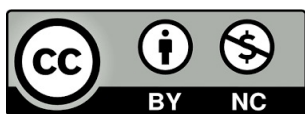Francisco Javier Santiago Arcos

Assembly and Characterization of Heterogeneous Biocatalyst for the Manufacturing of Omega Hydroxy Acids

Director/es

López Gallego, Fernando
López Cortajarena, Altziber

Tesis Doctoral

ASSEMBLY AND CHARACTERIZATION OF HETEROGENEOUS BIOCATALYST FOR THE MANUFACTURING OF OMEGA HYDROXY ACIDS

Autor

Francisco Javier Santiago Arcos

Director/es

López Gallego, Fernando
López Cortajarena, Altziber

UNIVERSIDAD DE ZARAGOZA
Escuela de Doctorado

Programa de Doctorado en Bioquímica y Biología Molecular

2024

Assembly and Characterization of Heterogeneous Biocatalyst for the Manufacturing of Omega Hydroxy Acids

Francisco Javier Santiago Arcos

CIC BIOMAGUNE

Assembly and Characterization of Heterogeneous Biocatalyst for the Manufacturing of Omega Hydroxy Acids

Dr. FERNANDO LÓPEZ GALLEGO, Profesor de investigación Ikerbasque

Dra. AITZIBER LÓPEZ CORTAJARENA, Profesora de investigación Ikerbasque

HACEN CONSTAR:

Que la memoria "Assembly and Characterization of Heterogeneous Biocatalyst for the Manufacturing of Omega Hydroxy Acids" realizada por Francisco Javier Santiago Arcos en el centro de investigación CIC BiomaGUNE y bajo su inmediata dirección, reúne las condiciones exigidas para optar al grado de Doctor en Bioquímica y Biología Molecular.

Agradecimientos

Table of contents

List of abbreviations

ω-hydroxyacids	ω-HA
2-Hydroxytetrahydropyran	lactol
2,2,6,6-Tetramethylpiperidin-1-yl)oxyl	TEMPO
Adenosine monophosphate	AMP
Adenosine triphosphate	ATP
ADH from *Bacillus* (*Geobacillus*) *stearothermophilus*	ADH1
Agarose microbeads	AG
Alcohol dehydrogenases	ADHs
Candida antartica Lipase B	CAL-B
Catalase from bovine liver	CAT
Catalase from *Bordetella pertussis*	BpCAT
Confocal laser scanning microscopy	CLSM
Continuous flow systems	CFS
Controlled porosity glass	CPG
Dimethyl sulfoxide	DMSO
Divinyl sulfone	DVS
ECR8204F	Pu
Ethylenediamine	EDA
Flame ionization detector	FID
Flavin adenine dinucleotide	FAD
Fluorescein isothiocyanate	FITC
Full width half maximum	FWHM
Glutaraldehyde	GA
High density	$Hd\text{-}AG\text{-}Co^{2+}$
Horse radish peroxidase	HRP
Imidodiacetates	IDA
Immobilized specific activity	iSA
Immobilization yield	ψ
Isopropylβ-d-1-thiogalactorpyranoside	IPTG
Lactonase from *Rhodococcus erythropolis*	ReLAC
Lactonase from *Sulfolobus Islandicus*	LAC
Low density	$Ld\text{-}AG\text{-}Co^{2+}$
Luria-Bertani	LB
Maximum normalized fluorescence fitted peak	yFWHM
NADH oxidase from *Thermus thermophilus*	NOX
Nicotinamide adenine dinucleotide	NAD
Nicotinamide adenine dinucleotide reduced	NADH
Nicotinamide adenine dinucleotide phosphate	NADPH
Nitrotriacetates	NTA
Penicillin G acylase	PGA
Phanero-chaete chrysosporium	PcAOX*

Polyethyleneimine-activated agarose	AG-PEI
Polymerase chain reaction	PCR
Porous silica particles	EziG
Radius	R
Recovered activity upon the immobilization	RA
Relative recovered activity	rRA
Room temperature	RT
TALON metal affinity resin	$tAG\text{-}Co^{2+}$
Theoretical immobilized activity	iA
Thermal denaturation temperature	Tm
Unspecific peroxygenase	UPO
Wall-coated reactors	WCR

Resumen

En la presente tesis doctoral se lleva a cabo un estudio sistemático para desarrollar un biocatalizador heterogéneo multienzimático para catalizar la transformación escalonada de dioles alifáticos en omega-hidroxiácidos. Primeramente, se desarrolló e intensificó la sincronización de un sistema multi enzimático "cell-free" sin precedentes con un sistema de reciclado de cofactor autosuficiente. Segundo, fue llevado a cabo un estratégico estudio de inmovilización de una de las enzimas del sistema acompañado por una caracterización funcional y estructural de los biocatalizadores heterogéneos ensamblados. Tercero, fue diseñado un soporte heterofuncional activado con tres diferentes químicas de funcionalización para la inmovilización una gran variedad diferente de enzimas y fue testeado con nuestra cascada enzimática. Finalmente, todo el conocimiento adquirido durante el estudio fue empleado para desarrollar un prometedor biocatalizador el cual co-inmoviliza y co-localiza nuestro sistema multi enzimático in la misma partícula y el cual fue aplicado exitosamente en condiciones de reacción, tanto en batch como en flujo.

Abstract

In this doctoral thesis, a systematic model to develop multi enzyme heterogenous biocatalysts to catalyze the stepwise transformation of aliphatic diols into ω-hydroxy acids is performed. Firstly, the orchestration of an unprecedent cell-free enzyme system with self-sufficient cofactor recycling was developed and intensified. Secondly, it was carried out a strategical immobilization study of one the enzymes of the system accompanied by a functional and structural characterization of the assembled heterogenous biocatalysts. Thirdly, a heterofunctional support activated with three different chemical functionalities to immobilize a wide variety of different enzymes was design and tested with the enzymatic cascade. Finally, all this gathered knowledge was employed to develop a promising biocatalyst which co-immobilizes and co-localizes our multi enzyme system in the same microparticle which was successfully applied in flow and batch reaction conditions.

CHAPTER 1: INTRODUCTION

1.1. Biocatalysis

Chemical industry produces most of the products that we consume every day. From textile and cosmetics to pharmaceutical and food products, all these manufactures are normally mediated by specific and sophisticated molecular processes named chemical reactions. A chemical reaction involves the rearrangement, in the molecular or ionic structure of reactants, to a different set of substances. These reactions are often restricted to the time and the energy required for the chemical transformation. The process can be irreversible, or reversible, where an equilibrium constant leads the rate relationship between product and substrate concentrations. Chemical reactions can occur as either single elementary reactions or as a series of successive reactions.. The latter is known as a stepwise reaction, where the rate of each step can be influenced by the preceding steps. Several factors influence the rates of chemical reactions, including the chemical nature of the involved substances (substrates, intermediates, and products): Physical state of the substances, reaction conditions (for instance, pH and temperature), substance concentrations, and the presence of a catalyst, which can play an important role in reaction effectiveness.

Catalysts are substances that increase the rate of a chemical reaction by lowering the activation energy of the chemical process by attaching itself to the reactant molecule, thereby interacting with it[1]. Depending on the nature of the catalyst, we can differentiate homogenous catalyst when the phase of substrate and catalyst are the same, whereas we denominate heterogenous those catalyst with different phase to the substrate. Heterogenous catalysis presents better perspective for industrial application such as easier separation between catalysts and reactants, application in flow reactions and reusability[2, 3]. However, homogenous catalysis still displays several advantages referred to higher selectivity, defined chemical structures (active site uniformity) and not limitations of mass transfer among catalysts. Catalyst (**Figure 1.1**). Catalysts are not consumed during the reaction course. This fact makes the possibility to reuse them in several synthesis cycle before their life-spam is out.
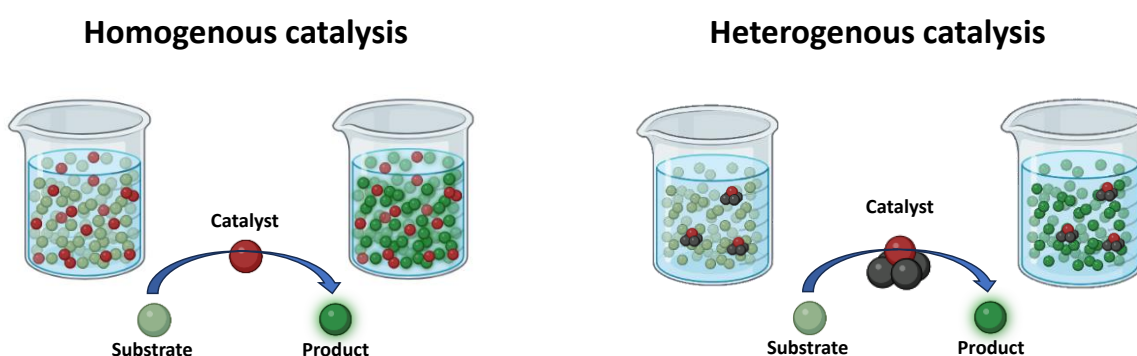
Figure 1.1: Scheme of the different types of catalysis: Homogenous catalysis and heterogenous catalysis.

Catalysis is classified based on the nature of the catalysts, in three main fields:

- ➢ Organometallic catalysis: The catalyst structure involves one chemical bond between a carbon atom of an organic molecule and a metal which includes alkali, alkaline earth, transition metals and metalloids[4]. Some reactions carried by organometallic catalysts are cross-coupling reactions to form carbon-carbon bonds employed in pharmaceutical synthesis[5] and carbonylation reactions to yield acids, esters and aldehydes from alkenes[6]

- ➢ Organocatalysis: It is the part of the organic chemistry that explore the chemical reactions carried out by organic substances without presence of metals. This kind of catalysis has become very important in industrial synthesis for its better selectivity compared to organometallic catalysis. Some of the organocatalysts employed: Amines such as L-Proline to form enamines with carbonyl compounds [7-9], chiral amides in aldol reactions[10] and carbenes to perform cross-coupling reactions, avoiding aldol condensation[11].

- ➢ Biocatalysis: It can be defined as the employment of natural proteins (enzymes) or nucleic acids to catalyze chemical reactions under non-physiological conditions. Most of the chemical processes where biocatalysis have been employed in industry, involve the kinetic resolution of chiral primary and secondary alcohols, amines or carboxylic acids, being hydrolases (such as *C. antarctica* lipase B (CAL-B)) or amidases (such as penicillin acylase) the mostly used family enzymes. Nowadays, the fact that biocatalysis carries out chemical reactions under non-toxicity and mild environmental conditions, adding the biodegradability of the substances, the exquisite selectivity and the high turnovers numbers makes biocatalysis an interesting strategy for industrial process sustainability. However, several drawbacks must be assessed to meet some exigent requirements demanded by industry. Hauer points out three majors aspects: Performance, market intelligence (the design of biocatalyst under process demand and costs and timeline[12]

1.2. Enzymes

Enzymes are complex and sophisticated catalysts found in nature to speed up catabolic and anabolic reactions involved in maintaining living systems[13, 14]. These proteins consist of a sequence of linked amino acids that determines the enzyme's final features, including their three-dimensional structure, the shape of their active site, and the reactions which they can perform.

The active-site is the part of the enzyme where the substrate molecules bind and undergo it chemical transformation into the final product [15-17]. This chemical process is carried out by

structural changes produced in the enzyme-substrate complex[18]. Some of the amino acids possess specific catalytic activity such as Aspartic and glutamic acids and Histidine which act in proton transfer reaction; serine, cysteine and tyrosine performing as nucleophiles or deprotonated lysines as a base, in catalytic reactions. The understanding of the role of these amino acids in the catalytic reactions and their location in the active-site allow us to explore the modification of the catalytic pocket of enzymes to improve the enzymatic reactions in terms of kinetics and selectivity (regio, chemo, and enantio), to increase substrate scope and to stabilize the enzymes for better operational performance.

Enzymes can be classified based on the catalytic reaction performed. Oxidoreductases catalyze redox reactions, being further categorized between oxidases and reductases. Hydrolases are the family of enzyme more employed in industrial biocatalysis and perform the hydrolysis of substrates. Ligases catalyses the reaction of the synthesis of two molecular substrates into one molecular compound, whereas Lyases carry out the elimination of a group from the substrate. Finally, transferases (transference of certain groups among substrates), Isomerase (speed-up the conversion of isomers, geometric isomers, or optical isomers) and Translocases (transference of substance along a membrane) complete the classification of the enzymes (**Figure 1.2**).
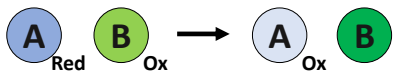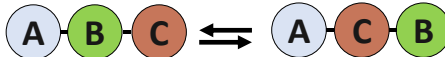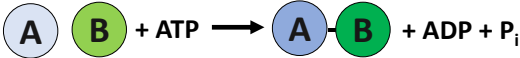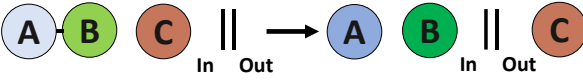
Enzyme class	General scheme of reaction
Oxidoredcutases	A$_{Red}$ B$_{Ox}$ ⟶ A$_{Ox}$ B
Transferases	A C B ⟶ A C–B
Hydrolases	A–B + H$_2$O ⟶ A$_H$ B$_{OH}$
Lyases	A–B ⇌ A B
Isomerases	A–B–C ⇌ A–C–B
Ligases	A B + ATP ⟶ A–B + ADP + P$_i$
Translocases	A–B C ‖ In Out ⟶ A B ‖ C In Out

Figure 1.2: Schemes of the different catalytic reactions carried out by enzymes.

Additional to enzymes, other molecules called cofactors are involved in the metabolic routes and are key in the efficiency of the reactions. Cofactors are non-protein, organic or inorganic, compounds which interact with the enzyme to carry out the chemical reaction. Indeed, as an active-site of the substrate, enzymes have specific binding-site for cofactors and these mechanisms is also relevant in Michaelis-Menten analysis biocatalytic reactions. Even cofactors have been explored to use them in organocatalysis[19]. Most of the organic cofactors contain the nucleotide adenosine monophosphate (AMP) as main core in the structure, such as adenosine triphosphate (ATP), flavin adenine dinucleotide (FAD) and nicotinamide adenine dinucleotide (NAD) as **Figure 1.3** exposes. Normally, these cofactors are consumed along the chemical reaction in a stoichiometry manner, thus additional enzymatic reaction are needed to recycle cofactors to be employed again in another turnover.
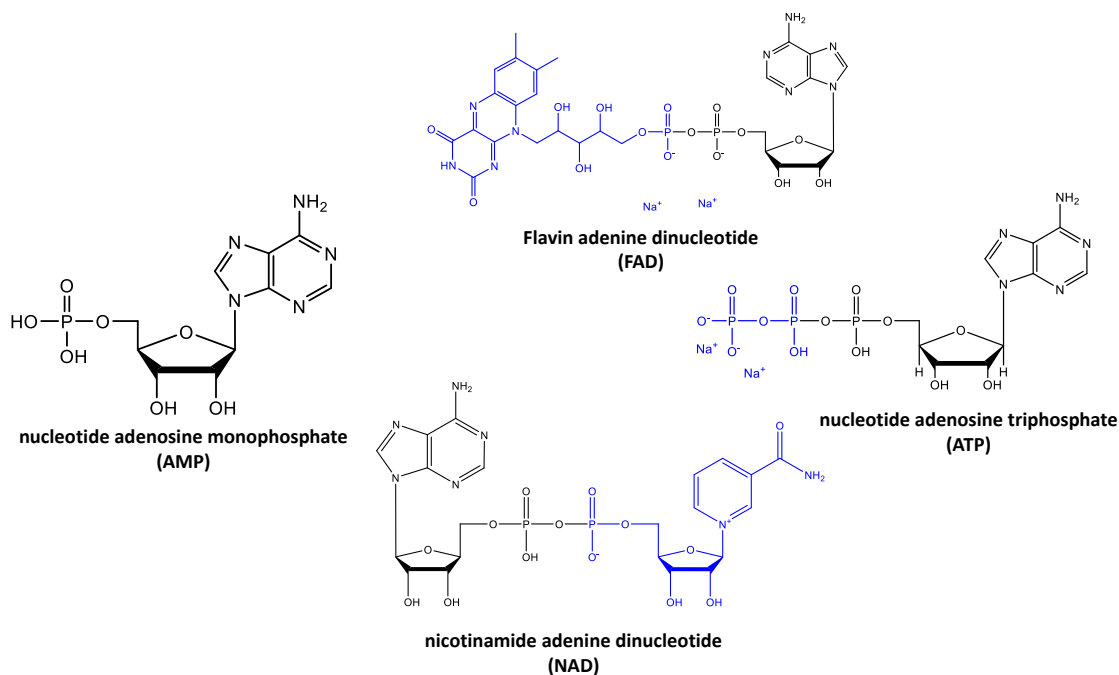
Figure 1.3: Structure of the different mainly cofactors employed in biocatalysis.

1.3.   Biocatalytic process in industry

Interestingly, biocatalytic processes have been linked to humanity since may not fully understand the mechanisms behind them. 3000 years ago, ancient civilizations employed yeast (*Saccharomyces cerevisiae* and *Saccharomyces carbelgensis*) to carry out the alcoholic fermentation of the sugars of grapes (Embden-Meyerhof route) to produce one of the most relevant drinks in human history: Wine. Fortunately, these microorganisms are already on grape skin. However, the assemble of biocatalyst is even older since Egyptians already used "sourdough" or "wild yeast" from bread dough exposed to the air as a carrier for yeast present in the environment. It took time to elucidate the science behind these processes. In the nineteenth century, Persoz and Payen isolated the enzyme amylase investigating the hydrolysis of starch to dextrin and sugar, leading the foundation of enzymology and its main role in biological processes. Both researchers formulated some basic principles of enzyme action in 1833[20]:

- Small amounts of the preparation were able to liquefy large amounts of starch.
- The material was thermolabile.
- The active substance could be precipitated from aqueous solution by alcohol, and thus be concentrated and purified. This active substance was called diastase (a mixture of amylases).

Eduard Buchner hypothesized that the substance inside yeast cells that carry out the alcoholic fermentation are proteins, and that living systems secrete these molecules to ferment sugar.

21

He named that protein zymase or enzyme, and his work was awarded with the Nobel prize in 1907. All these achievements make him be considered as the father of the enzymology. There is some controversial opinion about this title since the female Russian scientific Maria Mikhaïlovna Manàsseina was the first to claim that the fermentation process is due to the action of enzymes that can be isolated from the yeast cells, being a cell-independent process. However, Buchner and Rapp dismissed her claims, affirming that her experimental evidence was unconvincing, and she was subjectively convinced of the existence of an enzyme of fermentation.

The application of enzyme in industry was mainly focused on the synthesis or resolution of optically active intermediates. Two majority group of enzymes (lipases and amidases) are employed in the kinetic resolution of chiral primary and secondary alcohols, amines, or carboxylic acids. This toolbox was enhanced with nitrilases, ketoreductases and transaminases. Overall, the aimed final product was the manufacture of essential building blocks as starting point for the synthesis of more complex molecules, with an interesting potential in pharmaceutical synthesis.

The transference of biocatalysis into industry faces several challenges to assess issues as: efficiency of the performance and economic cost and timeline[12]. However, there are some examples to have overcome those drawbacks such as the well-stablished industrial scale-up biocatalytic process is the synthesis of acrylonitrile from acrylamide is carried out by a whole-cell system containing nitrile hydratase, exceeding 100 $g \cdot L^{-1} \cdot h^{-1}$ space-time yields.

In the last two decades, the employment of enzymes as catalysts in industrial manufacturing has experimented a revolution due to employment of modern bioinformatic and computer modelling tools which allowed the discovery of new enzymes and the rational design or directed evolution of new variants. The latter technology was developed by Frances H. Arnold, awarded the Nobel prize in Chemistry in 2018. The aim of this tendency is mostly to enhance the scope of substrates of the enzymes and increase the stability under operational conditions. Additionally, other approaches can be explored to improve biocatalytic performance in industry as the employment of artificial cascades that carry out the complete synthesis, avoiding the isolation of reaction intermediates and saving resources, reagents, and time.

1.4.   Multi-enzyme systems.

Multi-enzyme process refers to the combination of different enzymes and enzymatic complex to carry out specific cascade reactions. Living system employ the combination of different enzymes to assemble metabolic pathways which are fundamental in homeostasis by maximizing the capture of energy or minimizing its use[21]. The cellular machinery employs enzymes with specific activities across different metabolic pathways, showcasing the versatility that these biocatalysts provide in nature. Also, these pathways happen mostly in the cytoplasm

of microorganisms that we can consider as one-pot reaction, which is a relevant capacity of multi-enzyme systems on their application in industrial processes.

The term "cell-free cascade" refers to a reaction sequence designed to combine enzymes from different organisms without being part of a metabolic route in natural organisms. Indeed, the enzymes involve in this cascade can be employed in the non-natural reaction direction, increasing the catalytic possibilities of the cascades (For instance, the oxidation of fat acids, a catabolic route in nature that can act as anabolic one when it is assembled in an artificial cascade or in whole-cell system). Additionally, these biocatalytic reactions can be combined with other type of catalyst to form chemoenzymatic reactions[22]. The assemble of this *de novo* cascades allow to generate a great variety of reactions with great putative interest in industrial synthesis. Artificial cascades can be classified through different parameters (**Figure 1.4**):

- Number of steps
- Number of catalysts: Also, we must distinguish between the catalysts involve in the linear sequence and those for cofactor recycling, removal of co-substrates, etc.
- Type of combined catalysts: Biocatalysts, organocatalysts or metal catalysts
- Chronology: Simultaneously or concurrently and sequential
- Type of chemical reaction steps: hydrolysis, reduction (ketone/aldehyde, carboxylic acid, C=C, reductive amination) oxidation (alcohol, aldehyde, C-H, Baeyer-Villiger), C-C bond formation
- Type of biocatalyst preparation: Purified enzymes, cell-free extracts, whole cells, resting cells….
- Spatial organization of biocatalyst: In solution, immobilized, compartmentalized (membrane), colocalized, etc.
- Multi-enzyme cascades can be also classified based on the morphology of the cascade.
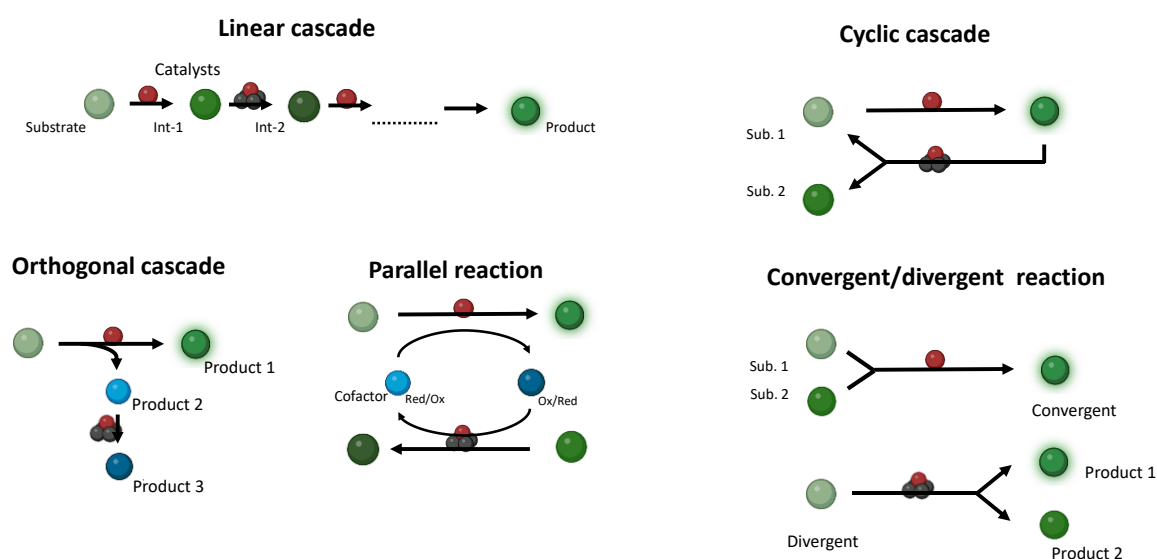
Figure 1.4: Different enzymatic cascades carried out by multi-enzyme systems.

Each time point of the cascade is denominated as stage. A stage may comprise one or more reaction steps. Overall, the employment of enzymatic cascades offers several advantages such as the no need of isolation during the process since the cascades are designed to concurrent carry out the different steps to the final product at the same pot[23]. Despite the expensive value of the cofactors employed in most of the cell-free cascades, there are effective regeneration systems that can allow not only the increase of use of the molecule, but also the possibility to shift an unfavourable equilibrium to the desired products[24]. We can find that some synthetic processes involve the generation of different unstable intermediates which may be affected during isolation and input on the next stage. Cascades avoid this event since once the molecule is formed already is taken by the next step[25].

Despite the modulation capacity for assembling a great variety of enzymatic cascades, nature is the major source of inspiration. The unveiling of the metabolic pathways involved in cellular machinery as glycolysis were key on the understanding the potential of enzymes in chemical synthesis[26]. The first assembly a cell-free cascade involved two enzymes in a linear sequence for the biotransformation of lactic acid to L-alanine in 1984. However, the orchestration of cell-free cascade requires the compatibility of the reaction conditions (for instance, temperature and pH) and the enzymes involved in the biotransformation.

Rational design and direct evolution to generate new branch of enzymes have dominated the research trend in biocatalysis in the last years, increasing the scope of substrates and the reactions possibilities[27]. Currently, new databases and IA machinery facilities the access to the analysis of biocatalysis data[28] which may even improve more the accuracy of computational designs. These new revolutionary tools have generated an efficient and fast biocatalysis cycle (Figure 5). Firstly, the selected enzyme is improved by enzyme mining and protein engineering to improve the catalytic efficiency. Later, the enzyme is coupled with the other catalysts in the desired cascade. Finally, the process is intensified to reach industrial demand values by controlling the reaction conditions (pH, temperature, substrate concentrations, oxygenation, and other parameters) (**Figure 1.5**)[12].
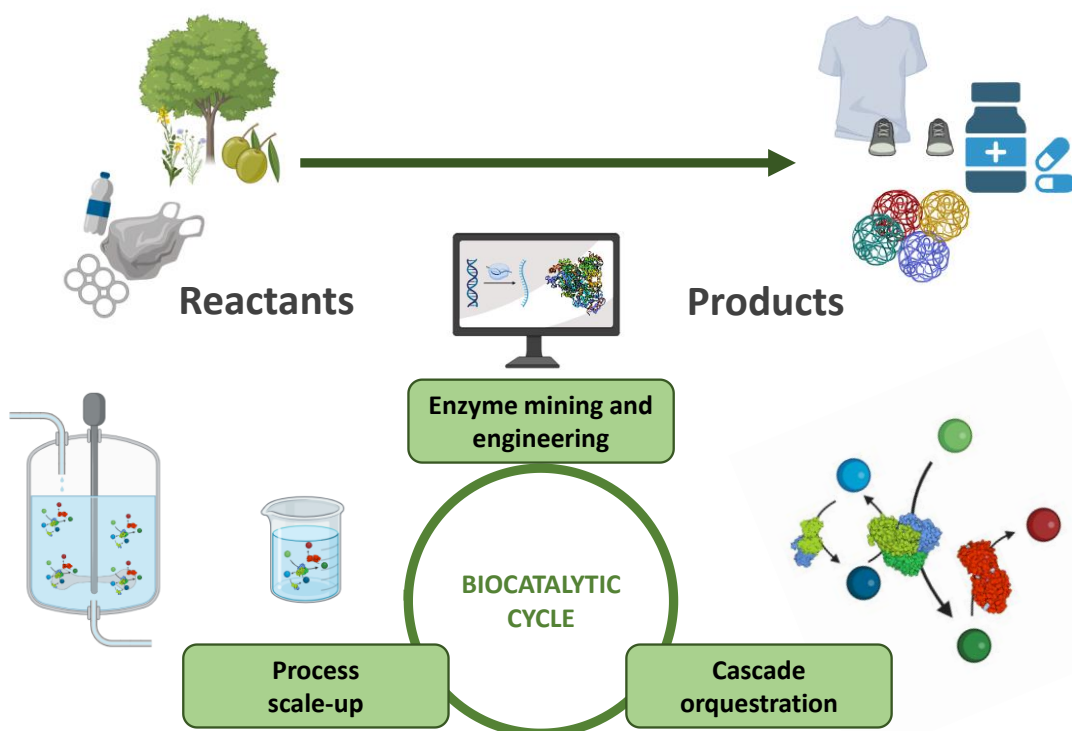
Figure 1.5: Biocatalytic cycle of multi enzyme cascades.

1.5. Enzyme immobilization

Enzyme immobilization relates to the state of enzyme molecules confined or attached to solid materials where enzymes are in a different phase respect to the reactants. These biocatalysts are considered as heterogenous catalysts since the enzymatic reaction happens in the solid-phase whereas substrates are in the liquid-phase. Since the substrates and products present in the liquid phase can diffuse across the heterogenous biocatalysts, enzyme immobilization allows an easy-downstream separation between the biocatalyst and reaction media at the end of the biotransformation, the reuse of the biocatalyst in several processes, the possibility of the use of the biocatalyst in a continuous flow system and the enhancement of the stability of the immobilized enzymes. However, there is not an "universal" methodology for an appropriate immobilization for every enzyme. Each enzyme must be studied individually to assess the best strategy for the immobilization and the most suitable carrier.

The immobilization of enzymes on carriers to assemble heterogenous biocatalyst has been employed to improve enzymatic reaction performance under industrial conditions[29, 30]. There are several advantages in assembling heterogenous biocatalysts such as: Easy downstream processing of the catalyst, reusability in several batches, increase of enzyme stability, specially towards organic solvents and high temperatures[31]. However, the negative effect in kinetic parameters and reaction rates compared to free enzymes and the decay of the biocatalyst efficiency by fouling or enzyme inactivation are challenges to be assessed[31]. Two main factors influence in this loss of activity: Conformational changes due to enzyme

immobilization and diffusional restrictions of substrates with the biocatalyst[32]. A new approach to expand the advantages of multi enzymes cascades in biocatalysis is the co-immobilization which allows us to control the spatial distribution on carrier surface, improving the overall efficiency of the cascade by, for instance, reducing mass transfer limitations among enzymes[29, 33, 34]. A crucial task for enzyme immobilization is the selection of both carrier and chemistry binding strategy. Despite having some limitations, enzyme immobilization has been widely employed in different chemical synthesis in different areas in industry.

- Food: Most of the heterogenous biocatalyst assembly involves the covalent binding to the carrier surface. Some examples: the immobilization of proteases on mesoporous zeolite/silica in the cheese manufacturing[35], and the immobilization of β-galactosidase on chitosan/silica[36] and polyvinyl alcohol[37] for the lactose hydrolysis in daily products.

- Detergents: Enzymes have long been added to detergents formulations for the removal of certain types of stains in ambient temperatures. Proteases has been immobilized on polymeric matrix and mesoporous silica nanospheres covalently for the removing blood and egg yolk stains[38, 39], whereas lipases were immobilized covalently on arylamine glass beads for oil stain removal[40].

- Textile: A considerable increase in the usage of enzymes in the textile sector has taken place recently. Enzyme are applied on textile processing steps due to their capability to modify cellulosic fibres, generating higher-quality textiles[41]. Cellulose has been employed immobilized in epoxy resins by adsorption for the biopolishing of fabrics without tensile strength loss. Other carriers employed for immobilization are polymers as Eudagrit L-100 and S-100 by noncovalent immobilization[42, 43]. Proteases employment aims to achieve shrink-resistant wool end products as substitute of environmental harmful chlorination processes[44]. The polymer carrier Eudragit S-100 also was employed to protease immobilization[45].

- Wastewater treatment: main focus of the enzyme employment of this area is focused on phenolics and dyes removal due to their carcinogenic and mutagenic properties, toxicity, and poor biodegradability[46]. Some laccases and peroxidases has been immobilized on different supports as Cu(II) ion chelated chitosan to manage the degradation of methyl orange, Cibacron blue and reactive black 5[47], managing interesting yields and operational stability (87% of degradation during 20 uses or immobilized covalently on epoxy functionalized silica to remove efficiently till 95 % of phenols[48].

1.6.   Support Materials Used for Enzyme Immobilization

Chemical, biochemical, mechanical, and kinetic properties of an immobilized enzyme directly depend on the properties of the enzyme, but also on the properties of the material in which the enzyme is immobilized. The support is a key factor, and some of its characteristics are important, such as the possibility to introduce many reactive groups to interact with the enzyme, to possess a flat surface, and to obtain a fully inert surface after immobilization[49]. Most employed supports can be synthetic organic polymers, biopolymers, inorganic materials, smart polymers, and hydrogels. No universal material has been described for all different applications in immobilized enzymes.

Synthetic organic polymers: most representative synthetic organic polymers used for enzyme immobilization are methacrylic resins, such as Purolite and Relizyme[50]. They are hydrophilic and both mechanically and chemically stable. Amberlite XAD-7 is another acrylic resin that can be used to covalently attach enzymes, and it was notably used for CAL-B immobilization by Novozymes[51]. However, the most commercially exploited methacrylic resin for CAL-B immobilization via interfacial activation is Lewatit VC OP 1600, which gave rise to the most ever commercialized biocatalyst, Novozyme435[52]. The main issue of acrylic resins are diffusion limitations. Plastic materials such as nylon[53, 54] or polyurethanes[55] are other synthetic organic polymers relevant for enzyme immobilization.

Biopolymers: a wide range of polymers of natural origin, such as polysaccharides including cellulose, agarose, starch, pectin, chitin, carrageenan, and chitosan, as well as some proteins, such as albumin, gelatin and collagen are mainly used as supportive materials for enzyme immobilization. These materials are disposed in matrixes that form very inert aqueous gels characterized by a high mechanical strength. Their chemical structure enables their easy activation to bind proteins both reversibly and irreversibly, mostly with aldehyde, carbodiimide, epoxide, hydrazide or active ester groups[56]. A clear advantage of these polymers is their natural availability: agro-industrial wastes have been used to develop efficient cellulose matrices for lipases or transaminases immobilization[57, 58], and a lignin-based matrix have been successfully implemented in flow biocatalysis[59]. We can find examples of intensified processes employing a biopolymer as carrier as agarose to the synthesis of melatonin by an acyl transferase or the manufacturing of 6-amino penicillanic acid by a penicillin G acylase (PGA) in organic solvent[60-62].

Inorganic materials: a huge variety of inorganic materials can be used for enzyme immobilization, such as alumina, silica, glass, zeolites and ceramics. Silica-based supports are the most suitable matrices due to their high mechanical strength, their easy functionalization with chemical groups and their easy fabrication to provide desirable morphology, pore structures and micro-channels. Furthermore, silica gels are chemically inert and therefore environmentally friendly for chemical manufacturing. Enzymes can be easily immobilized in silica by absorption[63-65]. Controlled porosity glass (CPG) is a silica glass composed by pores

with a particular size distribution and a wide variety of geometric forms[66, 67]. This material is platform for the bioamination of ketones in organic solvents by w-transaminase immobilization[68].

1.7. Enzyme immobilization techniques

Two major employed strategies are physical (adsorption or physical entrapment) and chemical immobilization (covalent binding and cross linking)[69-74].

1.7.1. Reversible bound

Enzymes binds to the carrier surface through weak non-covalent interactions (for example: van der Waals, hydrophobic interaction, hydrogen bond or salt linkages). These strategies allow the enzyme immobilization with no chemical modification of the enzyme residues. Even, enzymes can be easily removed for the carrier under gentle conditions, allowing the reusability of the support upon the enzyme inactivation. There are several advantages present in this immobilization technique:

- supports are chemically activated with high reactive groups, and hence they are very stable during transport, storage.
- Protocols are usually simple and carried out under mild conditions.
- The capacity to regenerate the heterogenous biocatalyst "*in situ*" after enzyme inactivation.

The main disadvantage of this process is the leaching of the immobilized enzyme due to non-permanent binding (**Figure 1.6.A**).

Ionic interaction

The most popular, simplest, and oldest technique for reversible immobilization. This entails the ionic interaction between the enzyme and the carrier material, by having the opposite charge the counterparts[75]. However, this noncovalent immobilization is easily reversed by varying the temperature, ionic strength or changing the pH[76]. Additionally, some distortions produced by excessive charges can hamper the enzyme structure, affecting the catalytical process effectiveness[77] (**Figure 1.6.B**).

Hydrophobic interaction

Enzyme immobilization technique where enzyme attaches to the carrier through the hydrophobic regions on its surface. Carriers have highly hydrophobic surfaces such as octyl-agarose and octadecyl-sephabeads. This technique mostly employed for the adsorption of lipases since the open and active form of lipase molecules becomes stabilized by strong adsorption on the support surface and, eventually, an hyperactivation of the enzyme (**Figure 1.6.D**).

Affinity interaction

This immobilization technique is based on creating (bio)affinity linkages between an activated carrier with, for instance lectin, avidin or metal chelates, and a specific domain or tag of the protein sequence such as: carbohydrate residue, biotin and histidine tails. The latter is widely used due to the specific interaction formed between the imidazole ring of histidine and metal ions (Co^{2+}, Cu^{2+}, Zn^{2+} or Ni^{2+}). Additionally, this methodology is highly employed in the enzyme purification from crude extracts, where the enzyme to purify is fused to a poly-histidine tag with high specific for metal chelates. This approach is named immobilized metal affinity chromatography (IMAC). Moreover, IMACS offers the possibility to control the enzyme orientation to avoid enzyme deactivation by the minimal effect in enzyme structure[78-81] (**Figure 6.C**).

Reversible immobilization
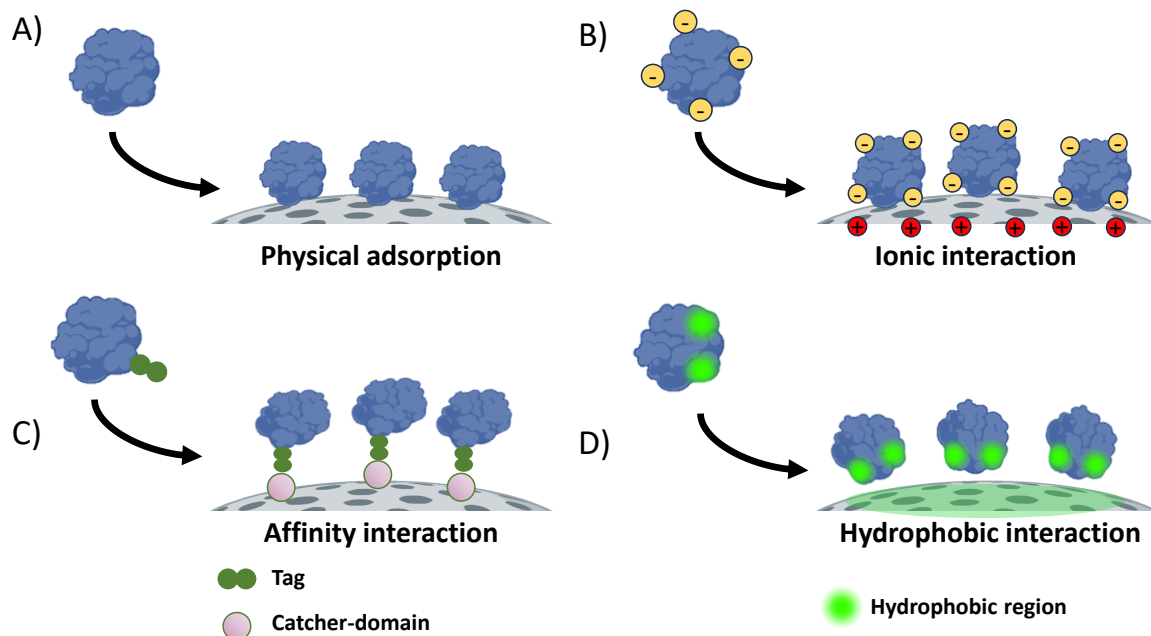
Figure 1.6: Different reversible enzyme immobilization techniques.

1.7.2. Irreversible bound

Enzymes usually bind to the surface of the carrier by the side chain of one of their residues or/and N-terminal residue to reactive group present in the support. These groups usually either possess electrophile character or are Michael acceptors (activated alkanes). Normally, the selected carrier is functionalized with reactive groups that react with several residues at the surface of the enzyme such as lysine (ε-amino group), cysteine (thiol group) and aspartic and glutamic acids (carboxylic group), which performs a nucleophilic attack to the reactive groups in the carrier surface. Normally, irreversible enzyme immobilization takes places at alkaline pHs since most of the nucleophile residues (Lysines, Histidines, Serines, and Tyrosines) of the enzyme surface are highly activated.

Irreversible immobilization present advantages such as enhancement of stability and reusability and improvement of product purity by avoiding leaching. However, the strategy confers high rigidity to immobilized enzymes which may hamper enzyme activity. Simply, not every enzyme is suitable for irreversible attachment. The selection of the chemical group to functionalize the surface carrier arise key on the successful immobilization of the enzyme, not only the complete attachment of the enzyme to the carrier, but also the recover activity after immobilization and the increase of the stability of the immobilized enzyme. The reactive groups employed in irreversible immobilization can be classified in three groups.

Aldehyde groups (electrophiles)

Small aliphatic groups that can be secluded from the support surface. Aldehyde groups promote multipuntual covalent bound with the nucleophile residues (Lys and N-terminus)) forming a Schiff's base with the amino groups of the amino acids. This reaction is normally carried out at alkaline pH due to the more activation as nucleophiles of the residues. These Schiff's bases are selectively reduced by secondary amines, sodium borohydride or sodium cyanoborohydride agents. Also, this reduction steps allows to eliminate the still reactive groups of the support (**Figure 1.7**).

Guisan et al. exposed the first immobilization protocol through glyoxyl agarose gels (Support-O-CH$_2$-CHO). This protocol promotes the bound of the enzyme to the surface carrier through short spacer arms, generating multipuntual covalent binding very strong. Additionally, the employment of other organic compounds as glutaraldehyde allows increasing the distance between the carrier surface and the anchoring immobilization point. Indeed, this activating group promotes a two-step immobilization: After ionic adsorption by rich glutamic and aspartic amino regions. Taking advantage of the structure of the molecule (symmetric di aldehyde group), glutaraldehyde can react, for instance, with amino-activated matrix, enhancing immobilization carrier properties by a double chemical interaction carrier enzyme (covalent due to aldehyde groups, whereas ionic interaction between enzyme and amine groups).

As previously described, after enzyme immobilization and formation of Schiff's base between nucleophile residue and reactive group of the carrier, reduction step arises mandatory to apply reduction agents (i.e., NaBH$_4$) to promote the irreversibility bound and reduce the remaining

aldehyde groups in the carrier surface. However, before this step, it is important to hamper the remaining reactive groups of the surface carrier to avoid undesired reactions. When the reduction agents do not reduce both Schiff´s bases and remaining aldehydes (i.e., picoline borane), blocking agents are usually employed to this task that, additionally, confer new characteristics to the surface carrier.
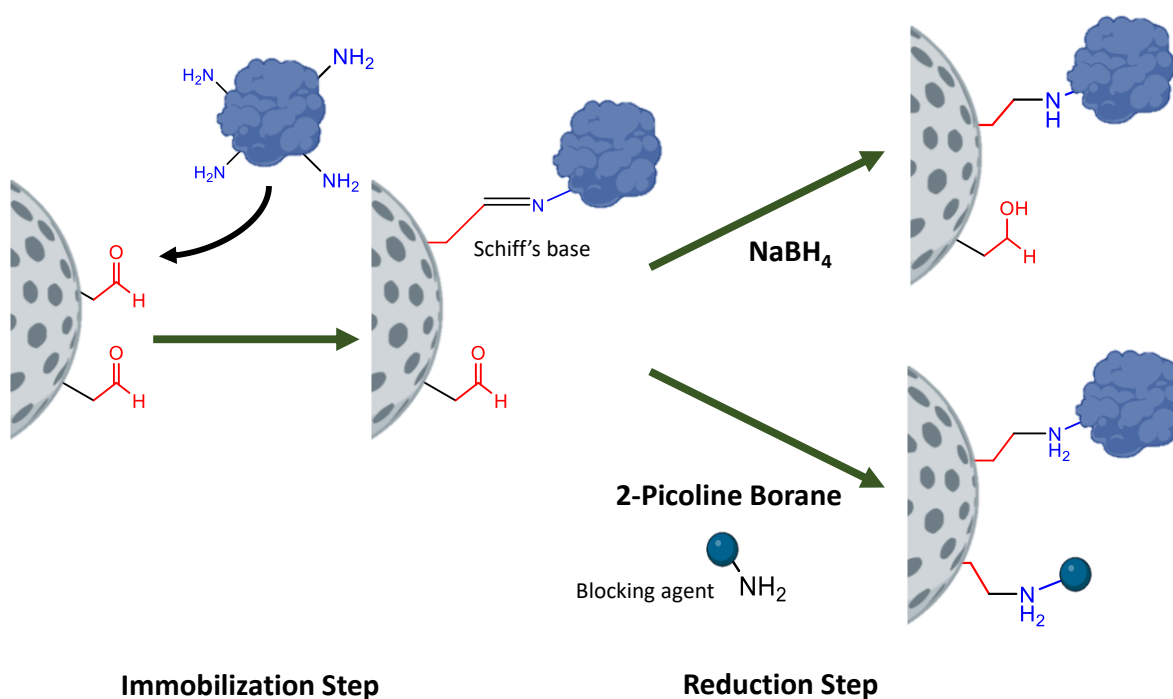
Figure 1.7: Scheme of enzyme immobilization.

Epoxy group (electrophiles)

Epoxy groups involves two carbons and oxygen atoms forming a three-membered ring structure. They present great stability at neutral pH values allowing the storage for long periods of time for functionalized carriers. Epoxy groups can react with very different chemical groups present in the amino acids: Cysteines (thiols), Lysines and Histidines (aminos), Tyrosine and Serine (aromatic alcohols); forming strong linkages (secondary amino, ether, or thioether bonds) with a minimal chemical modification of the protein because pK values of the new secondary amino groups are very similar to those of the pre-existing primary amino ones (Figure 1.8). At the end of the immobilization process, epoxy groups can be easily blocked by reaction with different thiol or amine compounds under mild conditions, avoiding uncontrolled reaction between the support and the enzyme that might decrease its stability.

The elimination of the remaining reactive epoxy groups is carried out by the employment of blocking agents. The variety of these blocking agents is wide since there are numerous compounds that can react with them, such as thiols, amino acids, and other amines. This fact allows to modulate the features of the carrier thorough the use of polar amino acids in the blocking step.
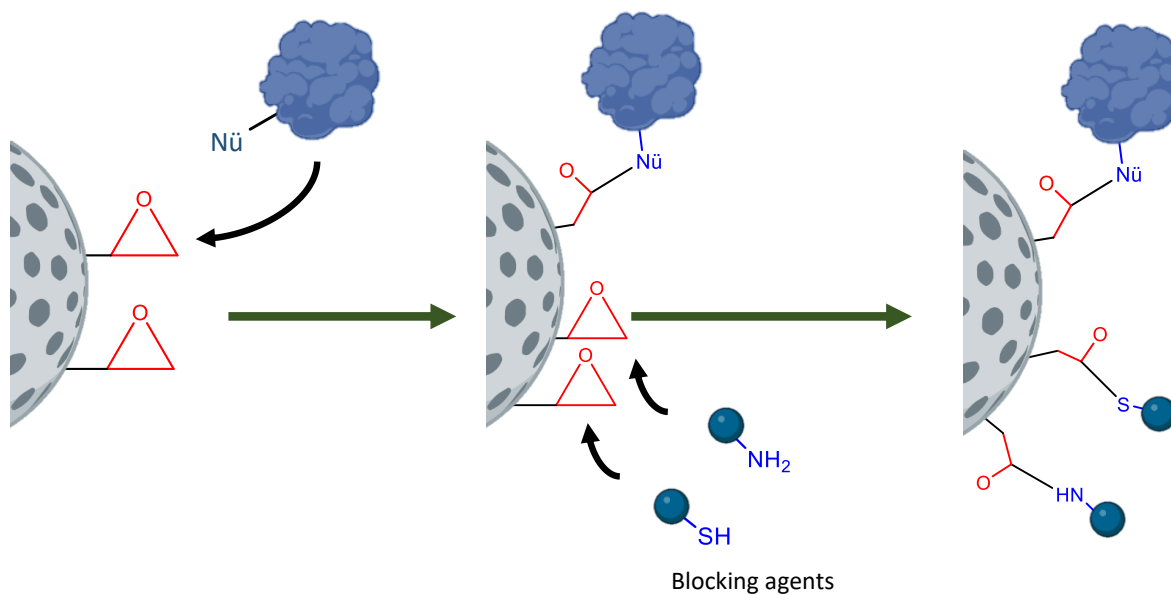
Figure 1.8: Scheme of enzyme immobilization.

Alkanes groups (Michael acceptors)

These groups are characterized by generating reactive conjugates that allows Michael addition of, commonly, amine or thiol groups on conjugated double bonds[82]. Among the different agents applied in functionalization, divinyl sulfone has emerged as a referent of this strategy.

Divinyl sulfone (DVS) groups take enzyme immobilization through a reactive vinyl sulfone group that react with, not only amino, phenol, imidazole or thiol groups of enzymes, but also moieties present in carrier surface. For surface activation, DVS reacts to different functional groups presents in surface supports such as amino, thiol or hydroxy groups[83, 84]. DVS shows a high number of enzyme-carrier interactions than its counter partner the glyoxyl-agarose[85-87]. Interestingly, enzyme immobilization can be carried out at a wide range of pH (from 5 to 10), involving in the first attachment different enzyme reactive groups[86] (**Figure 1.9**). DVS activations has been tested also in cellulose[88], silica[83] and super-paramagnetic hybrid nanoparticles[89]. Additionally, as epoxy groups, the elimination of the remaining no reacted groups is carried out through the employment of blocking agents, conferring additional properties to the carrier surface. β-galactosidase and trypsin were immobilized through this strategy, obtaining promising results[86, 90].
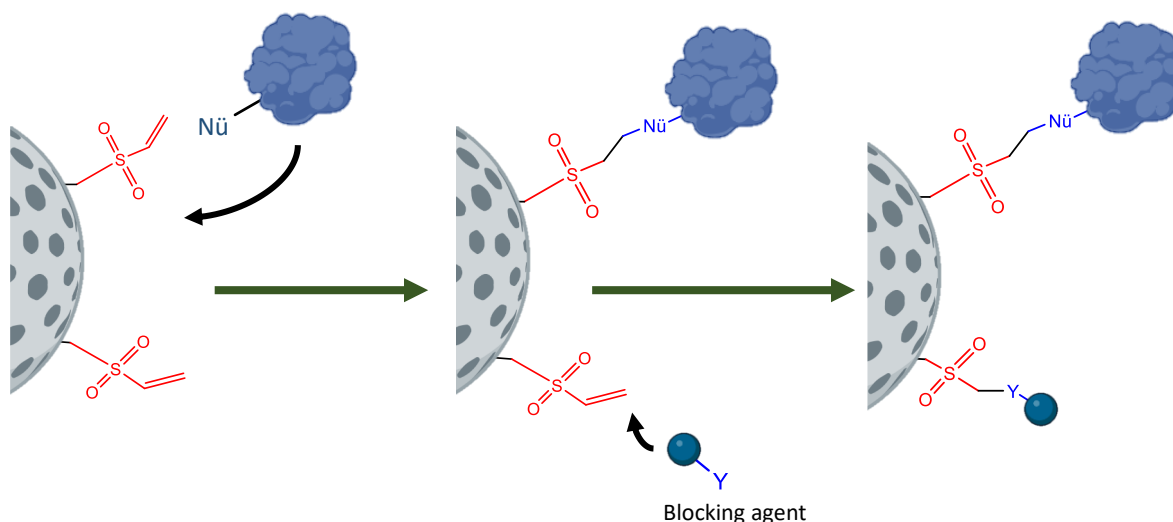
Figure 1.9: Scheme of different chemical strategies for irreversible immobilization

1.8.   Heterofunctional carriers

Enzyme co-immobilization is a current strategy to immobilize multi-enzyme systems. Bringing enzymes together inside solid materials may enhance the mass transport and increase the local concentration of intermediates between the co-immobilized enzymes[91]. However, the co-immobilization of two or more enzymes on the same support is not trivial, as one immobilization strategy might be beneficial for one enzyme but detrimental for the other(s). Therefore, co-immobilization by itself does not guarantee the activity and stability of a heterogeneous multi-enzyme system[92]. In this context, heterofunctional supports contain several functionalities (reactive groups) on their surface that react with several surface residues (Lys, His, Cys, Asp, etc.) of one or more enzymes under different conditions (pH, ionic strength, temperature). Heterofunctional carriers can be modified during and at the end of the enzyme immobilization. For instance, aldehyde groups can be blocked to direct the immobilization through non-covalent interactions (in the case of irreversible immobilization). This block-agents can modify the microenvironment of the immobilized enzymes. Another post-immobilization strategy is the coating of the surface carrier by a polymer that confers, for instance, more stability to the immobilized enzyme.

These heterofunctional supports emerge as an excellent solution to co-immobilize multi-enzyme systems on the same surface, where each enzyme is attached to the support through its optimal immobilization chemistry. The vast majority of heterofunctional supports offer the combination of only two groups: one (i.e., ionic, hydrophobic, metal chelate groups) to drive the enzyme adsorption and the other (i.e., epoxy, aldehyde, glyoxyl, and vinyl groups) to react with the exposed nucleophilic residues on the enzyme surface to form covalent and irreversible bonds[93, 94]. The combination of these two groups allows a two-step enzyme immobilization, in which the enzyme is first absorbed very quickly to the support (close contact) and then irreversible covalent attachment between the enzyme and the support is formed[95].

One of the primary benefits of employing these types of supports is their ability to enable the immobilization of enzymes in various regions on their surface, offering versatility in enzyme orientation. The presence of distinct hydrophobic/hydrophilic moieties on the surface carriers can modulate the enzyme orientation (**Figure 1.10**). New bioinformatics provide information about enzyme surface characteristics, which can allow us to predict and design the most suitable orientation for each enzyme immobilization[96].

Although heterofunctional supports have been mainly harnessed to accomplish the multivalent covalent immobilization of single enzymes at mild conditions, recent trends are more focused on their use as a chassis for the co-immobilization of multi-enzyme systems controlling their spatial organization[92, 97-99].
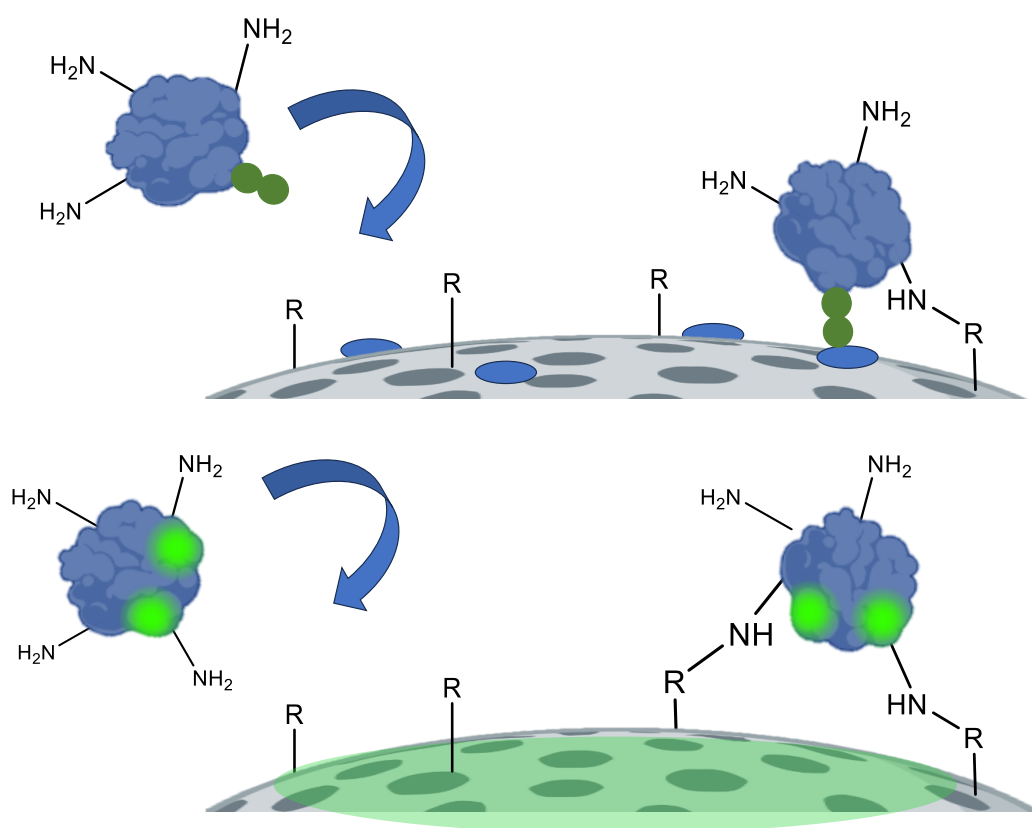
Figure 1.10: Scheme of enzyme orientation under immobilization. The enzyme orientates by affinity to the surface of the carrier prior to the attachment to the support.

1.8.1. Controlling the spatial distribution under enzyme immobilization

There are several factors that influences the heterogenous biocatalyst efficiency apart from the conformation adopted by the enzyme when it is immobilized. For instance, mass transfer limitations from the bulk to the material surface can affect the productivity of our biocatalyst due to the creation of intraparticle gradients of the reaction components (microscale), and by suboptimal reactor settings, like poor agitation (macroscale)[100]. The localization of the

enzyme on the particle has also a great influence in the biocatalyst productivity. In porous materials, the bounded enzymes might suffer from both external mass transfer issues and internal diffusion restrictions, limiting the productivity of the heterogenous biocatalyst. Recent published work showed that the nanometrical organization of a multi enzyme system increases till 5 times higher the specific productivity compared to a non-organized system[101]. Low enzyme loads, tunning carrier dimensions and reactor designs are some strategies to overcome these mass transport issues[102].

Another approach is controlling enzyme location within the carrier. This approach can intensify the efficiency of heterogenous biocatalyst since enzyme distribution impacts on substrate mass transference on the enzymatic system. For instance, glycosidases and acylases nonuniformly immobilized at the outer surface of porous microbeads outperform those uniformly distributed across the inner material porous surface[103]. Also, Benitez et al showed that the productivity of the NADH oxidase from *Thermus thermophilus* (NOX) increased several times when enzyme is localized in outer surface of the particle compared to an inner distribution due to limited oxygen diffusion inside the particle[100].

There are several strategies to control the enzyme location in the particle. One is controlling the chemical nature of the enzyme and the carrier interface[97, 104]. Rapid immobilization avoids enzyme perfusion along the particle, mainly immobilized at the outer surface of the particle, whereas slow immobilization allows enzyme diffusion before attachment. The immobilization rate can be easily controlled by adding immobilization competitors or modify the immobilization buffer and/or conditions.

1.9. Industrial processes

1.9.1. Batch reactions

Batch reactions refers to those chemical reactions in which the process is carried out in a non-continuous vessel where all reactants product and solvent do not flow in or out during the reaction[105] (**Figure 1.11**). Most of the batch consist of a vessel with an agitator and integral heating/cooling system. The usual agitator comprises a central driveshaft mounted with impeller blades, that depending on the viscosity of the mix reaction, can be adapted for an appropriate mixing. Temperature control is crucial in the right performance of a batch reactor Chemical reaction can liberate or absorb heat during the process requiring heating or cooling external jackets. These coils consist of: A single external jacket, half-coil jacket or a constant flux cooling jacket.
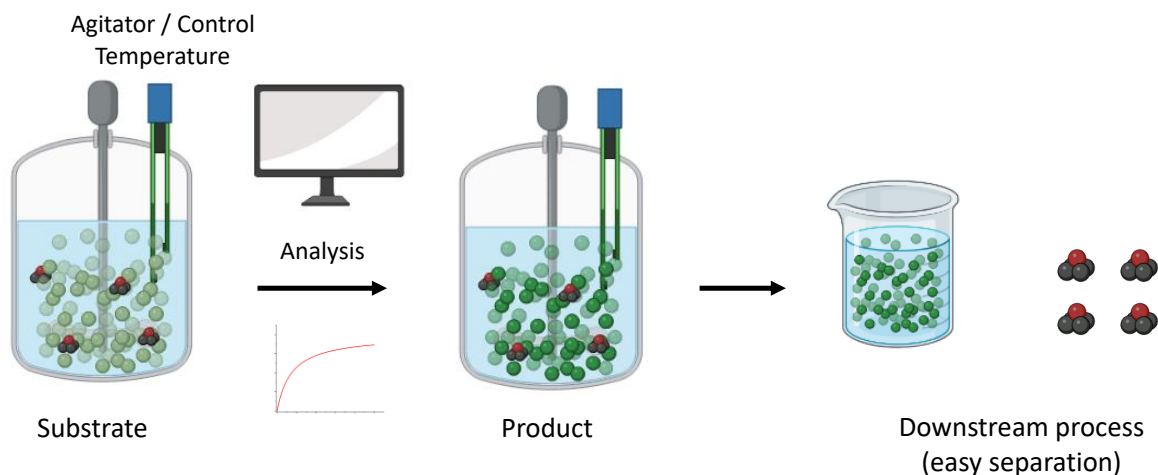
Figure 1.11: Classical Discontinuous Batch process composed of consist of a vessel with an agitator and integral heating/cooling system and analysis. Easy downstream purification due to different phase of product and biocatalyst.

Batch processes are commonly used in pharmaceutical and synthetic chemistry due to their flexible production planning, fast implementation as well as process and product traceability. Although companies favour batch processes due to the availability of sunk capital for this technique and accumulated knowledge, they require significant investment in material, large storage facilities for chemicals, solvents and, noteworthy, process intermediates. Also, the scalability is never straightforward as heat and mass transfer are a challenge[102, 106, 107]. A very interesting example of a heterogenous biocatalyst process to be applied in industry is the synthesis of emollient esters (i.e, myristyl myristate or coconut oil esters) by immobilized CALB. Chemical synthesis took place at high temperatures and caused formation of side-products, whereas new biosynthetic process reduces 100°C the temperature reaction (from 180°C to 60°C) and avoids downstream processing steps.

Some batch process requires of controlling substrate concentration due to that some enzymes may be inhibited at high concentrations of some of them. Fed batch reactors consists in supply one or more substrates to the bioreactor till the accomplish of the biocatalytic process[108]. This technique improved immobilized unspecific peroxygenase (UPO) hydroxylate performance by monitoring hydrogen peroxide concentration (inhibitor of UPOs) and feeding *in* or *ex situ* to manage a suitable concentration levels[108]. Additionally, a continuous process can be performed in a fed batch reactor adding a downstream output to collect final product. This flow reaction is very suitable for heterogenous biocatalyst which can generate a fluid bed reactor with an appropriate stirring.

1.9.2. Flow reactions

As aforementioned, immobilization of enzymes in solid materials represents a valuable tool for pharmaceutical and synthetic chemistry. Normally, immobilized enzymes are implemented in batch processes, due to their fast implementation and to their product traceability. However, continuous flow systems (CFS) present several advantages when compared with batch reactors, as they present better volumetric productivity, they are more easily transferrable to large-scale production and their modularity permits a much better control of the setup of the reaction[109]. CFS requirements are not particularly demanding and allow for the automation of the process. CFS strategies also guarantee the control in conditions such as pressure, temperature, or reactivity in a much safer way than batch. In addition, process intensification and feedback loop strategies can be implemented with continuous operations and usually improve the cost-efficiency. Multiphasic reactions benefit from flow systems as for example gaseous reagents often present poor interfacial mixing due to their low solubility, and pressurized flow reactors can increase this solubility[110]. Another key advantage is the easy integration of analytical devices to real-time monitoring in situ the reaction. Additionally, the continuous removal of product and substrate in flow reduces enzyme inhibition, improving the reaction rate of the enzyme[111]. Finally, continuous flow systems can also facilitate the performance of enzymatic and chemical cascade reactions by combining more than one reactor in series[106, 112, 113].

Flow reactors are normally miniaturized in a laboratory scale to utilize devices constituted by channels or tubes with different diameters from μm (microreactors) to mm (mesoreactors). Microreactors are characterized by a laminar flow and they are more effective in heat/mass transfer and temperature control, but mixing is limited by diffusion, while channel obstruction can easily occur [114, 115](**Figure 1.12**). Mesoreactors can present a turbulent flow when they operate at high flow rates, and they usually overcome issues related with mixing efficiency, that is why this kind of reactors is more extendedly used[116, 117]. Depending on how the enzyme immobilization is carried out, reactors can be classified in two types: wall-coated reactors (WCR), in which the enzyme is directly immobilized on the reactor's walls or on a membrane[118, 119]; and packed-bed reactors (PBR), in which the supported-enzyme particles are packed in a column[120]. WCR are often applied for microfluidic systems where solid carriers could cause obstructions, while PBR are more popular for any mesoreactor design.
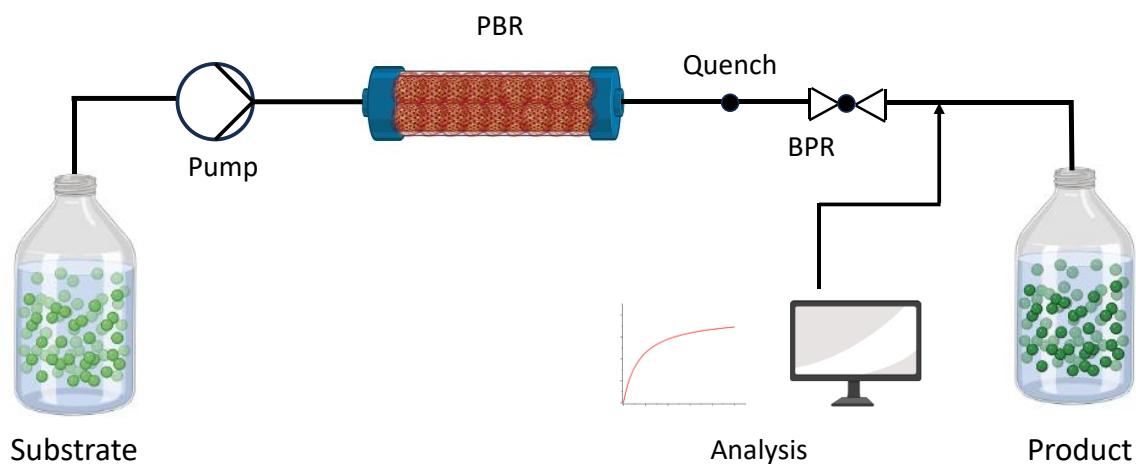
Figure 1.12: Classical Continuous Flow System (CFS) composed of the substrate delivery pump, the reactor, a quenching system, a back pressure regulator (BPR), and in-line collection, analysis and purification systems.

1.9.3. Production of omega hydroxy acids

Manufacturing of ω-hydroxyacids (ω-HA) exhibits a multitude of applications in the chemical industry since they are used in the production of several commodities such as resins, plasticizers, and lubricants [121, 122]. In the polymer industry, ω-HAs show high potential as precursors for the next generation of biodegradable polyesters (i.e., biomedical applications) [123]. Long-chain ω-HA are naturally occurring in cutin, a biopolyester that forms the plant cuticle [124]. However, medium and short-chain ω-HA are mainly accessed through chemical synthetic methods that require protected substrates and expensive metal catalysts, limiting the process sustainability [125-130](**Figure 1.13.A**). In a more environmentally friendly approach, engineered microbes have been exploited to efficiently synthesize medium and short-chain ω-HA from renewable organic acids [125-128]and 5-hydroxymethylfurfural [131], but also from fossil cycloalkanes [132, 133]and cyclohexanol [134](**Figure 1.13.B**). As an alternative, a 4-enzyme cell-free system has been assembled in solution to sequentially perform hydration, oxidation, Baeyer-Villiger oxidation, and hydrolysis steps that synthesize medium-chain ω-HAs from unsaturated fatty acids [135](**Figure 1.13.C**).
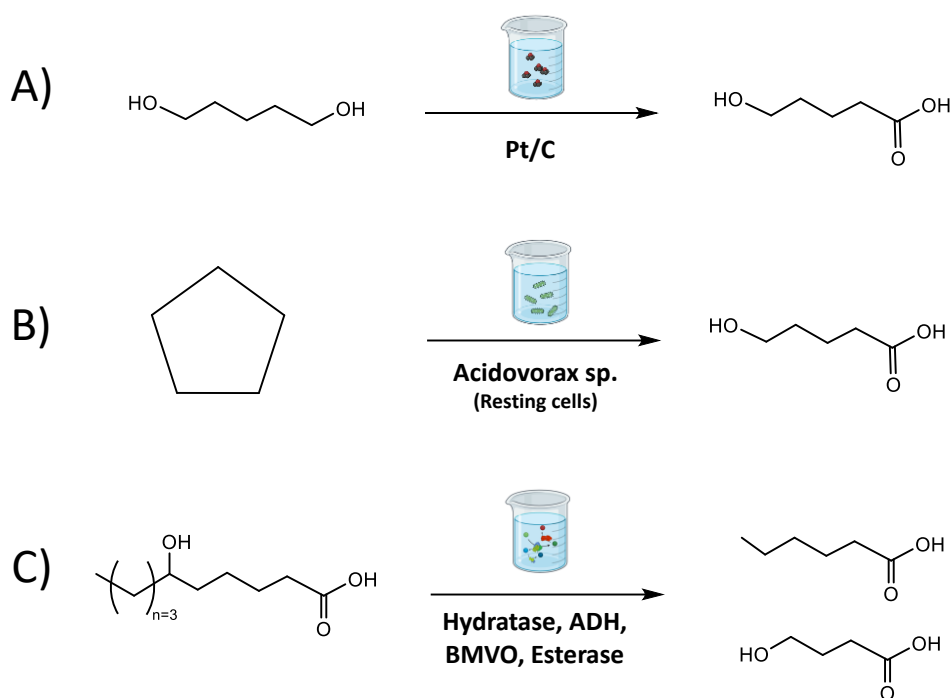
Figure 1.13: Different catalytic approaches for the synthesis of ω-HA.

Unfortunately, the atom economy of this process is rather low as the starting long-chain fatty acids are chopped down, yielding a mixture of the corresponding medium-chain ω-HAs and monocarboxylic acids. Besides the lack of product purity (ω-HAs are mixed with monocarboxylic acids), such a route cannot yield short-chain ω-HAs (≤6 carbon atoms). Hence, the cell-free biosynthesis of short-chain ω-HAs is an unmet need despite the large enzyme toolbox nowadays existing. Some successful cascades employed oxidoreductases (monooxygenases and dehydrogenases) to biosynthesize lactones (ω-HA precursor of ω-HA) from short-chain cyclic ketones[136-138] and cycloalkanes[139] using nicotinamide adenine dinucleotide phosphate (NADPH) as a cofactor.

Oxidation reactions have been employed as one of the most useful reactions in chemical manufacturing to produce aldehydes as building blocks for the synthesis of more complex molecules such as carboxylic acids and aminoalcohols[140, 141]. However, the most of the chemical procedures' present disadvantages such as poor selectivity and low sustainability. The biocatalyst driven oxidations allow performing the reactions under mild conditions and more importantly avoid the use of tedious protection groups due to the exquisite enzyme selectivity[142]. Alcohol dehydrogenases (ADHs; EC 1.1.1.1) are widely used for the oxidation of alcohols in combination with redox nicotinamide cofactors (NAD(P)+) as hydride acceptors[143]. Within this enzyme family, ADH from *Bacillus* (*Geobacillus*) *stearothermophilus* (ADH1) have been successfully exploited for the selective and versatile oxidation of 1,ω-diols [144]. In fact, this enzyme has been coupled to transaminases to sequentially transform 1,ω-

diols into aminoalcohols[140, 145]. ADH1 catalyzes the hydride transfer from one hydroxyl group of the substrate to NAD$^+$ through a compulsory ordered mechanism similar to other alcohol dehydrogenases[146]. For this reason, ADH1 requires an in situ recycling of NAD$^+$ when exploited in applied biocatalysis (**Figure 1.14.A**). Several enzymatic and chemoenzymatic recycling systems have been proposed for this type of biotransformations using laccases[147], NADH oxidases[148] and organocatalysts[149].
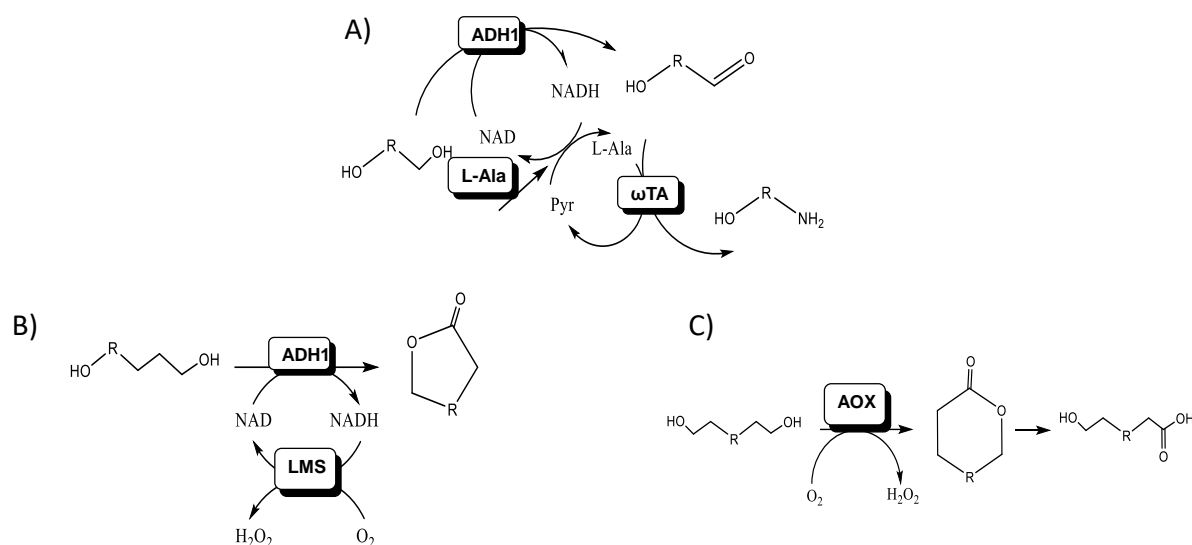
Figure 1.14: Different approaches for the synthesis of omega-hydroxy acids.

(2,2,6,6-Tetramethylpiperidin-1-yl)oxyl (TEMPO)-assisted laccase reaction has also proven useful for this biotransformation[150] (**Figure 1.14.B**). Recently, a similar double consecutive oxidation of aliphatic and aromatic diols elegantly yields ω-HA in a cofactor-free system using an engineered alcohol oxidase from Phanero-chaete chrysosporium (PcAOX*)[151]. However, the main limitation of those cascades is the use of the same enzyme to catalyze the two oxidation steps, being the lactol oxidation the rate-limiting one (**Figure 1.14.C**).

Due to the substrate of the cascade, selectivity is mandatory when the regioselective oxidation of only one primary hydroxyl group of the 1,ω-diols needs to be oxidized to its corresponding ω-hydroxy aldehydes. Several different chemical approaches (i.e., organometallics) are well known to carry out the oxidation of primary alcohols, but they lack the demanded selectivity and generate undesired overoxidized products, making the ADH2 the best candidate for the first step reaction.

1.9.4. Implementation of ADHs in industry

One of the major limitations of using isolated ADHs at the industrial level is their low stability under process operation conditions. Therefore, the industrial application of free

dehydrogenases faces several drawbacks in terms of operational stability and long-term use[31]. To solve these problems, enzyme immobilization allows the generation of robust heterogeneous biocatalysts that are easily separated from the reaction products, can increase the enzyme volumetric activity (high protein loads), can be readily recycled for several consecutive batch cycles and are easily integrated inflow reactors for continuous production of the target product[152]. When the immobilization protocol is well designed both catalytic efficiency and stability can be enhanced[153]. The selection of the carrier material is crucial to achieve highly robust and efficient heterogeneous biocatalysts[154]. Currently new immobilization trends based on self-assembled inorganic chassis have also proven their usefulness as protein carriers[155, 156]. Besides the carrier properties, the enzyme orientation upon binding must also be considered when designing an immobilization protocol that pursues maximizing the performance of the resulting heterogenous biocatalysts[157]. Enzymes can be immobilized on carriers through several strategies such as physical absorption, hydrophobic interactions and electrostatic forces[158]. However, these strategies fail to control the orientation of the enzyme in the carrier. Hence, oriented immobilization is gaining momentum in applied biocatalysis as endorses the most recent process developments, involving dehydrogenases. Immobilization of His-tagged enzymes is one of the most preferred strategies to control the enzyme orientation due to its versatility to purify and immobilize recombinantly expressed enzymes on a great variety of carries and in one-pot[159, 160]. Paradisi's and Flitch's groups are exploiting His-tagged enzymes to control their orientation upon immobilization on porous carriers functionalized with metal-complexes[154, 161]. These immobilized systems enable to carry out telescoped synthetic schemes in flow. One of the limitations of His-tag driven immobilization is the reversibility of the attachment between the enzyme and the carriers. Such issue may be overcome by using heterofunctional carriers that, besides the metal-complex, are also functionalized with either aldehydes or epoxides that ultimately establish irreversible bonds with the site-directed immobilized enzymes[157, 162]. Cobalt-chelates and epoxides have been exploited to fabricate highly robust biocatalysts that have been applied for large-scale biotransformations and flow-biocatalysis[154, 163]. As alternative to carriers functionalized with cobalt-chelates, a new generation of commercially available carriers based on porous glass functionalized with Fe^{3+}-catechol are gaining momentum in applied biocatalysis[67]. Although a wide range of enzymes have been successfully immobilized on solid carriers to enhance their functional properties, structural characterizations of the immobilized enzymes are also demanded to understand the structural changes occurred upon the immobilization and further optimize the fabrication of heterogeneous biocatalysts.

Furthermore, other drawbacks linked to the employment of enzymes as catalysts are the reusability of the biocatalysts, decreasing its final productivity, and the need for downstream processing. Additionally, enzymes are natural designed to act in cellular context, thus, their performance may be negatively affected for several reasons such as: loss of spatial organization hampering the catalytic coupling between different active sites, loss of activity and low solubility and stability. The immobilization of enzymes on solid surfaces provides a good strategy to assess these challenges.

CHAPTER 2: OBJECTIVES

To sum up the introduction, the employment of enzymes offers many advantages for chemical synthesis in industry. Multi enzyme cascades can carry out complex processes in one-pot. To scale-up the process at industrial levels, enzyme immobilization arises as an excellent strategy. The study of the effect of the immobilization is mandatory to find the suitable chemistry of immobilization. Additionally, this design is more complex in the case of immobilize multi enzyme system. Finally, the optimization of cascade reaction when the multi enzyme is in solution and immobilized is crucial to achieve high production levels.

Heterogenous biocatalysis is an optimal selection for the application of enzyme in chemical cascades. Taking advantage of the new brand of biochemical possibilities provided by computational machinery, the immobilization confers stability and reusability to enzymatic cascade. The design of specific heterofunctional carriers allows to optimize the yield of the biocatalyst by selecting the most suitable immobilization protocol for each enzyme. Additionally, the control of the spatial distribution may improve cascade synergy by reducing mass transfer limitations among catalysts. All these approaches path the way to assemble sophisticated and specific biocatalysts to meet industrial demands under different scenarios (**Figure 2.1**). Firstly, the selection and engineering of the enzymes and the orquestration of the cascade is carried out. Secondly, it is designed the heterogenous biocatalyst by the selection of the material and the chemistry of the immobilization. Thirdly, different spatial distributions and configurations are tested to optimize the biocatalyst. Finally, the process is intensified to optimize the desired synthesis in industrial demands.
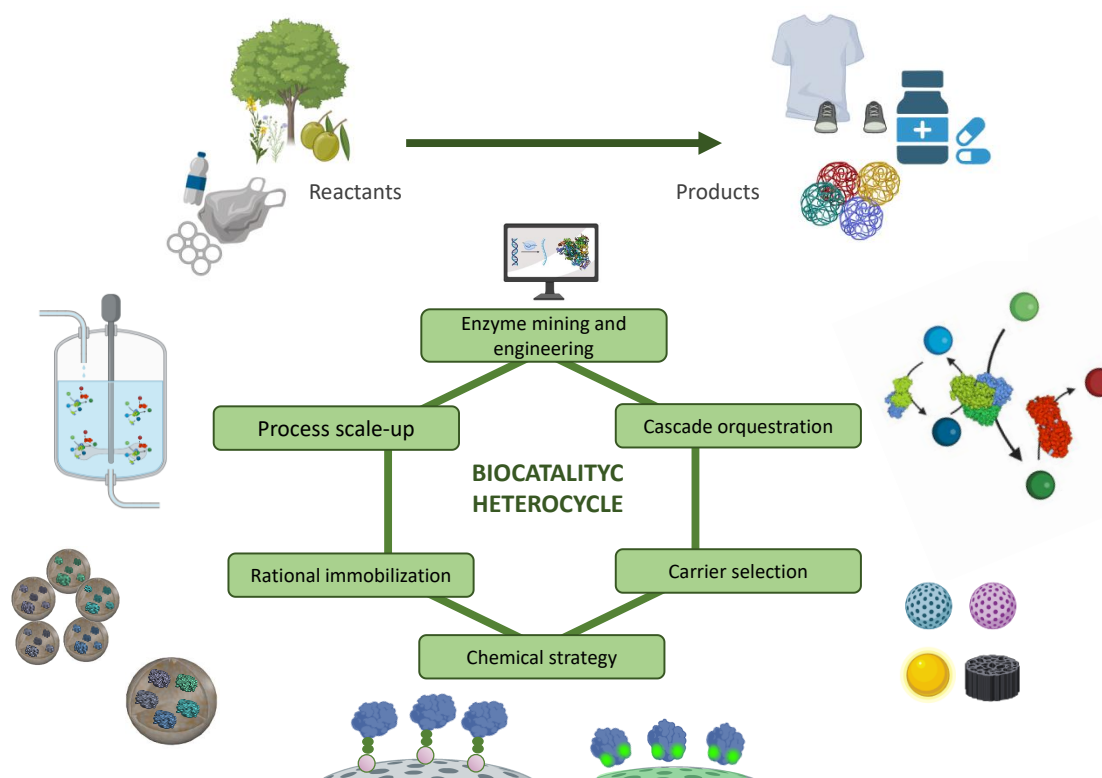
Figure 2.1: Scheme of biocatalytic heterocycle.

Overall, this thesis faces a holistic approach to improve the assembly of multi enzyme heterogenous biocatalysts by the path of the "biocatalytic heterocycle" through four different objectives:

- Development and optimization of a multi enzymatic system in solution for the production of ω-hydroxy acids.

- Methodology study for assembling heterogenous biocatalysts through the immobilization of the alcohol dehydrogenase from *Bacillus stearothermophilus* on different carriers.

- Development of a heterofunctional carrier to immobilize a multi-enzyme system, selecting the best chemical strategy for all enzymes.

- Study of the spatial distribution and post-immobilization processes for the optimization of heterogenous multi enzyme biocatalyst in batch and flow processes.

CHAPTER 3:

1.1.   Introduction

The application of multi-enzyme cascades for the synthesis of biopolymers presents interesting perspectives in the synthesis of short and medium ω-HA. As described before, the assembling of an efficient artificial cascade requires of the activity orchestration of the cell-free enzyme system. Inspired by the microbial non-phosphorylative oxidative pathway for pentose degradation[137], we envision an elegant yet unexplored route to directly access short-chain ω-HAs through the concurrent oxidative lactonization and lactone hydrolysis catalyzed by oxidoreductases and lactonases[164], respectively (**Scheme 3.1**).
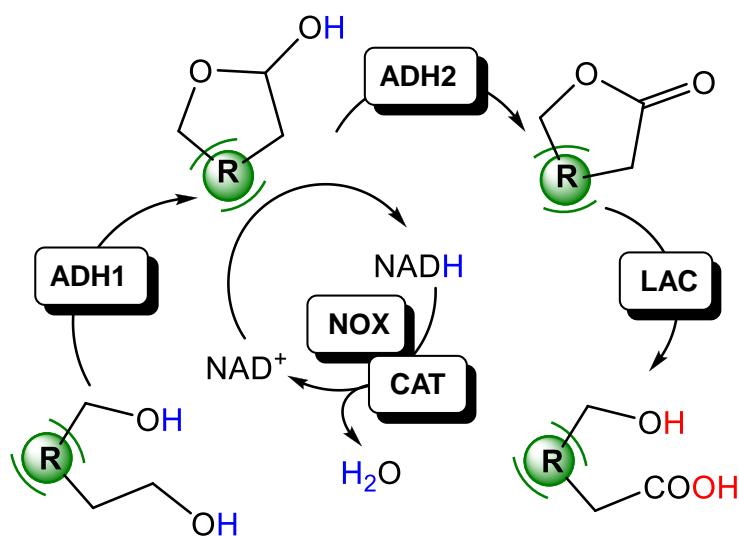
Scheme 3.1: Envision cascade to produce ω-HA.

The route is endorsed by the success of the already proven biosynthesis of lactones from short-chain cyclic ketones[135, 136] and cycloalkanes[134] using nicotinamide adenine dinucleotide phosphate (NADPH)-dependent cell-free multi-enzyme systems based on monooxygenases and dehydrogenases. Previous work showed the alcohol dehydrogenase equine liver (ADH2) as perfect candidate for the double oxidation of aliphatic diols into lactones employing a laccase mediator system as cofactor recycling[143]. Hence, new perspective to speed-up the reaction tests the employment of two alcohol dehydrogenases (EC 1.1.1.1; from equine liver; ADH2 (a dimeric enzyme with a isoelectric point of 5.4, already probed in lactone formation[143]) and *Bacillus stearothermophilus*-ADH1 with a tetrameric structure and probed in the synthesis of aminoalcohols[140]) and an alcohol oxidase from *Phanerochaete chrysosporium* (EC 1.1.3.13; 5.4 isoelectric point; already probed in ω-HA synthesis reactions[150]) for the double oxidation of diols combined with a Lactonase from *Sulfolobus Islandicus* (LAC; EC 3.1.1 with a isoelectric point of 4.84) for the hydrolysis of the lactone (widely employed in kinetic resolution reactions of racemic lactones[165]. As regeneration cofactor system is employed the combination of a dimeric enzyme with an isoelectric point of 4.8 NADH oxidase from *Thermus thermophilus* (NOX; EC 1.6.3.3) and a tetrameric enzyme with an isoelectric point of 5.4 catalase from Bovine liver (CAT; EC 1.11.1.6), both enzymes has been widely employed to regenerate NAD+ in oxidation cascades[140].

1.2. Experimental Section

1.2.1. Materials

Enzymes as alcohol dehydrogenase equine (ADH2) recombinant expressed in E. coli 0.5 U mg^{-1}, catalase from bovine liver (CAT) lyophilized powder 2000–5000U mg^{-1} of protein and Horse radish peroxidase (HRP)~150U·mg^{-1}; substrates1–7a, reaction products 1d, 4d, 5d, reagents as a flavin-adenine-dinucleotide sodium salt (FAD$^+$), sodium phosphate dibasic dihydrate, ABTS, *p*-nitrophenol, were acquired from Sigma-Aldrich (St.Louis,IL). Nicotinamide-adenine-dinucleotide sodium (NAD$^+$) was purchased from GERBU Biotechnik GmbH (Wieblingen, Germany). Lactones 2c and 7c, ω-HA as 7d, 5-oxopentanoicacid (2e), and 6-oxohexanoicacid (3e) were obtained from Enamine building blocks (Riga, Latvia). ω-Has 2d and 3d were purchased from Cymit (Barcelona, Spain). 6BCL agarose beads activated with glyoxyl groups (AG-G) were prepared as described elsewhere[166]. Cobalt-activated agarose microbeads 4BCL (AG-Co^{2+}) (particle size; 50 150 μm, pore size; 112 nm (mean value) and 15 μmol of Co^{2+} per g carrier) were purchased from ABT technologies (Madrid, Spain). Precision plus protein standards, microBio-spin chromatographic columns and Bradford reagent were acquired from BIORAD. All other reagents and solvents were analytical grade or superior.

1.2.2. Enzyme production and purification

Alcohol dehydrogenase from *Bacillus stearothermophilus*, lactonases from *Sulfolobus islandicus* (LAC), from *Rhodococcus erythropolis* (ReLAC), NADH oxidase from *Thermus thermophilus* (NOX) were over expressed in Escherichia coli BL21 cells, whereas alcohol oxidase from *Phanerochaete chrysosporium* F101S variant (PcAOX*) was overexpressed in Artic Express (DE3) E. coli cells.

1.2.3. Expression

A total of 1 mL of an overnight culture of E. coli transformed with the respective plasmids was inoculated in a 50 mL of Luria-Bertani (LB) broth containing kanamycin (final concentration of 30 μg mL^{-1}) for ADH2, LAC, ReLAC and ampicillin (100μg mL^{-1}) for NOX or a mixture of kanamycin and gentamycin (30 and 20 μg mL^{-1}, respectively) for PcAOX*. The culture was incubated at 37°C (in the case of ADH2, LAC, ReLAC, RePON1LAC and NOX) or 30°C (in the case of PcAOX*) at 250 rpm until the OD600 nm reached 0.6. At that point, the culture was induced with 1 mM of isopropylβ-d-1-thiogalactorpyranoside (IPTG) in the case of ADH2, NOX and PcAOX*, whereas for LAC, ReLAC and RePON1-LAC the induction IPTG concentrations were 1μM, 1 mM and 1μM, respectively. Cells were grown at 37°C for 3 h (in the case of ADH2 and NOX) or at 21°C (in the case of LAC, ReLAC and RePON1LAC) or at 13°C (in the case of PcAOX*) overnight and then harvested by centrifugation at 1290g during 30 min at 4°C.

1.2.4. Purification

All recombinantly expressed enzymes but NOX were purified by affinity as follows: the resulting pellet was resuspended in one-tenth of its original volume of 25 mM sodium phosphate buffer solution (pH=7) for ADH2, LAC, ReLAC and RePON1LAC and 50 mM sodium phosphate buffer pH 7.8 supplemented with 0.150 M NaCl, 0.1 M KCl, 20 mM imidazole, 0.1 mM FAD^+ for PcAOX*. Cells were broken by sonication at an amplitude of 40% with alternating cycles of 3s on/5s off during 20 min at 4°C (SonopulsHD4100, Bandelin). The cell lysate was centrifuged at 10528g for 30 min at 4°C. The supernatant containing the enzyme was collected and passed through a cobalt-activated agarose resin equilibrated with a binding buffer. The column was incubated for 1 h at 4°C to promote the protein binding to the column. Afterward, the column was washed three times with binding buffer before the protein elution with elution buffer (binding buffer supplemented with 300 mM imidazole). The eluted protein was gel-filtered by using PD-10 columns (GEhealthcare) to remove the imidazole and exchange the enzyme buffer to 25 mM sodium phosphate pH 7. NOX was purified as follows: the cells were resuspended in one-tenth of their original volume of 10 mM sodium phosphate buffer solution pH 7 and broken by sonication (SonopulsHD4100, Bandelin) at amplitude of 40% alternating cycles of 3s on/5s off during 20min at 4°C. The suspension was centrifuged at 10528g for 30min at 4°C. The supernatant containing the enzyme was incubated at 70°C for 1h to remove all mesophilic proteins, the thermophilic one remaining in the super-natant that is separated by centrifugation at 10528g for 30min at 4°C. The supernatant was passed through polyethyleneimine-activated agarose (AG-PEI) where this enzyme is not attached[167]. SDS-PAGE and Bradford assays were carried out after each production batch to determine the purity, concentration, and specific activity of the enzymes (**Figure 3.1**).
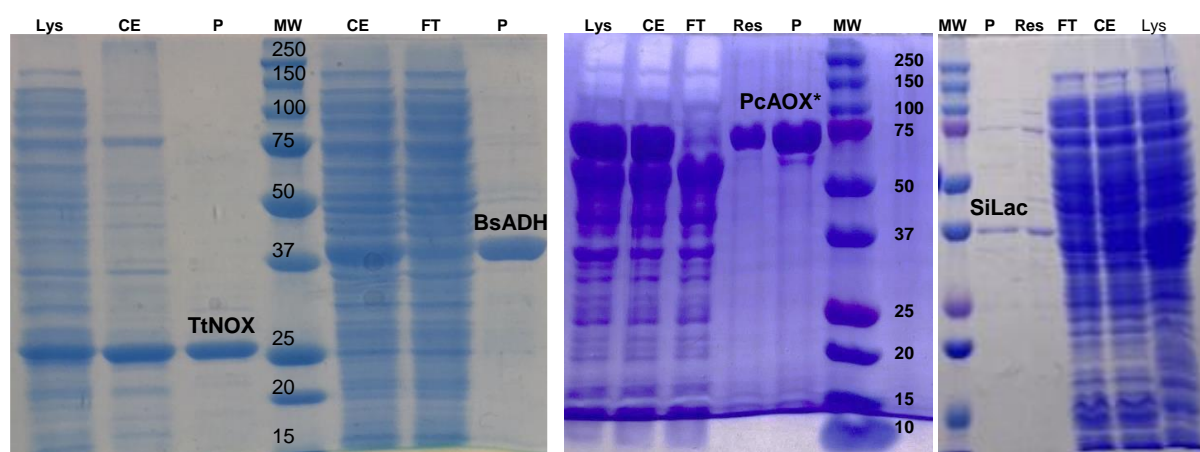
Figure 3.1: SDS-PAGEs of the enzyme purification. Lanes: MW (Molecular weight markers, BioRad Precision Plus Protein All Blue Standard). Lys (lysate), CE (soluble crude extract), FT (flow through of the purification), Res (washed resin after purification) and P (pure protein).

In the case of the commercial preparation of ADH1, we determined the enzyme concentration with a calibration curve of BSA in an SDS-PAGE gel (**Figure 3.1.B**). According to this calibration curve, the ADH1 commercial extract has 0.37 ± 0.014 mg of enzyme perm g of crude powder.
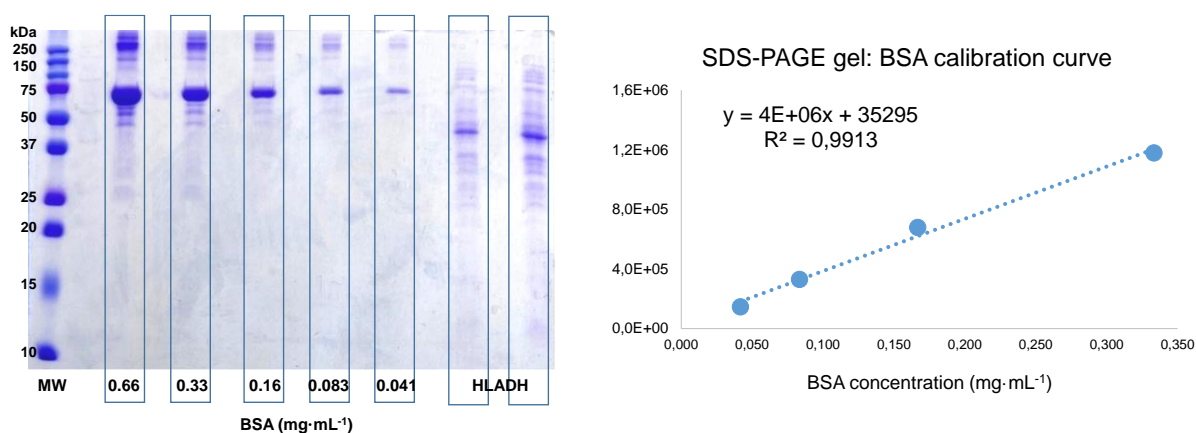
Figure 3.2: SDS-PAGE gel (left) containing different concentrations of BSA and the commercial crude ADH1. The BSA calibration curve obtained after the imaging analysis of the SDS-PAGE-gel (right).

1.2.5. Enzyme activity measurements

Enzyme activities were spectrophotometrically measured in transparent 96-well microplates, employing a Microplate Reader Epoch 2, BioTek with the software Gen5.

1.2.5.1. ADH activity

200 µL of a reaction mixture containing the substrate (diols or lactol) and the cofactor NAD^+ (at the specified concentrations) in sodium phosphate buffer at pH 8 were incubated with 5 µL of enzymatic solution or suspension (properly diluted) at 30°C. The increase in the absorbance at 340 nm due to the NADH formation was recorded. One unit of activity was defined as the amount of enzyme that was required to reduce 1 µmol of NAD^+ to NADH per minute at the assay conditions (**Figure 3.3**).
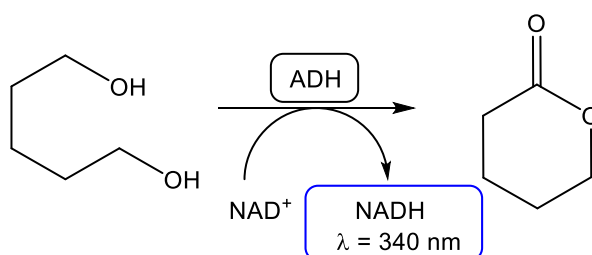
Figure 3.3: Colorimetric assays for biocatalysts kinetic characterization of the oxidative lactonization, recording increment in the absorbance at 340 nm. Reaction conditions: 0.2 mM NADH, 0.15 mM FAD^+ in 100 mM sodium phosphate buffer pH 8 at 30°C.

1.2.5.2. Alcohol oxidase activity

200 µL of a reaction mixture containing the substrate (2a, at the specified concentration), HRP 10 µg mL^{-1}, ABTS 1 mg mL^{-1} In sodium phosphate buffer at pH 8 were incubated with 5 µL of

enzymatic solution or suspension (properly diluted) at 30°C. The increase in the absorbance at 414 nm due to the ABTS oxidation triggered by the H_2O_2 formed by the oxidase, was recorded. One unit of activity was defined as the amount of enzyme that was required to produce 1 µmol hydrogen peroxide per minute at the assay conditions.

1.2.5.3.   Lactonase activity

Lactonase activity was indirectly monitored by the decrease in the pH triggered by the ω-HA formation from its corresponding lactone hydrolysis. Briefly, 200 µL of a reaction mixture containing the 1 mM of δ-valerolactone, 0.1% acetonitrile, 0.25 mM p-nitrophenol in 2.5 mM sodium phosphate buffer at pH7.0 were incubated with 5 µL of enzymatic solution or suspension (properly diluted) at 30°C. The decrease in the absorbance of *p*-nitrophenol (pH indicator) at 410 nm was recorded. One unit of activity was defined as the amount of enzyme that was required to produce 1 µmol ω-hydroxy acid per minute at the assay conditions.

1.2.5.4.   Catalase activity

The activity was determined by recording the decrease in the absorbance at 240 nm of 200 mL of a reaction mixture containing 35 mM hydrogen peroxide in 100 mM sodium phosphate pH8 at 30°C. The reaction was initiated by adding 5 µL of the enzymatic solution or suspension to the reaction mixture. One unit of CAT activity was defined as the amount of enzyme required for the disproportionation of 1 µmol of hydrogen peroxide per minute at the assay conditions.

1.2.5.5.   NOX activity

200 µL of a reaction mixture containing 0.2 mM NADH and 150 µM FAD^+ in 50 mM sodium phosphate buffer pH 8 at 30°C were incubated with 5 µL of enzymatic solution or suspension (properly diluted) at 30°C. The decrease in the absorbance at 340 nm was monitored. One unit of activity was defined as the amount of enzyme that was required to oxidize 1 µmol of NADH per minute at the assay conditions (**Figure 3.4**).
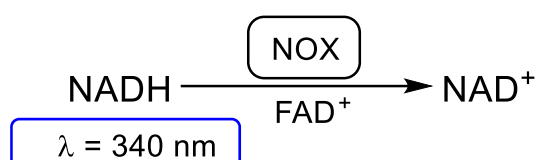
Figure 3.4: Colorimetric assays for biocatalysts kinetic characterization of the cofactor regeneration, recording decrease in the absorbance at 340 nm. Reaction conditions: 0.2 mM NADH, 0.15 mM FAD^+ in 100 mM sodium phosphate buffer pH 8 at 30°C.

1.2.6.   Synthesis of ω-HA

Either soluble or immobilized enzymes were placed inside a capped plastic tube (2 or 5 mL) containing a reaction mixture (0.5 or 1.5 mL, as indicated) consisted in either 20 or 100 mM of substrate (1a, 2a, 3a, 4a, 5a, 6a or 7a), 1 mM NAD^+, 0.15 mM FAD^+ in 200 mM sodium phosphate buffer pH 8. The cap of the tube was punched with an open needle to allow atmospheric oxygen supplementation. Reactions were incubated at 30°C at 250 rpm inside an orbital incubator. When specified, the pH was manually adjusted by the addition of 1 M NaOH. The reaction course was monitored by withdrawing samples at periodic intervals which were analyzed by chromatographic methods. The concentration of substrate, intermediates, and products were determined by GC analysis at different time points. Particularly, the lactone and ω-HA concentrations were calculated with a double analysis as described in **Figure 3.5**.
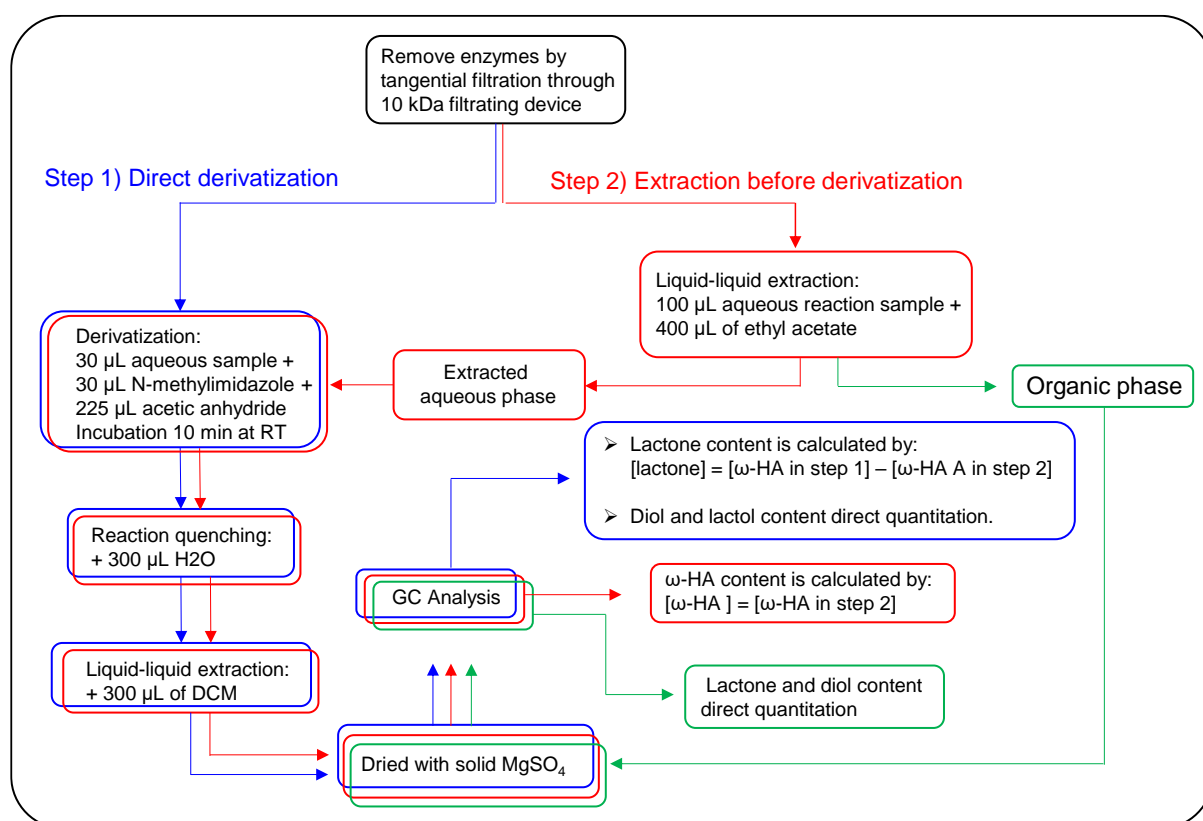
Figure 3.5: Sample treatment before GC and GC-MS analysis for content determination.

We estimated the 6d yield qualitatively by NMR analysis calculating the ratio between the integration values of the doublets relative to CH3 of 6d (3.00) at 0.90 ppm and CH3 of the unknown product (1.13) that lies between 0.95–1.00 ppm (**Annex 3.1**). When needed, the products were isolated for NMR analysis by sequentially flushing the samples through tangential ultrafiltration units (Amicon Ultra centrifugal filters, 10 kDa) to remove the enzymes and then through a column of agarose microbeads functionalized with polyethyleneimine (60 kDa) to remove the traces of phosphorylated cofactors (NAD^+ and FAD^+) via the ionic exchange.

1.2.7. Analytical measurements

1.2.7.1. Gas chromatography (GC)

Prior to GC analysis reaction samples were derivatized as described elsewhere[168]. During sample derivatization, lactones are hydrolyzed to their corresponding ω-HAs, therefore before sample derivatization, lactones must be removed by liquid-liquid extraction with ethyl acetate as follows: 100 µL of aqueous reaction sample were mixed with 400 µL of ethyl acetate and vortexed for 20 s and centrifuged 1 min at 1000 g. After extraction, the organic phase was stored for further GC analysis, and the aqueous phase was further derivatized. The lactone was determined in the organic phase, while the ω-HA was quantified in the aqueous phase. We analyzed every reaction sample both with and without lactone extraction. Diols and lactols were quantified by direct sample derivatization without lactone extraction. Samples were derivatized by placing 30 µL of the aqueous reaction in a 1.5 mL Eppendorf tube, followed by the addition of 30 µL of N-methylimidazole and 225 µL of acetic anhydride and incubated by 10min at room temperature. Afterwards, 300 µL of distilled water were added to the reaction mix and allowed to cool down. Later, liquid-liquid extraction of acetylated compounds was done by the addition of 300 µL of dichloromethane containing 2 mM eicosane as internal standard discarding the aqueous phase. 30–50 mg of anhydrous $MgSO_4$ were added to dry samples before GC analysis. Gas chromatography analyses were carried out in an Agilent 8890 GC system chromatograph afterward using a J&W HP-5 GC column (30 m × 0.32 mm × 0.25 µm), helium as the carrier gas, and equipped with a flame ionization detector (FID). Injector at 280°C, FID at 300°C. Separation of acetylated derivatives and extracted com- pounds in ethyl acetate were done by the following temperature program: the initial temperature at 60°C, maintained 2min, ramp to 160°C at a rate of 10°Cmin^{-1}, ramp 2 to 240°C at a rate of 20°Cmin^{-1} and finally maintained 4min. The samples were additionally analyzed using an Agilent 7820 A Series Gas Chromatograph a J&W HP-5 GC column (30 m × 0.25 mm × 0.25 µm), coupled to an Agilent 5975 C inert XL Mass Spectrometer with Electronic Impact ionization.

1.2.7.2. Chiral GC chromatography

Before chiral GC analysis, reaction samples were treated with ethyl acetate to remove residual lactones as aforementioned. Once lactones were removed aqueous samples were derivatized to obtain acetylated ω-HA as previously described. Once acetylated, samples were analyzed in an Agilent 8890 GC system chromato- graph using a chiral column (Alpha and Beta DEX^{TM} 120 Fused silica capillary column (30 m x 0.25 mm x 0.25 µm)), helium as the carrier gas, and equipped with a flame ionization detector (FID). Injector at 280°C, FID at 280°C.

1.2.7.3. High performance liquid chromatography (HPLC) analysis

Prior to HPLC analysis the reaction samples were derivatized as described elsewhere[169]. Briefly, 10 µL of aqueous sample (0.6–20 mM) were mixed with 50 µL of O-benzylhydroxylamine hydrochloride (130 mM in pyridine/methanol/water 33: 15: 2) and incubated for 5 min at 25°C. Afterwards, 500 µL of methanol were added and then centrifuged 5 min at 13450 g. HPLC analysis was conducted in an Agilent Technologies 1260 Infinity chromatograph equipped with

a Poroshell EC-C18 column (4.6mm ×100mm x 2.7μm). Samples were detected at 215nm and were eluted at 1 mL·min^{-1} flow rate employing two mobile phases; phase A composed of trifluoroacetic acid 0.1% in water, and phase B composed of trifluoroacetic acid 0.095% in 4: 1 acetonitrile: water. Elution conditions: 10% to 100% of B over 30 min. Retention times of O-benzylhydroxylamine derivatives were: 5-oxopentanoic acid (2e): 14.7 min, and 6-oxohexanoic acid (3e): 16.3 min.

1.2.7.4. *Nuclear magnetic resonance (NMR) analysis*

When specified, reaction samples were analyzed by ^{1}H NMR spectra acquired on a Bruker 500 MHz Ultra Shield spectrometer, operating at 500 MHz for ^{1}H NMR spectroscopy. Chemical shifts were reported in parts-per-million (δ, ppm) and referenced using the residual solvent peak (deuterium oxide δ=4.79 ppm). Coupling constants (J) were reported in hertz [Hz]. The multiplicity of the signals was reported as singlet (s), doublet (d), doublet of doublets of doublets of doublets (dddd), doublet of the quartet (dq), doublet of triplet (dt), triplet (t), and multiplet (m).

1.3. Results and Discussion

1.3.1. Cascade optimization

In our first attempt, we performed the synthesis of 5-hydroxypentanoic acid (2 d) combining a commercial crude extract of ADH from horse liver (ADH1) as sole dehydrogenase and the pure His-tagged lactonase from *Sulfolobus islandicus* (LAC) together with an excess of the widely used NAD$^+$ recycling system formed by a pure thermostable NADH oxidase NOX from Thermus thermophilus (NOX) and the catalase from bovine liver (CAT) (commercial crude extract)[140, 170]. We did not select the water-forming NOX, since our previous studies showed that the NOX outperforms the former one exhibiting higher operational stability[170, 171]. Furthermore, the tandem NOX/CAT stoichiometrically demands half of the oxygen for the NAD$^+$ recycling than the water-forming oxidases, a fact that positively impacts on the atom economy of the process. **Figure 3.6** shows the reaction time course of the four-enzyme system using an enzyme activity ratio of 2 : 1 : 10 : 100 (ADH1/LAC/NOX/CAT), where the lactol intermediate (2 b) is accumulated during the first 5h, and the ω-HA yield (2 d) reached 60% after 20h.
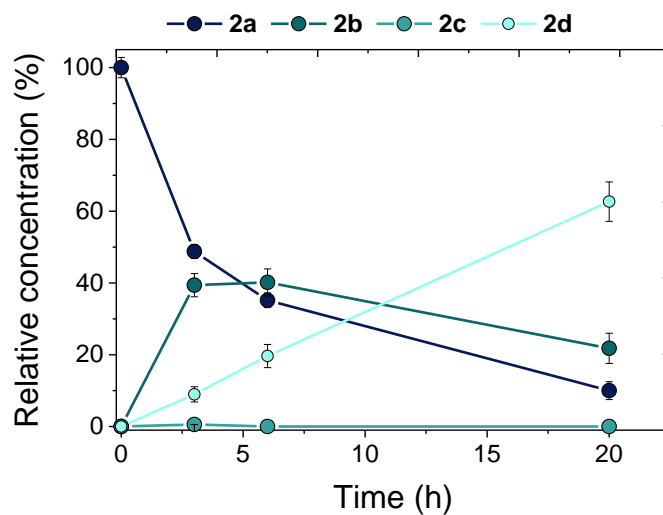
Figure 3.6: Multi-enzymatic synthesis of ω-hydroxy acids from diols. Reaction course consisting in 0.5 mL of 2a 20 mM, NAD$^+$ 1 mM, FAD$^+$ 0.15 mM in sodium phosphate buffer 100 mM pH 8 at 30°C and 250 rpm, containing ADH1 20 mU, NOX 200 mU, CATHL 2 U and Si-Lac 20 mU.

On the contrary, the lactone intermediate is negligibly accumulated as LAC hydrolyzes the lactone 2c 214 times more efficiently than the ADH1 oxidizes the lactol 2b according to the intrinsic kinetic parameters of these enzymes (**Table 3.1**).

Table 3.1: Steady state kinetic parameters of different enzymes.

Enzyme	Substrate	K_M (mM)	Vmax (Umg^{-1})	k_{cat} (s^{-1})	$k_{cat} \cdot K_M^{-1}$ (M^{-1}s^{-1})	Reaction conditions
ADH2	2a	33.8±2.34	12.5±0.35	30.2	894	1 mM NAD$^+$ in 100 mM phosphate buffer pH 8
	2b	> 2000	nd	-	-	
	NAD$^+$	0.89±0.20	1.32±11	3.2	3587	10 mM 2a in 100 mM phosphate buffer pH 8
ADH1	2a	1.29±0.75	1.99±0.04	2.6	2051	1 mM NAD$^+$ in 100 mM phosphate buffer pH 8
	2b	1536±332	0.074±0.006	0.099	0.064	
	NAD$^+$	0.61±0.08	19.24±0.76	25.5	41859	10 mM 2a in 100 mM phosphate buffer pH 8
PcAOX*	2a	171[*]±19	0.34[*]±0.01	3.3[*]	19	100 mM phosphate buffer pH 8
LAC	2c	19.1[**]±1.9	0.22[**]±0.0006	0.26[**]	13.7	0.25 mM pNP, 10% ACN in 2.5 mM phosphate buffer pH 7

*Apparent steady state kinetic parameters: activity was determined by coupling HRP assay. **Apparent steady state kinetic parameters: activity was indirectly determined by recording the decrease in the absorbance at 405 nm of *p*-nitrophenol at pH 7 due to the formation of the ω-HA. nd: not detected. PcAOX* is modified by exchanging a Serine (S) by a Phenylalanine (F).

Evaluating other lactonases, we found that LAC reaches 1.5 times higher and similar yield than the lactonases from *Rhodococcus erythropolis* (ReLAC) and Homo sapiens (RePON1), respectively, in agreement with their specific activities (**Figure 3.7 and Table 3.2**).
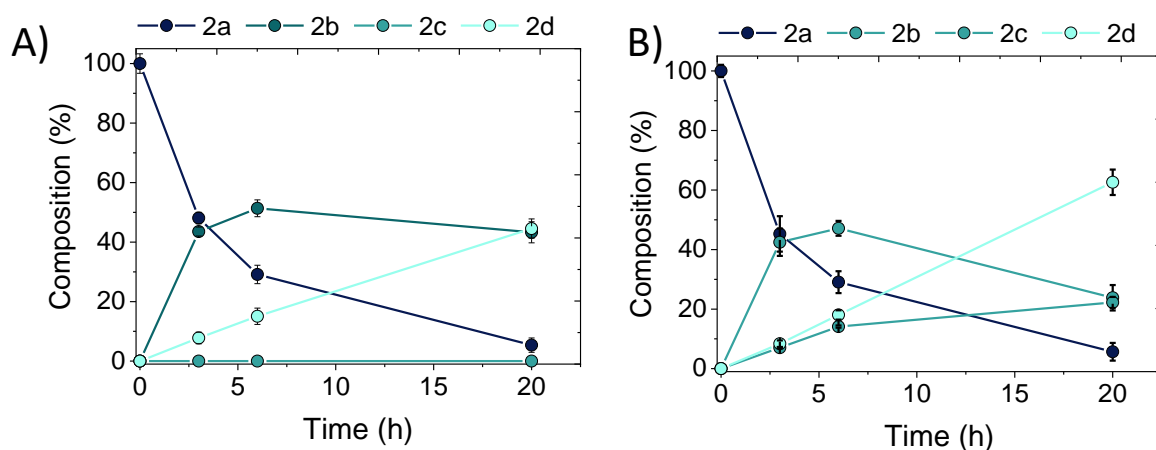
Figure 3.7: Reaction course. A) ReLac. B) RePON1Lac. Reaction mixture consisted in 0.5 mL of 1,5-pentanediol 20 mM, NAD$^+$ 0.2 mM, FAD$^+$ 0.15 mM in sodium phosphate buffer 100 mM pH 8 at 30°C and 250 rpm. Each reaction contained ADH1 20 mU, NOX 200 mU, CAT 2 U and Lactonases 20 mU.

Table 3.2: Activity of lactonases with δ-valerolactone (2d).

Lactonase	Specific activity (U·mg^{-1})
LAC	1.034 ± 0.081
ReLAC	0.058 ± 0.006
RePON1LAC	1.032 ± 0.041

Reaction mixture = δ-valerolactone (1 mM), p-nitrophenol (2.5 mM), ACN (10% v/v) in 2.5 mM sodium phosphate buffer pH 7 at 30°C.

To minimize the lactol accumulation, we incorporated an additional dehydrogenase that outperforms ADH1 for the diol conversion to dominate the first oxidation step, thus ADH1 can focus on the second and limiting lactol oxidation step. We found that the ADH from *Bacillus stearothermophilus* (ADH2) performed the first step with a catalytic constant (kcat=30.2 s^{-1} towards the diol (2a) 12-fold higher than that presented by ADH1 (**Table 3.1**), and poorly oxidized the lactol (2b) (**Figure 3.8.A**).
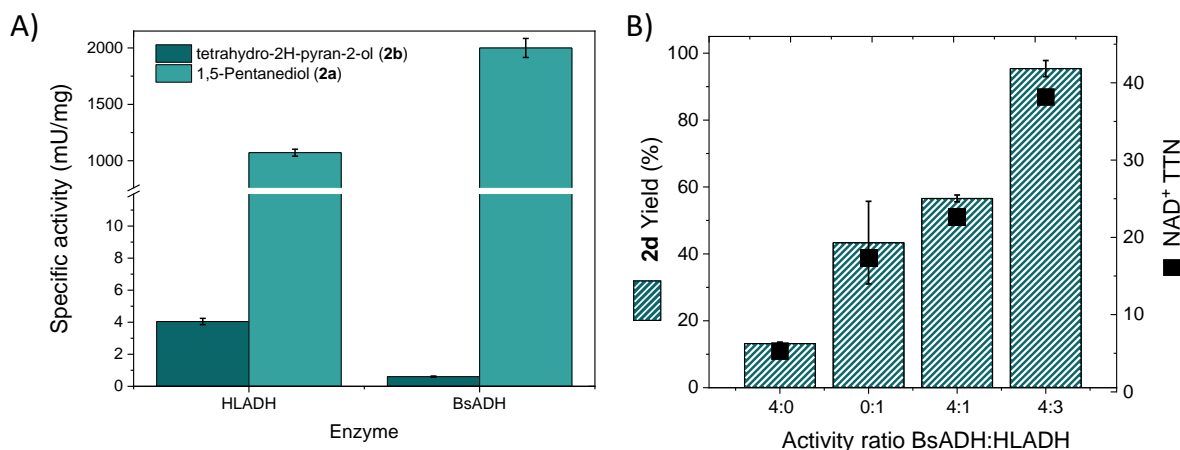
Figure 3.8: A) Activity of alcohol dehydrogenases towards different alcohols. Reaction conditions were 10 mM of substrate, 1 mM NAD$^+$ in 100 mM sodium phosphate buffer pH 8 at 30°C. B) Synthesis optimization all reactions consisted in 0.5 mL of 2a 20 mM, NAD$^+$ 1 mM, FAD$^+$ 0.15 mM in sodium phosphate buffer 100 mM pH 8 at 30°C and 250 rpm, containing one or two ADHs (where 1 equivalent corresponds to 0.33 nmol of enzyme), NOX 26 µg, CAT 46 µg and Lac 19 µg.

Moreover, ADH2 and ADH1 showed similar Michaelis-constant values (K_M = 0.6–0.9 mM) towards NAD$^+$, suggesting that both enzymes will work at their maximal rate under the substoichiometric concentration of cofactor typically used in bio-redox transformations. When different activity ratios ADH1/ADH2 were assayed, we identified such ratio as one of the key parameters to maximize ω-HA yield (**Figure 3.8.B**). In fact, when the system was conducted solely with ADH2, the ω-HA yield was extremely low (13%) despite the high conversion of the diol (86%), which gave rise to a large accumulation of lactol (70%) (**Figure 3.9**).
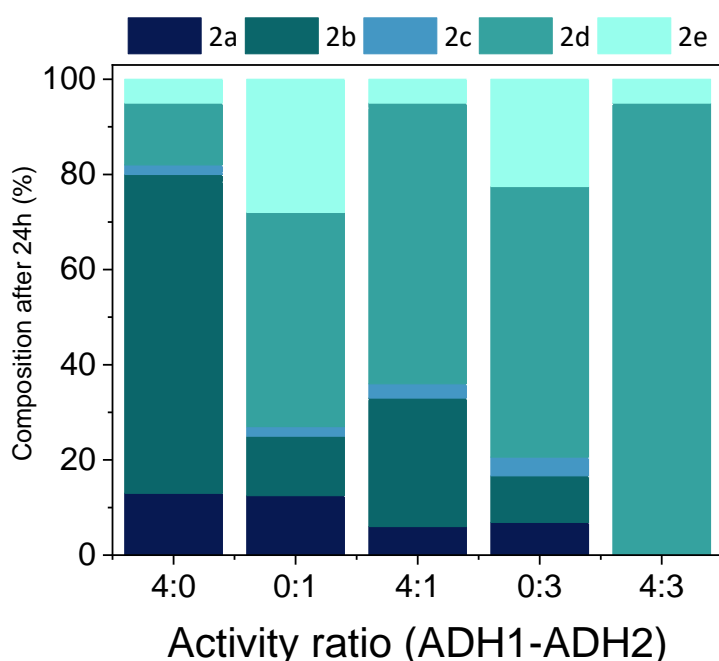
Figure 3.9: Product profile of 2d biosynthesis using different ADH1:ADH2 ratios. All reactions consisted in 0.5 mL of 20 mM 2a, 1 mM NAD$^+$, 0.15 mM FAD$^+$ in 100 mM sodium phosphate buffer pH 8 at 30°C and 250 rpm,

containing, NOX (200 mU), CAT (2 U) and LAC (20 mU) and ADH1 (40 or 120 mU) and/or ADH2 (160 mU). Values correspond to 24h of reaction.

This insight entails ADH2 as the specialist enzyme for the first oxidation within this enzyme cascade. A similar product distribution was found using the immobilized version of this enzyme towards the same substrate and under similar reaction conditions. Likewise, when the system was performed by the ADH1 as the unique ADH (even at different amounts, 40 (ratio 0:1) or 120 mU (ratio 0:3)), the transformation only reached 60% of ω-HA yield, similar to the yield achieved with the combination of the two ADHs using an activity ratio 4:1. Pleasantly, the activity ratio 4:3 (ADH2/ADH1) achieved the highest ω-HA yield (97%) with a quantitative conversion of the diol (2a), attaining a total turnover number for NAD^+ (TTN NAD^+) of 38.8 (close to the theoretical maximum of 40). Higher ADH2/ADH1 activity ratios drove to lower ω-HA yields (**Figure 3.8.B and 3.8**). The synergistic use and the activity orchestration of these two ADHs enhance the overall reaction yield due to the negligible accumulation of the lactol after 24h, demonstrating that ADH2 mainly oxidizes the diol, relegating ADH1 from its task in the first oxidation. This fact allows ADH1 to be focused exclusively on the lactol oxidation avoiding its accumulation in the reaction media and driving the cascade towards the target product. When we used the benchmark PcAOX* as the sole oxidative enzyme, we found that the cascade only reached 11% of ω-HA yield (2d) under the same conditions as the optimized cascade using ADH1 and ADH2 (**Figure 10**).
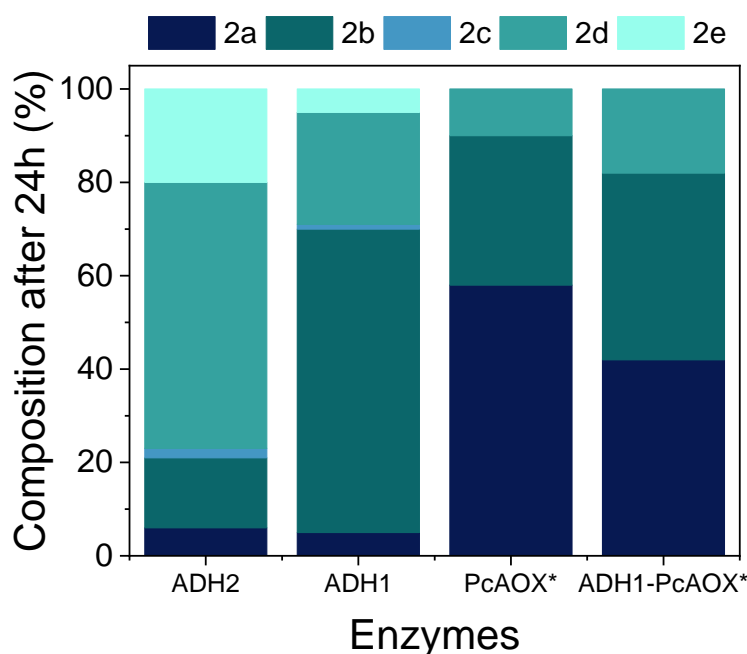
Figure 3.10: Product profile of the cell-free biosynthesis of 2d from 2a catalyzed by either ADHs or AOX enzymes. In the case of ADHs, the reaction mixture consisted in 0.5 mL of 20 mM 2a, 1 mM NAD^+, 0.15 mM FAD^+ in 100 mM sodium phosphate buffer pH 8 at 30°C and 250 rpm, containing either ADH1 (92 μg) or ADH2 (92 μg), LAC (20 mU), NOX (200 mU) and CAT (2 U). In the case of PcAOX*, the reaction mixture consisted in 0.5 mL of 20 mM

2a, in 100 mM sodium phosphate buffer pH 8 at 30°C and 250 rpm, containing PcAOX* (92 µg) and LAC (20 mU). In the case of ADH2-PcAOX*, the reaction mixture consisted in 0.5 mL of 20 mM 2a, 1 m NAD$^+$, 0.15 mM FAD$^+$ in 100 mM sodium phosphate buffer pH 8 at 30°C and 250 rpm, containing ADH2 (92 µg) and PcAOX* (92 µg), LAC (20 mU), NOX (200 mU) and CAT (2 U).

Moreover, when PcAOX* was combined with ADH2, we observed a slight increase in the ω-HA yield (17%), but still 3.4 and 5.6 times lower than the ones achieved with the sole ADH1 and the combination of ADH1 and ADH2, respectively, as oxidative enzymes. The low performance of PcAOX* as a standalone oxidative enzyme relies on its low kcat toward the starting diol (2a) compared to ADH2 (**Table 3.1**). Regarding the oxidation of the lactol intermediate (2b), PcAOX* accumulates 2 times more lactol than ADH1, (**Figure 3.10**), suggesting that neither does such oxidase outperform ADH1 in the second oxidation step.

Therefore, the synergistic use and the activity orchestration of these two ADHs enhance the overall reaction yield due to the negligible accumulation of the lactol after 24h, demonstrating that ADH2 mainly oxidizes the diol, relegating ADH1 from its task in the first oxidation. This fact allows ADH1 to be focused exclusively on the lactol oxidation avoiding its accumulation in the reaction media and driving the cascade towards the target product.

1.3.2. Substrate scope and enantioselectivity of the multi-enzyme system

Once we identified the best enzymes and their optimal stoichiometry, we applied the five-enzyme system for the synthesis of chemically diverse short-chain ω-HAs starting from a battery of seven linear and branched C4-C6 ω-diols (1-7a). The multi-enzyme system successfully consumed more than 99% of all these diols but diethylene glycol (4a) and 1,4-butyne diol (5a) (**Table 3.3**).

Table 3.3: Cascade multi-enzymatic synthesis of ω-hydroxy acids from diols

Substrate	Product	Diol Conversion (%)	TOF oxidation step[a] (h⁻¹)	ω-hydroxy acid Yield (%)	TOF hydrolysis step [b] (h⁻¹)
1a	1d	100	0.50	40	0.62
2a	2d	100	0.50	97	1.53
3a	3d	100	0.50	0	nd*
4a	4d	0	0	0	0
5a	5d	21	0.11	0	0
6a	6d	100	0.50	70	1.10
7a	7d	100	0.50	92	1.44

[a]TOFs of the oxidation step were calculated as the µmol of oxidized diol / µmol of ADHs after 24 hours. [b]TOFs of the hydrolysis step were calculated as the µmol of produced ω-HA / µmol of LAC after 24 hours. nd* The ω-HA was overoxidized to form the corresponding aldehyde, therefore after 24 hours 3d was not detected. All reactions consisted in 0.5 mL of 20 mM substrate, 1 mM NAD$^+$, 0.15 mM FAD$^+$ in100 mM sodium phosphate buffer pH 8 at 30°C and 250 rpm, containing ADH2 (160 mU), ADH1 (120 mU), NOX (200 mU), CAT (2 U) and LAC (20 mU).

These results are aligned with the measured spectrophotometric activities of both ADHs towards these diols, where 4a and 5a were the least preferred ones (**Figure 3.11**).
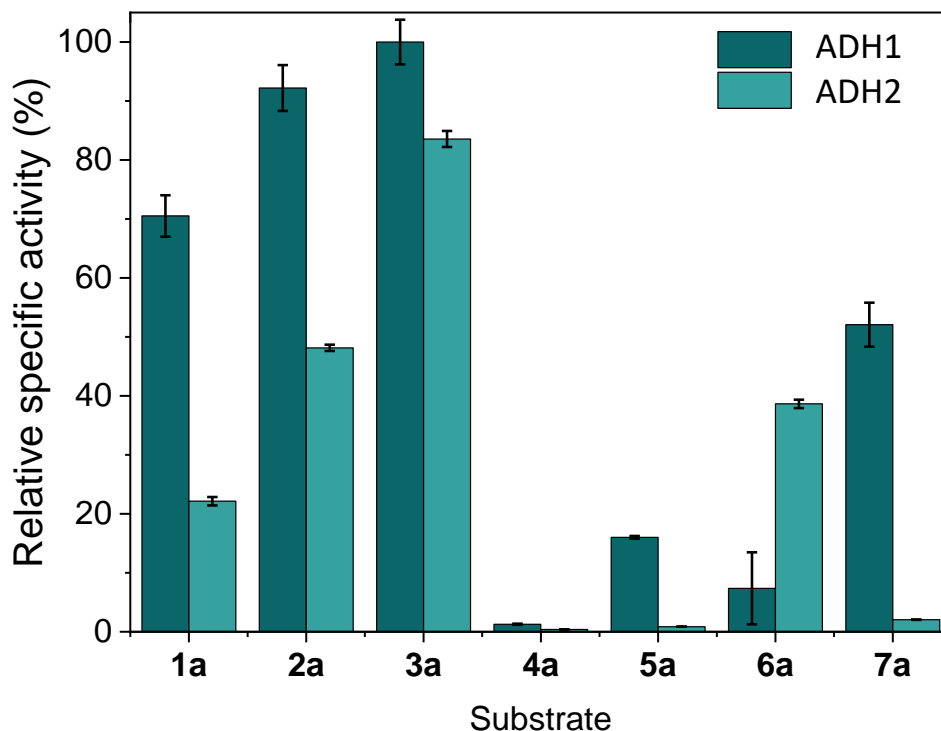
Figure 3.11: Activity of ADHs towards different linear and substituted diols. In all cases, reaction mixtures consisted in 10 mM diol, 1 mM NAD⁺ in 100 mM sodium phosphate buffer pH 8 at 30°C. 100% of relative specific activity corresponds to the activity of ADH2 towards substrate 3a (2.17 U·mg⁻¹).

Besides, the cyclization of 5b is precluded due to the C2-C3 planar triple bond structure, supporting its unsuccessful lactonization and subsequent hydrolysis. Unlike PcAOX*, which was engineered to accept polyols, the active site of both ADH2 and ADH1 seems to hardly accommodate non-alkylic diols. Furthermore, ADH2 exhibits higher specific activity than the ADH1 towards all assessed diols but 6a (**Figure 3.11.A**), supporting the fact that ADH2 relieves the workload of ADH1 in the first oxidative step, letting the latter focus on the lactol oxidation. As a general trend, the hydrolysis turnover frequency (TOF) was higher than the oxidation TOF (**Table 3.3**). Regarding the diol oxidation, similar trends were reported by Kara[143] and co-workers, who described the preparation of lactones from diols (1a, 2a, 3a, 6a, and 7a) employing ADH1 coupled to a laccase mediator system. Despite 5 out of the 7 assayed diols being completely consumed, the cell-free cascade only reached ω-HA yields higher than 70% for 2a, 6a, and 7a. Using the shortest diol (1a), the cell-free system reached a 40% yield of 1d, which can be attributed to the high stability of 1c preventing its hydrolysis. Likewise, this system failed to synthesize the 6-hydroxyhexanoic acid (3d) despite its corresponding diol (3a) being quantitatively oxidized to the lactol. When we inspected deeper the product profile of 3a after 24 h, we identified 6-oxohexanoic acid (3e) as an overoxidation product (**Annex 3.2**). This finding agrees with the high oxidative activity reported for ADH2 towards long-chain ω-HA to produce biobased polyamides where the formation of oxocarboxylic acids intermediates is desired. Unlike shorter ω-HAs, the 6C ω-HA (3d) reveals itself as the substrate for the two dehydrogenases when it is accumulated (**Annex 3.3**) unlike the 5C ω-HA, supporting the accumulation of the latter but not the former. In fact, when we analyzed the reaction products

at 2 h, 4 h, and 24 h by GC-MS, we could not detect 3d even at the early reaction times, meanwhile, all the aldehyde intermediates formed within this cascade could be detected (**Annex 3.2-4**).

Additionally, we tested the enantioselectivity of our cell-free biocatalytic cascade. To that aim, we challenged the multi-enzyme system with the prochiral 3-methyl-1,5-pentanediol (6a) to address its desymmetrization. After 24 hours of reaction, 6a was 100% consumed, yielding 70% of 6d but accumulating the lactol intermediate and the overoxidation product 6-oxo-3-methylpentanol (**Annex 3.4-5**). The enantiopurity of 6d was determined by chiral GC (**Annex 3.6**) where the presence of only one enantiomer (one chromatographic peak) points out that the cell-free cascade yields the ω-HA with ee>99%. According to the previously reported exquisite S-enantiopreference (ee>99%) of ADH1 during the oxidation of symmetric diols into 3-substituted δ-valerolactones, we conclude that our cell-free multi-enzyme system enantioselectivity synthesizes S-6d. On the contrary, the multi-enzyme system showed null enantioselectivity for oxidizing the racemic mixture of 4-hydroxypentanol 7a (rac-7a). After 24 hours of reaction, rac-7a was converted into its corresponding ω-HA, yielding 92% of rac-7d and suggesting that neither the ADHs nor the LAC are enantioselective for the oxidation and the hydrolysis step, respectively (**Annex 3.7**). Again, this insight matches with the lack of enantioselectivity reported for ADH1 towards the oxidation of rac-7a (82%), which yields a racemic mixture of the corresponding lactone (rac-7c, ee=2%). The low enantio preference of the multi-enzyme system towards rac-7a is also supported by the poor enantioselectivity found for LAC towards the hydrolysis of the racemic lactone rac-7c ee<2%; (**Annex 3.8**). A similar lack of enantioselectivity was observed for ReLAC (**Annex 3.9**), which meant that the kinetic resolution of 7a was not possible using the dehydrogenases and lactonases here tested. This means that the preparation of enantiopure 7d is forbidden using the cell-free biocatalytic cascade we described here.

Motivated by the excellent results we achieved with the transformation of diol 2a, we scaled the substrate concentration up to 100 mM using the optimized system stoichiometry. Under these conditions, a steady pH drop was observed during the reaction course that slowed down the ω-HA production after 4 hours (**Figure 3.12.A**).
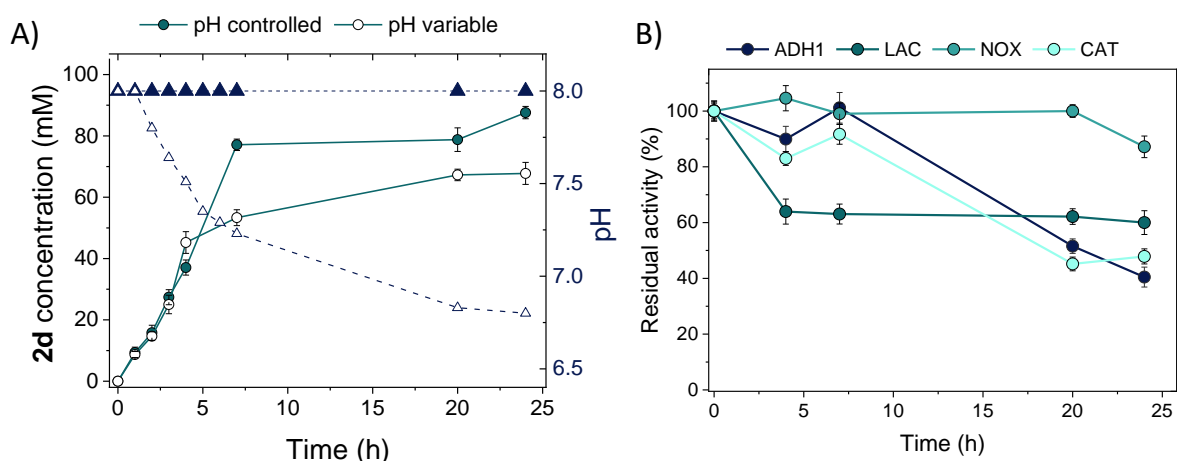
Figure 3.12: Multi-enzymatic synthesis of ω-hydroxy acids from diols. All reactions consisted in 1.5 mL of 2a 100 mM, NAD$^+$ 1 mM, FAD$^+$ 0.15 mM in sodium phosphate buffer 100 mM pH 8 at 30°C and 250 rpm, containing ADH2 0.52 mg, ADH1 1.58 mg, NOX 0.084 mg, CAT 0.34 mg and LAC 0.112 mg. A) Effect of the pH in the initial ω-hydroxy acid production rate; reactions without pH control (black and red squares) and reactions with pH control (black and red triangles). B) Enzyme stability under the following operation conditions without pH controlling: 100 mM 2a, 1 mM NAD$^+$, 0.15 mM FAD$^+$ in 200 mM sodium phosphate buffer pH 8 at 30°C and 250 rpm.

The reduction of the ω-HA production rate relied on the inactivation of the cascade enzymes under operation conditions without pH control, where the ADHs and the CAT enzymes lost 60% of their initial activity after 24 hours (**Figure 3.12.B**). To overcome the negative effect of the pH value decreasing, we manually kept the pH at 8 along the whole biotransformation to assure a steady ω-HA production rate during the entire reaction course (**Figure 3.12.A**). Controlling the pH value, the cell-free cascade attained a 90% yield of 2d after 24 hours and using 100 mM substrate, without detecting any intermediate. Upon passing the crude reaction mixture through an ultrafiltration unit to remove the enzymes and through a weak anionic exchange column to trap the cofactors (NAD$^+$ and FAD$^+$), the aqueous and buffered solution of ω-HA (2d) was characterized by GC-MS and ^{1}H NMR spectroscopy (**Annex 3.10** and **3.11**). At this substrate load, the cell-free biotransformation results in a mass titer of 11 g L-1, a volumetric productivity of 0.4 g L^{-1} h^{-1}, and a mass-specific yield of 9.3 g product g biocatalyst^{-1}. These mass metrics fall close to the range that Meissner and Woodley have reported for the industrial implementation of high-priced valued products. Unfortunately, when we scaled up the reaction volume from 1.5 mL up to 10 and 20 mL (at 100 mM 2a), the system achieved 46% and 45% of 2d yield after 48 and 72 hours, respectively (**Table 3.4**). The low yields were attained due to visible enzyme precipitation, which may be highly related to the increased air-liquid interface as previously reported with other enzymes.

Table 3.4: Scale up reaction volume during the synthesis of 2d.

Substrate 2a (mM)	Product 2d (mM)	2d Yield (%)	Molar mass product (μmol)	Reaction scale (mL)	Cofactor TTN
100	90	90	135	1.5	180
100	46	46	460	10	92
100	45	45	900	20	90

Reactions consisted in 100 mM 2a, 1 mM NAD^+, 0.15 mM FAD^+ in 100 mM buffer pH 8 at 30°C and 250 rpm.

1.4. Conclusions

We have developed an orchestrated multi-enzyme system that sequentially catalyzes the double oxidation of diols into lactones and their hydrolysis to ultimately yield ω-HA, integrating an efficient NAD^+ regeneration system that uses oxygen as the ultimate electron acceptor. High ω-HA yields were achieved through the synergistic combination of two ADHs possessing different catalytic efficiencies towards the diol and lactol oxidation, respectively.

Furthermore, this multi-enzyme system was proven to transform a wide scope of linear and branched short-chain diols into their corresponding ω-HAs, demonstrating an excellent enantioselectivity for the desymmetrization of prochiral 3-methyl-1,5-pentanediol. In our study, oxygen mass transport was not intensified; however, we envision oxygen bubbling as an efficient approach to enhance the NAD^+ recycling by boosting NOX activity, which will ultimately accelerate the overall cascade rate, yielding higher ω-HA titers in shorter times. Thoroughly exploiting synergies in biocatalytic cascade reactions, this new artificial multi-enzyme cascade can open up new paths to upgrade diols into molecules with higher industrial value, if the bottlenecks and challenges in scaling up can be overcome.

CHAPTER 4:

4.1. Introduction

Enzyme immobilization presents an interesting solution to enhance the properties of the free-enzyme catalyzed processes. The success of assembling a successful heterogenous biocatalyst relays on the selection of carrier and chemistry binding strategy. An easy and fast characterization of the assembled heterogenous biocatalyst may allow us to identify the best strategies for enzyme immobilization. Although a wide range of enzymes have been successfully immobilized on solid carriers to enhance their functional properties, structural characterizations of the immobilized enzymes are also demanded to understand the structural changes occurred upon the immobilization and further optimize the fabrication of heterogeneous biocatalysts.

In this work, we present an immobilization screening for His-tagged ADH2 (His-ADH2) aiming at maximizing the activity and the stability of the resulting heterogeneous biocatalysts for their further integration in one-pot multi-enzyme systems to selectively oxidize 1,ω-diols to yield ω-hydroxy aldehydes. In previous attempts, the immobilization of ADH2 resulted in an active heterogeneous biocatalyst that could be reused[140], nevertheless, the clues underlying the enzymatic stabilization remain to be elucidated. We have performed an extensive characterization of the immobilized enzymes on the different porous carriers, analyzing their immobilization parameters, thermal stability, spatial distribution, and the structural changes that enzymes undergo on the surface of each carrier. The optimal heterogeneous biocatalyst selected among the different porous carriers tested herein, was then applied for the selective oxidation of five different diols in combination with the best enzyme partner for the in situ recycling of NAD$^+$[172] selected from two different NADH oxidases.

4.2. Experimental section

4.2.1. Materials

Substrates as 1,4-butanediol (1s), 1,5-propanediol (2s), 1,6-hexanediol (3s), diethylene glycol (4s), 3-methyl-1,5-pentanediol (5s), 5-hydroxypentanal (2p),2-Hydroxytetrahydropyran (lactol), δ-valerolactone, the enzyme catalase from bovine liver, kanamycin sulfate from Streptomyces kanamyceticus, ampicillin, flavin-adenine-dinucleotide sodium salt (FAD$^+$), fluorescein isothiocyanate (FITC), rhodamine B isothiocyanate, acetic anhydride and n-methylimidazole were purchased from Sigma-Aldrich (St. Lous, IL, United States). Isopropyl β-D-thiogalactopyranoside (IPTG), nicotinamide adenine dinucleotide sodium salt (NAD$^+$) and β-nicotinamide adenine dinucleotide reduced (NADH) were purchased from GERBU Biotechnik GmbH (Wieblingen, Germany). Low density (LdAG-Co^{2+}; 15 µmol of Co^{2+} x g $_{carrier}^{-1}$) and high density (HdAG-Co^{2+}; 30 µmol of Co^{2+} x g $_{carrier}^{-1}$) cobalt-activated agarose microbeads 4BCL (particle size; 50–150 µm) were purchased from ABT technologies (Madrid, Spain). TALON metal affinity resin (tAG-Co^{2+}) (particle size 45–165µm; 20 µmol of Co^{2+} x g $_{carrier}^{-1}$) was purchased from Takara Bio Group (Göteborg,Sweden). Metal-ion affinity enzyme immobilization EziG (1, 2 and 3; particle size 75–150µm; 10 µmol Fe^{3+} x g^{-1} were kindly donated by EnginZyme (Solna, Sweden). 6BCL glyoxyl-agarose beads were prepared as described

elsewhere (Guisán, 1988). Precision plus protein TM standards, micro Bio-spinTM chromatographic columns and Bradford reagent were acquired from BIORAD. All other reagents and solvents were of analytical grade or superior.

4.2.2. Bacterial Strains and Growth Conditions

His-ADH1[173], LpNOX[148] and NOX[167] were cloned and overexpressed in competent Escherichia coli BL21 cells transformed with the respective plasmids. Briefly, 1 mL of an overnight culture of E. coli BL21 (DE3) harboring each plasmid was used to inoculate 50 mL of Luria-Bertain (LB) medium containing kanamycin for BsADH2 and LpNOX (final concentration 30 µg × mL^{-1}) and ampicillin for NOX (final concentration 60 µg × mL^{-1}). The resulting culture was aerobically incubated at 37°C with orbital shaking at 250 rpm until the OD600 nm reached 0.6. Afterwards, the culture was induced with 1 mM IPTG. His-ADH2 and NOX were induced for 3h at 37°C, while LpNOX was induced for 16 h at 21°C. After the induction time, cells were harvested by centrifugation at 1,157g for 30min at 4°C. Supernatants were discarded and the pellet was resuspended in 5 mL of a solution of 50 mM NaCl, 10 mM imidazole in 25 mM sodium phosphate buffer solution at pH 7. Cells were lysed by sonication using an Ultrasonic sonicator LABSONIC P, at 50% amplitude (0.5s ON/ 0.5s OFF) for 15min in an ice-water bath. The suspension was then centrifuged at 12,298g for 30min at 4°Cand the supernatant containing the cell extract with the His-tagged protein was collected and employed for further purification and/or immobilization.

4.2.3. Purification and Immobilization of His-ADH1 on the Different Carriers

10 volumes of crude cell extract containing the His-ADH1 were mixed with 1 volume of carrier and incubated under orbital shaking for 1h at 4°C. Later, the suspension was filtered and the microbeads containing the enzyme were washed with 5 volumes of 25 mM phosphate buffer at pH 7. Resulting resins were stored at 4°C until their usage. Additionally, 10 volumes of crude cell extract containing the His-ADH1 were mixed with 1 volume of LdAG-Co^{2+} microbeads and incubated under orbital shaking for 1h at 4°C. Later, the suspension was filtered and the microbeads containing the enzyme were washed with 5 volumes of 25 mM phosphate buffer at pH 7. Sequentially, His-ADH1 was eluted by the addition of 10 volumes of 300 mM imidazole in 25 mM phosphate buffer at pH 7 for 1h at 4°C under orbital shaking. Lastly, SDS-PAGE and Bradford protein assay[174] were carried out after each production batch to determine the purity, the concentration, the bound enzyme to the carriers and the specific activity of the enzyme.

4.2.4. Immobilization of the Co-Factor Regeneration System NOX/CAT on Glyoxyl and LpNOX in LdAG-Co^{2+}

One volume of glyoxyl-6BCL carrier equilibrated with 100 mM sodium bicarbonate buffer at pH 10 was incubated with 10 volumes of enzymatic solution containing 0.26 mg·mL^{-1} of purified NOX and 10 mg·mL^{-1}of CAT in 100 mM sodium bicarbonate buffer at pH 10 and incubated for 3–4h at 4°C. Afterwards, the supernatant was discarded, and the carrier was incubated with 10

volumes of a solution containing 1 mg·mL^{-1}of sodium borohydride in 100 mM sodium bicarbonate buffer at pH 10 for 30min. Finally, the suspension was filtered and washed with 5 volumes of 25 mM sodium phosphate buffer at pH 7. 10 volumes of crude cell extract containing the His-tagged LpNOX were mixed with 1 volume of LdAG-Co^{2+} microbeads and incubated under orbital shaking for 1h at 4°C. Later, the suspension was filtered and the microbeads containing the enzyme were washed with 5 volumes of25 mM phosphate buffer at pH 7.

4.2.5. Calculation of Immobilization Parameters

For any immobilization protocol herein performed, we calculated the following immobilization parameters: Load is defined as the mass of immobilized protein per gram of carrier. It is calculated as follows:

$$\text{Load (mg} \cdot \text{g}^{-1}) = \text{immobilized protein (mg} \cdot \text{mL}^{-1})\text{x } (\frac{\text{Immobilization volume (mL)}}{\text{carrier mass (g)}})$$

Immobilization yield (ψ) is defined as the percentage of the offered enzyme that is immobilized on the carrier. It is calculated as follows:

$$\psi = \left(\frac{\text{Offered activity} - \text{supernatant activity}}{\text{Offered activity}}\right)\text{x } 100$$

Immobilized activity (iA) is defined as the theoretical activity bound to the carrier. It is calculated as follows:

$$\text{iA (U x g}^{-1}) = (\text{Offered activity})\text{x } (\frac{\psi}{100})$$

Recovered activity (RA/U·g^{-1}) is defined as the real enzyme activity per mass of carrier measured through the corresponding colorimetric assay upon the immobilization.

Relative recovered activity is defined as the percentage of the theoretically immobilized activity (iA) exhibited by the enzyme upon the immobilization protocol. It is calculated as follows:

$$\text{rRA (\%)} = \left(\frac{\text{RA}}{\text{iA}}\right)\text{x } 100$$

Immobilized specific activity (iSA) is defined as the activity per mass of the immobilized enzyme. It is calculated as follows:

$$\text{iSA (U x mg}^{-1}) = (\frac{\text{RA}}{\text{Load}})$$

4.2.6. Enzymatic activity measurement of both free and immobilized enzymes

Enzyme activity of the different systems was spectrophotometrically measured in UV flat bottom and transparent 96-well microplates, employing a Microplate Reader Epoch 2, BioTek ®. Data processing was done with Gen5 software.

4.2.6.1.   ADH Activity Assay

200 µL of a reaction mixture containing 10 mM 1,5-pentanediol, 1 mM NAD^+, in 50 mM Tris-HCl buffer at pH 8 were incubated with either 5 µL of free enzyme or 10 µL suspension 1:10 of the different immobilized biocatalysts at 30°C. The increase in absorbance was monitored at 340 nm. One unit of activity was defined as the amount of enzyme that was required to reduce 1 µmol of NAD^+ per minute at the assayed conditions.

4.2.6.2.   NOX Activity Assay

200 µL of a reaction mixture containing 0.2 mM NADH, 0.15 mM FAD^+ in 50 mM Tris-HCl buffer at pH 8 were incubated with either 5 µL of free enzyme or 10 µL suspension 1:10 of the different immobilized biocatalysts at 30°C. The decrease in absorbance was monitored at 340 nm. One unit of activity was defined as the amount of enzyme that was required to oxidize 1 µmol of NADH per minute at the assayed conditions.

4.2.6.3.   Catalase Activity Assay

200 µL of a reaction mixture containing 35 mM H_2O_2, in 50 mM Tris-HCl buffer at pH 8 were incubated with either 5 µL of free enzyme or 10 µL suspension 1:10 of different immobilized biocatalysts at 30°C. The decrease in the absorbance at 240 nm was monitored. One unit of activity was defined as the amount of enzyme that was required to disproportionate 1 µmol of H_2O_2 per minute at the assayed conditions.

4.2.7. Protein labeling with fluorescent probes

Fluorescent labeling of the enzyme was done using a methodology reported elsewhere[175]. Briefly, an enzyme solution of 0.25 mg·mL^{-1} in 100 mM of sodium bicarbonate buffer at pH 8.5 was mixed with FITC or rhodamine B solution at 1:10 molar ratio (FITC and rhodamine B stocks were prepared in DMSO at 10 mg·mL^{-1}). The labelling reaction was then incubated for 1h under gentle shaking at 25°C. Later, unreacted FITC or rhodamine B was eliminated by either filtering the enzyme solution through a tangential ultrafiltration unit (10 kDa) or dialyzing the enzyme solution with a 25 mM sodium phosphate buffered solution at pH 7 until no coloration was observed in the filtered solution.

4.2.8. Confocal laser scanning microscopy (CLSM) imaging

The localization and distribution of fluorophore-labelled His-ADH1 immobilized along the different carriers were visualized with a confocal microscope Spectral ZEISS LSM 880

microscope equipped with an excitation laser, λ_{ex} 561 nm for Rhodamine Band emission filter. Confocal imaging was done using a ×20 and ×40 water objectives and a 1:200 (w:v) buffered suspension in 25 mM phosphate buffer at pH 7, of each biocatalyst with the fluorescently labeled immobilized enzymes. The resulting micrographs were analyzed with FIJI[176]. From confocal images, we obtained an average and normalized fluorescence radius profile, using FIJI software and its plugin module for radial profile generation (developed by Paul Baggethun). Subsequently, a Gaussian fit was applied to the obtained profiles of 10 single beads of similar size. Then, we searched for the fitted data point that corresponds to the 50% of the maximum normalized fluorescence fitted peak (yFWHM), and the corresponding radius coordinate (xFWHM) to that data point was then subtracted from the radius (R) of the analyzed bead to finally obtain the FWHM (full width half maximum) that means the infiltration distance of the enzyme into the bead surface.

4.2.9. Thermal inactivation

Inactivation of both soluble and immobilized biocatalysts were carried out by incubating them in 25 mM sodium phosphate at pH 7 at 25–90°C for 1h. The residual activity upon the thermal incubation was quantified and the T_{50} was calculated as the temperature where the enzyme exhibits the 50% of its initial activity (prior to the thermal incubation). For the kinetic thermal inactivation, both free and immobilized enzymes were incubated in a suspension 1:10 (w:v) with 25 mM sodium phosphate at pH 7at 70°C. Samples were withdrawn at different times and their residual activities were measured by the ADH activity assay. The activity of the different time points was normalized with the enzyme activity at time zero as reference. To calculate the half-life times, the obtained experimental measurements were adjusted to a 3-parameters biexponential kinetic inactivation model[177].

4.2.10. Analysis of intrinsic tryptophan fluorescence

Immobilized biocatalysts loading 0.5 mg of protein·g $_{carrier}^{-1}$ were used for this experiment. The intrinsic fluorescence of free and immobilized His-ADH2 was measured before and after the samples were incubated at 80°C for 1 h. To that aim, 70 µg of either free or immobilized enzymes were placed in a 96-well dark plate and the fluorescence emission spectra was recorded between300 and 500nm upon the sample excitation at 280 nm, using emission band widths of 5nm. All spectroscopic measurements were performed in 25 mM phosphate buffer at pH 7.

4.2.11. Anisotropy measurements

The polarized fluorescence of immobilized samples loaded with 0.5 mg of FTIC-labelled His-ADH1 was measured to determine the fluorescence anisotropy of FTIC conjugated to the free and immobilized proteins. To calculate the anisotropy values, 3 ng of either free or immobilized enzyme were placed into a 96-well dark plate and measured in a Microplate Reader Synergy H1, BioTek®. Anisotropy values were obtained according to the equation:

$$r = \frac{I_z - I_y}{I_T}$$

where I_z represents the parallel fluorescence intensity, I_y represents the perpendicular fluorescence intensity and I_T represents the total fluorescence intensity that is calculated by: $I_T = I_z + I_y$.[178]

The anisotropy values of all immobilized samples were normalized to the anisotropy of the free enzyme. Values higher than one mean enzymes with higher rotational tumbling than the free enzyme, while values lower that none mean enzyme with lower rotational tumbling than the free enzyme.

4.2.12. Operational stability of the immobilized biocatalysts

50 mg of His-ADH1 immobilized on LdAG-Co^{2+}, AG-Co^{2+}/E and EziG1 plus 125 mg of NOX/CAT on glyoxyl were placed inside a 1.5 mL Bio-spinTM chromatographic column with 600 µL of reaction mixture composed by 20 mM of 2s, 1 mM of NAD$^+$, 0.15 mM of FAD$^+$ in 50 mM Tris-HCl at pH 8. All reactions were performed at atmospheric pressure facilitating the oxygen diffusion to the reaction pot through an open syringe needle. After each reaction cycle (24 h), the reaction crudes were removed and collected for analysis, and the immobilized biocatalysts kept for the discontinuous use in the next batch cycle. Additionally, prior to continue with the next batch cycle, biocatalysts were washed with one volume of 25 mM of phosphate buffer at pH 7.

4.2.13. Regioselective reduction of diols

25 mg of His-ADH1 immobilized on EziG1 plus 62.5 mg of NOX/CAT on glyoxyl were placed inside a 1.5 mL Bio-spinTM chromatographic column with 800 µL of reaction mixture composed by 20 mM of substrate (1, 2, 3, 4 or 5s)1 mM of NAD$^+$, 0.15 mM of FAD$^+$ in Tris-HCl 50 mM at pH 8. All samples were incubated through orbital shaking (250 rpm) at atmospheric pressure, facilitating the oxygen diffusion to the reaction pot through an open syringe needle. After 24 h, all mixture reactions were removed and collected for analysis.

4.2.14. Kinetic analysis of the cofactor regeneration system

125 mg of His-ADH1 immobilized on EziG1 plus 312.5 mg of NOX/CAT in glyoxyl and LpNOX-LdAG-Co^{2+} were placed inside a 5 mL Tube with 1.5 mL of reaction mixture consisted of 20 mM of 1,5-Pentanediol 1 mM of NAD$^+$, 0.15 mM of FAD$^+$ in Tris-HCl 50 mM at pH 8. All samples were incubated through orbital shaking (250 rpm) at atmospheric pressure, facilitating the oxygen diffusion to the reaction pot through an open syringe needle. To analyze the reaction course of each system, 200 µL of the suspension were collected at different time points: 0.30, 1, 2, 4,8, and 24 h. Suspensions were filtered through 1.5 mL Bio-spinTM chromatographic column to collect the reaction crudes collected for further chromatographic analysis.

4.2.15. Analytical measurements

4.2.15.1. Gas chromatography (GC)

All reaction samples were derivatized as described elsewhere[179]. Additionally, 50 µL of aqueous reaction sample were placed in a 1.5 mL Eppendorf tube. Later, 150 µL of ethyl acetate were added and vortexed for 20 s 20–50 mg of anhydrous MgSO4 were added to dry samples before GC analysis using eicosane 2 mM as external standard. Gas chromatography analyses were carried out in an Agilent 8,890 System gas chromatograph using a column of (5%-phenyl)-methylpolysiloxane (Agilent, J&W HP-5 30m × 0.32mm × 25µm), helium as a carrier gas, and equipped with a flame ionization detector (FID). The temperature of the injector and FID detector were 280°C and 300°C, respectively. Separation of compounds were done by the following temperature ramp: initial temperature 60°C, maintained 2min, two ramps, first to 160°C at a rate of $10°C·min^{-1}$ and finally to 240°C at a rate of $20°C·min^{-1}$. Retention times for substrates are: 1s: 4.17min, 2s: 5.78min, 3s: 7.46min, 4s: 4.49min, 5s: 6.95min, 2-Hydroxytetrahydropyran (lactol): 3.38min, δ-valerolactone: 6.01min, and eicosane (external standard): 16.60min.

4.2.15.2. HPLC Analysis

Before HPLC analysis samples were derivatized as described elsewhere[180]. Briefly, 10 µL of aqueous sample (0.6–20 mM) were mixed with 50 µL of O-benzylhydroxylamine hydrochloride (130 mM in pyridine/ methanol/water 33:15:2) and incubated for 5min at 25°C. Afterwards, 500 µL of methanol were added and then centrifuged 5min at 13,450g. HPLC analysis was conducted in an Agilent 1,260 Infinity II chromatograph equipped with a Poroshell EC-C18 column (4.6 × 100 mm, 2.7 µm). Samples were detected at 215nm and were eluted at $1 mL·min^{-1}$ flow rate employing two mobile phases, phase A composed by trifluoroacetic acid 0.1% in water, and phase B composed by trifluoroacetic acid 0.095% in 4:1 acetonitrile/water. Elution conditions: 10–100% of B over 30min. Retention time of derivatized 5-hydroxypentanal was 14.39min.

4.3. Results and Discussion

4.3.1. Enzyme immobilization and kinetic characterization

Initially, we studied the effect of different porous carriers and activation chemistries in the immobilization of a ADH1. For these studies we selected two types of commercially available materials with different types of functionalization; porous agarose microbeads (AG) functionalized with different types of ligands (imidodiacetates (IDA) and nitrotriacetates (NTA)) and density of cobalt-chelates and porous silica particles (EziG) functionalized with Fe^{3+}-catechol complexes (**Table 4.1**).

Table 4.1: Characteristics of the different carriers

Material	Name	Functional group	Density groups (μmol/g)	Particle size (μm)
Agarose	LdAG-Co^{2+}	IDA-Co^{2+}	15	50-150
	HdAG-Co^{2+}	IDA-Co^{2+}	30	50-150
	AG-Co^{2+}/E	IDA-Co^{2+}/ Epoxide	20	50-150
	tAG-Co^{2+}	NTA-Co^{2+}	20	45-165
Silica	EziG1	Catechol-Fe^{3+}	10	75-125
	EziG2	Catechol-Fe^{3+}	10	75-125
	EziG3	Catechol-Fe^{3+}	10	75-125

According to previously reported protocols[157], we functionalized agarose porous microbeads with two different reactive groups; IDA-Co^{2+} and epoxides, giving rise to the carrier abbreviated as AG-Co^{2+}/E (**Figure 4.1**).
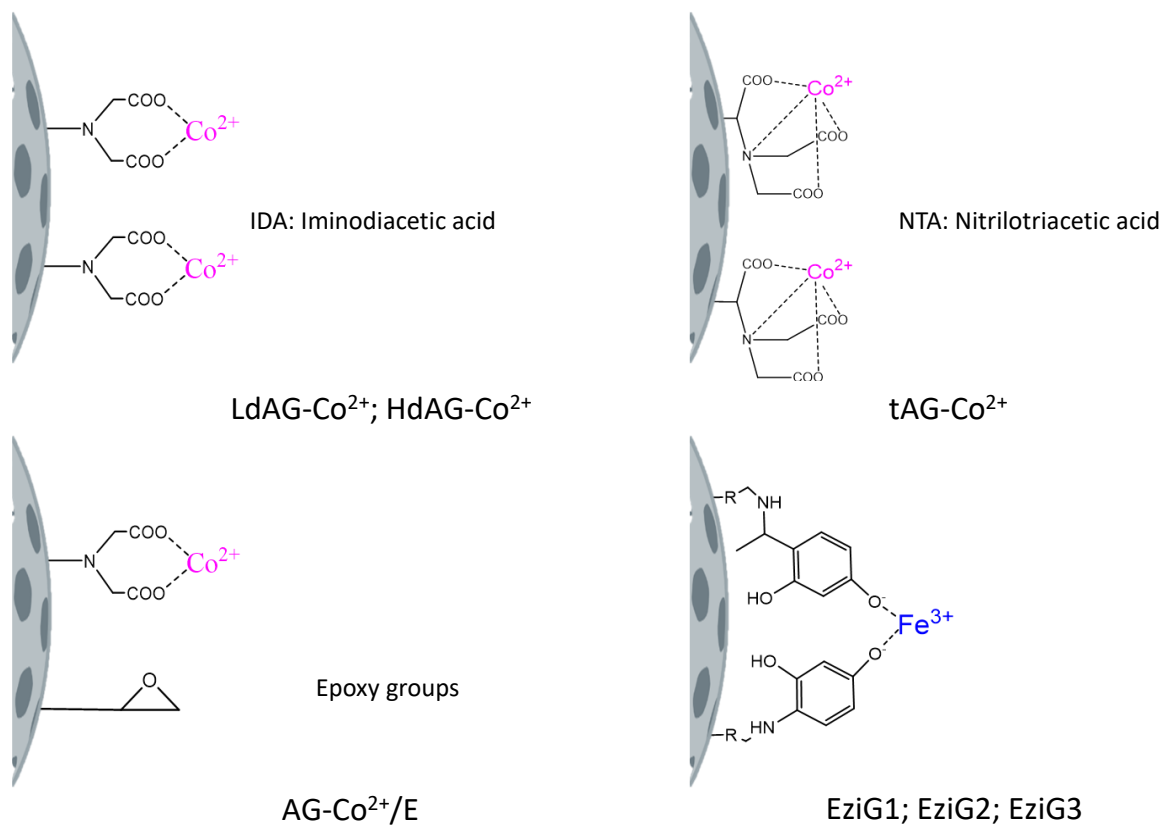
Figure 4.1: Chemical of structure of the different functional groups displayed at the porous surface of carriers.

Among the different controlled-pore glass carriers, we tested three different ones presenting low (EziG1), medium (EziG2) and high (EziG3) hydrophobicity. When cell-free extracts of overexpressed His-ADH2 in *E. coli* were incubated with the different carriers, we achieved immobilization yields higher than 95% with protein loads of at least 0.1 mg x g^{-1} (**Table 4.2**).

Table 4.2: Immobilization parameters of His-ADH1 on different porous carriers.

Name	Load (mg/g)[a]	Ψ (%)[b]	iA (U/g)[c]	RA (U/g)[d]	rRA (%)[e]	iSA (U/mg)[f]
LdAG-Co^{2+}	0.11	94 ± 3	0.94	0.44	47	4
HdAG-Co^{2+}	0.11	98 ± 1	0.97	0.45	47	4.1
AG-Co^{2+}/E	0.11	99 ± 4	0.98	0.22	22	2
tAG-Co^{2+}	0.11	96 ± 4	0.95	0.46	49	4.2
EziG1	0.14	99 ± 2	0.99	0.48	48	3.4
EziG2	0.14	98 ± 2	0.98	0.23	23	1.6
EziG3	0.13	99 ± 1	0.99	0.23	23	1.7

For details of the immobilization parameters see Materials and Methods. ψ: Immobilization yield. iA: theoretical immobilized activity. RA: recovered activity upon the immobilization. rRA: relative recovered activity. iSA: immobilized specific activity. The activity of ADH1 was measured using 2s as substrate under the assay conditions described in methods. IDA:Imidodiacetic acid.

In contrast, the recovered enzymatic activity (RA) significantly varied depending on the hydrophobicity of the carrier but negligibly changed when depended on the metal type and density of the carrier. While ADH1 recovered roughly 50% of its initial activity upon the immobilization on hydrophilic surfaces of all agarose-based carriers (LdAG-Co^{2+}, HdAG-Co^{2+}, tAG-Co^{2+}), similar activity recoveries were only achieved when using the most hydrophilic silica-based carrier (EziG1). However, the more hydrophobic EziG2-3 resulted to lower recovered activities upon the immobilization process. When agarose-based carriers were functionalized with both cobalt and epoxide groups (AG-Co^{2+}/E), the enzyme recovered the half of the activity recovered with the carriers functionalized only with cobalt-chelates. Hence, we suggest that AG-Co^{2+}/E promotes irreversible covalent bonds between the enzyme and the carrier that may distort the structure of the immobilized enzyme, negatively affecting its activity. To confirm the irreversibility of the immobilization on these hetero-functional carriers, we incubated all immobilized enzymes under denaturing conditions (10% SDS and 100°C for 5 minutes), and the supernatants were analyzed by SDS-PAGE (**Figure 4.2**).
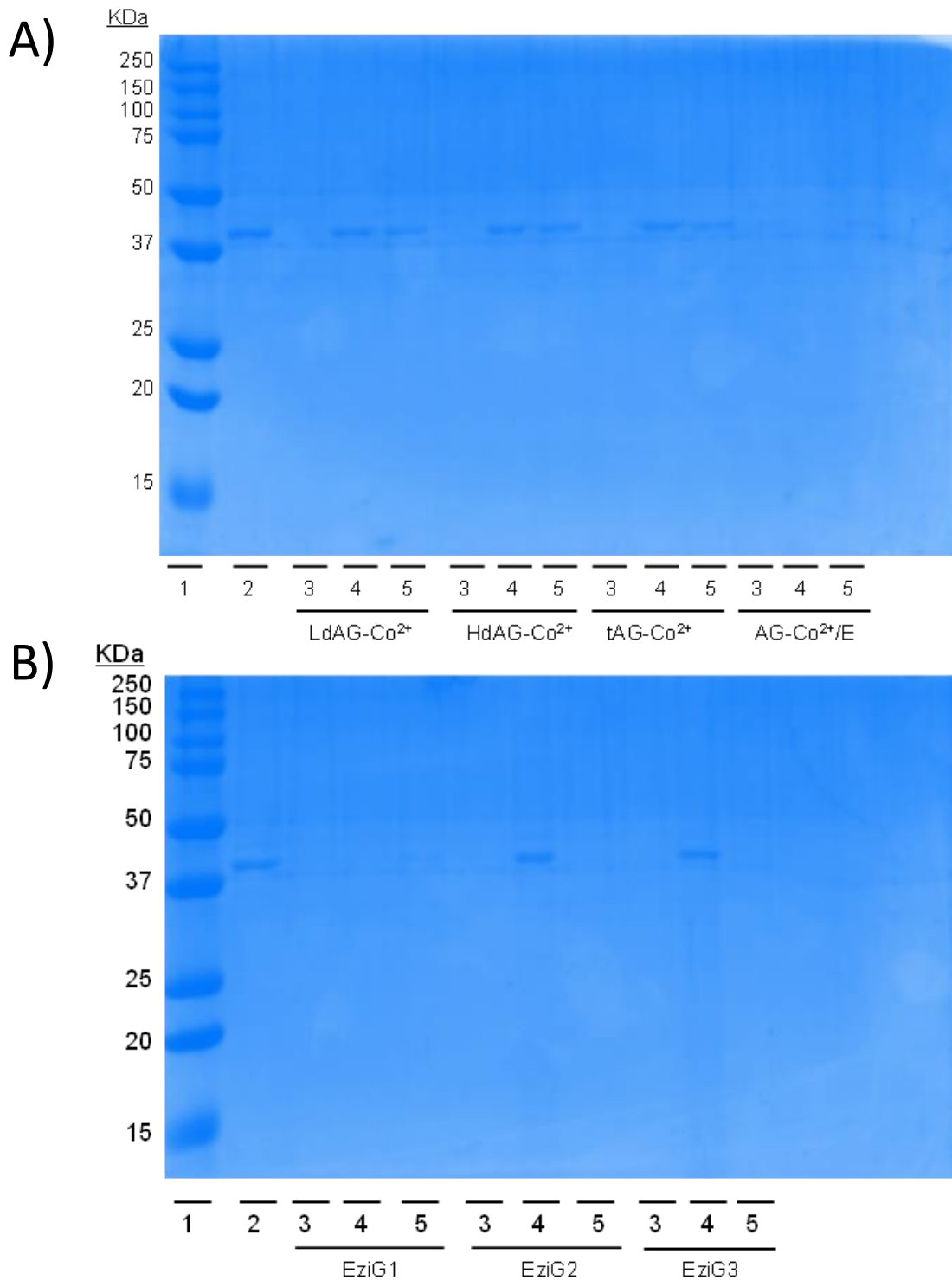
Figure 4.2: SDS-PAGEs gels of the immobilization process on different agarose-based (A) and glass-based (B) porous carriers. MW: Molecular weight markers (BioRad Precision Plus Protein All Blue Standard); 1 and 2: ADH1 crude extract; 3: Flow through upon binding; 4: Resin harboring the immobilized enzyme; 5: Elution sample (0.3 M imidazole)

As expected, His-ADH1 was released from all carriers but AG-Co^{2+}/E confirming that only those carriers functionalized with epoxy groups can irreversibly attach the enzyme. Similar results

have been reported for other enzymes immobilized on other types of carriers functionalized with epoxide groups[157]. Surprisingly, neither was the enzyme released fromEziG1 although it was immobilized through reversible interactions between the His-tag and the Fe^{3+}-catechol complexes (**Figure 4.2**). Other strong interactions (i.e, electrostatic bonds) between the surface carrier and the enzymes may explain this unexpected behavior of ADH1 bound to EziG1.

Furthermore, when we measured the specific activity of the immobilized enzymes, we observed higher values in the agarose-based carriers functionalized only with cobalt-chelates. This finding points out that the combination of agarose matrix and cobalt-chelates enables a more selective and effective immobilization of His-tagged proteins as only ADH1 was bound to the resins, recovering a high activity. On the contrary, EziG1 binds proteins unspecifically thus reducing the specific activity of the immobilized His-ADH1 but recovering similar volumetric activities ($U \cdot g^{-1}$) as with the AG carriers. As expected, the agarose matrix turns out to be the best system for the one-pot purification and immobilization of this His-tagged enzymes. In fact, this material is widely used to pack the chromatographic columns for protein purification[157].

4.3.2. Spatial distribution of His-ADH1 across the porous surface of different carriers

Once the immobilization was characterized, we investigated the spatial organization of His-ADH1 across the surface of the different porous carriers through confocal laser scanning microscopy (CLSM) imaging and through 3D image reconstruction (**Figure 4.3**).
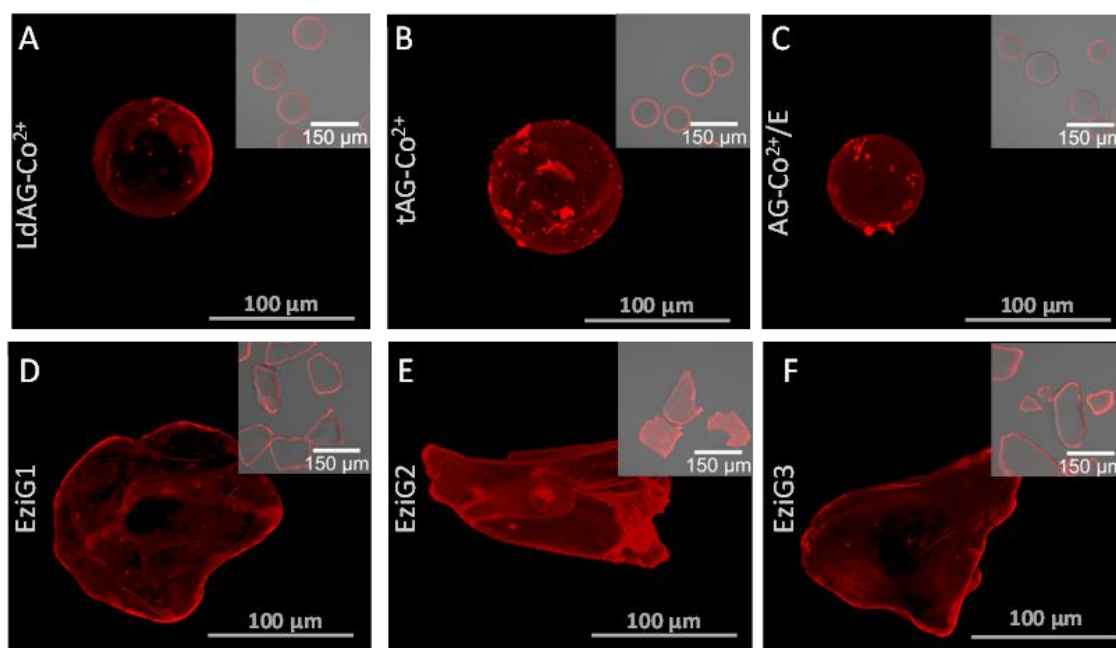
Figure 4.3: Confocal fluorescence microscopic Z-stack section images of immobilized His-ADH2 labelled with Rhodamine (red channel) on LdAG-Co^{2+}(A), tAG-Co^{2+}(B), AG-Co2+/E(C), EziG1(D), EziG2(E), EziG3(F). Top right insets are lower magnification confocal fluorescence micrographs where red and brightfield channels are overlaid.

ADH1 immobilized on agarose-based materials was similarly located at the most outer regions of the beads regardless the metal-complex ligands and the presence of epoxide groups (**Figure 4.3.A-C**). A similar distribution pattern was found when EziG1 and EziG3 were used as carriers

(**Figure. 4.3. D-E**). In all these carriers the enzyme was infiltrated only 2-3 μm inside the particles (**Figure 4.4**). However, the more hydrophobic iron-complexed glass particles (EziG2) immobilized His-ADH1 through a more uniform distribution, which meant that the proteins were infiltrated up to 35-42μm towards the inner surface of the particles. Interestingly, the 3D image reconstruction of the different immobilized biocatalysts revealed some different surface patterns for those samples with similar spatial distribution. While the enzymes immobilized on glass carriers regardless their spatial organization showed minor protein aggregates at their surface (inset **Figure 4.3. D-F**), the agarose-based carriers promoted the protein aggregation at the surface of the particles. However, these different spatial organizations negligibly affected the functional parameters of the immobilized enzymes according to the **Table 4.1**.
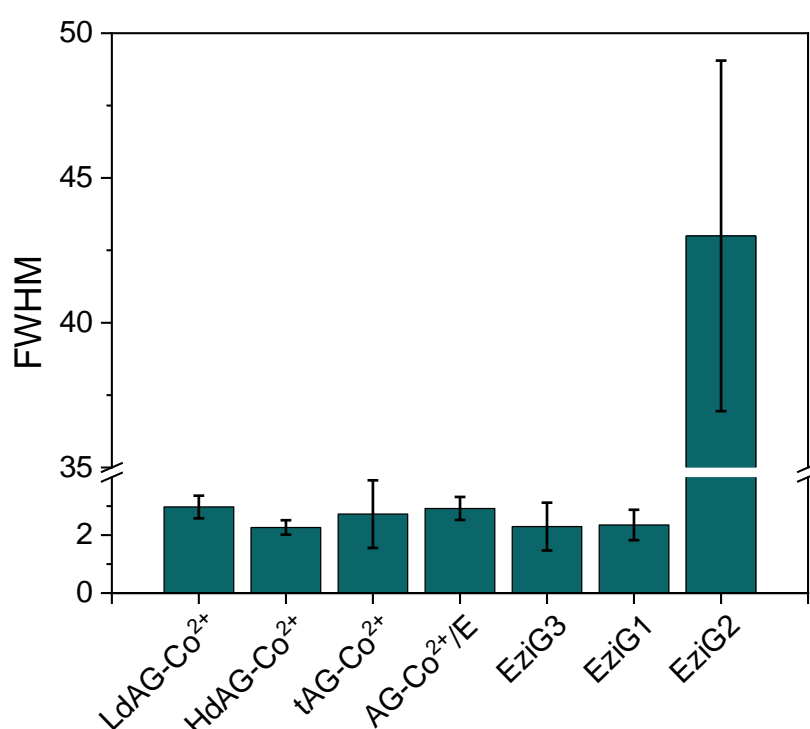
Figure 4.4: Infiltration distance (FWHM / μm) of His-ADH1 across the surface of different porous carriers. FWHM: full width half maximum.

4.3.3. Thermal inactivation

All biocatalysts (including free enzyme) were incubated in a range of temperatures (from 20°C to 90°C) to calculate their T_{50}, temperature to which enzyme activity is reduced after 1 hour of incubation (**Figure 4.5**).
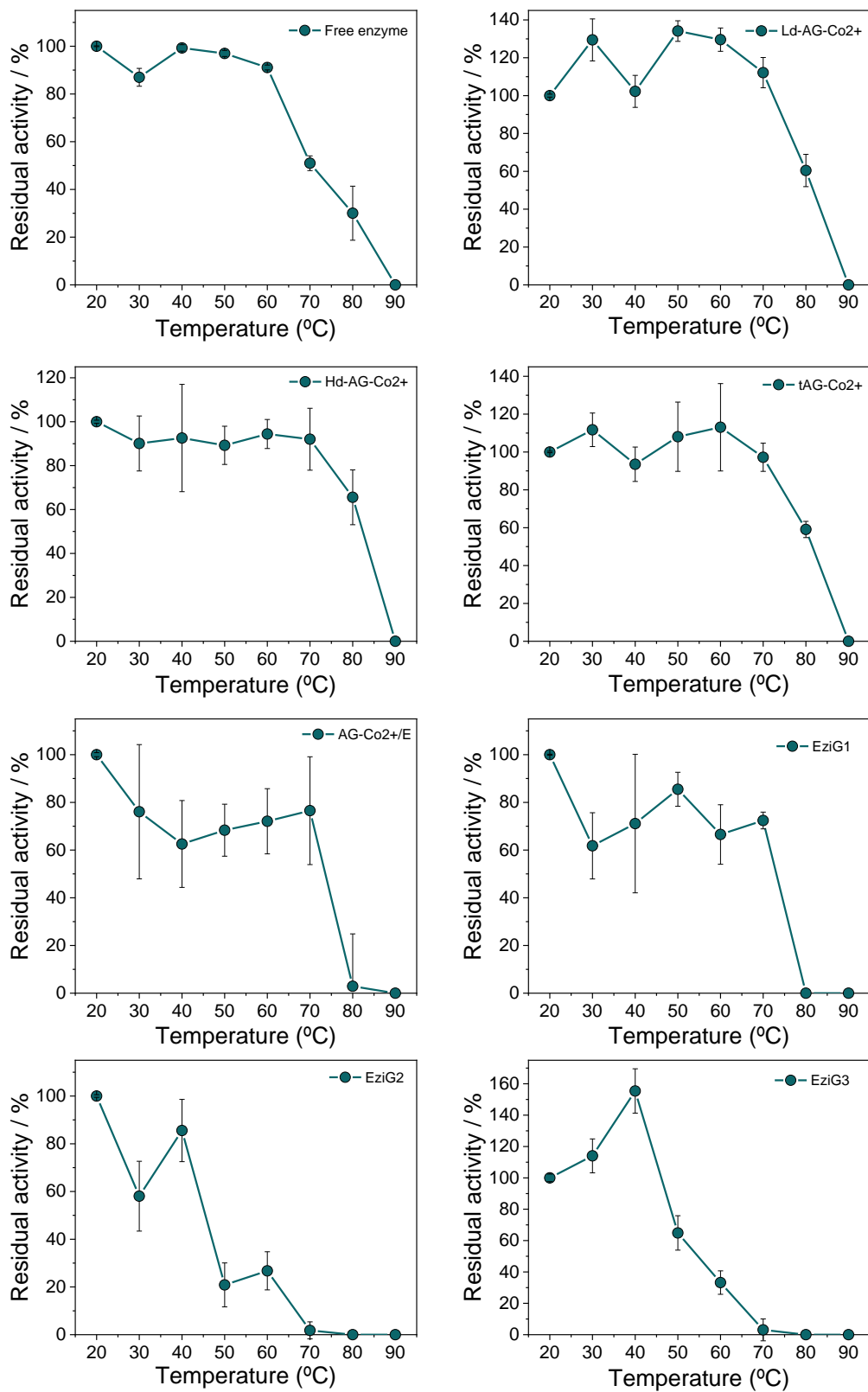
Figure 4.5: Thermal inactivation of free and immobilized ADH1 on different carriers. Samples prepared in phosphate buffer 25 mM at pH 7 were incubated at different temperatures for 1 hour. After the thermal

incubation, enzyme activity was measured with a reaction mixture composed by 10 mM of 1,5-pentanediol, 1 mM of NAD^+ in 50 mM Tris-HCl 50 mM pH 8.

Figure 4.6.A shows that all agarose carriers raised up 5–10°C the T_{50} of ADH1 compared to the free counterpart. Among glass carriers, only EziG1 was able to stabilize the enzyme, while its immobilization on EziG2 andEziG3 led to heterogeneous biocatalysts with lower T_{50} than the free enzyme.
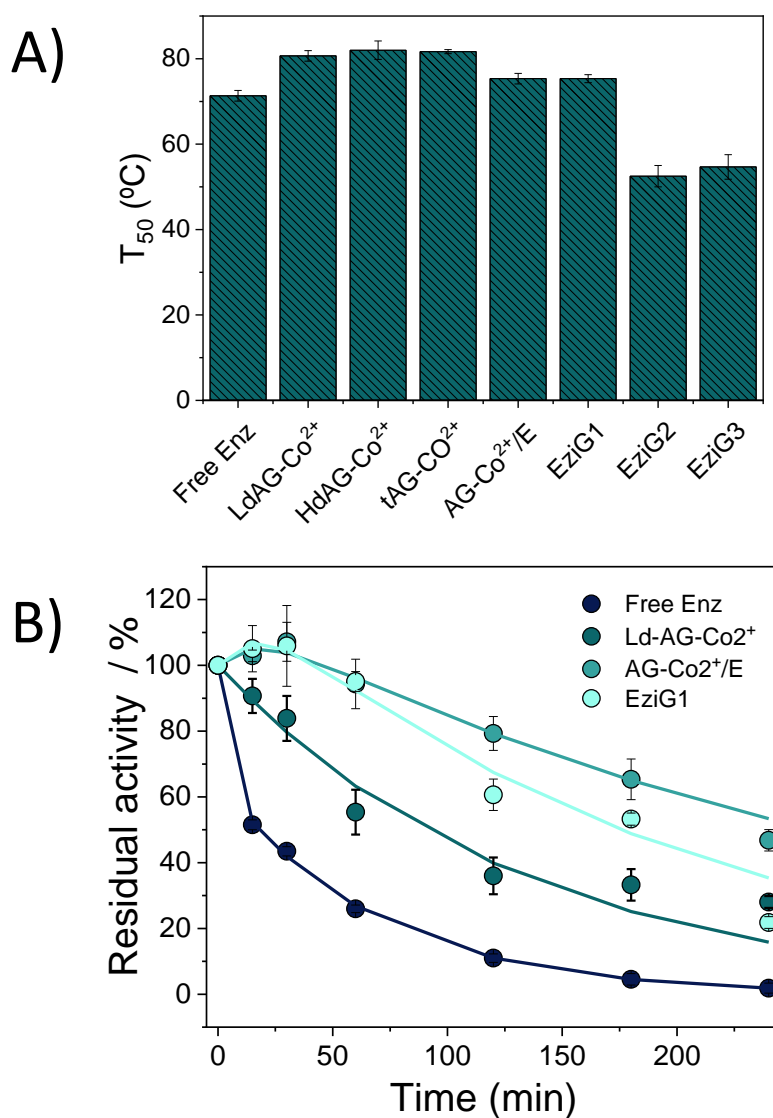
Figure 4.6: Thermal inactivation of soluble and immobilized ADH1 on different carriers. A) T_{50} means the temperature to which either the soluble or the immobilized enzyme lost 50% of its initial activity after 1 h incubation. B)Thermal kinetic inactivation of different soluble and immobilized biocatalysts incubated at 70°C in sodium phosphate buffer25 mM pH 7. The activity was measured with2sas substrate under the assay conditions described in methods. Symbols represent the obtained experimental values, while the solid lines correspond to their fitting to 3-parameters biexponential kinetic inactivation model (Aymard and Belarbi,2000). Half-life time of the different samples: ADH1: 0.58h; ADH1 immobilized on LdAG-Co^{2+}: 1.51h, EziG1: 2.93h, AG-Co^{2+}/E:4.62h.

To further investigate the inactivation kinetics of the immobilized ADH1, we evaluated the thermal inactivation at 70°C for three selected carriers: LdAG-Co^{2+}, AG-Co^{2+}/E and EziG1. The inactivation courses (**Figure 4.6.B**) show that the immobilization of His-ADH1 on LdAG-Co^{2+}, EziG1 and AG-Co^{2+}/E led to the enzyme stabilization, resulting in half-lives 3, 6 and 9 times higher than the free enzyme, respectively. Remarkably, EziG1 promotes a 2 times higher stabilization than LdAG-Co^{2+} but such carrier yielded a lower enzyme thermal stability than the AG-Co^{2+}/E carrier where ADH1 is immobilized through a similar orientation but attached through irreversible bonds. These results are aligned with previous data reported for enzymes immobilized on heterofunctional carriers involving irreversible immobilization[181].

4.3.4. Structural analysis of immobilized His-ADH2

To understand the effect of the immobilization on the structure of His-ADH1, we performed a set of biophysical techniques to elucidate whether structural rearrangements occur during the immobilization and inactivation processes. The emission fluorescence of aromatic residues reveals their microenvironment within the protein structure[182], thus structural changes upon immobilization and further thermal shock can be monitored through measuring the intrinsic fluorescence of proteins (**Figure 4.7**).
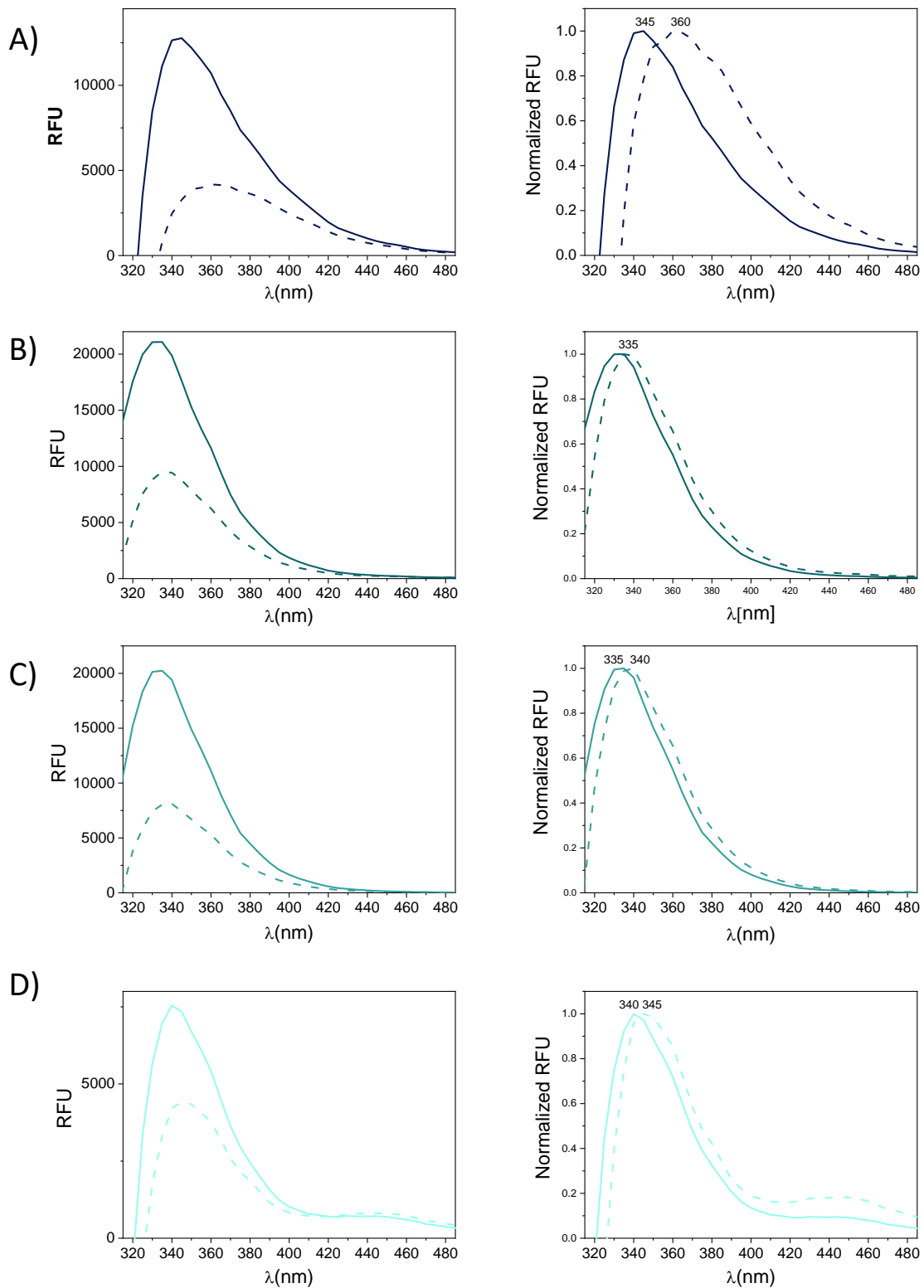
Figure 4.7: Spectra of intrinsic protein fluorescence. Left Column represents RFU vs λ, whereas right column represents the spectra normalized to the RFU at the maximum wavelength. Straight lines represent samples incubated at 25°C, whereas dash lines represent samples after thermal incubation (1 hour at 80°C). A: Free enzyme; B: LdAG-Co^{2+}; C: AG-Co^{2+}/E; D: EziG1.

All immobilized enzymes shifted their max λ towards lower wavelengths compared to the free enzyme, indicating that the aromatic residues of ADH1 are less solvent exposed upon the immobilization process, most likely due to the interactions with the carrier surfaces (**Figure 4.8.A**).
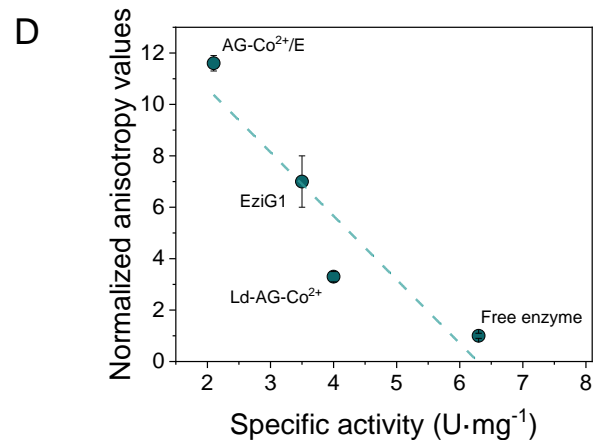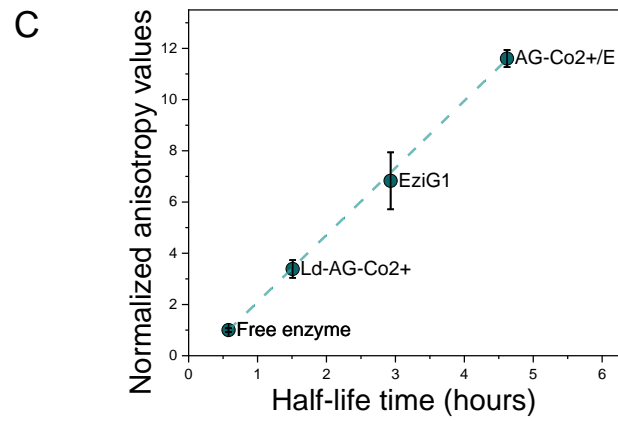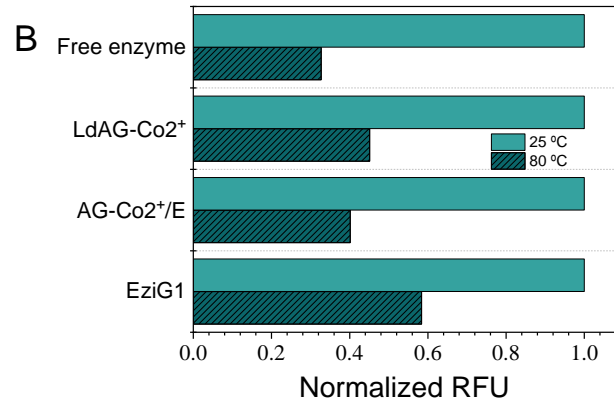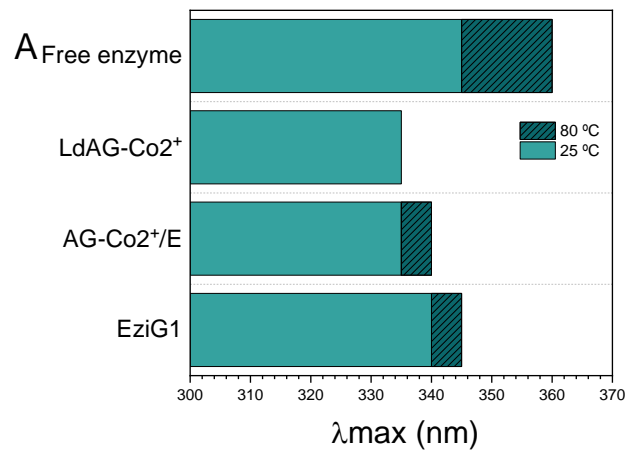
Figure 4.8: Intrinsic fluorescence of free and immobilized ADH1. A) λmax of each biocatalyst before (solid orange bars) and after (red stripped bars) 1h incubation at 80°C. B) Normalized RFU values for each biocatalyst before (orange bars) and after (red stripped bars) 1h incubation at 80°C. The RFUs of each sample before the thermal incubation were set as reference value of 1. C) Normalized anisotropy as a function of the half-life time at 70°C (from Figure 7) of different ADH1 immobilized on the different carriers. Fitting linear regression: y=2.62x—0.52; R^2= 0.999. D) Normalized anisotropy as a function of the specific activity (from Table 1) of different ADH1 immobilized on the different carriers. Fitting linear regression: y=2.21+14.74; R^2= 0.932. Anisotropy values of each sample were normalized with the value of anisotropy of the free enzyme (Anisotropy of sample/Anisotropy of free enzyme).

When the biocatalysts were incubated at 80°C for 1h, the free enzyme exhibited a 15nm red-shifted λ_{max} due to thermally induced unfolding, whereas that λ_{max} shift was minimized with all immobilized enzymes (**Table 4.3**).

Table 4.3: Structural analysis of immobilized His-ADH1

	Free Enzyme	**Ld-AG-Co^{2+}**	**AG-Co^{2+}/E**	**EziG1**
Δshift (nm) after incubation[a]	15	0	5	5
% after immobilization[ba]	-	80.16	78.26	30.44
% after incubation[cb]	19.48	47.52	41.87	55.97
Fluorescence Polarization[dc]	28 ± 2	91 ± 9	292 ± 8	140 ± 31
Anisotropy values[d]	19 ± 1	63 ± 6	216 ± 6	127 ± 20

[a]Δshift (nm) after incubation: Wavelength at maximum RFU after incubation – wavelength at maximum RFU before incubation; [b]% after immobilization: (Maximum RFU after immobilization/Maximum RFU free enzyme) x 100; [c]% after incubation: (Maximum RFU after incubation/Maximum RFU after immobilization) x 100; [d]Fluorescence Polarization: values were calculated with Gen5 software using the parallel fluorescence intensity, the perpendicular fluorescence intensity and the G Factor values.

Remarkably, there was no shift when the enzyme was immobilized on LdAG-Co^{2+}. Additionally, we analyzed the maximum fluorescence intensity at the ⬜max of each sample before and after thermal incubation. As shown in **Figure 4.8.B** the immobilized enzyme reduced its maximum fluorescence intensity upon thermal shock. However, after the thermal incubation, all immobilized samples experienced a lower fluorescence decay than the free enzyme in agreement with the results obtained for the λmax shift. These results point out a structural stabilization of ADH1 upon the immobilization process, which is manifested in longer half-life times under high temperatures in comparison to the free enzyme.

Besides the structural rearrangements promoted by the immobilization, we also study the local motion of the immobilized enzymes when immobilized on this set of porous carriers. To that aim, we chemically labelled ADH1 with FITC and then immobilized those fluorophores

conjugated enzymes to perform anisotropy studies with both soluble and immobilized samples. **Figure 4.8.C** reveals that the relative anisotropy of the immobilized enzymes is higher than the free one, indicating that all the herein tested immobilization protocols reduce the enzyme mobility. When comparing the normalized anisotropy values among the different immobilizes, we observe that the irreversible covalent immobilization on AG-Co^{2+}/E dramatically reduces the rotational tumbling of the anchored enzymes. Remarkably, there is a strong positive linear correlation (R^2 = 0.999) between the anisotropy values and the half-life time of the immobilized enzyme incubated at 80°C. Therefore, the less mobile the immobilized enzyme is, the higher the stability. A similar trend was also found for the super folded green fluorescence protein immobilized on agarose porous microbeads through different chemistries[183]. On the contrary, Figure 8.D shows a negative correlation (R^2 = 0.932) between the specific activity of the immobilized enzymes and their normalized anisotropy values. Hence, our findings support those inverse correlations between activity and stability often found when comparing different immobilization protocols, is related with rotational mobility (anisotropy) of the immobilized enzyme. Single-molecule studies provided direct evidence that come to the same conclusion; the activity and the stability of immobilized enzymes must be balanced by controlling the extent of the enzyme attachment[184].

4.3.5. Operational performance of the different immobilized biocatalysts in batch

In order to select the optimal carrier to immobilize ADH1 for its application in the regio-selective oxidation of 1,ω-diols, the three immobilized preparations previously characterized were incubated with a NAD$^+$ enzymatic recycling partner for the oxidation of 1,5-pentanediol to 5-hydroxy pentanal using catalytic amounts of the cofactor. First, we tested two putative recycling cofactor systems: one involving a His-tagged NADH oxidase from *Lactobacillus pentosus* (LpNOX) immobilized on LdAG-Co^{2+}, and another one composed by NOX from Thermus thermophilus (NOX) and Catalase from bovine liver (CAT) co-immobilized on agarose porous microbeads functionalized with aldehyde groups (AG-G). Using a diol: NAD$^+$ molar ratio 1:10, we incubated ADH1 and the immobilized cofactor recycling systems in the same vessel to favor the in-situ cofactor recycling. After 24h, the NOX/CAT system consumed close to 90% of the diol, nevertheless the recycling system based on immobilized LpNOX only reached a conversion of 50% (**Figure 4.9**).
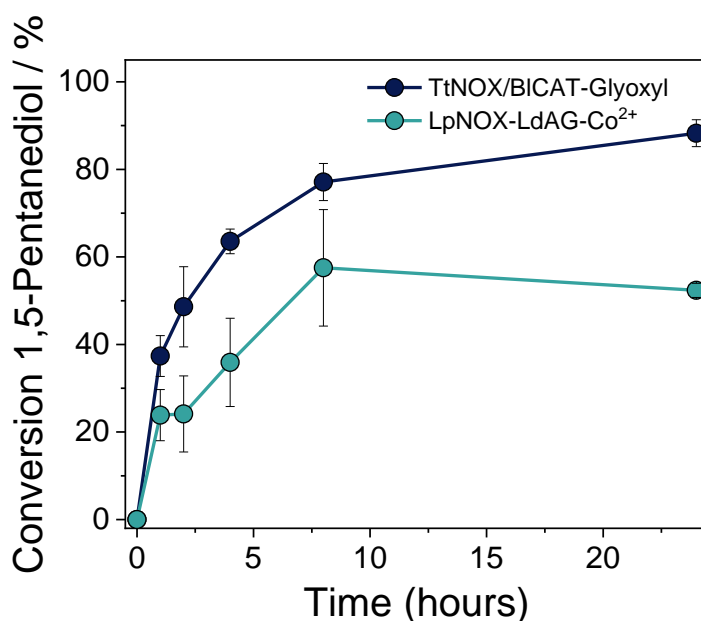
Figure 4.9: Oxidation of 1,5-pentanediol catalyzed by immobilized His-ADH1 on EziG1mixed with two different regenerator systems: NOX/CAT immobilized on Glyoxil and LpNOX immobilized on LdAG-Co^{2+}. Reactions were carried out at 20 mM of 1,5-Pentanediol and 1 mM of soluble NAD+ in 50 mM Tris-HCl buffered solution 50 mM pH 8 at 30°C for at 24 hours.

The superior performance of NOX/CAT system might be explained by the 40% higher catalytic efficiency of immobilized NOX compared to the immobilized LpNOX (Table 4.4).

Table 4.4: Immobilization parameters of regeneration systems.

Porous carrier	Enzyme	Load (mg/g)	ΨA (%)[a]	iA (U/g)[b]	RA (U/g)[c]	rRA (%)[d]	Km[e]	Vmax[e]
Glyoxil	NOX	0.26	85	8.5	0.57	6.66	1.29 ± 0.18	2.19 ± 0.19
	CAT	8.9	93	9300	615	6.6	-	-
LdAG-Co^{2+}	LpNOX	0.82	95	9.5	0.95	10	0.9 ± 0.01	1.11 ± 0.04

[a]Immobilization yield, ΨA = (immobilized activity/offered activity) x 100. [b]Immobilized activity (iA) (U x g^{-1}) = Offered activity per gram of carrier x (ΨA/100). [c]Recovered activity (RA) (U x g^{-1}) means the activity measured upon the immobilization protocol. [d]Relative recovered activity (rRA) (%) = (RA/iA) x 100 [e]Kinetic parameters were calculated through fitting the experimental data with the Michaelis-Menten equation using Origin Lab 10.

Hence, we selected the co-immobilized NOX/CAT systems to be coupled with the three immobilized preparations of ADH1 to further test their operational stability. Figure 4.10.A shows that all immobilized biocatalysts achieved 90% conversion of 1,5-pentanediol in the first cycle, majorly converting such diol into the 5-hydroxy pentanal (50-75% yield) and its corresponding lactol (33-14% yield) detected through HPLC and GC-FID (Annex 4.1 and 4.2), respectively.
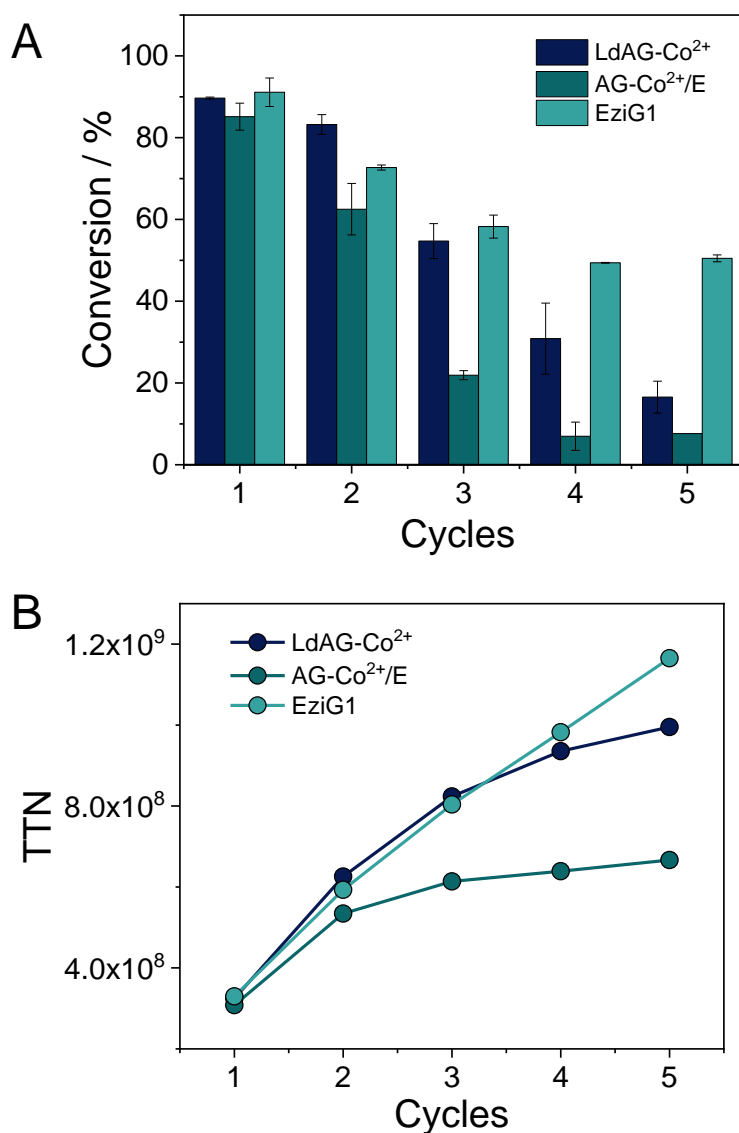
Figure 4.10: Chromatographic conversion(A)and enzyme total turnover number (TTN)(B)during the oxidation of 2s catalyzed by ADH1 immobilized on different carriers: LdAG-Co^{2+}(blue), AG-Co^{2+}/E (orange) andEziG1 (green) in consecutive batch reactors. Reactions were carried out at 20 mM of 2s and 1 mM of soluble NAD$^+$ in 50 mM Tris-HCl buffered solution pH 8 at 30°C. TTN was calculated as the sum of moles of 2s oxidized after each cycle by one mole of immobilized enzyme.

It is described that these two molecules are in equilibrium under reaction conditions[143]. Remarkably, the oxidation was practically regioselective towards only one of the hydroxy groups, as low yields (< 1.5%) of δ-valerolactone and none of the other overoxidized products (dialdehyde, 5-hydroxy pentanoic) were detected upon the enzymatic reaction (**Annex 4.1** and **Table 4.5**).

Table 4.4: Reactants concentration upon 24 hours of reaction in presence of different assembled biocatalysts.

Biocatalyst (carrier)	[1,5-Pentanediol] (mM)[a] / (%)[b]	[Lactol] (mM)[a] / (%)[c]	[δ-varelolactone] (mM)[a] / (%)[c]
LdAG-Co^{2+}	2.06 ± 0.05 / 10	5.71 ± 0.37 / 28.5	0.09 ± 0.04 / 0.5
AG-Co^{2+}/E	2.97 ± 0.66 / 15	6.56 ± 0.86 / 32.8	0.13 ± 0.10 / 0.7
EziG1	1.77 ± 0.70 / 9	2.89 ± 0.46 / 14.4	0.24 ± 0.08 / 1.2

Reaction condition: 20 mM 1,5-Pentanediol, 1 mM NAD$^+$, 0.15 mM FAD in buffer Tris-HCl 50 mM at pH 8. [a]Concentration substrate: Quantity values were determined applying calibration curve previously obtained. [b]Conversion = ([Diol]24 h /[Diol]0 h) x 100. [c]Yield = ([Lactol or lactone]24 h /[Diol])) x 100.

However, ADH1 immobilized on both AG-Co^{2+}/E and LdAG-Co^{2+} experienced a steady decrease in their productivity after the second batch cycle. In contrast, the enzyme immobilized on EziG1 kept a productivity close to 50% after 5 reaction cycles. This higher operational stability was manifested in a 2 and 1.2 higher accumulated enzyme TTN (defined as the moles of 1,5-pentanediol oxidized per mol of tetramerADH1) after 5 reaction cycles and in comparison, with the enzyme immobilized on AG-Co^{2+}/E and LdAG-Co^{2+} respectively (**Figure 4.10.B**). When we studied the leaching of ADH1 from the carriers, we observed that the enzyme remains in the resins AG-Co^{2+}/E and EziG1 upon their incubation under denaturing conditions for SDS-PAGE analysis (**Figure 4.2**), entailing that 100% of the protein remained bound to AG-Co^{2+}/E and EziG1 after 5 batch operational cycles. On the contrary, the operational conditions were sufficient to cause the quantitative lixiviation of the enzyme from the resin LdAG-Co^{2+} (**Figure 4.11**).
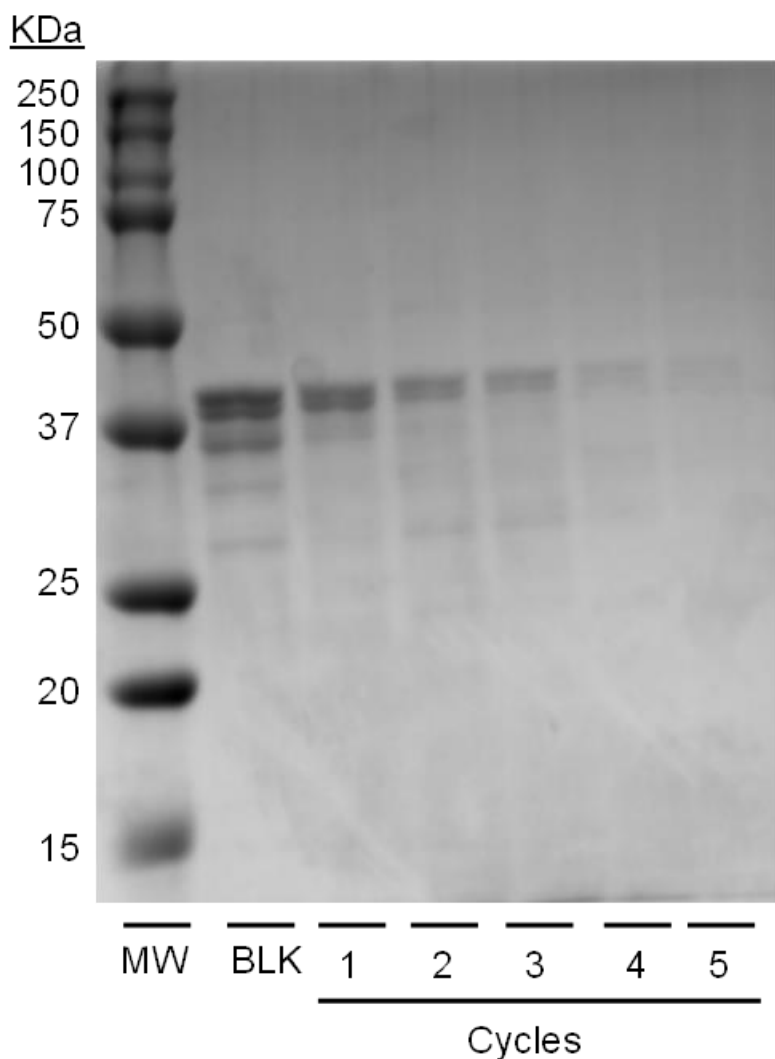
Figure 4.11: SDS-PAGEs gel to analyze the enzyme lixiviation of His-ADH2 immobilized on LdAG-Co^{2+} after several operational cycles. MW: Molecular weight markers (BioRad Precision Plus Protein All Blue Standard); BLK: Eluted His-ADH1 from LdAG-Co^{2+} before the operational cycle and after each 24 hour reaction cycle.

In the light of these data, we suggest that the operational inactivation of ADH1 immobilized on LdAG-Co^{2+} is mainly caused by the enzyme lixiviation. In contrast the enzymes immobilized on AG-Co^{2+}/E on EziG seems to be operationally inactivated through structural distortion, rather than through enzyme leaching after each reaction cycle. Similar negligible enzyme leaching was observed for other His-tagged enzymes immobilized as protein-inorganic hybrids (Ashok et al., 2018).

Remarkably, the accumulated TTN after re-using the immobilized enzyme in EziG1 reached values as high as 4 x10^5 one of the highest values ever reported for an immobilized alcohol dehydrogenase[185]. In comparison to the TTN estimated for upscaled selective oxidation of lactols using a soluble ADH/NOX system (Bartsch et al., 2020), the herein reported heterogeneous biocatalyst presents 1 order of magnitude higher TTN for the oxidation of 1,ω-

diols to their corresponding lactols. It is worth mentioning that the most robust and efficient heterogeneous biocatalysts under operational conditions (ADH1 immobilized on EziG) was not the most thermostable one. On the contrary the most thermostable heterogenous biocatalyst (ADH1 immobilized on AG-Co^{2+}/E) was the least productive and stable operationally. This divergence between thermal and operational stability might rely on the different inactivation mechanisms triggered during either the thermal shock (in absence of substrates) or the batch oxidation process (in presence of substrate and cofactor). A similar divergence has been reported for a pyruvate aldolase thermostabilized through directed evolution[186].

The excellent immobilization parameters, the structural integrity, the high thermal and operational stability and the high accumulated TTN of His-ADH1 immobilized on EziG1 led us to select this heterogeneous biocatalyst for its application in the oxidation of a battery of different diols, employing the co-immobilized NOX/CAT NAD$^+$ recycling system (**Figure 4.12**).

To that aim, we evaluated the substrate conversion, the enzyme productivity, and the volumetric productivity of this heterogeneous multi-enzyme system towards the oxidation of five different 1,ω-diols (). As expected, the system achieved the oxidation of linear aliphatic 1,ω-diols, but failed to convert branched and etherified 1,ω-diols. The immobilized His-ADH2 oxidizes the 5 and 6 carbon 1,ω-diols more rapidly than the shorter ones.

Figure 4.12: [a]Enzymatic productivity = μmol substrate x μmol enzyme^{-1} x hour -1. [b]Productivity = mg x L^{-1} x d^{-1} [c]Productivities were determined after 24 h at 30°C. [b]250 rpm. shaking. All reaction mixtures consisted in substrate 20 mM, NAD$^+$ 1 mM in Tris-HCl 50 mM at pH 8.
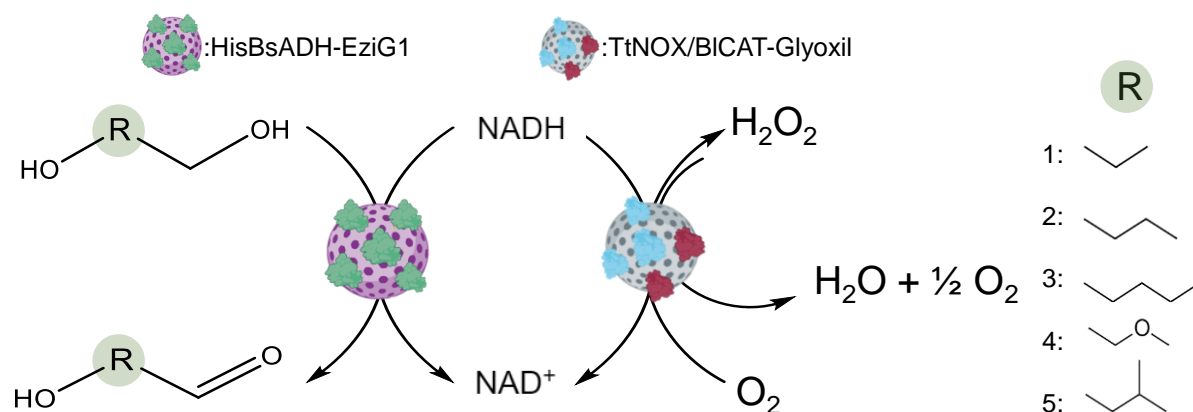
Substrate	Product	Enzymatic productivity	Productivity[b,c]
1s	2p	2641 ± 294	743 ± 52
2s	2p	3268 ± 690	1021 ± 230
3s	3p	2292 ± 382	1027 ± 187
4s	4p	0	0
5s	5p	0	0

4.4. Conclusions

In this study, we have screened a battery of porous carriers and immobilization chemistries to enhance the robustness of a His-tagged variant of ADH1. Through characterizing the activity and structural changes undergone by the enzyme upon the immobilization, we reveled the impact of the different immobilization protocols on the enzyme properties. While the irreversible attachment of ADH1 to agarose microbeads functionalized with cobalt-complexes and epoxides (AG-Co^{2+}/E) enhances the enzyme thermal stability, such immobilization protocol yields a less operationally stable biocatalyst. On the contrary when the enzyme was immobilized on glass-based carriers functionalized with iron-complexes (EziG1), its thermal stability was lower, but the heterogeneous biocatalyst was surprisingly more stable under operation conditions. This latter heterogeneous biocatalyst was successfully mixed with a NADH oxidase and a catalase co-immobilized on a different porous carrier to selectively oxidize 1,ω-diols, integrating an *in situ* NAD$^+$ recycling system in batch. This immobilized multi-enzyme systems could be recycled up to 5 cycles, retaining more than 50% of its initial conversion. Finally, we tested the substrate scope of ADH1 immobilized on EziG1, proving the versatility of this enzyme towards the oxidation of linear aliphatic 1,ω-diols. This work illustrates how the optimization of a heterogeneous biocatalyst must be accompanied by its functional and structural characterization. Remarkably, the determination of the anisotropy exhibited by the fluorophore-labelled and immobilized enzymes is revealed as a very informative parameter that unveils an activity/stability trade-off that depends on the structural dynamics of the

immobilized enzyme. The optimization and characterization pathway herein reported will surely help to rationalize new immobilization protocols to fabricate more active and robust immobilized biocatalysts.

CHAPTER 5:

5.1. Introduction

Enzyme coimmobilization is a recurrent strategy to solve some of the drawbacks presented in multistep biocatalysis by providing a suitable compartmentalized microenvironment, spatially organized, that increase cascade efficiency, easing reaction workups, enabling the biocatalyst reutilization and mass transport substrates among enzymes. However, the coimmobilization of two or more enzymes on the same support is not trivial as one immobilization strategy might be beneficial for one enzyme but detrimental for the others.

Heterofunctional supports emerge as an excellent solution to coimmobilize multienzyme systems on the same surface where each enzyme is attached to the support through its optimal immobilization chemistry. In this chapter, we have exploited and characterized porous supports functionalized with three reactive groups: metal chelates to site-directed immobilize His-tagged enzymes, cationic amines to ionically absorb them, and electrophile groups (aldehydes or epoxides) to promote their multivalent covalent attachment to the support surface (**Scheme 5.1A** and **B**). While the cationic amines and the metal chelates establish reversible bonds between the immobilized enzymes and the support surface, the electrophile ones do establish irreversible bonds that may avoid the enzyme leakage during the biocatalyst utilization. A similar trifunctional support was reported for the immobilization of a sole enzyme but never intended for the coimmobilization of a multienzyme system[187]. We immobilized a pall of six different enzymes on this trifunctional support and characterized their immobilization kinetics, stability, and structural rearrangements upon the immobilization process. To demonstrate the potential of this trifunctional support for the coimmobilization of multienzyme systems, we challenged it with a model system composed of three enzymes that orthogonally work to selectively oxidize 1,5-pentanediol into its corresponding lactol within situnicotinamide adenine dinucleotide (NAD^+) regeneration and H_2O_2 removal (**Scheme 5.1C**)[171]. Finally, we evaluated the stability and reusability of the coimmobilized enzyme preparations in a batch reactor operated for consecutive and discontinuous reaction cycles.
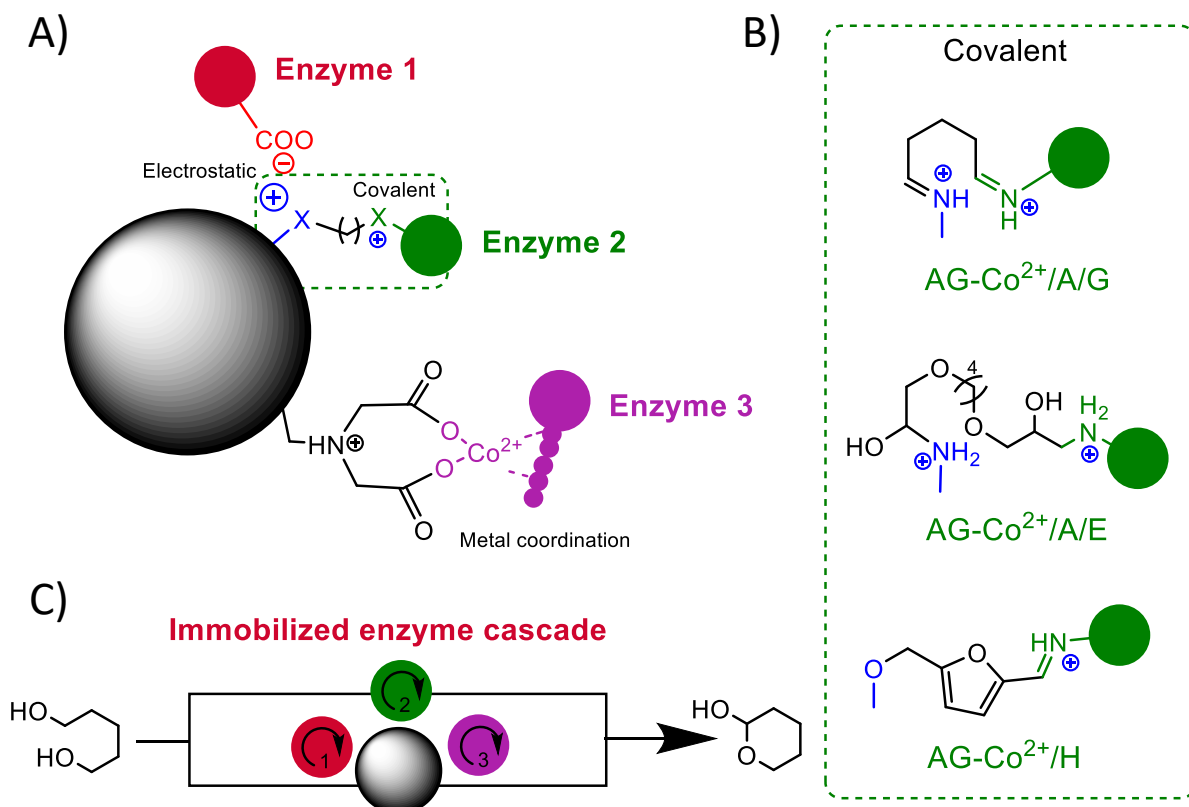
Scheme 5.1: A) Surface of a trifunctional support that coimmobilizes several enzymes through three different immobilization chemistries. B) Chemical scheme of the different electrophiles that covalently bind enzymes. C) One-pot oxidation of 1,5-pentanediol into 2-tetrahydropyranol catalyzed by a three-enzyme cascade coimmobilized on the trifunctional support described in panel A).

5.2. Experimental section

5.2.1. Materials

The enzymes alcohol dehydrogenase (ADH) from *Bacillus stearothermophilus* (ADH1), reduced nicotinamide adenine dinucleotide (NADH) oxidase from *Thermus thermophilus* HB27 (NOX), catalase from *Bordetella pertussis* (BpCAT), and the lactonase from *Sulfolobus islandicus* (LAC) were produced as previously reported.[20] Four percent cross-linked agarose (AG) beads (particle size 50–150μm; pore diameter 300nm) were purchased from Agarose Bead Technologies (Madrid, Spain); epoxy meth- acrylate microbeads ECR8204F (Pu) (particle size 150–300 μm; pore diameter 300–600 Å) so were kindly donated by Purolite; and Cellulose MT200 (particle size 100–250 μm; pore diameter 32 nm) was purchased from IONTOSORB (Usti and Labem, Czech Republic). Compounds such as ethylenediamine (EDA), imidazole, iminodiacetic acid, cobalt chloride, sodium periodate, sodium hydroxide fluorescein isothiocyanate (FITC), rhodamine B isothio- cyanate, sodium acetate, sodium chloride, sodium phosphate, sodium bicarbonate, glutaraldehyde (GA), SYPRO Orange Protein Gel Stain, 1,5-pentanediol, 5-hydroxypentanal, tetrahydro-2H-pyran-2-ol, δ- valerolactone, as well as the enzymes catalase from bovine liver (CAT) and alcohol dehydrogenase from horse liver (ADH2)

were acquired from Sigma-Aldrich Chemical Co. (St. Louis, IL). All other reagents were of analytical grade.

5.2.2. Preparation of tri-heterofunctional support activated with cobalt-chelates, secondary amine groups and aldehydes (AG-Co^{2+}/A/G)

For the first step we prepared epoxy-activated agarose (AG-E) as described elsewere[92]. Then, we activated the AG-E with iminodiacetic acid (AG-E/IDA) by preparing a suspension of 10 g ($\approx$ 14 mL) of AG-E in 100 mL of 1 M iminodiacetic acid at pH 11. The suspension was maintained under gentle agitation at 200 rpm for 1h at room temperature (RT). Afterwards, the support was filtered and rinsed with 10 volumes of water. Once AG-E/IDA was obtained, we introduced amino groups by incubating it over night with 10 volumes of 1 M ethylenediamine at pH 11 (AG-A/IDA) under gentle agitation at 200 rpm at room temperature. Later, the support was filtered and gently rinsed with water. Then, the introduction of aldehyde moieties was conducted by incubating the support over night with 25% glutaraldehyde solution in 200 mM sodium phosphate buffer pH 7 (AG-IDA/A/G) under gentle agitation at 200 rpm at room temperature. Once the incubation concluded, the support was filtered and washed with at least 10 volumes of water. Finally, to introduce the metal group, the support was incubated with 10 volumes of 30 mg·mL^{-1} CoCl$_2$ during 2h at room temperature (AG-Co^{2+}/A/G). At the end, the support was filtered and washed with abundant water and stored at 4°C protected from light (**Figure 5.1**).
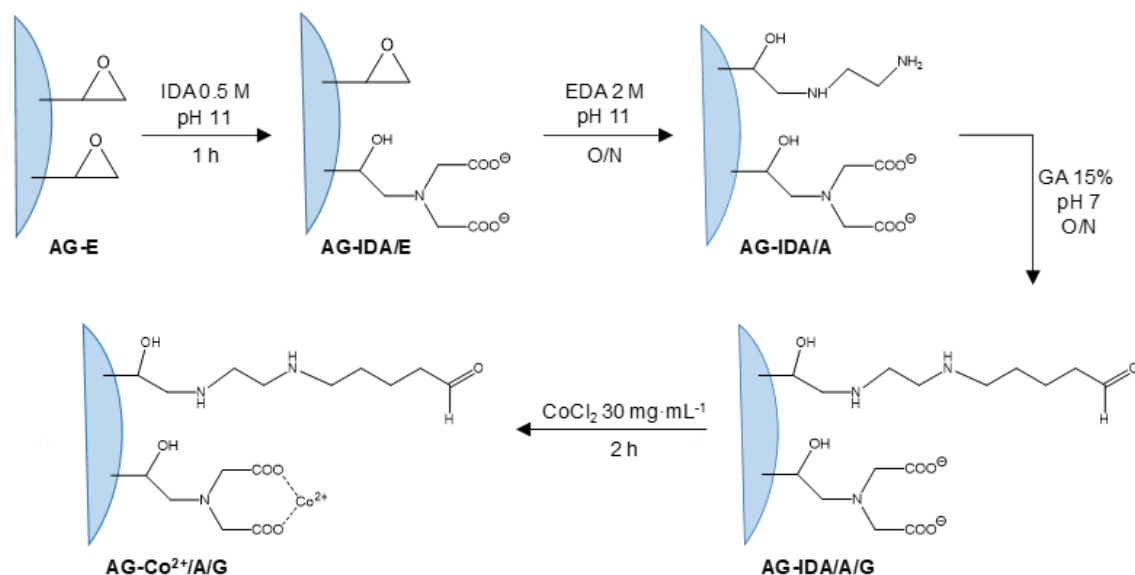
Figure 5.1: Preparation pathway of AG-Co^{2+}/A/G.

5.2.3. Preparation of tri-heterofunctional support activated with cobalt-chelates, secondary amine groups and epoxides (AG-Co^{2+}/A/E)

1 volume of AG-A/IDA was suspended in 20 volumes of 0.4 M 1,4-butanediol diglycidyl ether (BD), 12% acetone in 80 mM bicarbonate buffer pH 9 and incubated overnight under gentle

agitation at 200 rpm at room temperature. Once the incubation concluded, the support was filtered and washed with at least 10 volumes of 20% acetone in water, and then with only water. Finally, to introduce the metal group, the support was incubated with 10 volumes of 30 mg·mL^{-1} CoCl$_2$ during 2h, at room temperature (AG-Co^{2+}/A/E). At the end, the support was filtered and washed with abundant water and stored at 4°C protected from light (**Figure 5.2**).
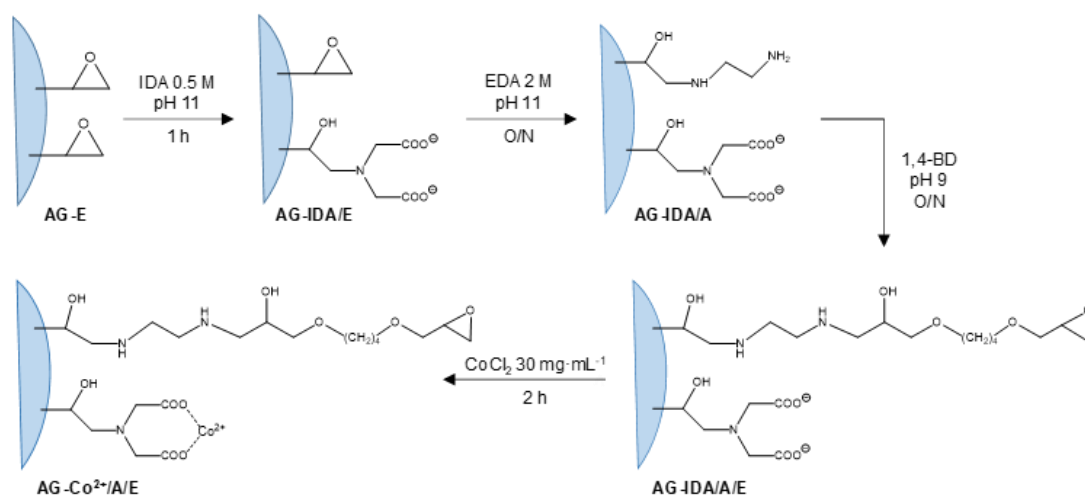
Figure 5.2: Preparation pathway of AG-Co^{2+}/A/E.

5.2.4. Preparation of bi-heterofunctional support activated with cobalt chelates and hydroxymethyl furfural AG-Co^{2+}/H

1 volume of AG-E/IDA was suspended in 10 volumes of 100 mM hydroxymethylfurfural (HMF), in 100 mM sodium phosphate buffer pH 8 and incubated overnight under gentle agitation at 200 rpm at RT (AG-H/IDA). Once the incubation concluded, the support was filtered and washed with at least 10 volumes of water. Finally, to introduce the metal ligand, the support was incubated with 10 volumes of 30 mg·mL^{-1} CoCl$_2$ during 2h, at room temperature (AG-Co^{2+}/H). At the end, the support was filtered and washed with abundant water and stored at 4°C protected from light (**Figure 5.3**).
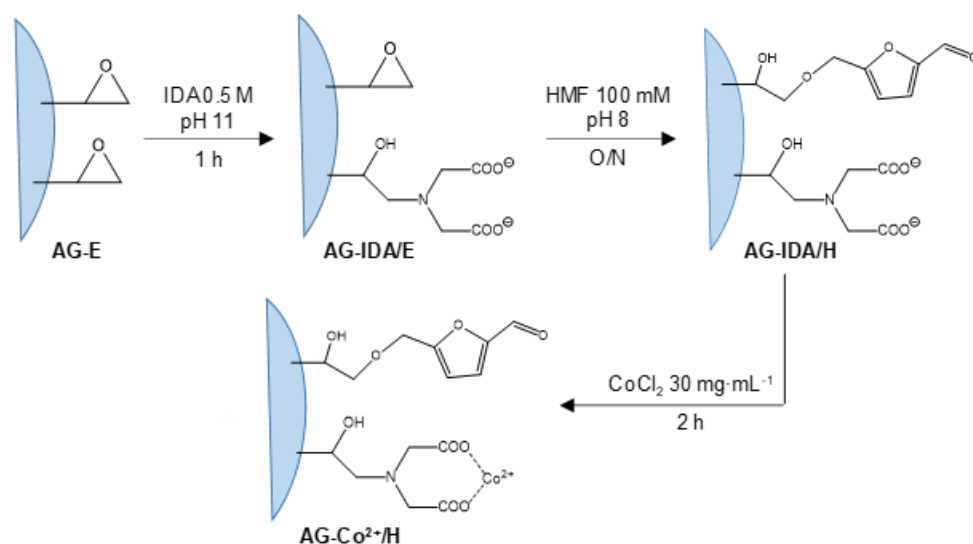
Figure 5.3: Preparation pathway of AG-Co^{2+}/A/H.

5.2.5. Preparation of tri-heterofunctional supports CEL-Co^{2+}/A/G and Pu-Co^{2+}/A/G

The functionalization of cellulose-microbeads (CEL) and polymethacrylate-microbeads (Pu) were done following the same activation protocol to prepare AG-Co^{2+}/A/G but replacing AG by CEL (CEL-Co^{2+}/A/G) or Pu microbeads (Pu-Co^{2+}/A/G). While the Pu microbeads are commercially supplied with epoxides (ECR8204F), cellulose was activated with the epoxy groups following the same protocol as for agarose[92].

5.2.6. Degree of activation of the supports

5.2.6.1. Epoxy groups quantitation

NaIO4 as described elsewhere[188]. Briefly, 1 g of the support was incubated with 10 mL of 0.5 M H_2SO_4 for 2h at room temperature to hydrolyze the epoxy groups. Afterwards, the hydrolyzed carrier (yielding vicinal diols) was oxidized with 20 mM NaIO$_4$ (1:10 suspension) by incubation at room temperature (typically 1-2 hours). The number of epoxy groups was calculated by the difference in NaIO$_4$ consumption between the hydrolyzed support and the initial epoxy support. Different consumption degree of periodate was quantified by titration with potassium iodide (KI). Briefly, 20 μL of remnant NaIO$_4$ in the supernatant were mixed with 200 μL of 10% KI in saturated bicarbonate solution and measuring the absorbance at 405nm.

5.2.6.2. IDA groups quantitation

IDA groups were indirectly quantified following the same hydrolysis procedure as for epoxy groups quantitation but hydrolysing both AG-IDA/E and AG-E with H_2SO_4 for 2h at room temperature to hydrolyze the epoxy groups. Once epoxy groups were hydrolyzed, the formed diols were measured by oxidative titration with NaIO$_4$. IDA groups were calculated as the

difference in NaIO$_4$ consumption of hydrolyzed both AG-E (before IDA groups introduction) and AG-IDA/E. The consumption of periodate was spectrophotometrically measured by titration with KI as previously described.

5.2.6.3. Amino groups quantitation

Introduced amino groups were quantified by titration with picrylsulfonic acid[189]. Briefly, 0.25 mL of picrylsulfonic acid solution (5% w/v) diluted 500 times in 100 mM sodium bicarbonate buffer pH 8.5 (Cat. P2297 Sigma-Aldrich) were mixed with 0.5 mL of a suspension 1:10 of AG-IDA/A in 100 mM sodium bicarbonate buffer pH 8.5. The mixture was incubated at 37°C during 2h with gentle mixing. Afterwards, the support was washed 4 times with 0.75 mL of 1 M NaCl followed by 5 washes of 0.75 mL of distilled water. The washed support was resuspended 1:10 in distilled water to measure the absorbance of 200 µL at 335nm against a support control without amino functionalization (AG-IDA/E). Calibration curve of ethylenediamine (linear range 0.03 − 0.25 mM) was also prepared under the same conditions. Micrographs of the picrylsulfonic activated AG-IDA/E were acquired by placing 100 µL of a 1:20 water suspension of the support in a 96-well clear microplate and visualized in bright field mode in a Cytation5 Cell Imaging Reader (BioTek Instruments) (**Figure 5.4.A**).
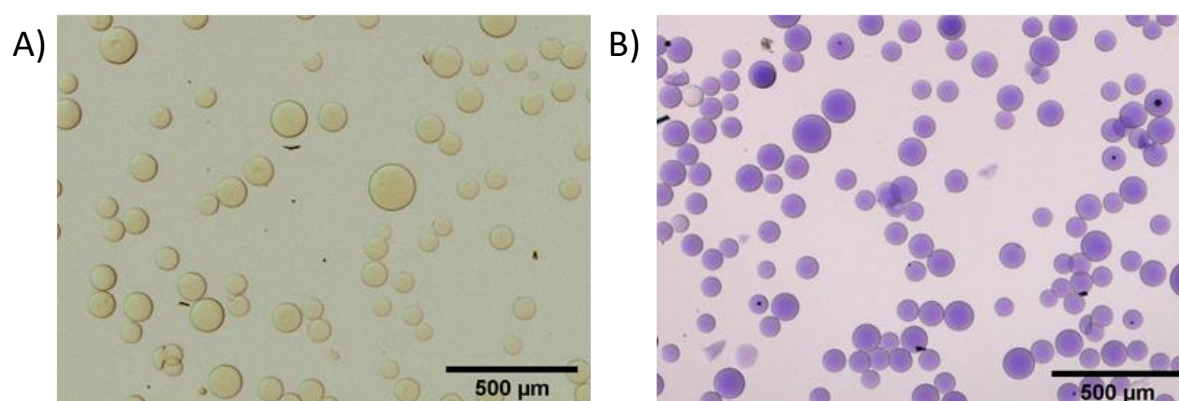
Figure 5.4: Distribution of agarose-activated microbeads with different functionalities. A) AGA/IDA. B) AG-A/G/IDA.

5.2.6.4. Aldehyde groups quantitation

Aldehyde functionalization with glutaraldehyde was quantified by titration with Schiff's reagent[190]. Briefly, 20 µL of Schiff's reagent (Cat. 1.09034 Sigma-Aldrich) were mixed with 200 µL of a suspension 1:10 of AG-Co^{2+}/A/G in distilled water. The mixture was incubated at room temperature during 30min with gentle mixing. Later the support was washed 4 times with 0.5 mL of 1 M NaCl followed by 5 washes of 0.5 mL of distilled water. The washed support was resuspended 1:10 in distilled water in order to measure the absorbance of 100 µL at 570 nm against a support control without GA activation (AG-IDA/A). Calibration curve of glutaraldehyde (linear range 0.15 − 2.5 mM) was also prepared under the same conditions.

Micrographs of the Schiff activated AG-IDA/A were acquired by placing 100 µL of a 1:20 suspension of the support in water and visualized in a bright field mode in a Cytation5 Cell Imaging Reader (BioTek Instruments) (**Figure 5.4.B**).

5.2.6.5. HMF groups quantification

Agarose functionalization with HMF was spectrophotometrically quantified by a using a HMF calibration curve (linear range 0.19 mM − 1.56 mM). To properly determine the calibration curve, we measured the absorbance of 200 µL of a suspension (1:20) of AG-IDA/H or AG incubated with different concentrations of HMF in water at 285nm in a Microplate Reader Epoch 2 (BioTek Instruments).

5.2.6.6. Enzyme immobilization

The immobilization was conducted by mixing 10 mL of enzyme solution (in 100 mM sodium phosphate buffer pH 7) with 1 g of support (AG-Co^{2+}/A/G or AG- Co^{2+}/A/E or AG-Co^{2+}/H). The suspension was maintained under gentle agitation at 25 rpm at 4°C. The immobilization course was followed by measuring the activity for both the supernatant and the suspension. Once the immobilization was completed (typically 30 minutes), the immobilization mixture was incubated for 2h at 25 rpm and 4°C to promote the formation of multivalent attachment between the nucleophiles on the enzyme surface (mainly Lys) with the either the aldehydes or the epoxide of the carrier surface. Subsequently, a blocking step was done by addition of glycine (1 M pH 8) followed by soft agitation over night at 25 rpm and 4°C. Once the carrier was blocked, the immobilized sample was washed 5 times with 5 volumes of 25 mM sodium phosphate buffer pH 8, filtered and stored at 4°C.

5.2.6.7. Enzyme co-immobilization

Enzyme co-immobilization was conducted following the same methodology previously described but incorporating the enzymes in two different orders. For the sequential immobilization, 10 mL of NOX in 100 mM sodium phosphate buffer at pH 7 were firstly incubated with 1 g of AG-Co^{2+}/A/G during 2h at 25 rpm and 4°C. Afterwards, the suspension was filtered and 10 mL of a solution of CAT in the same buffer was added, followed by incubation for 2h at 4°C and 25 rpm. Later, the suspension was filtered again and 10 mL of ADH1 in the same buffer were added and incubated for 2 more hours at 4°C and 25 rpm. Then, the suspension was filtered and incubated overnight at 4°C and 25 rpm with 1 M glycine at pH 8 to block the remaining aldehyde groups. Finally, the biocatalyst was filtered ad washed with 25 mM sodium phosphate buffer pH 7 and stored at 4°C.

5.2.7. Enzyme activity assays

Enzyme activities were spectrophoto- metrically measured in transparent 96-well microplates with a flat bottom (Nunc), employing a Microplate Reader Epoch 2 (BioTek Instruments) provided with the software Gen5.

5.2.7.1. ADH Activity.

200 μL of a reaction mixture containing 10 mM of 1,5-pentanediol and 1 mM of NAD^+ in sodium phosphate buffer at pH 8 were incubated with 5 μL of enzymatic solution or 10 μL of suspension (properly diluted) at 30°C. The increase in the absorbance at 340nm due to the reduction of NAD^+ was recorded. One unit of activity was defined as the amount of enzyme that was required to reduce 1 μmol of NAD^+ to NADH per minute at the assayed conditions.

5.2.7.2. NADH Oxidase Activity

200 μL of a reaction mixture containing 0.2 mM of NADH and 150 μM of flavin adenine dinucleotide (FAD^+) in 50 mM sodium phosphate buffer pH 8 at 30°C were incubated with 5 μL of enzymatic solution or 10 μL of suspension (properly diluted) at 30°C. The oxidation of NADH was monitored as a decrease in the absorbance at 340nm. One unit of activity was defined as the amount of enzyme that was required to oxidize 1 μmol of NADH to NAD^+ per minute at the assayed conditions.

5.2.7.3. Catalase Activity.

200 μL of a reaction mixture containing 35 mM of hydrogen peroxide in 100 mM sodium phosphate pH 8 at 30°C were incubated with 5 μL of the enzymatic solution or 10 μL of suspension (adequately diluted). The catalase activity was measured by recording the decrease in the absorbance at 240nm. One unit of CAT activity was defined as the amount of enzyme required for the disproportionation of 1 μmol of hydrogen peroxide per minute at the assessed conditions.

5.2.7.4. Lactonase Activity.

Lactonase activity was indirectly monitored by the decrease in the pH triggered by the formation of 5- hydroxypentanoic acid from its corresponding lactone hydrolysis. Briefly, 200 μL of a reaction mixture containing 1 mM δ- valerolactone, 0.1% acetonitrile, and 0.25 mM p-nitrophenol in 2.5 mM sodium phosphate buffer at pH 7 was incubated with 5 μL of enzymatic solution or 10 μL of suspension (properly diluted) at 30°C. The decrease in the absorbance of p-nitrophenol (pH indicator) at 410nm was recorded. One unit of activity was defined as the amount of enzyme that was required to produce 1 μmol of 5- hydroxypentanoic acid (titrated by pH change) per minute at the assayed conditions.

5.2.8.   Thermal inactivation

Thermal inactivation kinetics of the biocatalysts were conducted by incubating a solution or a suspension of the free or immobilized enzymes in 100 mM sodium phosphate buffer pH 8.0 at the indicated temperature until more than 50% of the initial activity was lost. To calculate half-life times, the obtained experimental measurements were adjusted to a three-parameter biexponential kinetic inactivation model[177]. Additionally, we deter- mined the thermal denaturation temperature (Tm) of the biocatalysts by fluorescent thermal shift assay. Briefly, 25 µL of 1 µM enzyme solution or suspension in 25 mM sodium phosphate buffer pH 8 containing 5 µL 60× of SPYRO Orange Protein Gel Stain was placed into a 200 µL clear thin-wall polypropylene eight-tube strip for polymerase chain reaction (PCR). The protocol was set with a temperature analysis range from 25 to 95°C in 1h, recording the fluorescence in a CFX Real-Time PCR system (Bio-Rad). Raw fluorescence data were analyzed to determine the denaturation temperature (Tm) from nonlinear fitting of thermal denaturation data[191] employing OriginLab software.

5.2.9.   Protein labeling with fluorescent probes

Fluorescent labeling was done accordingly with a methodology reported elsewhere[175]. An enzyme solution (typically 0.25 mg·mL−1) in 100 mM of sodium bicarbonate buffer at pH 8.5 was mixed (1:10 molar ratio) with either rhodamine B isothiocyanate or fluorescein isothiocyanate (FITC) in dimethyl sulfoxide (DMSO) (5 mg·mL^{-1}) and incubated 1h with gentle agitation at 25°C in darkness. Afterward, the remaining fluorophore was eliminated by dialysis through a centrifugal filter unit (cutoff of 10 kDa) with 25 mM sodium phosphate buffer pH 8.0.

5.2.10. Confocal laser scanning microscopy (CLSM) imaging

The distribution of immobilized fluorophore-labeled proteins was analyzed with a confocal microscope Espectral ZEISS LSM 510 with an excitation laser (λ_{ex}: 561 nm) and emission filter (LP575). Confocal imaging was carried out at both 20× and 40× (water, 1.2 NA) objectives and a 1:200 (w/v) buffered suspension in 25 mM phosphate at pH 7. The resulting micrographs were analyzed with FIJI[176] using an image analytical routine previously reported[192]. From confocal images, we obtained an average and normalized fluorescence radius profile, using FIJI software and its plugin module for radial profile generation (developed by Paul Baggethun). Subsequently, a Gaussian fit was applied to the obtained profiles of at least 10 single beads. Subsequently, we searched for the fitted data point that corresponds to 50% of the maximum normalized fluorescence fitted peak (yFWHM), and the corresponding radius coordinate (xFWHM) to that data point was then subtracted from the radius (R) of the analyzed bead to finally obtain the full width at half-maximum (FWHM), which means the infiltration distance of the enzyme into the bead surface. Dividing this infiltration distance between the radius size, we obtained the relative infiltration distance.

5.2.11. Fluorescence Anisotropy

The polarized fluorescence of immobilized samples loaded with 0.5 mg of FTIC-labeled enzymes was measured to determine the fluorescence anisotropy of FTIC conjugated to the free and immobilized proteins. To calculate the anisotropy values, 3.5 ng of either free or immobilized enzymes was placed into a 96-well dark plate and measured in a Microplate Reader Synergy H1, BioTek. Anisotropy values were obtained following the methodology described elsewhere[171].

The anisotropy values of all immobilized samples were normalized to the anisotropy of the free enzyme. Values higher than one mean enzymes with higher rotational tumbling than the free enzyme, while values lower than one mean enzymes with lower rotational tumbling than the free enzyme.

5.2.12. Intrinsic fluorescence of aromatic residues

Immobilized biocatalysts loading 0.5 mg of protein·g$_{support}^{-1}$ were used for this experiment. The intrinsic fluorescence of free and immobilized His-ADH1 was measured before and after the samples were incubated at 80°C for 1h. To that aim, 70 µg of either free or immobilized enzymes was placed in a 96-well dark plate and the fluorescence emission spectra were recorded between 300 and 500nm upon the sample excitation at 280nm, using emission bandwidths of 5 nm. All spectroscopic measurements were performed in 25 mM phosphate buffer at pH 7.

5.2.13. Batch reactions and recycling of co-immobilized enzymes

50 mg of heterogeneous biocatalyst were placed inside a capped plastic tube (2 mL) containing 300 µL of a reaction mixture consisted in 20 mM 1,5-pentanediol, 1 mM NAD^+, 0.15 mM FAD^+ in 200 mM sodium phosphate buffer pH 8 allowing atmospheric oxygen supplementation by punching the tap with an open needle. Reactions were incubated at 30°C at 250 rpm inside an orbital incubator. The reaction course was monitored by withdrawing samples at periodic intervals which were analyzed by chromatographic methods.

5.2.14. Analytical measurements

5.2.14.1. Gas chromatography

Prior to GC analysis, 50 µL of the reaction sample was mixed with 200 µL of ethyl acetate to perform a liquid–liquid extraction of the compounds of interest containing 2 mM eicosane as the external standard. After the extraction, 30–50 mg of anhydrous $MgSO_4$ was added to dry samples before GC analysis. Gas chromatography analyses were carried out in an Agilent 8890 GC system chromato- graph using a J&W HP-5 GC column (30m × 0.32mm × 0.25µm), helium as the support gas, and equipped with a flame ionization detector (FID). The injector was set at 280°C and the FID at 300°C. Separation of extracted compounds in ethyl acetate was done by

the following temperature program: the initial temperature at 60°C, maintained 2min, ramp to 160°C at a rate of 10°C·min^{-1}, ramp 2– 240°C at a rate of 20°C·min^{-1} and finally maintained 4min.

5.2.14.2. *High performance liquid chromatography (HPLC) analysis*

5-Hydroxypentanal was quantified by HPLC through derivatization into its corresponding O-benzylhydroxylamine derivative[180]. Briefly, 10 µL of aqueous reaction sample (0.6–20 mM) was mixed with 50 µL of O-benzylhydroxylamine hydrochloride (130 mM in pyridine/methanol/water 33:15:2) and incubated for 5 min at 25 °C. Afterward, 500 µL of methanol was added and then centrifuged 5min at 13450g. HPLC analysis was conducted in an Agilent Technologies 1260 Infinity II chromatograph equipped with a Poroshell EC-C18 column (4.6mm × 100mm x 2.7µm). Samples were detected at 215nm and were eluted at 1 mL·min^{-1} flow rate employing two mobile phases: phase A composed of trifluoroacetic acid 0.1% in water and phase B composed of trifluoroacetic acid 0.095% in 4:1 acetonitrile/water. Elution conditions: 10–100% of B over 30 min, followed by 10 min to recover the initial conditions. The retention time of O-benzylhydrox- ylamine derivatized 5-hydroxypentanal was 14.4min.

5.3.   Results and Discussion

5.3.1. Support functionalization

Ideally, an heterofunctional support should enable the efficient co-immobilization of different enzymes through chemistries that improve the overall properties of the multi-enzyme system. Inspired by a previously described tri-heterofunctional support exploited for the immobilization of single enzymes[187], we also functionalized porous agarose microbeads with cobalt-chelates to site-directed immobilize His-tagged enzymes, with positively charged secondary amines to ionically absorbed negatively charged enzymes and electrophile groups (aldehyde and epoxide) to react with the nucleophile residues at the enzyme surface. These three reactive groups should allow the immobilization of three different enzymes through three different chemistries (Figure I) comprised in a two steps enzyme immobilization process: a first and fast enzyme adsorption followed by a covalent enzyme binding.

As support, we selected 4BCL porous agarose microbeads (300nm average pore size and 90-150µm bead diameter), which have a suitable pore diameter for the immobilization of enzymes, a suitable particle size for the use of the heterogeneous biocatalysts in both batch and flow reactors, and a great versatility to be functionalized with a plethora of reactive groups[193]. We first functionalized agarose microbeads with epoxy groups (AG-E)[194], and then AG-E was incubated with iminodiacetic acid (IDA) to generate the bifunctional support containing epoxy and IDA groups (AG-IDA/E) (**Figure 5.1**). The degree of IDA functionalization is easily controlled by the pH and the incubation time (**Table 5.1**).

Table 5.1: Activation degree of agarose-microbeads 4 BCL

IDA (mM)	pH	Incubation Time (h)	Activation degree (μmol·g^{-1})	
			IDA	Epoxy
500	11	0.5	22.2	16.5
500	9	1	5.2	33.5
500	11	1	20.2	18.5
500	9	3	25.3	13.4
500	11	3	26.0	12.7

Total epoxy-groups after epichlorhydrin treatment = 38.7 μmol·g^{-1}
Total diols after epichlorhydrin treatment & H$_2$SO$_4$-hydrolysis = 82.2 μmol·g^{-1}

After this step, we introduced a 1:1 molar ratio of epoxy: IDA groups on the modified agarose surface (19 and 20 μmol·g^{-1}, respectively) (**Table 5.2**).

Table 5.2: Heterofunctional activation of agarose microbeads

Support	Step	Introduced functional group	Activation degree (μmol·g^{-1})
AG-Co^{2+}/A/G	1	Epoxy	19 ± 1.5
	2	IDA	20 ± 2.1
	3	EDA	12 ± 2.6
	4	GA	26 ± 3.5
AG-Co^{2+}/A/E	1	Epoxy	18 ± 1.5
	2	IDA	20 ± 2.1
	3	EDA	13 ± 1.8
AG-Co^{2+}/H	1	Epoxy	18 ± 1.5
	2	IDA	20 ± 2.1
	3	HMF	4.3 ± 0.7

Afterwards, we introduced the first target functionality, by incubating the AG-IDA/E with ethylenediamine (EDA), which converted the remaining epoxy groups into amine ones but maintaining intact the IDA ligands (AG-IDA/A). Then, the second functionality was introduced by incubating the AG-IDA/A with glutaraldehyde (G), a bifunctional agent, which reacts quantitatively with the primary amine of EDA, giving rise to a functionalized support with aldehyde and secondary amine groups (AG-IDA/A/G) (**Figure 5.1**). The functionalization of AG-IDA/A with primary amines and AG-IDA/A/G with aldehydes was confirmed by titration with picrylsulfonic acid and with the Schiff reagent, respectively (**Figure 5.4**). Optical microcopy images reveal that the functionalization of the agarose microbeads is uniform throughout their porous structure. Finally, we incubated AG-IDA/A/G with a cobalt chloride solution to form cobalt-chelates, which are the third functional group of the tri-functional support (AG-

Co^{2+}/A/G) (**Figure 5.1**). We found out that the functional groups are uniformly distributed over the porous surface of the agarose beads, enabling the enzymes to be potentially immobilized on any region (outer and inner) of the support particles. Apart from the aliphatic aldehydes, we also explored other two possible activation chemistries that functionalize the support with epoxy and aryl aldehydes (**Figure 5.1**). To that aim, we employed 1,4-butanediol diglycidyl ether to replace aldehyde groups of AG-Co2+/A/G by epoxide ones, yielding a heterofunctional support functionalized with cobalt, amino and epoxide groups (AG-Co^{2+}/A/E, **Figure 5.2**). On the other hand, we replaced GA and EDA by hydroxymethylfurfural, finally yielding an heterofunctional support functionalized with cobalt and aromatic aldehyde groups (AG-Co^{2+}/H, **Figure 5.3** and **Table 5.2**). After titration of epoxy, aldehydes, amine and cobalt chelates, the three supports were functionalized with different reactive groups in almost equimolar ratios per gram of support, and similar reactive group density but HMF, which its density was 3 times lower than the aldehydes and epoxy groups (**Table 5.2**). Detailed abbreviation of all the prepared supports is provided in supplementary **Table 5.3**.

Table 5.3: Abbreviation of the different prepared supports

Abbreviation	Functionalities	Matrix	Support description
AG-E	Mono-functional	Agarose	Epoxy activated agarose
AG-IDA	Mono-functional	Agarose	Iminodiacetic activated agarose
AG-IDA/E	Bi-functional	Agarose	Epoxy and iminodiacetic activated agarose
AG-IDA/A	Bi-functional	Agarose	Amino and iminodiacetic activated agarose
AG-IDA/A/G	Tri-functional	Agarose	Glutaraldehyde, amino and iminodiacetic activated agarose
AG-Co^{2+}/A/G	Tri-functional	Agarose	Glutaraldehyde, amino and cobalt activated agarose
AG-Co^{2+}/A/E	Tri-functional	Agarose	Epoxy, amino and cobalt activated agarose
AG-Co^{2+}/H	Bi-functional	Agarose	Hydroxymethylfurfural and cobalt activated agarose
Pu-Co^{2+}/A/G	Tri-functional	Methacrylate	Glutaraldehyde, amino and cobalt activated methacrylate
CE-Co^{2+}/A/G	Tri-functional	Cellulose	Glutaraldehyde, amino and cobalt activated cellulose

5.3.2. Enzyme immobilization on heterofunctional supports

We selected an enzyme panel to evaluate the immobilization efficiency on the three heterofunctional supports and the stabilization effects they promote on the immobilized enzymes. Herein, the enzyme panel studied is composed of an homotetrameric His-tagged alcohol dehydrogenase from Bacillus stearothermophilus (ADH1) a dimeric alcohol dehydrogenase from horse liver (ADH2), an untagged homodimeric NADH oxidase from Thermus Thermophilus HB27 [167, 195](NOX), an His-tagged homodimeric lactonase from

Sulfolobus islandicus (LAC)[196], an untagged tetrameric catalase from bovine liver (CAT)[197] and an His-tagged tetrameric catalase from Bordetella pertussis (BpCAT) which expresses both, higher specific activity and stability than CAT[197]. All enzymes were immobilized on the three heterofunctional supports in less than two hours.

Regardless the nature of the reactive groups displayed in the supports, His-tagged enzymes (as ADH1, BpCAT and LAC) were quantitatively immobilized, in contrast to the untagged ones (CAT, ADH2 and NOX), which achieved slightly lower immobilization yields (> 92 %) (**Table 5.4**).

Table 5.4: Single-enzyme immobilization parameters on different heterofunctional activated agarose microbeads.

Enzyme	Immobilization support	Enzyme load (mg·g^{-1})	Ψ (%) [a]	Recovered activity (U·g^{-1}) / (%) [b]	Half-life time (t$_{1/2}$) (h) [c]
ADH2	AG-Co^{2+}/A/G	0.47	100	0.42 (21)	0.51
	AG-Co^{2+}/A/E	0.47	100	0.58 (30)	0.85
	AG-Co^{2+}/H	0.47	100	0.37 (19)	0.42
ADH1	AG-Co^{2+}/A/G	1.52^d	99	0.24 (45)	54
	AG-Co^{2+}/A/E	1.54^d	100	0.25 (47)	21
	AG-Co^{2+}/H	1.51^d	98	0.22 (40)	26
NOX	AG-Co^{2+}/A/G	1.23	92	0.76 (8.1)	9.2
	AG-Co^{2+}/A/E	1.14	94	0.14 (1.3)	15.7
	AG-Co^{2+}/H	1.16	99	0.11 (1.1)	24.0
CAT	AG-Co^{2+}/A/G	0.54^d	96	12 (6.5)	4.4
	AG-Co^{2+}/A/E	0.52^d	92	8 (4.3)	4.0
	AG-Co^{2+}/H	0.55^d	98	11 (6.0)	3.4
BpCAT	AG-Co^{2+}/A/G	0.25	99	19 (22)	17.0
	AG-Co^{2+}/A/E	0.25	100	0 (0)	25.0
	AG-Co^{2+}/H	0.25	100	0.6 (0.7)	17.0
LAC	AG-Co^{2+}/A/G	0.43	100	0.18 (42)	7.4
	AG-Co^{2+}/A/E	0.43	100	0.05 (12)	4.7
	AG-Co^{2+}/H	0.43	100	0.09 (21)	6.4

[a]Immobilization yield, Ψ = (immobilized activity/offered activity) x100. [b]% Recovered activity is defined as the coefficient between the specific activity of the immobilized enzyme and the specific activity of the soluble one x 100. [c]Half-life time studies were assayed at different temperatures accordingly with each enzyme, thus 65°C for ADH1, 45°C for AHD2, 80°C for NOX, 40°C for BpCAT, 45°C for CAT, and 50°C for LAC. [d]Total protein content of semi-pure enzyme solutions.

With these results in hands, we demonstrate the feasibility of these heterofunctional supports to effectively immobilize a wide variety of His-tagged and untagged enzymes of different sizes and electrostatic surfaces under neutral pH conditions. These heterofunctional supports attain higher immobilization performance compared with agarose microbeads activated with cobalt-chelates and epoxy groups (AG-Co^{2+}/E), a benchmarked heterofunctional support widely used in applied biocatlaysis[196](**Table 5.5**).

Table 5.5: Single-enzyme immobilization parameters on AG-Co2+/E microbeads

Enzyme	Ψ (%) [a]	Recovered activity (%) [b]
ADH2	100	23
ADH1	97	49
NOX	54	0
CAT	15	0
LAC	100	7.4

[a] Immobilization yield, Ψ = (immobilized activity/offered activity) x100. [b] Recovered activity is defined as the coefficient between the specific activity of the immobilized enzymes and the specific activity of the soluble one x 100.

For example, the positively amine groups displayed in the AG-Co^{2+}/A/G and AG-Co^{2+}/A/E surfaces seem to increase the immobilization yield up to > 90% for enzymes with few exposed lysine residues, as it is the case of NOX (4 exposed lysine residues, PDB 1NOX) which only reached a 54% immobilization yield on AG-Co^{2+}/E.

On the other hand, we evaluated the performance of the different heterofunctional supports by comparing the recovered activity of each immobilized preparation. An ideal support would have 100% recovered activity (or immobilization effectiveness of 1), while lower values indicate enzyme inactivation upon immobilization. Immobilized enzymes follow a trend of activity reduction in all cases (**Table 5.4**).

Particularly ADHs suffer 50-80% enzyme inactivation upon their quantitative immobilization on these matrixes. These results agree with our previous report, where ADH1 was immobilized on different epoxy-activated matrixes[95]. Unlike ADHs, the oxygen dependent NADH oxidase (NOX) undergoes a marked enzyme activity reduction upon immobilization (losing more than 90% of its initial activity), recovering the highest activity when using AG-Co^{2+}/A/G (8.1%). This large activity reduction effect is mainly attributed to a hampered oxygen diffusion inside the macroporous agarose structure previously reported by our group[197]. Likewise, both catalases show marked activity reduction upon immobilization, where CAT retains less than 7% of its

initial activity, while BpCAT expresses three-fold higher residual activity only when immobilized on AG-Co2+/A/G (22%). This high activity loss has been also reported by other authors when immobilizing CAT on highly glutaraldehyde-activated agarose microbeads[198]. Finally, the studied lactonase maintains 12% to 42% of its initial activity upon immobilization, where AG-Co^{2+}/A/G provides the highest recovered activity of this enzyme. Previously, we co-immobilized both, the LAC and ADH2 on the same AG-Co^{2+} microbeads recovering 100% of its initial activity upon co-immobilization by metal-ligand affinity[199], thus we suggest that the enzyme inactivation of lactonase is triggered by the multivalent covalent attachment promoted by the GA groups.

Additionally, we assessed the thermal stability of the different heterogeneous biocatalysts at specific temperature conditions accordingly with their respective Tm values to observe any minimal enhancement (**Table 5.6** and **Figure 5.6**).

Table 5.6: Thermal stability of soluble enzymes

Soluble Enzyme	Half-life time (h)	Temperature (°C)
ADH2	3.8	65
ADH1	2.5	45
NOX	3.6	80
CAT	4.2	45
BpCAT	14.5	50
LAC	3.9	50

In all cases enzymes were incubated at 100 mM sodium phosphate buffer pH 8 at the indicated temperature. Half-life times were obtained by fitting the experimental data to a 3-parameters biexponential kinetic inactivation model.[177]
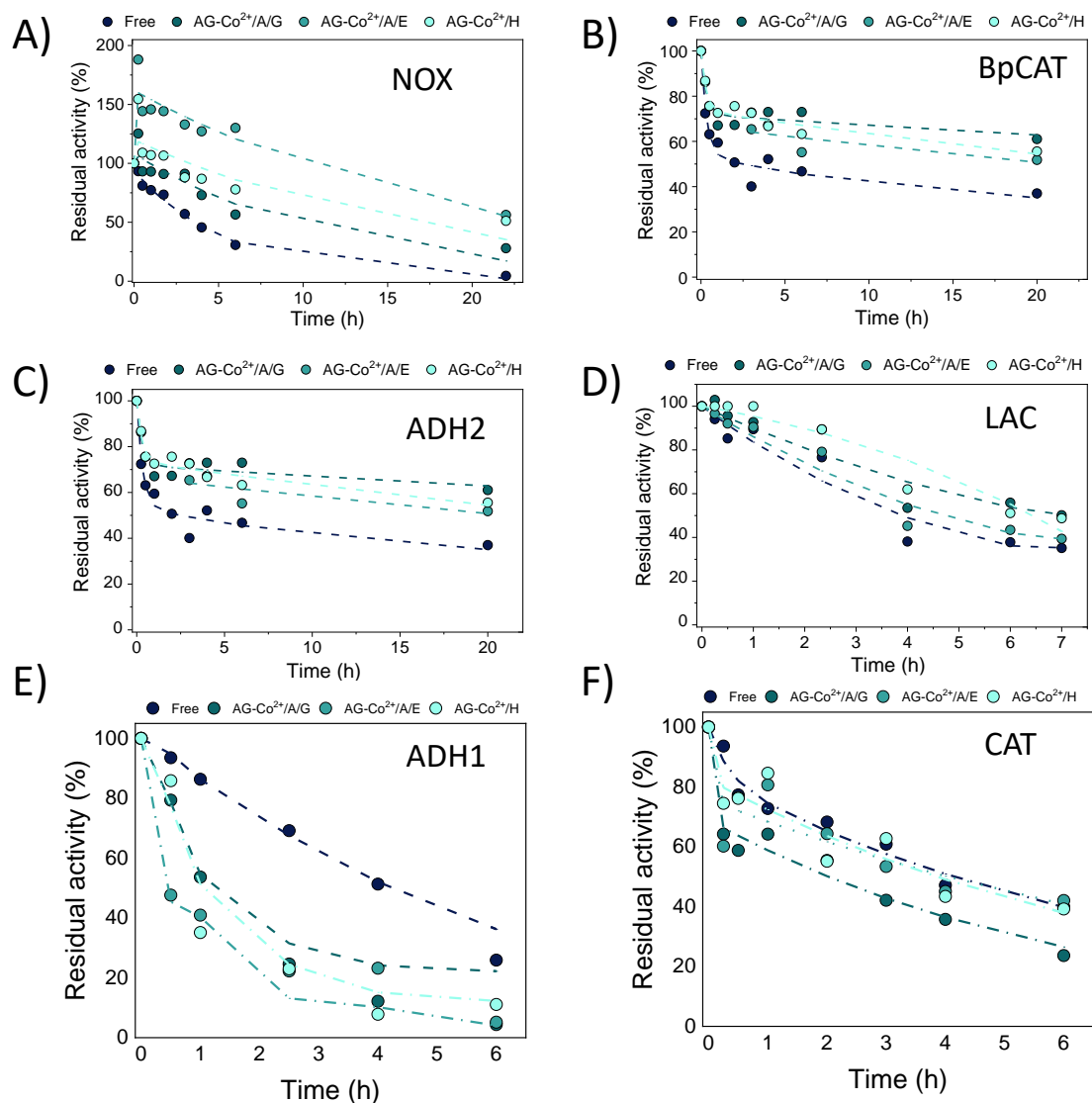
Figure 5.6: Thermal inactivation kinetics of soluble and immobilized enzymes on different heteroactivated supports. A) NOX at 80°C. B) BpCAT 40°C. C) ADH2 at 45°C. D) LAC at 50°C E) ADH1 at 70°C. F) CAT at 45°C. All thermal inactivations were conducted in 100 mM sodium phosphate buffer pH 8. Filled circles represent the obtained experimental measurements and the continuous dashed lines correspond to the fitting 3-parameters biexponential kinetic inactivation model[177]. ADH1, BpCAT, and LAC, are His-tagged at their N-terminus, while ADH2, CAT and NOX are untagged.

This result may be related to the thermophile nature of the enzyme. Also, this phenomenon was observed in the BpCAT thermal inactivation but in lower grade. Surprisingly, immobilized ADH1, regardless the support, is less stable than its free counterpart. The physical and chemical congruence of ADH1 and support surfaces might cause protein structural distortions that lead to a less stable biocatalyst when it is supported. Inter This specific issue we find for ADH1 may be addressed by post-immobilization polymeric coatings that stabilize the quaternary structure of oligomeric enzymes[198]. Despite the three supports efficiently immobilize all the tested enzymes with high yields, AG-Co^{2+}/A/G proves to be the optimal one to maximize the recovered activity and stability (high t$_{1/2}$ values) of a wider range of enzymes. For this reason, we select this support for further characterization studies.

5.3.3. Orthogonality of the immobilization chemistries in the tri-functional support AG-Co^{2+}/A/G

AG-Co^{2+}/A/G displays three different reactive groups that may immobilize enzymes through three different mechanisms to prepare immobilized multi-enzyme systems with industrial relevancy. Herein, we selected three different enzymes whose immobilization requires three different chemistries: His-ADH1, NOX and CAT. In particular, NOX hardly interacts with cationic exchangers[167], unlike CAT, which strongly does with positively charged supports[200]. On the other hand, metal-chelates binds His-ADH1 very efficiently and NOX has been successfully immobilized on supports functionalized with aldehyde as standalone reactive group[167]. Understanding the mechanism that drive the immobilization of each enzyme will allow us to design more efficiency co-immobilization protocols to fabricate highly active and stable multifunctional heterogeneous biocatalysts. The combination of these three enzymes presents a great potential in applied biocatalysis for the selective oxidation of diols into their corresponding aldehydes or lactols[171], lactones and ω-hydroxy acids[139], but also for the synthesis of aminoalcohols when coupled to transaminases[140].

To that aim, we evaluated the individual contribution of each reactive group displayed in AG-Co^{2+}/A/G to the enzyme immobilization kinetics. To study the sole contribution of cobalt-chelates, we blocked the support with glycine to remove the contribution of the aldehyde groups and performed the immobilization in presence of high salt concentration to avoid ionic interactions (sample coordination-chemistry, pink line in **Annex 5.1**). For the sole contribution of amine groups, we also blocked the aldehydes with glycine and performed the immobilization in presence of imidazole (sample ionic-chemistry, orange line in **Annex 5.1**). Finally, to study the sole contribution of the aldehydes, the immobilization was performed in presence of high concentration of salt and imidazole (sample covalent-chemistry, purple line in **Annex 5.1**).

This tri-heterofunctional support was designed to perform the enzyme immobilization in two sequential steps comprising a fast and first step of enzyme adsorption mainly driven by the cobalt chelates or by the secondary amine groups which can help that the second immobilization step take place (the enzyme covalent bounding mediated by glutaraldehyde moieties) by the gained proximity of the enzyme on the support's surface. **Annex 5.1.A** shows that the immobilization of His-ADH1 is driven by the cobalt-chelates groups as the immobilization rate was significantly reduced only when coordination chemistry was blocked by incubation with imidazole (purple line). For this enzyme, the aldehydes thus contribute to the first step of the immobilization to a lower extent than metal chelates. In the case of untagged NOX, we observe that cobalt-chelates and aldehyde groups dominate the immobilization kinetics as the enzyme is immobilized with a similar rate regardless of whether interactions with one or the other group are blocked (**Annex 5.1.B**). This insight agrees with the fact that aldehyde chemistry based on agarose activated with glyoxyl groups enables an efficient immobilization of that enzyme. Likewise, it has been reported that untagged NOX

interacts nonspecifically with metal chelates through some exposed histidine residues at its surface[167]. Finally, the immobilization of untagged CAT on AG-Co^{2+}/A/G is dominated by the aldehyde and amine groups, since the immobilization negligibly occur when the aldehydes were blocked and the immobilization was performed in presence of salt (**Annex 5.1.C**). Blocking the interactions with the aldehydes slows down the immobilization to a similar extent as avoiding the electrostatic interactions between CAT and the amine groups of the support. Therefore, for the three enzymes herein studied and under this experimental set-up, AG-Co^{2+}/A/G drive the immobilization through a mixed mechanism. The type of interactions that dominate the immobilization kinetics of each enzyme therefore depends on their intrinsic physio-chemical properties. Although the specific blocking of the different reactive groups allows us understanding the mechanisms that drive the immobilization of these three model enzymes, the fastest immobilization rates were achieved when the three reactive groups of AG-Co^{2+}/A/G were available for the enzyme attachment.

In the light of this results, the aldehyde groups do not play a fundamental role for the immobilization of ADH1 in the first immobilization step, however they may participate in a slower second step where a multivalent and irreversible attachment between the enzyme and the support is promoted. The irreversibility of this immobilization was confirmed by SDS-PAGE (**Figure 5.7**).

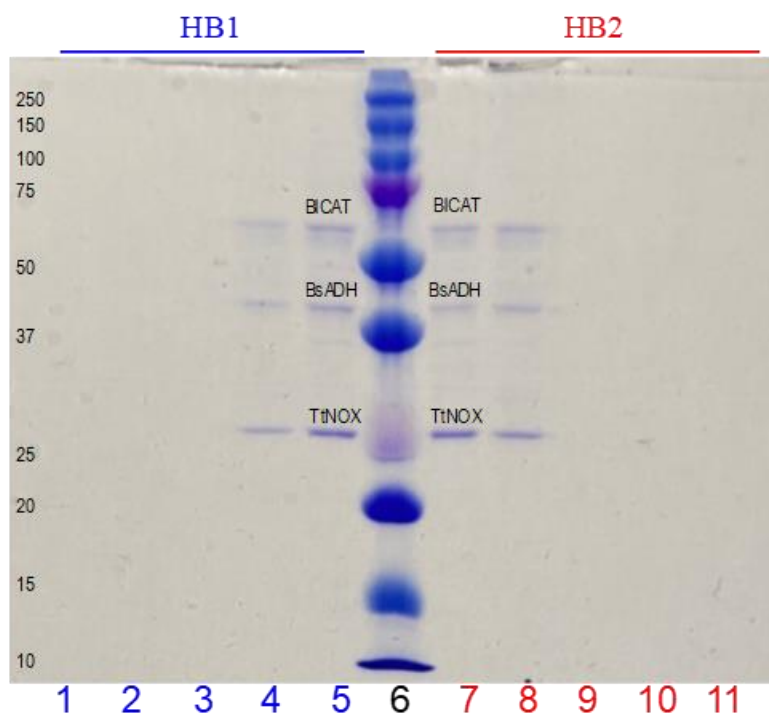**Figure 5.7:** Enzyme desorption assays. Biocatalysts HB1 (sequentially coimmobilized enzymes) and HB2 (coimmobilized enzymes at the same time addition order) were incubated 1h with 10 volumes of: A) 0.3 M imidazole pH 7; or B) 1 M NaCl; or C) 0.3 M imidazole and 1 M NaCl. After incubation, the suspensions were filtered and the eluted enzymes in the supernatant were analyzed by SDS-PAGE gel. Lanes 1-5 correspond to HB1.

Lanes 7 to 11 correspond to HB2. Lanes: 1, 11: eluted enzymes at C conditions; 2, 20: eluted enzymes at B conditions; 3, 9: eluted enzymes at A conditions; 4, 8: Boiled HBs (1:10 suspension in 100 mM sodium phosphate buffer pH 8) in Laemmli buffer without any desorption treatment; 5, 7: Soluble enzymes; 6: Molecular weight marker. ADH1 is His-tagged at its N-terminus, while CAT and NOX are untagged.

Enzymes are undetectably lixiviated after incubating the immobilized preparations with 0.3 M imidazole, 1 M NaCl or a combination of both. Under these conditions the enzymes only bound through cobalt-chelates and/or ionic interactions should be eluted to the bulk. However, partial enzyme lixiviation is only observed when incubating the immobilized biocatalysts at denaturing conditions (10min boiling in β-mercaptoethanol-SDS Laemmli's lysis buffer). This fact may be related to the subunit leaching of the oligomeric enzymes due to a suboptimal geometric congruence with the support surface (**Figure 5.7**).

5.3.4. Spatial distribution of immobilized enzymes across differently activated supports

In order to study the spatial distribution of different enzymes (CAT, BpCAT, ADH1, ADH2, NOX and LAC) across the inner surface of the tri-functional support, we labelled the enzymes with a fluorescent probe (Rhodamine isothiocyanate) prior their immobilization. Then, we immobilized the labelled enzymes on AG-Co^{+2}/A/G to investigate the enzyme distribution along the microparticle by confocal laser scanning microscopy (CLSM). From the CLSM images we calculated the relative infiltration distance defined as the percentage of radius where more than 50% of maximum fluorescence intensity of the sample is detected according to Diamanti et al[192]. His-tagged enzymes (BpCAT, ADH1 and LAC) are located at the very outer surface of the porous agarose microbeads colonizing less than 15% of the particle radius (**Figure 5.8**). On the contrary, the untagged enzymes colonize inner regions of the beads, occupying up to the 67% of the bead radius in the case of NOX. The spatial organization found for the different enzymes is supported by their immobilization kinetics. As previously reported by our group, high immobilization rates lead the enzymes to colonize the outer surface of porous materials since the enzyme immobilization is faster than the protein diffusion throughout the beads. On the contrary, low immobilization rates promote the enzyme infiltration toward inner regions of the beads because the protein diffusion is equal to or faster than the immobilization process. According to this, a His-tagged enzyme like ADH only colonizes the most outer 5 μm of the bead radius (10% relative infiltration distance) thanks to its fast immobilization (100% yield in 5 minutes, Figure 10.A). In contrast untagged enzymes colonize more inner regions due to their lower immobilization kinetics. For example, NOX is uniformly distributed across the radius of the beads because its immobilization rate is rather low (80% yield in 60 minutes, Figure 10.B). This spatial organization of NOX explains its low recovered activity upon immobilization on this tri-functional support as oxygen mass transport restrictions are more severe when the enzyme is located at the inner regions of porous supports. A similar insight was observed when NOX was uniformly distributed across aldehyde-activated agarose microbeads[100]. Regarding other untagged enzymes, we find the same trend for CAT (Figure 10.C), yet this enzyme is infiltrated to a lower extent than NOX (50 kDa) likely due to its higher molecular weight (240 kDa) that may hamper its diffusion across the porous structure of the support.
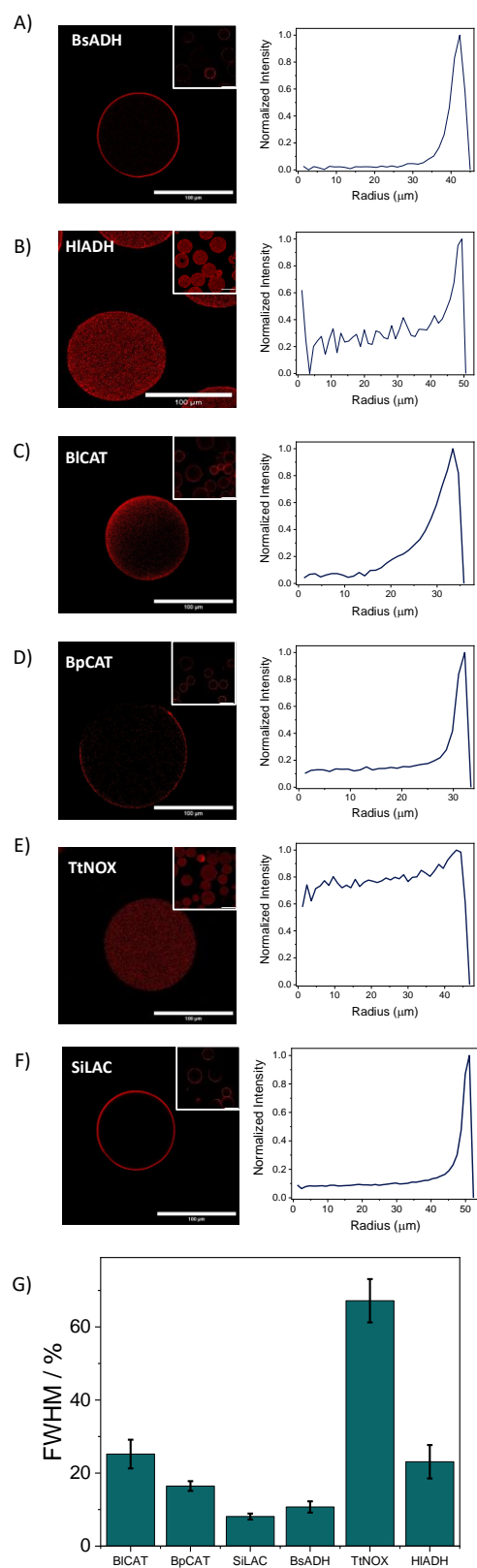
Figure 5.8: A-F) Confocal fluorescence microscopy presenting the spatial organization of different enzymes labeled with rhodamine B (red channel, λ_{ex}: 561nm) inside AG-Co^{2+}/A/G and the corresponding radial profiles. ADH1, BpCAT, and LAC are His-tagged at their N-terminus, while ADH2, CAT and NOX are untagged. G) Infiltration penetration percentage of each immobilized enzyme across the surface of different porous supports.

5.3.5. Stability and structural analysis of immobilized enzymes on tri-heterofunctional supports

To better explain the effect of the immobilization on the enzyme properties, we used a set of biophysical techniques to elucidate the structural rearrangements undergone in 6 different enzymes (ADH1, ADH2, NOX, CAT, BpCAT and LAC) when immobilized on AG-Co^{+2}/A/G, AG-Co^{+2}/A/E and AG-Co^{+2}/H. In one hand, we studied the intrinsic fluorescence spectrum of both immobilized and free enzymes (**Figure 5.9**) in order to acquire information about their microenvironment within the protein structure[182]. Most of the graphs show a remarkable decrease in the intrinsic fluorescence of the enzyme under immobilization compared to the free enzymes.
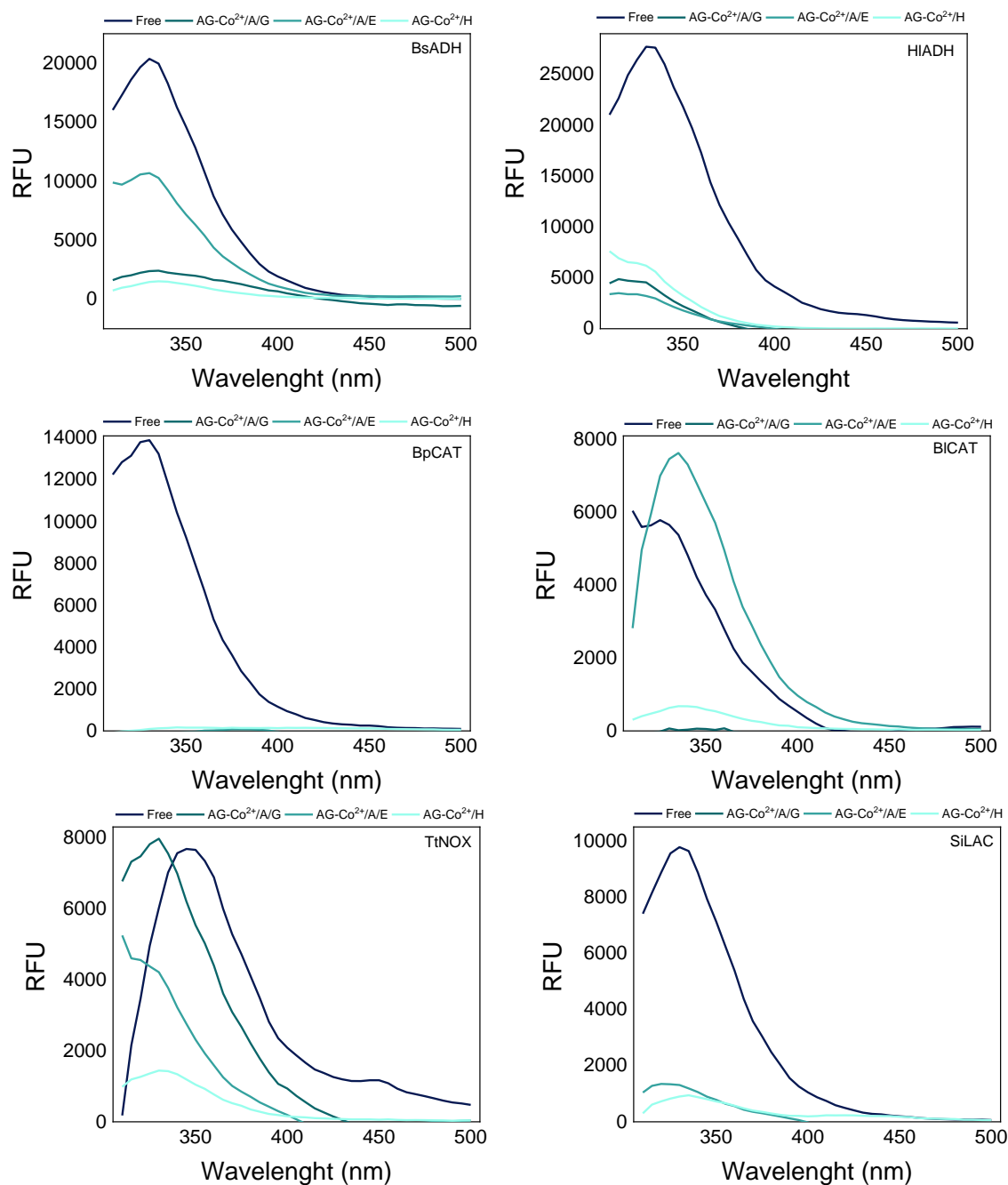
Figure 5.9: Spectra of intrinsic protein fluorescence before the immobilization (black lines, free) and upon the immobilization (purple, blue and red lines for AG-Co^{2+}/A/G, AG-Co^{2+}/A/E and AG-Co^{2+}/H, respectively). ADH1, BpCAT, and LAC, are His-tagged at their N-terminus, while ADH2, CAT and NOX are untagged.

On the other hand, we determined the relative anisotropy of free and immobilized enzymes labelled with fluorescein B isocyanate. The fluorescent anisotropy of small fluorophores tethered to the enzyme structure informs us about the apparent mobility of the protein through its rotational tumbling. The relative anisotropy of immobilized enzymes with respect to the anisotropy of their free counterpart reflects the changes in protein mobility promoted by the immobilization process. Normally, this relative anisotropy is greater as more stable the immobilized enzyme is, thus presenting a positive correlation with the half-life time of the

immobilized biocatalysts[183, 201]. Finally, we determined the unfolding transition temperature (Tm) of both free and immobilized enzymes by a thermal shift assay. All these data, together with the half-life time of the free and immobilized enzymes, are compiled in **Table 5.7** for comparative purposes.

Table 5.7: Stabilization of immobilized enzymes on AG heterofunctional activated agarose microbeads

Enzyme	Immobilization support	$\Delta\lambda_{max}$ (nm)	Tm (ºC)	Half-life time (h) [a]	Anisotropy
ADH2	Free	330	73	3.8	1
	AG-Co^{2+}/A/G	0	70	0.51	2.35
ADH1	Free	335	51	2.5	1
	AG-Co^{2+}/A/G	0	58	54	1.14
NOX	Free	335	78	3.6	1
	AG-Co^{2+}/A/G	30	84	9.2	4.62
CAT	Free	330	49	4.2	1
	AG-Co^{2+}/A/G	0	57	4.4	2.18
BpCAT	Free	330	56	14.5	1
	AG-Co^{2+}/A/G	-30	61	17	1.61
LAC	Free	335	53	3.7	1
	AG-Co^{2+}/A/G	0	62	6.7	2.23

[a] Half-life times studies were assayed at different temperatures accordingly with each enzyme, thus 65°C for ADH2, 45°C for HLAHD, 80°C for NOX, 40°C for BpCAT, 45°C for CAT, and 50°C for LAC

The immobilized preparation of the two ADHs, CAT and LAC present the same λ_{max} values than their free counterparts, indicating that the enzyme structure suffers negligible changes upon the immobilization process. In contrast all these immobilized enzymes experience a reduction in their protein mobility (rotational tumbling) and enhancement of their Tm values and halves-lives, except ADH1 which is less stable than the free enzyme although the anisotropy of the immobilized one was doubled. Specifically, immobilized NOX presented a red shifted λ_{max}, which suggests that their aromatic residues are more exposed to the solvent upon the immobilization process. The more solvent accessible conformation of the immobilized NOX exhibits a Tm 6°C higher than the soluble form. This conformational change is accompanied by a reduced enzyme rotational tumbling supported by an anisotropy value almost 5 times higher than its free counterpart. Oppositely, the immobilization of BpCAT on AG-Co^{2+}/A/G results in a blue shifted λmax in comparison with its free counterpart, suggesting that its interactions with the support promote less solvent exposed aromatic residues. In this case, this interaction seems to be beneficial for BpCAT folding stability as the Tm of the immobilized enzyme is 5°C higher than the free one. Moreover, the higher Tm values align with the higher half-life times under thermal inactivation. In summary, almost all tested enzymes are stabilized upon their immobilization on

AG-Co^{2+}/A/G reflected in their increased Tm values and half-life times, except ADH1, which shows lower thermal and folding stabilities that its free counterpart.

All assembled biocatalysts show higher anisotropy values than the free enzymes, indicating that the immobilization decreases the enzyme local mobility (rotational tumbling). Indeed, we find a trend between the anisotropy values and the thermodynamic and kinetic stability of the immobilized enzymes. Tm and half-life times increase when the relative anisotropy does except for the ADH1 biocatalysts. In most enzymes, the stabilization effects were accompanied by a reduction of the enzyme mobility within the porous microenvironment provided by the immobilization process and reflected in their augmented anisotropy values. In contrast, ADH1 is more unstable when its rotational mobility is limited, suggesting that less flexible conformation fixed upon its immobilization on AG-Co^{2+}/A/G is less thermally stable.

5.3.6. Co-immobilization of multi-enzyme systems

Once we characterized the separately immobilized enzymes, we assembled the multi-enzyme system formed by ADH1, NOX and CAT co-immobilizing them on the same AG-Co^{2+}/A/G microparticle. Initially, we evaluated the effect of the enzyme immobilization order on the biocatalyst activity performance. To that aim, we prepared a sequentially co-immobilized heterogeneous biocatalyst (HB1) by firstly immobilizing NOX, followed by the CAT and lastly attaching the ADH1. Likewise, we prepared a co-immobilized heterogeneous biocatalyst with the three enzymes co-immobilized at the same time (HB2) (**Table 5.8**). The immobilization yield of NOX was lower when all three enzymes were co-immobilized simultaneously than when they were immobilized sequentially. This effect could be related to protein steric hindrances triggered by the fastest ADH1 immobilization firstly colonizing the available matrix surface, thus exhibiting the same immobilization yields independently of the immobilization order (Table 10). The three enzymes recovered similar activities upon the immobilization regardless of whether they were immobilized sequentially (HB1) or simultaneously (HB2).

Table 5.8: Effect of the immobilization order on the immobilization parameters of multi-enzyme systems co-immobilized on AG-Co^{2+}/A/G.

Biocatalyst	Immobilization order	Enzymes	Enzyme load (mg·g^{-1})	Ψ (%) [a]	Recovered activity (U·g^{-1})[b] /(%)[c]
HB1	1st	NOX	0.78	75	1.17 (14)
	2nd	CAT	0.78^e	55	598 (11)
	3rd	ADH2	0.36	100	1.25 (42)
HB2	At the same time	NOX	0.53	51	0.93 (16)
		CAT	0.80^d	57	696 (11)
		ADH2	0.36	100	1.23 (41)

[a]Immobilization yield, Ψ = (immobilized activity/offered activity) x100. [b]Recovered activity of the immobilized enzyme per gram of support after the immobilization process. [c](%) is defined as the coefficient between the specific activity of the immobilized enzymes and the specific activity of the soluble ones. [d]Total protein content.

Afterwards, we evaluated both biocatalysts HB1 and HB2 under operational conditions by performing a model biotransformation. For that purpose, we applied HB1 and HB2 to selectively oxidize of 1,5-pentanediol to its corresponding products (5-hydroxypentanal, tetrahydro-2H-pyran-2-ol and δ-valerolactone) in batch operation conditions according to the enzyme selectivity previously reported by our group[100]. We selected this model biocascade since allows us evaluating the coupling efficiency of the three enzymes to simultaneously oxidizing the substrate, recycling a cofactor; the NAD$^+$, and removing a toxic by-product; the H$_2$O$_2$ (**Figure 5.10.A**). After 24 hours, both heterogeneous biocatalysts consumed more than 70% of the initial substrate 1,5-pentanediol, yielding a similar product profile, where tetrahydro-2H-pyran-2-ol was the major product (around 60%) (**Figure 5.10.B**). In agreement with the recovered activity (**Table 5.10**), the performance of the multi-enzyme system was negligibly affected by the co-immobilization order. However, after 5 hours the reactions reach a plateau for the consumption of the diol, suggesting the partial inactivation of the ADH1.
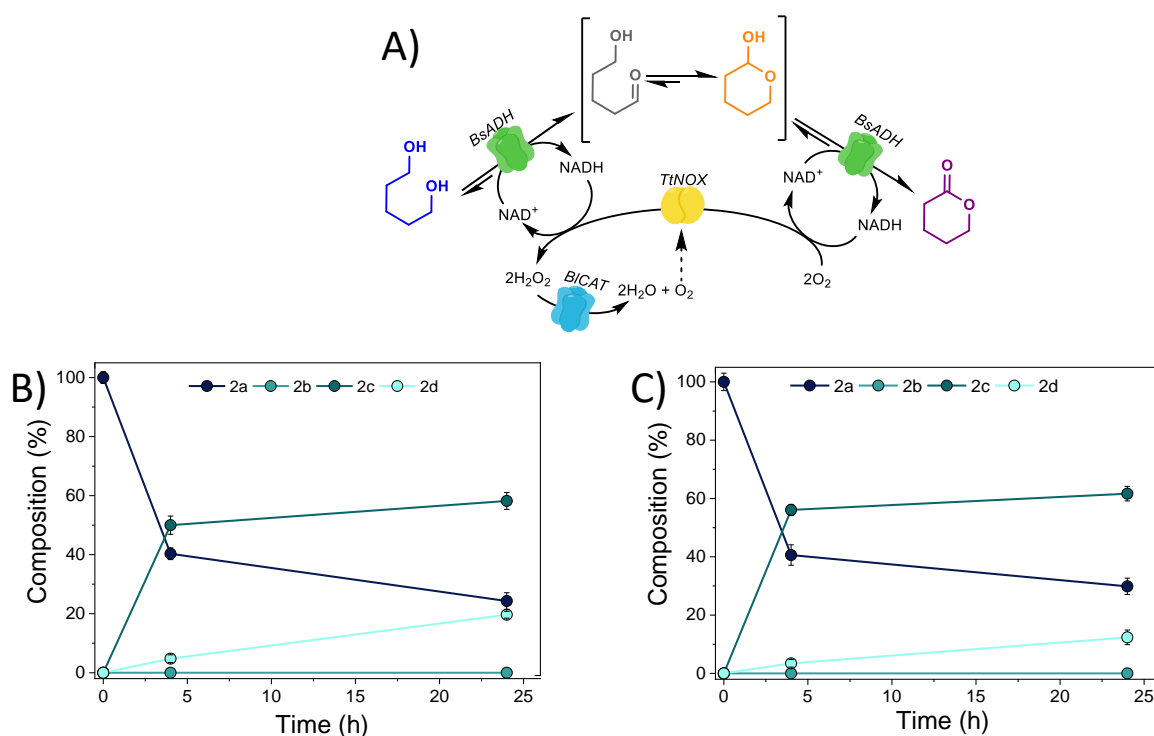
Figure 5.10: A) Reaction scheme of the selective oxidation of 1,5-pentanediol integrating NAD$^+$ recycling and H$_2$O$_2$ removal systems. Time courses of the 1,5-pentanediol oxidation catalyzed by trienzyme systems coimmobilized on AG-Co^{2+}/A/G either B) sequentially (solid lines and full squares) or C) simultaneously (dashed lines and empty circles). 1,5-Pentanediol (blue line), 5-hydroxypentanal (gray line), tetrahydro-2H-pyran-2-ol (orange line), and δ-valerolactone (magenta line). In all cases, reactions were performed by incubating 50 mg of heterogeneous biocatalyst with 300 µL of reaction mixture composed by 20 mM 1,5-pentanediol, 1 mM NAD$^+$, 0.15mM FAD$^+$ in 100mM sodium phosphate buffer pH 8 at 30°C. ADH1, BpCAT, and LAC, are His-tagged at their N-terminus, while ADH2, CAT and NOX are untagged.

A spectrophotometric assay confirmed that ADH2 is dramatically inactivated upon 8 h of operational use maintaining only 20% of its initial activity after 24h (**Annex 5.2**).

Despite this inactivation issue, the co-immobilized multi-enzyme system (HB2) reaches a 18% higher substrate consumption after 24h than their soluble and separately immobilized counterpart enzymes, supporting the fact that catalytic efficiency increases when multi-enzyme system is immobilized within the same confined space (**Figure 5.11**). Additionally, we observed an increase in the residual activity of the CAT in both distributions (**Figure 5.10**) at the first time-points of the operational stability. This effect was also observed at thermal inactivation but in NOX and BpCAT.
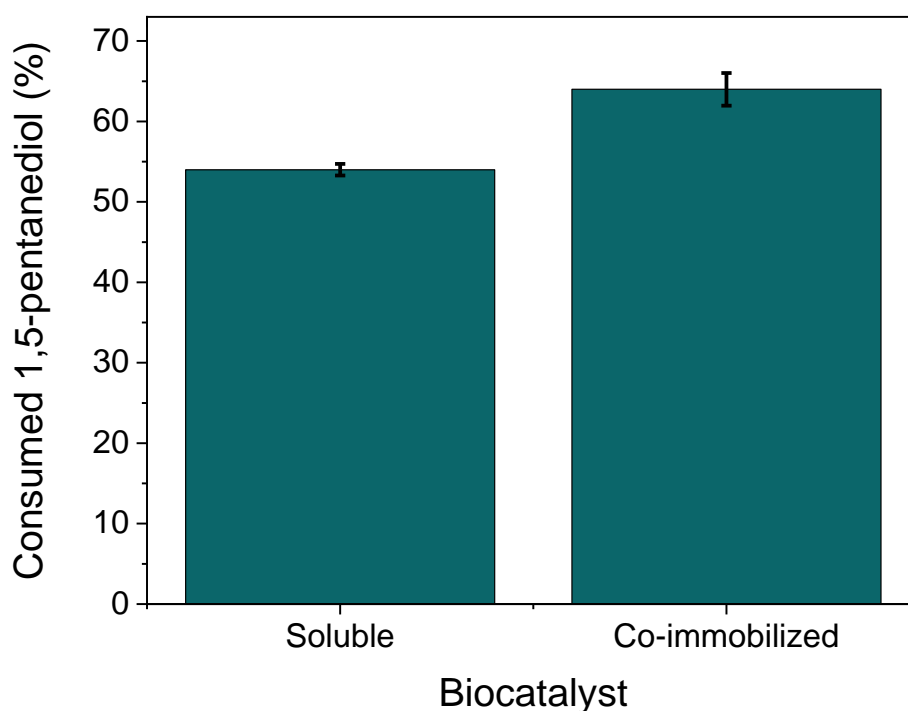
Figure 5.11: Consumed 1,5-pendanediol after 24h. In both cases reactions were performed by incubating 50 mg of HB2 of its equivalent in soluble enzymes with 300 µL of reaction mixture composed by 20 mM 1,5-pentanediol, 1 mM NAD^+, 0.15 mM FAD^+ in 100 mM sodium phosphate buffer pH 8 at 30°C.

5.3.7. Expanding the functionalization chemistry to other materials

Apart from agarose microbeads, we expanded the developed functionalization chemistry to other typically employed materials for enzyme immobilization. To this aim, we functionalized commercially available methacrylate microbeads and macroporous cellulose beads with the same active groups than AG-Co^{2+}/A/G (referred as Pu-Co^{2+}/A/G and CE-Co^{2+}/A/G, respectively). Then, we simultaneously co-immobilized ADH1, NOX and CAT on these two other materials to evaluate their performance (**Table 5.9**).

Table 5.9: Co-immobilization of multi-enzyme systems on tri-hetero-activated supports

Biocatalyst	Support	Enzymes	Enzyme load (mg·g^{-1})	Ψ (%) [a]	Recovered Activity (U·g^{-1})/ (%) [b]
HB2-AG	AG-Co^{2+}/A/G	NOX	0.53	51	0.93 (16)
		CAT	0.80^c	57	626 (11)
		ADH2	0.36	100	1.23 (41)
HB2-Pu	Pu-Co^{2+}/A/G	NOX	0.68	97	0.95 (13)
		CAT	0.75^c	74	254 (5)
		ADH2	0.30	100	0.84 (34)
HB2-CE	CE-Co^{2+}/A/G	NOX	0.35	50	1.1 (29)
		CAT	0.36^c	35	107 (4)
		ADH2	0.30	73	0.068 (3)

[a]Immobilization yield, Ψ = (immobilized activity/offered activity) x100. [b]Recovered activity of the immobilized enzyme (%) is defined as the coefficient between the specific activity of the immobilized enzymes and the specific activity of the soluble ones. [c]Total protein content

ADH1 achieves similar immobilization yield on AG-Co^{2+}/A/G and Pu-Co^{2+}/A/G, but slightly lower on CE-Co^{2+}/A/G. However, the cellulose-based carrier promoted a dramatic inactivation of this enzyme upon the immobilization. NOX behaves very similar when co-immobilized on hydrophilic matrixes as AG-Co^{2+}/A/G and CE-Co^{2+}/A/G but recovering 1.8-times higher activity when immobilized on cellulose matrix. In contrast, this enzyme achieves higher immobilization yields when immobilized on Pu-Co^{2+}/A/G but recovers 2.3-times lower activity upon its immobilization on this hydrophobic support. According to our previous results[100], the hydrophobicity of the support surfaces favors the immobilization of NOX at the expense of enzyme inactivation. Finally, CAT attains different immobilization yields depending on the matrix composition but expressing two times higher specific activity on agarose-based supports than on cellulose and methacrylate ones. In summary, all enzymes recovered the highest activities upon the immobilization on the most hydrophilic support (agarose microbeads) herein tested. Therefore, the physicochemical properties of the support directly affect the performance of the immobilized enzymes, even though they are immobilized through the same chemistry.

5.3.8. Biocatalyst recycling

As the last part of our study, we compared the reusability performance of HB2-AG, HB2-Pu and HB2-CE during the oxidation of the same model substrate in repeated batch cycles (**Figure 5.12**).
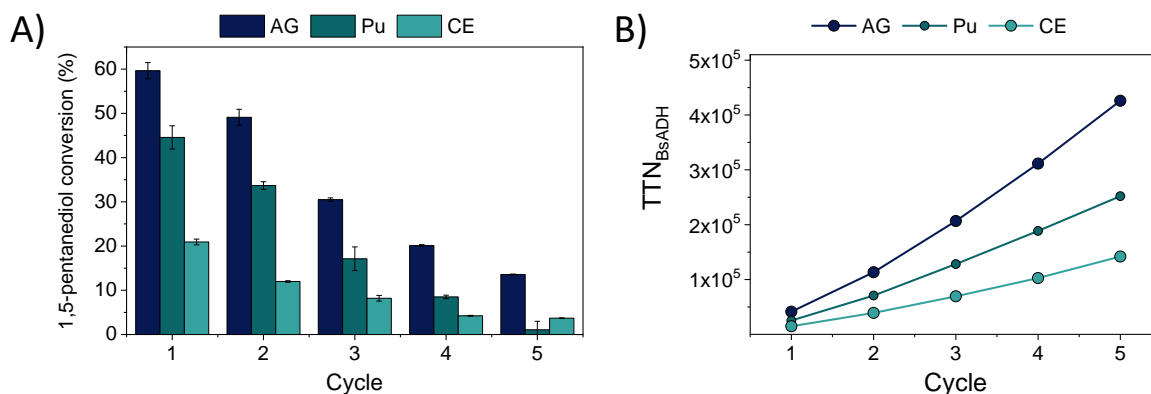
Figure 5.12: Recycling of coimmobilized heterogeneous biocatalysts during the oxidation of 1,5-pentanediol. A) Each cycle corresponds to 24h working at 20 mM 1,5-pentanediol, 1 mM NAD^+, and 0.15mM FAD^+ in 100mM sodium phosphate buffer pH 8 at 30°C. B) Accumulated TTN of ADH1 during recycling, defined as the mol of oxidized 1,5-pentanediol and tetrahydro-2H-pyran-2-ol per mol of tetrameric ADH1 after the fifth cycle; standard deviation is depicted in the shadows of the same color.

The agarose-based biocatalyst (HB2-AG) shows the higher yield and operational stability among the supports studied. The first cycle conversion of 1,5-pentanediol was 1.3 and 2.8 times larger when immobilized the multi-enzyme system on AG-Co^{2+}/A/G than on Pu-Co^{2+}/A/G and CE-Co^{2+}/A/G, respectively. Remarkably, the system immobilized on agarose microbeads maintain more than 80% of its initial activity after the second batch reaction cycle. Hence, this multi-functional heterogeneous biocatalyst is stable for more than 48 h of discontinuous operation as each reaction cycle corresponds to 24 h of reaction at pH 8 and 30°C. In the three support herein analyzed, the decrease of the product yield along the cycles is supported by the dramatic inactivation found for the co-immobilized ADH1 and CAT after the 5th batch cycle (**Table 5.12**).

Table 5.12: Individual residual activity of co-immobilized enzymes after five batch cycles.

Biocatalyst	Support	Enzyme	Residual activity (%)
HB2-AG	AG-Co^{2+}/A/G		0
HB2-Pu	Pu-Co^{2+}/A/G	ADH2	7
HB2-CE	CE-Co^{2+}/A/G		1
HB2-AG	AG-Co^{2+}/A/G		24
HB2-Pu	Pu-Co^{2+}/A/G	NOX	27
HB2-CE	CE-Co^{2+}/A/G		27
HB2-AG	AG-Co^{2+}/A/G		9
HB2-Pu	Pu-Co^{2+}/A/G	CAT	6
HB-CE	CE-Co^{2+}/A/G		11

Each reaction cycle corresponds to 24h working at 20 mM 1,5-pentanediol, 1 mM NAD^+, 0.15 mM FAD^+ in 100 mM sodium phosphate buffer pH 8 at 30°C.

However, the further stabilization of these enzyme under these operational conditions is out of the scope of this work. Previously, ADH1 was thermostabilized by its immobilization on agarose supports functionalized with epoxy and cobalt chelates, noteworthy the ADH1

thermostabilization did not afford enhanced operational stability[95]. The highest operational stabilization achieved when the multi-enzyme system is immobilized on AG-Co^{2+}/A/G leads to an accumulated total turnover number (TTN, defined as the mol of oxidized 1,5-pentanediol and tetrahydro-2H-pyran-2-ol per mol of tetrameric ADH1) of 1×10^5 after 5 batch cycles (**Figure 5.14.B**). This TTN is 333% higher than the same multi-enzyme system immobilized on CE-Co^{2+}/A/G, respectively. Expectedly, the accumulated TTN reaches a plateau upon the 4th cycle due to the inactivation of the enzymes. To note, the lower turnover of the multi-enzyme system immobilized on the cellulose-based support is attributed to the low recovered activity of ADH1 upon its immobilization on CE-Co^{2+}/A/G, respectively (**Table 5.13**).

Table 5.13: Co-Immobilization of multi-enzyme systems on tri-hetero-activated supports.

Biocatalyst	Support	Enzymes	Enzyme load (mg·g^{-1})	Ψ (%) [a]	Recovered Activity (U·g^{-1})/ (%) [b]
HB2-AG	AG-Co^{2+}/A/G	NOX	0.53	51	0.93 (16)
		CAT	0.80[c]	57	626 (11)
		ADH2	0.36	100	1.23 (41)
HB2-Pu	Pu-Co^{2+}/A/G	NOX	0.68	97	0.95 (13)
		CAT	0.75[c]	74	254 (5)
		ADH2	0.30	100	0.84 (34)
HB2-CE	CE-Co^{2+}/A/G	NOX	0.35	50	1.1 (29)
		CAT	0.36[c]	35	107 (4)
		ADH2	0.30	73	0.068 (3)

[a]Immobilization yield, Ψ = (immobilized activity/offered activity) x100. [b]Recovered activity of the immobilized enzyme (%) is defined as the coefficient between the specific activity of the immobilized enzymes and the specific activity of the soluble ones. [c]Total protein content

5.4.   Conclusions

We describe the preparation of an heterofunctional support that enables the co-immobilization of a variety of enzymes requiring different immobilization chemistries. The herein characterized support possesses three chemical functionalities, namely amino, aldehyde and cobalt moieties which synergistically permit a fast irreversible enzyme immobilization at neutral pH values of His-tagged and untagged enzymes. Moreover, it is also possible to change the chemical nature of the aldehyde moiety by replacing it by an epoxide or aromatic aldehyde such as hydroxymethylfurfural. However, we found that aldehyde groups as electrophiles to establish covalent bonds between the enzymes and the support outperform the other two (epoxides and HMF ones). With this information in hand, we exploited this tri-functional carrier to co-immobilize a tri-enzyme system for the regioselective oxidation of 1,5-pentanodiol to its corresponding lactol and lactone derivatives. Additionally, we also showed the possibility to expand this surface chemistry to different porous materials such as cellulose and methacrylate microbeads, however the physicochemical properties of the support surface impact on the operational performance and stability of the co-immobilized systems. Thus, this tri-functional support demonstrates its versatility to co-immobilize a wide variety of different enzymes under

mild immobilization conditions, opening the possibility to co-immobilize multi-enzyme systems aimed at enhancing the efficiency of cascade biotransformations.

CHAPTER 6:

6.1. Introduction

The recently developed cell-free biosynthetic cascade that transforms 1,ω-diols into ω-hydroxyacids (Chapter 4) is an excellent candidate to be benefited by multi-enzyme system co-immobilization through tuning the enzymes intraparticle spatial organization. In this 5-enzyme cascade, two NAD^+-dependent dehydrogenases (ADHs) synergistically catalyze the double oxidation of 1,ω-diols to their corresponding lactones (LAC) that are subsequently hydrolyzed by a lactonase to yield the target ω-hydroxyacids. The efficiency of the process relies on the in-situ recycling of NAD^+ driven by a NADH oxidase (NOX) that concomitantly produces hydrogen peroxide; a harmful oxidant that is removed by a catalase (CAT) to avoid enzymes inactivation. A previous work proposes a similar biosynthetic pathway towards the synthesis of ω-HA from cyclopentane but using resting cells as enzyme chassis. In the whole-cell biotransformation, the maximum product titer is 5 mM concentration of ω-HA (**Scheme 6.1.A**). In contrast, our cell-free system is able to increase the product titer 20 times with superior sustainable metrics (**Scheme 6.2.B**). Nevertheless, the incompatibility between the immobilization chemistries needed for each enzyme forced us to heterogenize the system using two different supports where the biosynthetic cascade was physically segregated, having one of the dehydrogenases far away from the NAD^+ recycling system[139]. This segregation yielded lower product titer than the system in solution and presented limited reusability as product yield dramatically decreased after the first operational cycle.
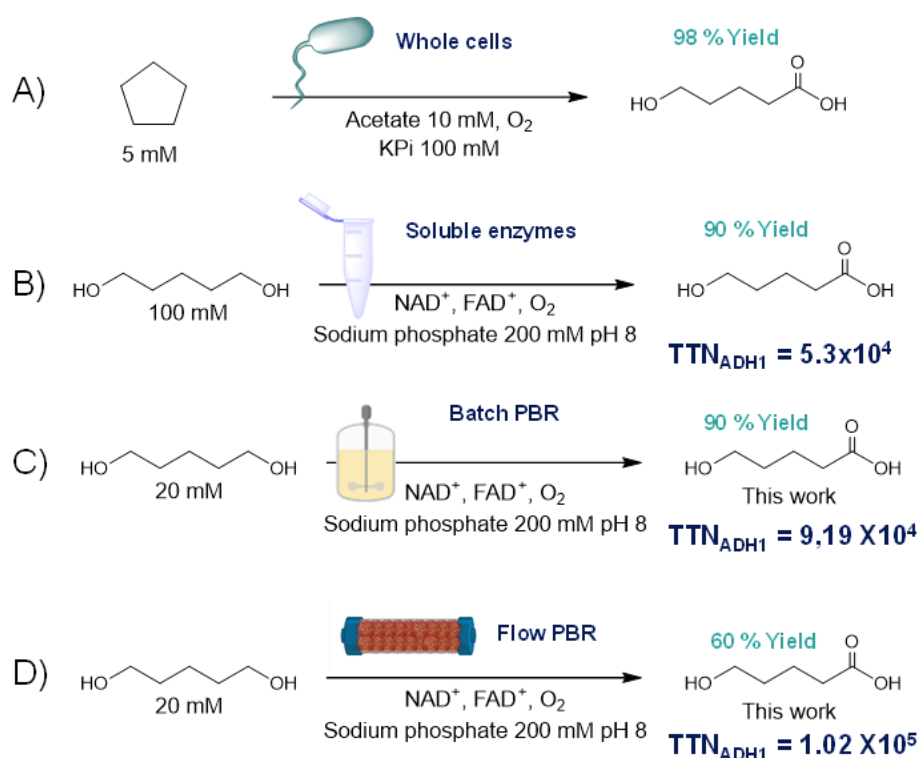
Scheme 6.1: Multi-enzyme biosynthesis of ω-hydroxyacids. A) Resting cells. B) Soluble enzymes. Co-immobilized enzymes (this work) in C) Batch and D) in Flow.

In this chapter, we have heterogenized this 5-enzyme system using the tri-functional support (AG-Co^{2+}/A/G) developed in Chapter 6. This support has proven successful to individually immobilize the 5 enzymes forming the biocascade, achieving active and stable heterogenous biocatalyst for most of them (see Chapter 6). Enzymes can be immobilized through His-tag coordination, ionic adsorption and covalent bonds as this support displays cobalt-chelates, positively charged secondary amines and aldehyde (from glutaraldehyde) groups. In this chapter, upon the kinetic characterization, the co-immobilized multi-enzyme system was optimized by tuning the intraparticle enzyme spatial distribution, finding the key role of the NOX localization for the overall productivity and stability of the cascade. Finally, the multi-functional heterogeneous biocatalyst was further stabilized by post-immobilization polymeric coating and increasing of the CAT load. The optimal solid biocatalyst was submitted to one-pot transformation of 1,5 pentanediol (1,5-PD) as model diol to yield 5-hydroxy pentanoic (5-HP) acid in consecutive batch cycles, demonstrating an excellent operational stability and scalability. Finally, we packed this heterogeneous multi-enzyme system in a plug-flow column to set a packed bead reactor for which the oxygen supplied was optimized to maximize both 5-HP titer and space-time yield.

6.2. Experimental section

6.2.1. Materials

The enzymes alcohol dehydrogenase (ADH2) from *Bacillus stearothermophilus* (ADH1), reduced nicotinamide adenine dinucleotide (NADH) oxidase from *Thermus thermophilus* HB27 (NOX) and the lactonase from *Sulfolobus islandicus* (LAC) were produced as previously reported[139]. Four percent cross-linked agarose (AG) beads (particle size 50–150 μm; pore diameter 300 nm) were purchased from Agarose Bead Technologies (Madrid, Spain). Compounds such as ethylenediamine (EDA), imidazole, iminodiacetic acid, cobalt chloride, sodium periodate, sodium hydroxide, rhodamine B isothiocyanate, Atto 390 NHS ester, Atto 488 NHS ester, sodium acetate, sodium chloride, sodium phosphate, sodium bicarbonate, glutaraldehyde (GA), Poly(allylamine), Protein Gel Stain, 1,5-pentanediol, tetrahydro-2H-pyran-2-ol, δ-valerolactone and 5-hydroxy pentanoic acid, alcohol dehydrogenase from horse liver (ADH2) were acquired from Sigma-Aldrich Chemical Co. (St. Louis, IL). Alexa Fluor™ 647 NHS ester was purchased from Fisher Scientific. All other reagents were of analytical grade

6.2.2. Preparation of tri-heterofunctional support activated with cobalt-chelates, secondary amine groups and aldehydes (AG-Co^{2+}/A/G)

We prepared AG functionalized with GA, EDA, and IDA/cobalt groups (AG-Co^{2+}/A/G) as described elsewhere. Briefly, we prepared epoxy-activated agarose (AG-E), and then, we activated with iminodiacetic acid (AG-E/IDA) by preparing a suspension of 10g of AG-E in 100 mL of 0.5 mM iminodiacetic acid at pH 11 under gentle agitation at 200 rpm for 1h at room temperature (RT). After filtering and rinsing with 10 volumes of water, AG-E/IDA was incubated with 10 volumes of 1 M ethylenediamine at pH 11 under gentle agitation at 200 rpm at room temperature overnight (AG-E/IDA/A). Afterward, the support was filtered and washed with 10 volumes of water, and then, incubated with a 15% glutaraldehyde solution in a 200 mM sodium

phosphate buffer pH 7 (AG-IDA/A/G) under gentle agitation at 200 rpm at room temperature. Subsequently, after filtering and washing, the support was incubated with 10 volumes of 30 mg·mL^{-1} of CoCl$_2$ for 2h at room temperature (AG-Co^{2+}/A/G) Finally, the carrier was filtered and washed with abundant water and stored at 4°C protected from light.

6.2.3. Optimization of the spatial organization in a heterogeneous 5-enzyme system

6.2.3.1. *Enzyme immobilization*
6.2.3.1.1. *HB1-HB5*

The assembly of heterogenous biocatalysts were conducted by mixing 10 mL of each enzyme solution at concentration showed in **Table 6.1**. in 100mM sodium phosphate buffer, pH 7 with 1 g of support AG-Co^{2+}/A/G. The suspension was maintained under gentle agitation at 25 rpm at 4°C for 2h. Subsequently, a blocking step was done by the addition of glycine (1 M, pH 8) followed by soft agitation overnight at 25 rpm and 4°C. Once the support was blocked, the immobilized sample was washed five times with five volumes of 25 mM sodium phosphate buffer, pH 8, filtered, and stored at 4°C. Specifically, Co-immobilization was conducted by the following order: HB-6: 1º NOX/CAT and 2º ADH1; HB-7: 1º NOX/CAT and 2º ADH2; HB-8: 1º NOX/CAT, 2º ADH1 and 3º ADH2; HB-9: 1º NOX/CAT, 2º ADH1, 3º ADH2 and 4º LAC. Between enzyme immobilization steps, immobilized samples were washed 3 times with five volumes of 25 mM sodium phosphate buffer, pH 8 and filtered.

6.2.3.1.2. *HB6-HB7*

The assembly of heterogenous biocatalyst conducted by mixing 10 mL of each enzyme solution at concentration showed in Table.1. in 100mM sodium phosphate buffer, pH 7 with 1 g of support AG-Co^{2+}/A/G. The suspension was maintained under gentle agitation at 25 rpm at 4°C for 2h. In these cases, NOX and CAT were immobilized firstly, and after filtering, ADH2 and ADH1 were immobilized to assemble HB-6 and HB-7 respectively. Finally, a blocking step was done by the addition of glycine (1 M, pH 8) followed by soft agitation overnight at 25 rpm and 4°C.

6.2.3.1.3. *HB-8*

The assembly of heterogenous biocatalyst conducted by mixing 10 mL of each enzyme solution at concentration showed in **Table 6.1**. in 100mM sodium phosphate buffer, pH 7 with 1 g of support AG-Co^{2+}/A/G. The suspension was maintained under gentle agitation at 25 rpm at 4°C for 2h. In this case, NOX and CAT were immobilized first, ADH2 secondly, and finally ADH1 were immobilized to assemble HB-8 and HB-7. Finally, a blocking step was done by the addition of glycine (1 M, pH 8) followed by soft agitation overnight at 25 rpm and 4°C.

6.2.3.1.4. *HB-9*

The assembly of heterogenous biocatalyst conducted by mixing 10 mL of each enzyme solution at concentration showed in **Table 6.1**. in 100mM sodium phosphate buffer, pH 7 with 1 g of support AG-Co^{2+}/A/G. The suspension was maintained under gentle agitation at 25 rpm at 4°C for 2h. In this case, NOX and CAT were immobilized first, ADH2 secondly, thirdly ADH1, and finally LAC were immobilized to assemble HB-9. Finally, a blocking step was done by the addition of glycine (1 M, pH 8) followed by soft agitation overnight at 25 rpm and 4°C.

6.2.3.1.5. HB-10

The assembly of heterogenous biocatalyst conducted by mixing 10 mL of each enzyme solution at concentration showed in **Table 6.1**. in 100mM sodium phosphate buffer, pH 7 with 1 g of support AG-Co^{2+}/A/G. The suspension was maintained under gentle agitation at 25 rpm at 4°C for 2h. In this case, NOX was incubated first in presence of a gradient of NaCl concentration (0, 0.1, 0.5 and 1 M). Then, CAT and ADH2 were immobilized, after ADH1, and finally LAC. Finally, a blocking step was done by the addition of glycine (1 M, pH 8) followed by soft agitation overnight at 25 rpm and 4°C.

6.2.3.1.6. HB-11, HB-12, and HB-13

The assembly of heterogenous biocatalysts were conducted as the HB-10. In the case of HB-11, after the immobilization of the 5 enzymes, the biocatalyst was incubated at 4°C overnight in sodium phosphate buffer pH 8, afterward it was blocked with 1 M glycine at 4°C for 3h, whereas HB-13, after the 5 enzymes immobilization, biocatalyst was incubated at 4°C overnight with poly allylamine (PAH) 10 mg·mL^{-1} in HEPES 25 mM buffer at pH 8.

6.2.4. Kinetic analysis of Distributions 1-4 in a 24 hour batch reaction course.

All distributions were assembled by adding each HB quantity specified in **Annex 6.1**. Distributions (100 mg) were placed inside a capped plastic tube (5 mL) containing 300 μL of a reaction mixture consisting of 20 mM of 1,5-pentanediol, 1 mM of NAD$^+$, and 0.15 mM of FAD$^+$ in 100 mM sodium phosphate buffer pH 8 allowing atmospheric oxygen supplementation by punching the tap with an open needle. Reactions were incubated at 30°C at 250 rpm inside an orbital incubator. The reaction course was monitored by withdrawing samples at periodic intervals, which were analyzed by chromatographic methods.

6.2.5. Operational stability of the Distributions

Briefly, 100 mg of Distributions 1 and 4 were placed inside a capped plastic tube (5 mL) containing 300 μL of a reaction mixture consisting of 10-20 mM of 1,5-pentanediol, 1 mM of NAD$^+$, and 0.15 mM of FAD$^+$ in 100 mM sodium phosphate buffer pH 8 allowing atmospheric oxygen supplementation by punching the tap with an open needle. Reactions were incubated at 30°C at 250 rpm inside an orbital incubator and samples collected at 24 hours. The

operational stability was monitored by withdrawing samples at periodic intervals, which were analyzed by chromatographic methods.

6.2.6. Enzyme activity assays

Enzyme activities were spectrophotometrically measured in transparent 96-well microplates with a flat bottom (Nunc), employing a Microplate Reader Epoch2 (BioTek Instruments) provided with the software Gen5.

6.2.6.1. ADH1 and ADH2 activity

200 µL of a reaction mixture containing 10 mM of 1,5-pentanediol and 1 mM of NAD$^+$ in sodium phosphate buffer at pH 8 were incubated with 5µL of enzymatic solution or 10µL of suspension (properly diluted) at 30°C. The increase in the absorbance at 340nm due to the reduction of NAD$^+$ was recorded. One unit of activity was defined as the amount of enzyme that was required to reduce 1 µmol of NAD$^+$ to NADH per minute at the assayed conditions.

6.2.6.2. NOX activity

200 µL of a reaction mixture containing 0.2 mM of NADH and 150µM of flavin adenine dinucleotide (FAD$^+$) in 50 mM sodium phosphate buffer pH 8 at 30°C were incubated with 5µL of enzymatic solution or 10µL of suspension (properly diluted) at 30°C. The oxidation of NADH was monitored as a decrease in the absorbance at 340nm. One unit of activity was defined as the amount of enzyme that was required to oxidize 1µmol of NADH to NAD$^+$ per minute at the assayed conditions.

6.2.6.3. CAT activity

200 µL of a reaction mixture containing 35 mM of hydrogen peroxide in 100 mM sodium phosphate pH 8 at 30°C were incubated with 5µL of the enzymatic solution or 10µL of suspension (adequately diluted). The catalase activity was measured by recording the decrease in the absorbance at 240nm. One unit of CAT activity was defined as the amount of enzyme required for the disproportionation of 1µmol of hydrogen peroxide per minute at the assessed conditions.

6.2.6.4. LAC activity

Lactonase activity was indirectly monitored by the decrease in the pH triggered by the formation of 5-hydroxypentanoic acid from its corresponding lactone hydrolysis. Briefly, 200 µL of a reaction mixture containing 1 mM δ-valerolactone, 0.1% acetonitrile, and 0.25mM p-nitrophenol in 2.5 mM sodium phosphate buffer at pH 7.0 was incubated with 5µL of enzymatic solution or 10 µL of suspension (properly diluted) at 30°C. The decrease in the absorbance of

p-nitrophenol (pH indicator) at 410nm was recorded. One unit of activity was defined as the amount of enzyme that was required to produce 1 μmol of 5-hydroxypentanoic acid (titrated by pH change) per minute at the assayed conditions.

6.2.7. Colorimetric assays for distribution kinetic characterization

6.2.7.1. Oxidative lactonization

Oxidative lactonization was monitored as showed in **Figure 6.1.A** Briefly, 200 μL of a reaction mixture containing 10 mM tetrahydro-2H-pyran-2-ol and 1mM of NAD^+ in 100 mM sodium phosphate buffer at pH 8 wee incubated with 10 μL of suspension (properly diluted) at 30°C. The increase in the absorbance at 340nm due to the reduction of NAD^+ was recorded. One unit of activity was defined as the amount of enzyme that was required to reduce 1 μmol of NAD^+ to NADH per minute at the assayed conditions.
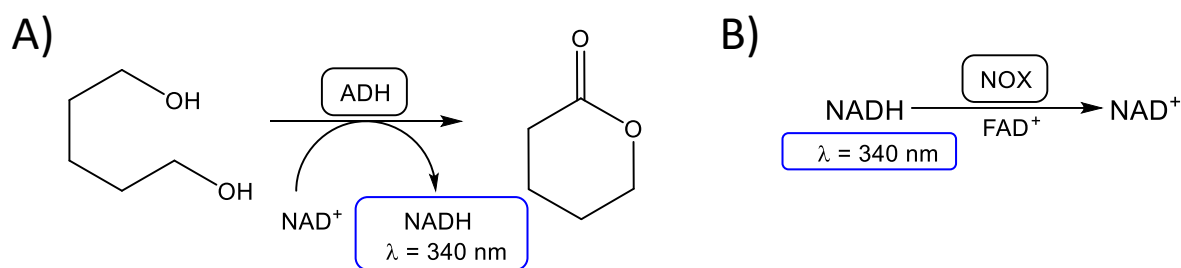

Figure 6.1: Colorimetric assays for biocatalysts kinetic characterization. A) Oxidative lactonization, recording increment in the absorbance at 340nm. Reaction conditions: 0.2 mM NADH, 0.15 mM FAD^+ in 100 mM sodium phosphate buffer pH 8 at 30°C. B) Cofactor regeneration, recording increment in the absorbance at 340nm. Reaction conditions: 0.2 mM NADH, 0.15 mM FAD^+ in 100 mM sodium phosphate buffer pH 8 at 30°C.

6.2.7.2. Cofactor regeneration

Cofactor regeneration was monitored as showed in **Figure 6.1.B** Briefly, 200 μL of a reaction mixture containing 0.2 mM of NADH and 0.15 mM of FAD^+ in 100 mM sodium phosphate buffer at pH 8 wee incubated with 10 μL of suspension (properly diluted) at 30°C. The increase in the absorbance at 340nm due to the reduction of NAD^+ was recorded. One unit of activity was defined as the amount of enzyme that was required to oxidize 1 μmol of NADH to NAD^+ per minute at the assayed conditions.

6.2.7.3. Hydrogen peroxide accumulation

Hydrogen peroxide accumulation was monitored as showed in **Figure 6.2**. Briefly, 200 μL of a reaction mixture containing 0.5 μg·mL^{-1} HRP, 20 mM 1,5-pentanediol, 1 mM NAD^+, 0.15 mM FAD+, 50 μM AmplifluRED in 100 mM sodium phosphate buffer at pH 8 wee incubated with 10 μL of suspension (properly diluted) at 30°C. The increase in the absorbance at 560 nm due to the formation of resorufin was recorded. One unit of activity was defined as the amount of

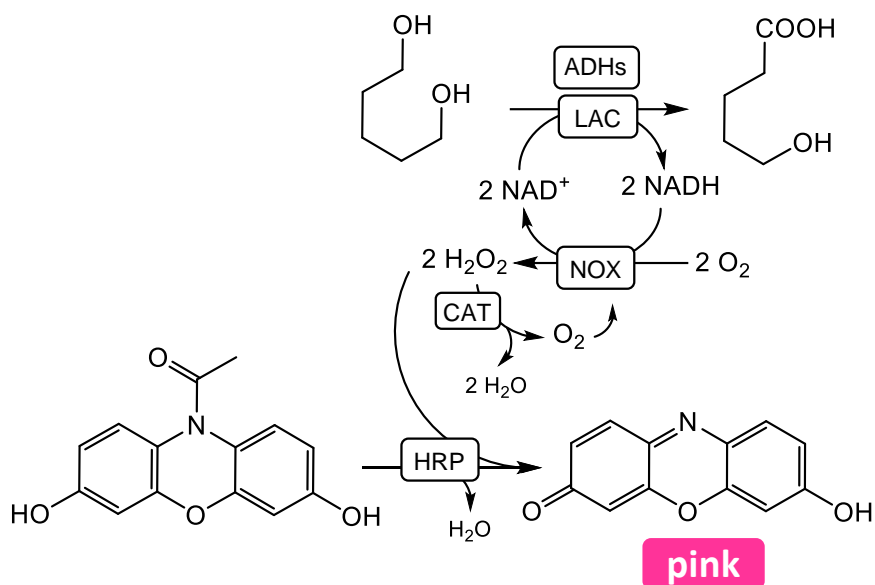enzyme that was required to disproportionate 1 µmol of hydrogen peroxide per minute at the assayed conditions.

Figure 6.2: Colorimetric assay for measuring the hydrogen peroxide accumulation. Recording the absorbance increase at 560nm due to the formation of resorufin. Reaction conditions consisted in 0.5 µg·mL^{-1} HRP, 20 mM 1,5-pentanediol, 1 mM NAD$^+$, 0.15 mM FAD$^+$, 50 µM AmplifluRED in sodium phosphate buffer 100 mM pH 8.

6.2.7.4. *ω-Hydroxyacid production*

ω-Hroxyacid production was monitored as showed in **Figure 6.3**. Briefly, 200 µL of a reaction mixture containing 20 mM 1,5-pentanediol, 1 mM NAD$^+$, 0.15 mM FAD$^+$, 0.1 mM Cresol Red in 100 mM sodium phosphate buffer at pH 8 wee incubated with 10 µL of suspension (properly diluted) at 30°C. The decrease in the absorbance at 580 nm due to the decrease in the pH was recorded. Also, the absorbance at 340nm was recorded at the same time to guarantee that there is not NADH accumulation since it decreases the pH. One unit of activity was defined as the amount of enzyme that was required to produce 1 µmol of hydroxyacid per minute at the assayed conditions.
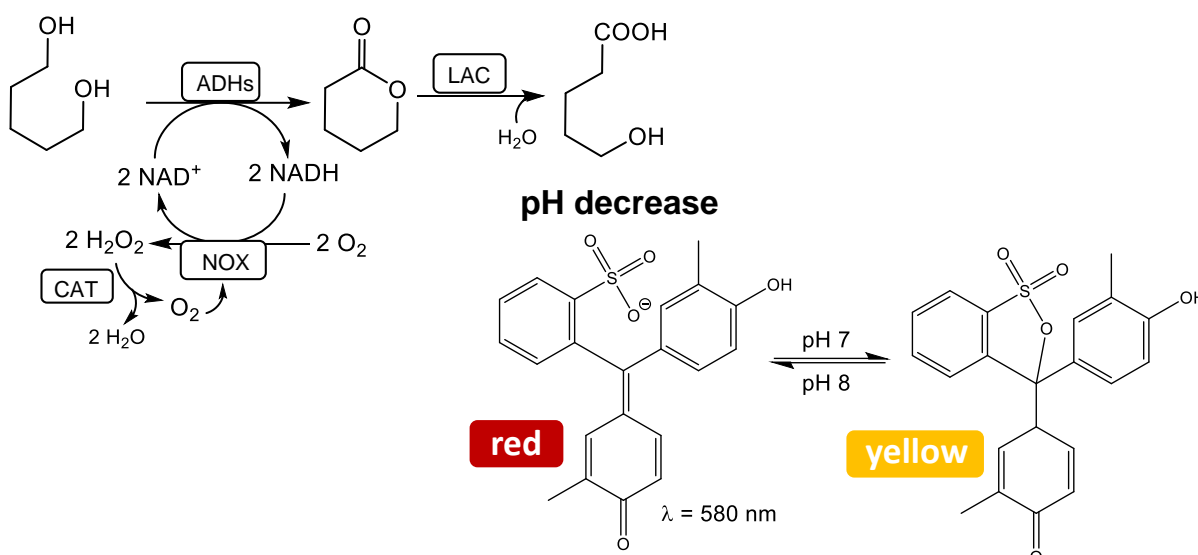
Figure 6.3: Colorimetric assay for measuring the ω-hydroxyacid production. Recording the decrease in the absorbance at 580nm and at the same time recording the absorbance at 340nm in order to guarantee that there is not NADH accumulation since it also decreases the pH. Reaction conditions consisted in 20 mM 1,5-pentanediol, 1 mM NAD$^+$, 0.15 mM FAD$^+$, 0.1 mM Cresol Red in sodium phosphate buffer 2.5 mM pH 8.

6.2.8. Protein labeling with fluorescent probes

Fluorescent labeling of enzymes was done using a methodology reported elsewhere[175]. Each enzyme solution in 100 mM of sodium bicarbonate buffer at pH 8.5 (ADH1: 0.2 mg mL-1, ADH2: 1 mg mL-1, LAC: 1 mg mL-1, CAT: 3.9 mg mL-1 and NOX: 1.2 mg mL-1) was mixed with the respective fluorophore: rhodamine B (ADH1), Atto 488 (ADH2), Atto 390 (LAC and CAT) and A647 (NOX) at 1:1 molar ratio (stocks of each fluorophore were prepared in DMSO). The labeling reaction was then incubated for 2 hours under gentle shaking at 25°C. Later, buffer exchange and removal of unreacted fluorophore was done by filtering the enzyme solution through a tangential ultrafiltration unit (10 kDa) equilibrated in 25 mM sodium phosphate buffered solution at pH 7.

6.2.9. Confocal laser scanning microscopy (CLSM) imaging

The localization and distribution of fluorophore-labelled immobilized enzymes along the different distributions were visualized with a confocal microscope Spectral ZEISS LSM 880 (Carl Zeiss, Germany) confocal microscope. Imaging was performed using 20x (0.8 NA) and 40x (immersion: water, 1.2 NA) objectives and different excitation lasers, λex: 405 nm for Atto 390, λex: 488 nm for Atto 488, λex: 561 nm for Rhodamine B, and λex: 633 nm for A647. All samples of each biocatalyst with the fluorescently labeled immobilized enzyme were suspended in an 8-well chamber slide (Ididi) in a 1:200 (w:v) buffered suspension in 25 mM phosphate buffer at pH 7, of each biocatalyst with the fluorescently labeled immobilized enzymes. The resulting micrographs were analyzed with FIJI[176], software to determine the relative infiltration radius and the colocalization parameters[192].

6.2.10. Batch reactions and recycling of co-immobilized enzymes

50 mg of heterogeneous biocatalyst were placed inside a capped plastic tube (2 mL) containing 300 μL of a reaction mixture consisted in 20 mM 1,5-pentanediol, 1 mM NAD^+, 0.15 mM FAD^+ in 200 mM sodium phosphate buffer pH 8 allowing atmospheric oxygen supplementation by punching the tap with an open needle. Reactions were incubated at 30°C at 250 rpm inside an orbital incubator. The reaction course was monitored by withdrawing samples at periodic intervals which were analyzed by chromatographic methods.

6.2.11. Flow reaction

The continuous flow biotransformations were conducted by preparing a 1 g packed bead reactor (PBR) in a plastic column and pumped it a reaction mixture containing 10-100 mM of 1,5-pentanediol, 1 mM of NAD^+, and 0.15 mM of FAD+ (and additionally 0-90 mM of hydrogen peroxide) in 100 mM sodium phosphate buffer pH 8 with a syringe pump. Temperature was maintained at 30°C with heated bath. The operational stability was monitored by withdrawing samples at periodic intervals, which were analyzed by chromatographic methods.

6.2.12. Analytical measurements

6.2.12.1.   Gas chromatography

(Extraction) Prior to GCanalysis, 50μL of the reaction sample was mixed with 200μL of ethylacetate to perform a liquid–liquid extraction of the compounds of interest containing 2 mM eicosane as the external standard. After the extraction, 30–50mg of anhydrous MgSO4 was added to dry samples before GC analysis. (Derivatization) All reaction samples were derivatized as described elsewhere[179]. Additionally, 50μL of aqueous reaction sample were placed in a 1.5 mL Eppendorf tube. Later, 150μLofethyl acetate were added and vortexed for 20s 20–50 mg of anhydrous $MgSO_4$were added to dry samples before GC analysis using eicosane 2 mM as external standard. Gas chromatography analyses were carried out in an Agilent 8890GC system chromato-graph using a J&WHP-5GC column (30m × 0.32mm × 0.25μm), helium as the support gas, and equipped with a flame ionization detector (FID). The injector asset at 280°C and the FID at 300°C. Separation of extracted compounds in ethyl acetate was done by the following temperature program: the initial temperature at 60°C, maintained 2 min, ramp to 160°C at a rate of 10°C·min^{-1}, ramp2–240°C at a rate of 20°C·min^{-1} and finally maintained 4 min.

6.2.12.2.   Nuclear magnetic resonance (NMR) analysis

When specified, reaction samples were analyzed by 1H NMR spectra acquired on a Bruker 500 MHz Ultra Shield spectrometer, operating at 500 MHz for 1H NMR spectroscopy. Chemical shifts were reported in parts-per-million (δ, ppm) and referenced using the residual solvent peak (deuteriumoxideδ=4.79ppm). Coupling constants (J) were reported in hertz[Hz]. The multiplicity of the signals were reported as singlet(s), doublet(d), doublet of doublets of doublets of doublets(dddd), doublet of the quartet (dq), doublet of triplet (dt), triplet(t), and multiplet (m).

6.3. Results and Discussion

6.3.1. Optimization of the spatial organization in an heterogeneous 5-enzyme system

The enzyme cascade is composed by two NAD$^+$-dependent alcohol dehydrogenases from *Bacillus stearothermophilus* (ADH1) and horse liver (ADH2) to synergistically oxidize 1,5-PD to δ-valerolactone through its corresponding lactol intermediate. As mentioned above, the pool of NAD$^+$ is replenished by an oxygen-dependent NADH oxidase from *Thermus thermophilus HB27* (NOX) coupled to a catalase from bovine liver (CAT) that depletes the hydrogen peroxide generated as by-product of NOX. Finally, a lactonase from *Sulfolobus islandicus* (LAC) hydrolyzes δ-valerolactone to 5-HP **(Scheme 6.2)**.
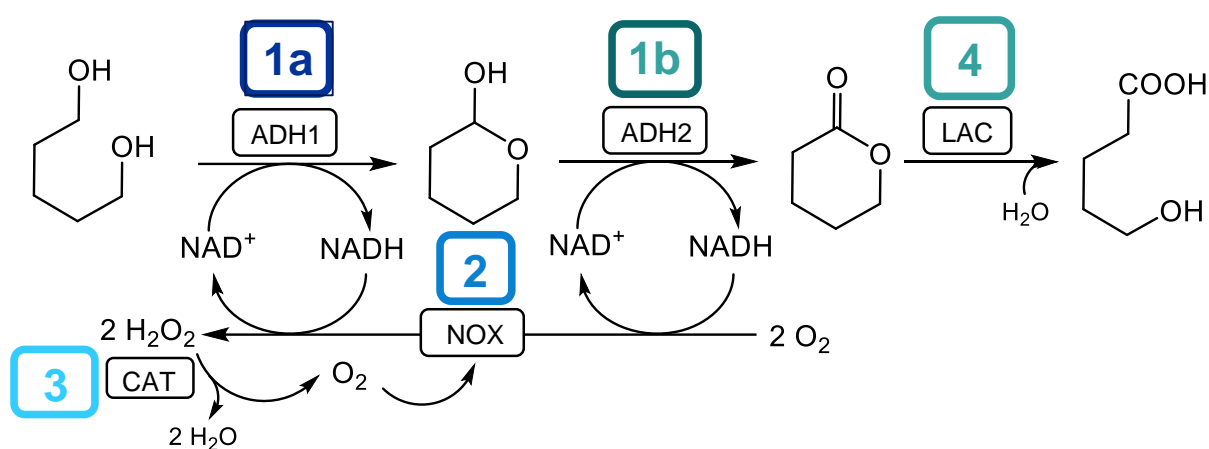
Scheme 6.2: Reaction scheme.

Previous work of this multi enzyme systems showed very promising conversion yields under pH control of the reaction mix by optimizing the enzyme ratio to overcome the bottleneck of the reaction (the second oxidation of the lactol step)[139]. However, we encountered important problems when try to scale-up the reaction (from 2mL to 10 and 25 mL). This fact leads us to assemble an heterogenous biocatalyst with our multi enzyme system. The 5 free-enzyme involved in the cascade were (co)immobilized on the tri-functional carrier above described (AG-Co^{2+}/A/G) following different spatial configurations **(Table 6.1)**. First, we individually immobilized all enzymes on the same support giving rise to five monofunctional heterogeneous biocatalyst (Entry 1, HB1 to HB5) **(Table 6.1)**.

Table 6.1. Immobilization parameters of enzymes on AG-Co^{2+}/A/G

Entry	Distribution	Heterogeneous biocatalyst	Enzyme	Enzyme load (offered / final) (mg·g^{-1})	Ψ ^{a} (%)	Recovered activity ^{b} (U·g^{-1}) /(%)
1	D1	HB1	ADH2	15 / 15^c	100	0.42 (23)
		HB2	NOX	0.51 / 0.41	81	0.67 (5)
		HB3	CAT	0.016 / 0.010^c	40	107 (25)
		HB4	ADH1	5 / 5	100	1.52 (11)
		HB5	LAC	1.58 / 1.49	98	0.35 (21)
2	D2	HB6	ADH2	7.50 / 7.41	99	0.5 (26)
			NOX	0.21 / 0.7	33	0.21 (15)
			CAT	0.007 / 0.004	56	109.7 (26)
		HB7	ADH1	2.50 / 2.45	98	1.19 (28)
			NOX	0.13 / 0.12	94	0.67 (5)
			CAT	0.007 / 0.004	65	127.3 (30)
		HB5	LAC	1.58 / 1.49	98	0.35 (21)
3	D3	HB8	ADH2	4.21 /4.20	99	na (na)
			NOX	0.23 / 0.13	57	0.40 (20)
			CAT	0.010 / 0.004	38	237 (61)
			ADH1	1.26 / 1.26	100	0.66 (23)
		HB5	LAC	1.58 / 1.49	98	0.35 (21)
4	D4	HB9	ADH2	3.0 / 3.0	100	na (na)
			NOX	0.18 / 0.12	65	0.53 (30)
			CAT	0.012 / 0.0023	19	343 (36)
			ADH1	1.0 / 1.0	100	0.9 (50)
			LAC	0.32 / 0.30	85	0.33 (46)
5	D4a	HB10	ADH2	3.0 / 3.0^c	100	na (na)
			NOX	0.18 / 0.14	79	0.50 (26)
			CAT	0.12 / 0.12^c	99	104 (8)
			ADH1	1.0 / 0.99	99	1.08 (50)
			LAC	0.32 / 0.32	100	0.18 (23)
6	D4b	HB11	ADH2	3.0 / 3.0^c	100	na (na)
			NOX	0.18 / 0.15	82	0.51 (26)
			CAT	0.12 / 0.12^c	99	120 (9)
			ADH1	1.0 / 1.0	100	1.04 (47)
			LAC	0.32 / 0.32	100	0.18 (23)
7	D4c	HB12	ADH2	3.0 / 3.0^c	100	na (na)
			NOX	0.90 / 0.66	74	1.25 (17)
			CAT	1.20 / 0.87^c	73	770 (35)
			ADH1	1.0 / 1.0	100	1.07 (49)
			LAC	0.32 / 0.32	100	0.20 (25)
8	D4d	HB13	ADH2	3.0 / 3.0^c	100	na(na)
			NOX	0.90/0.72	80	1.7 (20)
			CAT	1.20/1.14	95	116 (5)

ADH1	1.0/1.0	100	1.5 (53)
LAC	0.32/0.32	100	0.26 (32)

[a] Immobilization yield, Ψ = (immobilized activity/offered activity) × 100. [b]Recovered activity of the immobilized enzyme (%) is defined as the coefficient between the specific activity of the immobilized enzymes and the specific activity of the soluble ones. [c] Total protein content. Special post immobilization conditions of D4a-c: HB10: after the immobilization of the 5 enzymes, the biocatalyst was blocked overnight with 1 M glycine at 4°C. D4b: after the immobilization of the 5 enzymes, the biocatalyst was incubated at 4°C overnight in sodium phosphate buffer pH 8, afterward it was blocked with 1 M glycine at 4°C for 3h. HB12 was prepared as Hb11 but loading 5 and 20 times higher NOX and CAT, respectively. HB13: after the immobilization of the 5 enzymes, the biocatalyst was incubated at 4°C overnight with poly allylamine (PAH) 10 mg·mL^{-1} in HEPES 25 mM buffer at pH 8.

In this configuration each enzyme is immobilized on a bead different from the others, naming this spatial distribution as D1. Secondly, ADH1 and ADH2 were immobilized separately on AG-Co^{2+}/A/G but co-immobilized with NOX and CAT resulting in biocatalyst HB6 and HB7, respectively, and finally mixed with LAC immobilized on AG-Co^{2+}/A/G by its own (HB5) to assemble the configuration D2 (**Entry 2**, **Table 6.1**). Thirdly, NOX, CAT were co-immobilized with both ADHs (ADH1 and ADH2) on AG-Co^{2+}/A/G yielding the heterogeneous biocatalyst HB8 that was mixed with HB5 containing only LAC to assemble configuration 3, D3 (**Entry 3**, **Table 6.1**). Finally, the five enzymes were sequentially co-immobilized on AG-Co^{2+}/A/G to prepare biocatalyst HB9 with a configuration D4 (**Entry 4**, **Table 6.1**). All HBs were incubated with 1 M glycine upon 2 hours enzyme immobilization to block the remaining aldehydes which do not intervene in the enzyme attachment. These four spatial configurations imply that intermediates must follow different intraparticle diffusion pathways towards the final product. Accordingly, in D1 all intermediates must travel from one particle to the other to be processed by their corresponding enzyme (**Figure 6.5.A**).
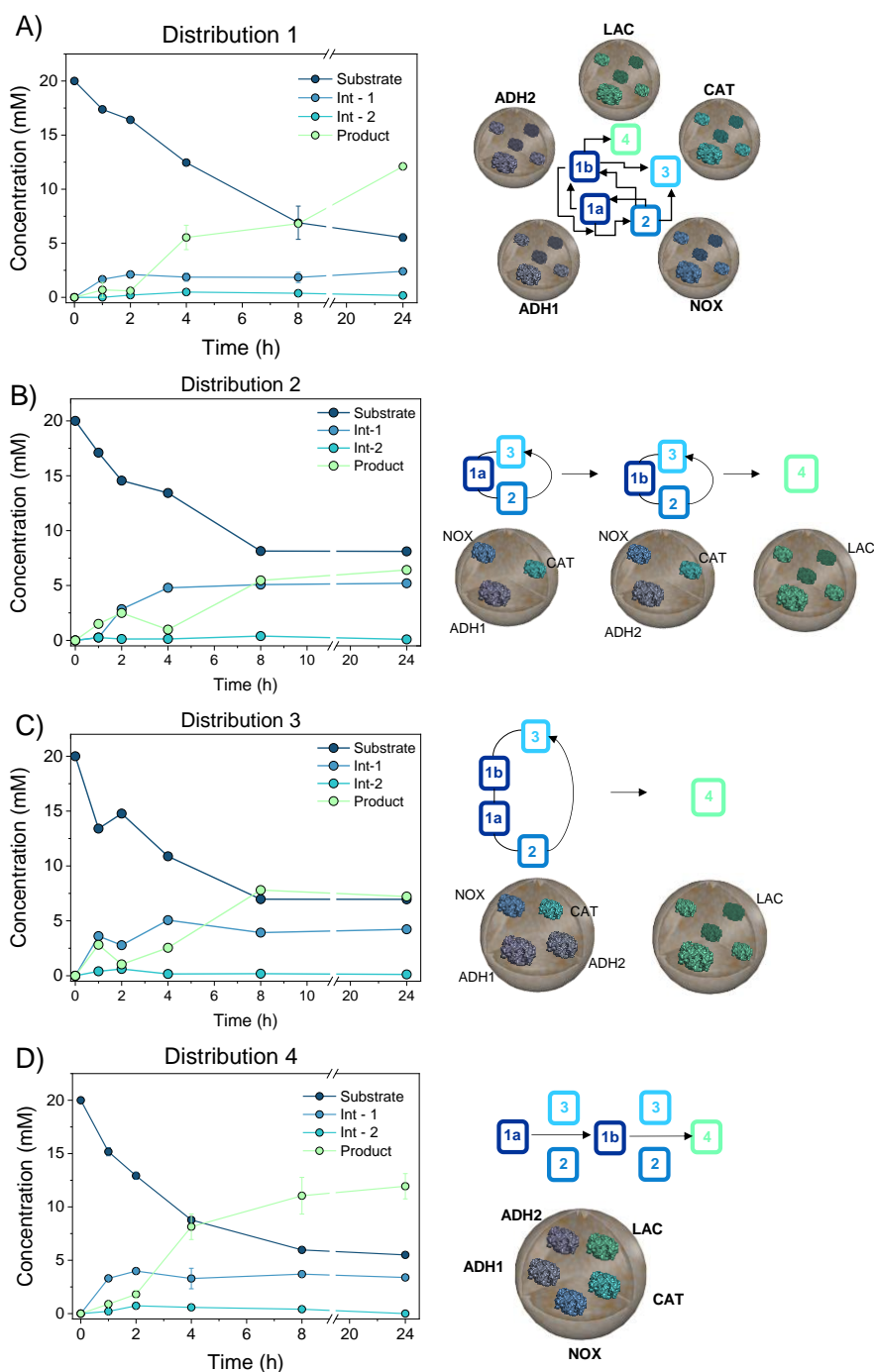
Figure 6.5: Different spatially organized multi-enzyme systems and their catalytic kinetic performance in the synthesis of 5-HPA. All reaction mixes containing 20 mM 1,5-PD, 1 mM NAD+, 0.15 mM FAD+, 200 mM sodium phosphate buffer pH 8 at 30°C.

In contrast, as D2 segregates each oxidation step but confines the NAD$^+$ recycling and H$_2$O$_2$ removal, the only intermediates forced to travel between particles are the lactol and the lactone. (**Figure 6.5.B**). In the case of D3, only the lactone must diffuse between different particles to be hydrolyzed by LAC (**Figure. 6.5.C**). Finally, as D4 confines the five enzymes inside the same particle, interparticle transport of intermediates is not needed to complete the cascade target product (**Figure 6.5.D**). Expectedly, the immobilization parameters for each

enzyme varied depending on whether the enzymes are individually immobilized o co-immobilized together (**Table 6.1**). This phenomenon was already reported for ADH1, as its recovered activity varied under individual immobilization or co-immobilization with other enzymes of the cascade[140].

Once the 9 different HBs (HB1-9) were prepared, they were mixed to assemble the multi-enzyme systems with the corresponding spatial distribution (D1-D4) in reaction, keeping a mass ratio of 1:3:0.18:0.012:0.32 for ADH1:ADH2:NOX:CAT:LAC respectively. Monitoring the reaction courses, we observed that D1 and D4 converted 75% of 1,5-PD yielding up to 60% of 5-HP in 24 hours, whereas D2 and D3 only reached a 35% 5-HP chromatographic yield (CY) after the same time (**Figure 6.5.B** and **C**). Remarkably, all enzymes co-immobilized on the same particle (Entry 4, HB9 with configuration D4) transform 1,5-PD into 5-HP 1.6 times faster (**Figure 6.6**) than all enzymes physically segregated into different particles (Entry 1, HB1-HB5 with configuration D1). Since the oxidation of the lactol intermediate (tetrahydro-2H-pyran-2-ol) is the rate-limiting step in this cascade[139] due to the high apparent K_M of ADH2 towards it (1.29 mM with 1,5-PD, 1.54 M with lactol and 19.06 mM with δ-valerolactone), its greater accumulation using the HB9 with D4 configuration may speed-up the lactone production, contributing so to enhance the overall higher throughput of the cascade when using this biocatalyst spatial configuration. Beyond the 5-HPA titer and productivity, we calculated the cascade coupling efficiency defined as the mol of 5-HPA per mol of 1,5-PD, where the ideal system would reach a coupling efficiency value of 1, indicating a perfect cascade orchestration where the substrate (1,5-PD) and intermediates (lactol and lactone) are quantitatively converted into the final target product (5-HPA). In agreement with the reached 5-HPA productivity, HB9 in configuration D4 (**Entry 4, Table 6.1**) presents a higher production rate value compared the mix of HBs in configuration D1 (**Entry 1, Table 6.1**) during the first 8 h. As D1 and D4 configurations present most promising results in terms of product yield and productivity, we discarded D2 and D3 configurations for further studies.
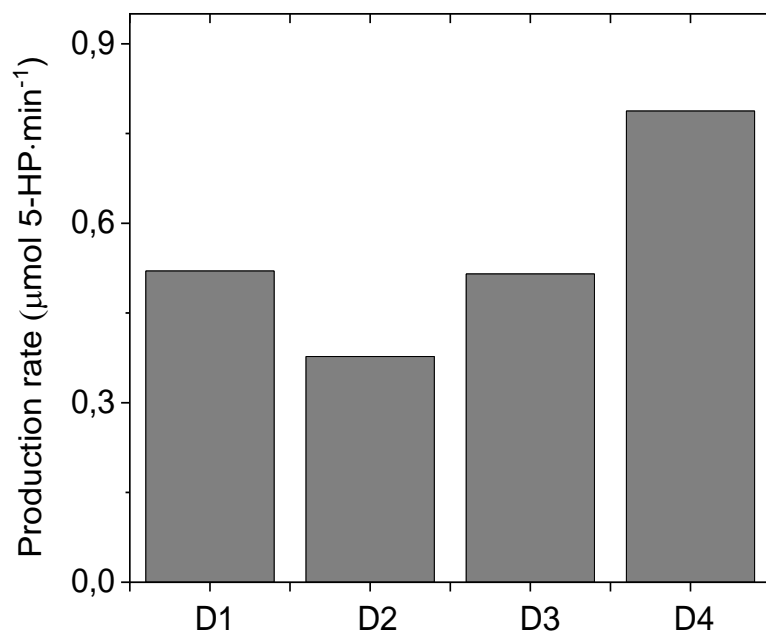
Figure 6: Production rate of 5-HPA of each Distribution at 4 hour of reaction course. In both cases reaction mixtures consisted in 20 mM 1,5-PD, 1 mM NAD^+, 0.15 mM FAD^+ in 100 mM sodium phosphate buffer pH 8.

6.3.2. Operational stability of the heterogeneous multi-function biocatalyst with different spatial configurations

Due to the promising performance of HBs under D1 and D4 spatial configurations, we tested their operational stability in consecutive batch reaction cycles by assessing the cascade coupling (**Figure 6.7**).
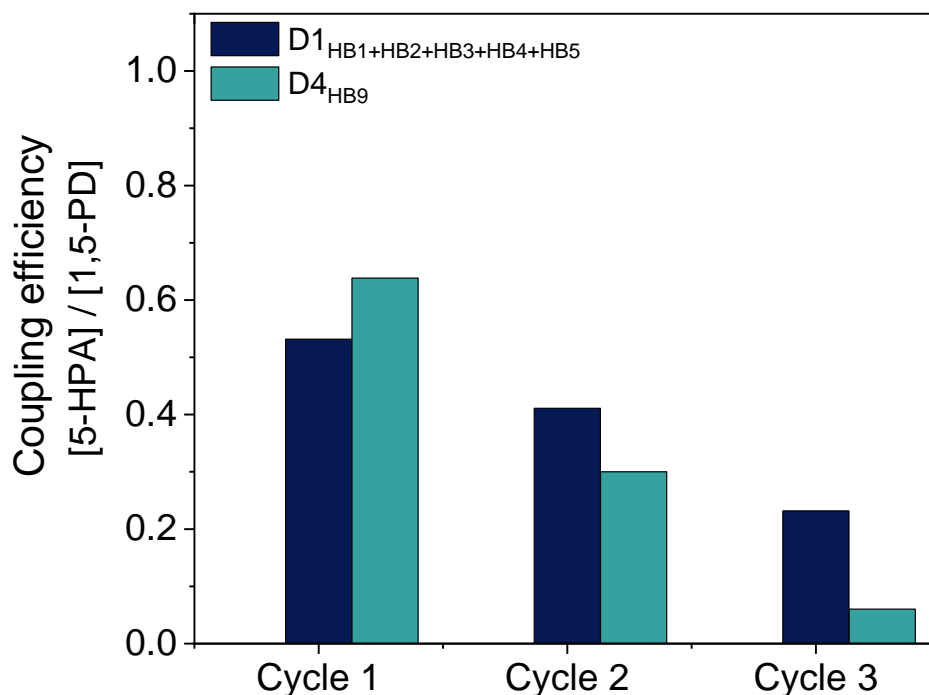
Figure 6.7: Cascade efficiency parameters of Distributions 1 and 4. Reaction mixtures consisted in 20 mM 1,5-PD, 1 mM NAD⁺, 0.15 mM FAD⁺ in 100 mM sodium phosphate buffer pH 8 at 24h, 250 rpm at 30°C.

Although HB9 with D4 configuration (**Entry 4**, **Table 6.1**) outperforms HB1-5 in configuration D1 (**Entry 1**, **Table 6.1**) in the first cycle, the cascade coupling efficiency was higher with D1 than with D4 in the second and third consecutive cycles, pointing out that the 5 enzymes co-immobilized together are less stable than those separately immobilized on the same carrier. To understand the lower operational stability of the co-immobilized systems (D4), we investigated the catalytic efficiency of each cascade step using a set of spectrophotometric assays that allowed us determining the activity of the diol oxidation, the NADH oxidation, the hydrogen peroxide accumulation (**Figure 6.3**) and the omega-hydroxy acid production (**Figure 6.4**).

Figure 8 shows that HB9 in configuration D4 is 3 and 4 times faster for the diol oxidation and NADH recycling, respectively, than the configuration D1 using HB1-5. These results match the time reaction courses (**Figure 6.5.A** and **D**), supporting the higher overall throughput of this cascade when it is catalyzed by the 5-enzymes co-immobilized on the same porous particle of AG-Co2⁺/A/G. However, the D4 spatial configuration accumulates H_2O_2 5 times faster than the configuration D1, suggesting that CAT in the co-immobilized system cannot pair the activity of the NOX. As H_2O_2 is a liaison for enzymes, its accumulation in the reaction catalyzed by HB9 in configuration D4 explains the system inactivation during the process despite its higher initial volumetric productivity. Despite the unsatisfactory operational stability, the high efficiency of the co-immobilized biocatalysts encouraged us to enhance its operational stability through optimizing its capacity to remove the in situ formed H_2O_2 without limiting the NADH recycling.
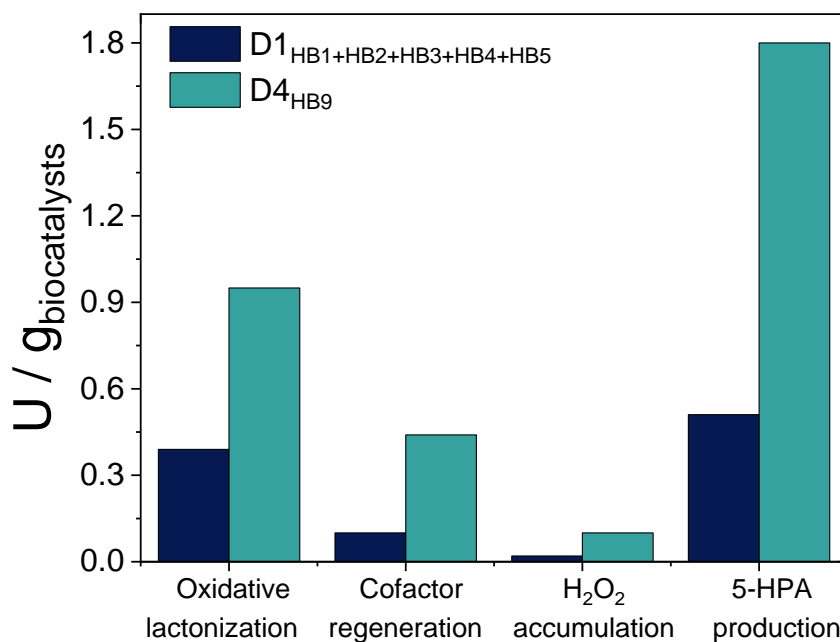
Figure 6.8: Specific productivity of Distributions 1 and 4 measured by colorimetric assays.

6.3.3. Optimization of the intraparticle spatial distribution and loading of 5-enzymes co-immobilized system (HB10) to maximize its performance

To investigate why hydrogen peroxide is accumulated when the cascade is catalyzed by HB9 in configuration D4, we studied the intra-particle spatial distribution of co-immobilized enzyme system by confocal laser scanning microscopy (CLSM) using enzymes labelled with compatible fluorophores for colocalization studies. **Figures 6.9.A** and **Annex 6.2** show that four of the co-immobilized enzymes are located at the outer surface of the particle, whereas NOX is located at the inner regions of the beads. This spatial distribution agrees to our previous results where the five enzymes were individually immobilized on this carrier[202]. The intra-particle segregation of NOX and CAT may explain their impaired activities and thus the accumulation of hydrogen peroxide during biotransformation as it is produced at large distances (inner regions of the particle) from where it can be removed (outer regions of the particle), not being immediately depleted once produced and thus damaging the other enzymes.
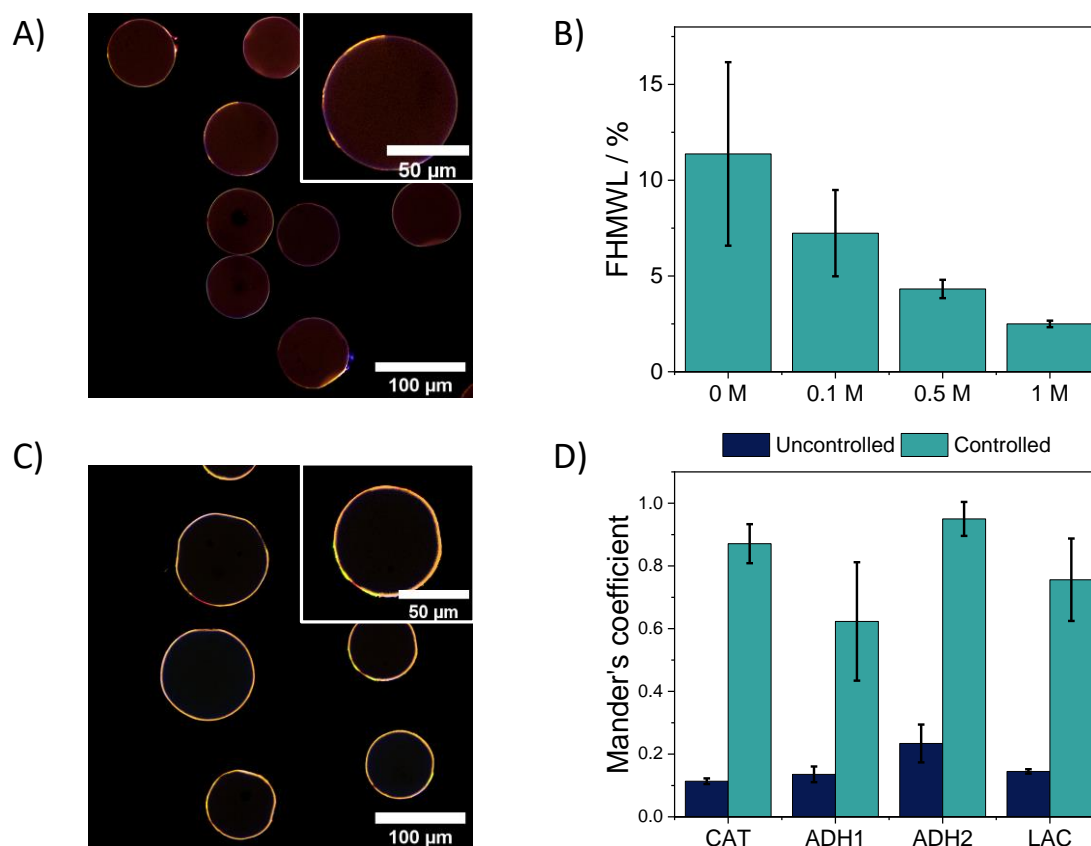
Figure 6.9: Study of spatial distributions. A) and C) confocal image of labelled enzymes in distributions 4 and 5 respectively. B) Infiltration penetration percentage of NOX at different concentrations of NaCl under immobilization. D) Mander's coefficient of Fraction NOX overlapping each enzyme.

To improve the hydrogen peroxide removal, we optimized the spatial distribution of NOX by tuning its immobilization kinetics, gathering all 5 enzymes forming the system in the outer surface of the beads. As previously demonstrated, the fast enzyme immobilization rate yields immobilized enzymes located at the outer parts of a microbead, while slowly immobilized enzymes are uniformly distributed inside and outside the beads. The immobilization rate can be easily controlled by adding immobilization competitors or modify the immobilization buffer and/or conditions. To favour a more rapid NOX immobilization rate and enable its localization at the outer surface of the beads, we performed its immobilization on AG-Co^{2+}/A/G in the presence of a gradient of NaCl concentration (0, 0.1, 0.5 and 1 M) and assessing the enzyme infiltration by CLSM (**Figures 6.9.B** and **Annex 6.3**). 1 M NaCl was needed to locate NOX at the outer surface of the carrier, colonizing the most outer 2% radius of the beads (15 µm in average) (**Figure 6.9.B**). Additionally, we corroborated that this new spatial location of NOX negligibly affected the immobilization pattern of the other enzyme members of the cascade. **Figure 6.9.C** and **Annex 6.4** show the CLSM images that demonstrate the co-localization of the 5 enzymes at the outer region of the same bead. When 1M NaCl is added to the immobilization buffer, the Manders´s coefficients of NOX regarding the other enzymes (**Figure 6.9.D**) determined from the CLSM images confirmed us that NOX co-localizes with the rest of the enzymes to a higher

extent than when NaCl was not added. As positive charges in the surface carrier repeal NOX slowing down its immobilization, we hypothesize that the chlorides will act as counter ions of the positive amine groups of AG-Co^{2+}/A/G, minimizing the enzyme repulsion and consequently immobilizing NOX faster and in the most outer surface. The outer localization of NOX brings it closer to CAT, enhancing their cooperative action, but also increase the NAD$^+$ recycling efficiency as the oxygen transport from the bulk to the more exposed NOX is facilitated. The HB bearing the 5 enzyme co-localized at the outer surface of the beads is hitherto referred as HB10 (D4a, **Entry 5**, **Table 6.1**). Next, we evaluated the effect on the intraparticle NOX spatial distribution on the biocatalyst productivity and operational stability. First, we observe that the localization of NOX at the outer surface of the beads (HB10, **Entry 5, Table 6.1**) increases 5-HPA titter upon 24 h reaction (**Figure 6.10.A**) and maintains the chromatographic product yield (CY ≈ 70%) constant for 3 consecutive batch cycle unlike the HB9 (**Entry 4**, **Table 6.1**) where NOX is localized in the deeper surface of the porous carrier (**Figure 6.10.B**).
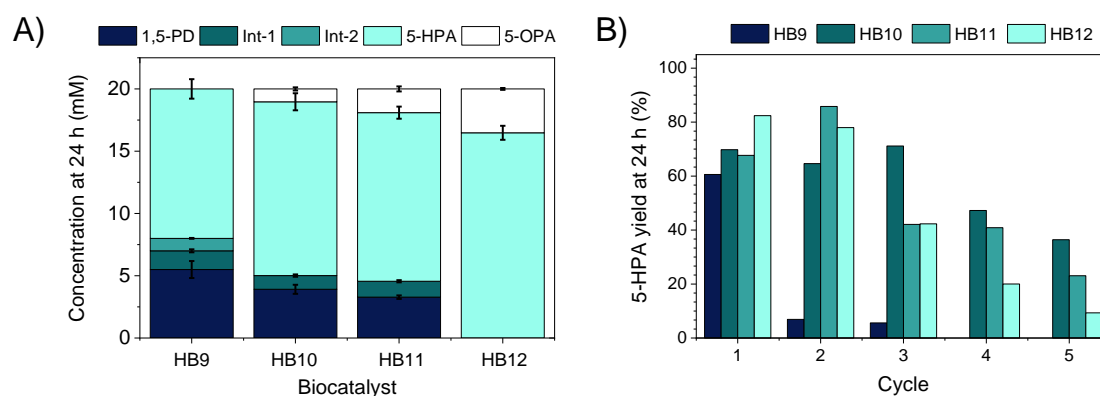

Figure 6.10: Effect of polymer coating. A) and B) Reaction-time course of HB12 (**Entry 7**, **Table 1**) and HB13 (**Entry 8**, **Table 6.1**) with and without polymer coating, respectively. c) Operational batch stability. All reaction mixes containing 20 mM 1,5-PD, 1 mM NAD$^+$, 0.15 mM FAD$^+$, 200 mM sodium phosphate buffer pH 8 at 30°C.

Unfortunately, the HB10 suffer operational inactivation upon the 4th operational cycle, observing a CY decay of 20%. To further increase the operational stability of HB10, we incubated the immobilized enzymes for longer times (16 h at 4°C) before the blocking step to fabricate HB11 (**Entry 6**, **Table 6.1**). Longer immobilization times pursues to promoting the formation of more attachments between the enzymes surface residues and the aldehydes of AG-Co^{2+}/A/G, to ultimately improving the enzyme stability as reported elsewhere for other enzymes immobilized on heterofunctional carriers of similar nature[194]. Nevertheless, the increase of the immobilization time increases neither enhanced the efficiency nor the operational stability of the HB10. Finally, to further optimize the performance of HB10 biocatalyst, we increased the load of NOX and CAT by 4.7 and 7.25 times, respectively, resulting in a heterogeneous biocatalyst named as HB12 (**Entry 7**, **Table 6.1**) where the specific activity of the immobilized NOX decreased 1.8 times due to the higher protein density within the porous beads. Previous studies support the fact that NOX is less catalytically efficient at high protein loads, suggesting that protein crowding negatively affect the performance of this enzyme[100]. Despite this activity reduction, HB12 converted 100% 1,5-PD to yield 80% 5-HPA. Surprisingly, we observed 20% of the 5-oxopentanoic acid (5-OPA), indicating the overoxidation

of the target 5-HPA. This product overoxidation hints a very efficient NAD$^+$-recycling system that boosts the oxidative activity of both co-immobilized dehydrogenases (ADH1 and ADH2). Regarding the operational stability, the excess of immobilized CAT drove to a less operationally stable biocatalyst as the product yield dramatically decayed to 10% upon re-using this biocatalyst in 5 consecutive batch cycles. In summary, the overall efficiency and operational stability of HB9 are optimized by localizing NOX at the outer surface of the beads and increasing the NOX and CAT loading in the biocatalyst, yet longer immobilization times drove to insignificant improvements in the biocatalyst performance. To note, higher enzyme loads resulted in a HB less operationally stable. To understand whether the operational inactivation of HB12 was due to the enzyme lixiviation because an excessive protein load, we performed SDS-PAGE analysis of HB10-HB12. This electrophoretic analysis reveals that enzyme lixiviation similarly occurred in all HB10-12 preparations (**Figure 6.11**), thus operational inactivation cannot only be explained by the enzyme subunit leaching (quaternary structure disassembly) under reaction conditions, but some structural distortions may also contribute to the overall biocatalyst deactivation.
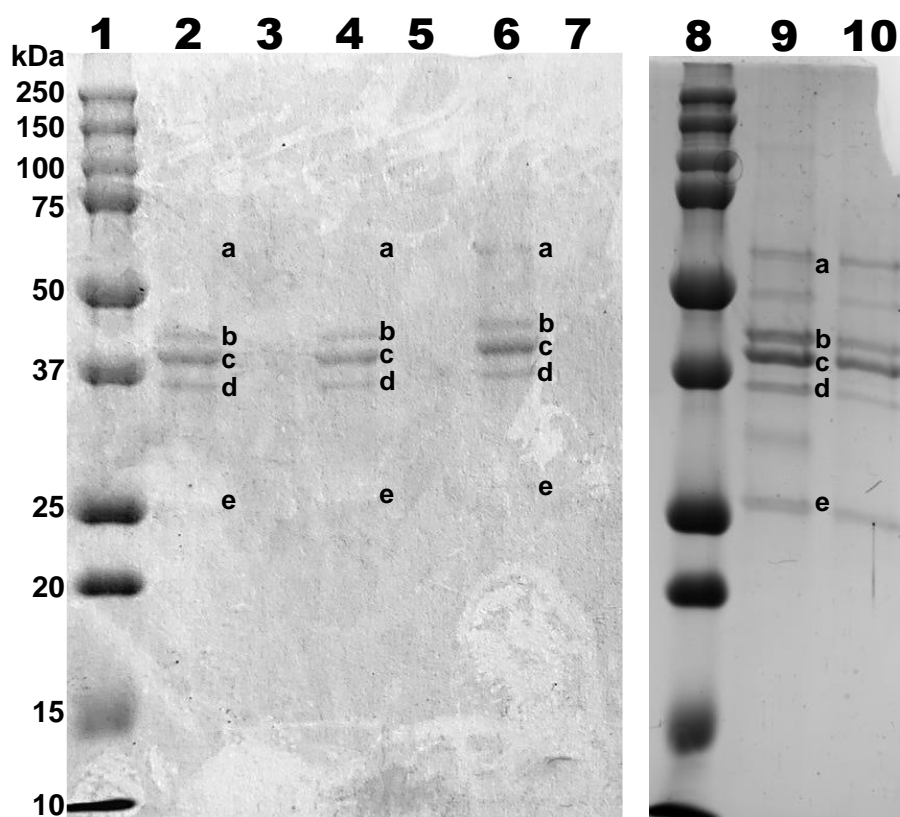

Figure 6.11: SDS-PAGE gels of HBs after five batch cycles. Lanes correspond: 1, molecular weight marker; 2. Freshly prepared HB9; 3, HB9 after 5 batch reaction cycles; 4. Freshly prepared HB10; 5, HB10 after 5 batch reaction cycles; 6. Freshly prepared HB11; 3, HB11 after 5 batch reaction cycles; 8, molecular weight marker; 9, Freshly prepared HB9-10, Freshly prepared HB12. a: CAT, 58 kDa, b: ADH1, 41 kDa, c: ADH2, 36 kDa, d: LAC, 35 kDa, and e: NOX, 23 kDa.

6.3.4. Polymer coating to improve heterogenous biocatalysts operational performance and stability

As we observed the subunit lixiviation of the most enzyme forming the most efficient heterogeneous biocatalyst HB-12, we decided to stabilize their quaternary structure by polymer coating using polyallylamine (PAH) since we previously demonstrated that such a coating enhances the performance of dehydrogenases and oxidases[203]. To that aim, after sequentially co-immobilizing the 5 enzymes with the optimal spatial distribution and enzyme loading, we coated them with PAH, fabricating a new version of HB-12 named as HB-13 (**Entry 8**, **Table 6.1**). The primary amine of PAH reacts with the remaining aldehyde groups of the carriers not involved in enzymes attachment, acting as ionic macromolecular crosslinker of enzyme subunits and blocking agent to make the carrier inert after the immobilization processes. This polymer coating increased the recovered activity of ADH1, ADH2, and NOX (**Table 6.1**), hinting the stabilization effect promoted by the aminated polymer in the enzyme quaternary structure. This quaternary structure stabilization is supported by the reduction of enzyme subunits lixiviation from the HB-13 when it is submitted to SDS-PAGE analysis (**Figure 6.11**, lanes 9 and 10). When we challenged HB-13 to the one-post step-wise oxidation/hydrolysis of 1,5-PD into 5-HPA, we pleasantly found that the coating/blocking with PAH achieves a CY of 100% using 10 mM substrate in only 2 hours in comparison with the 60% conversion achieved with the same catalyst but blocked with glycine (HB-12) in the same time (**Figure 6.12. A** and **B**).
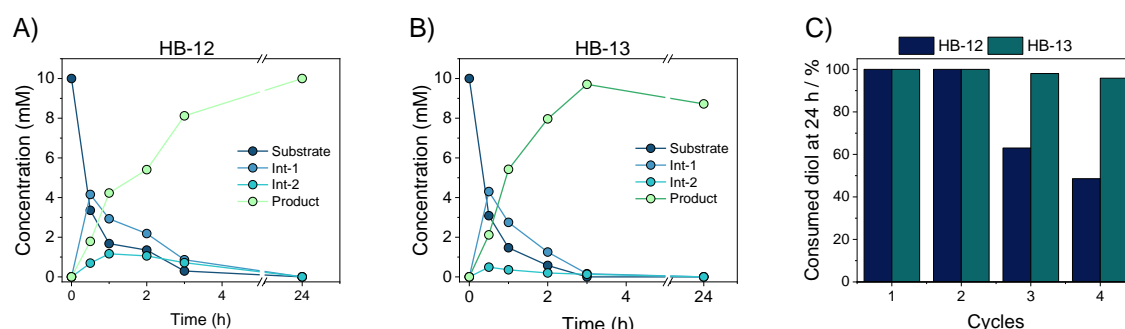

Figure 6.12: Effect of polymer coating. A) and B) Reaction-time course of HB12 (**Entry 7**) and HB-13 (**Entry 8**) with and without polymer coating, respectively. C) Operational batch stability. All reaction mixes containing 20 mM 1,5-PD, 1 mM NAD$^+$, 0.15 mM FAD$^+$, 200 mM sodium phosphate buffer pH 8 at 30°C.

When the substrate load was scaled up 20 mM, HB13 reached 90% CY in 6 hours (**Figure 6.13.A**). Next, we tested the operational stability of this new biocatalysts' version HB9 by submitting to consecutive recycling in 24 hours batch cycles. **Figure 6.12.C** shows how the PAH-coating heterogeneous biocatalyst was operationally stable for 4 consecutive cycles, while the substrate conversion decayed below 50% when using the non-coated HB12. This operational stability is also reflected in product titer along the batch cycles, which shows a similar trend as the substrate conversion using these two types of biocatalysts (**Figure 6.13.B**).
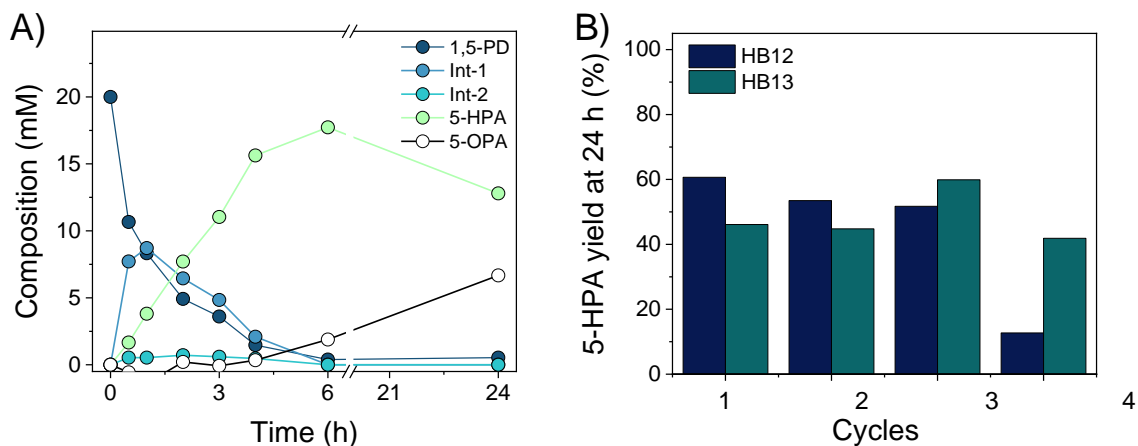
Figure 6.13: Reaction-time course of Distribution 5c covered with polymer at a) 10 mM of substrate and b) 20 mM of substrate. All reaction mixes containing 1 mM NAD+, 0.15 mM FAD+, 200 mM sodium phosphate buffer pH 8 at 30°C.

After successful assembling a productive and stable multi-functional heterogeneous biocatalyst (HB-13, **Entry 8**, **Table 6.1**), we scaled the batch reaction volume up to 30 mL with mol 5% biocatalyst load and monitored the product titer, the oxygen concentration, and the pH along the reaction course. Moreover, the pH was maintained constant to a value of 8 by NaOH titration since a pH-decay occurs concomitantly to the 5-HPA production (**Annex 6.5**). The performance of HB-13 in this scaled cascade is notorious as CY = 80% is achieved after 96 h (**Figure 6.14**).
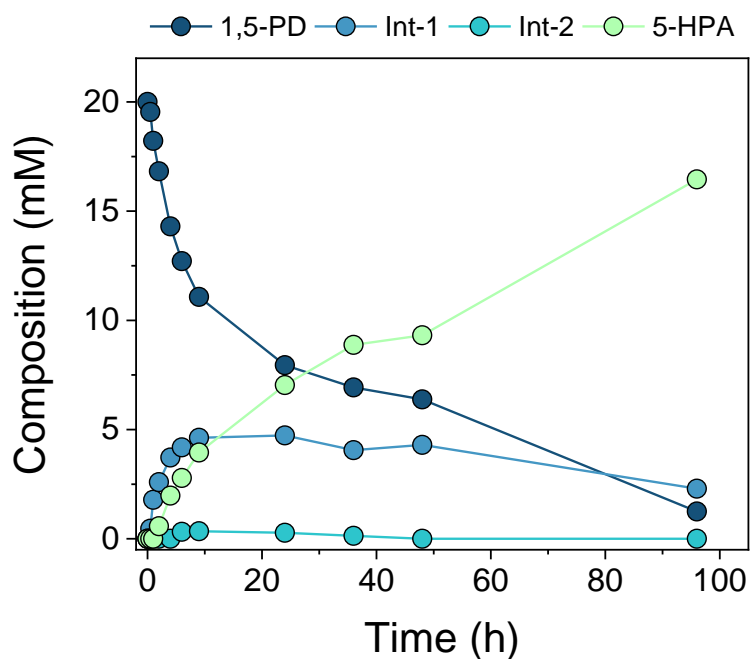

Figure 6.14: Operational stability of HB-13 at batch reaction. All reaction mixes containing 20 mM 1,5-PD, 1 mM NAD+, 0.15 mM FAD+, 200 mM sodium phosphate buffer pH 8 at 30°C in 600 rpm stirring. 1 g of biocatalyst in 30 mL of reaction volume.

This means a titer of 16.4 mM 5-HPA, with a maximum volumetric productivity of 59 mg $L^{-1} \cdot h^{-1}$ and an excellent cofactor recycling that reached a total turnover number of 1100 for NAD^+, meaning a 92% of conversion (**Annex 6.6**). We observe that, the oxygen level medium decreases (to more than 20% compared to initial rate at the beginning of reaction (**Annex 6.5**). This decrease in the oxygen level may relate to the fast consume of diol in the first steps, which relates to reduction of NAD^+ to NADH. Thus, the regeneration system consumes the oxygen presented in the reaction mix to oxidize NADH to NAD^+ covering the demand of the cofactor for the principal system. This fact may present a valuable proof for the perfect coupling between ADH dehydrogenases and regenerator cofactor system.

6.3.5. Employ of the biocatalyst in flow reaction

In our efforts to intensify the process, we decided to integrate HB-13 into a packed bed reactor (PBR). This PBR was firstly flushed with 10 mM 1,5-PD at 0.02 mL·min^{-1} showing no product formation. The UV-Vis spectra of samples collected from the PBR outlet demonstrated that all redox cofactor was in its reduced form; NADH, indicating the premature cascade halt due to an inefficient NAD^+ recycling (**Figure 6.15**).
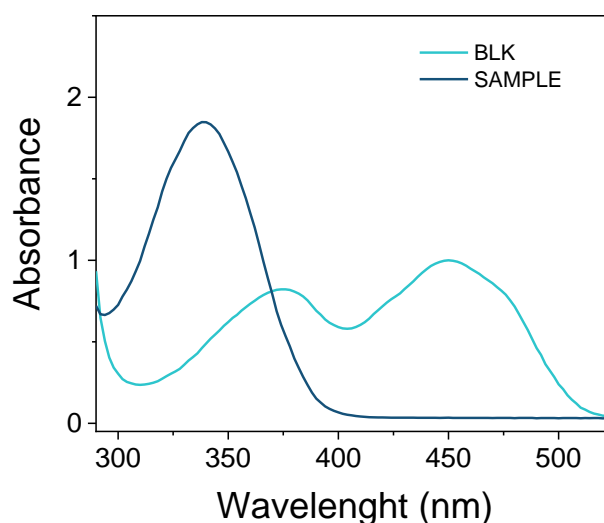

Figure 6.15: Spectra of the mix reaction before (BLK) and after reaction on the PBR (SAMPLE). All reaction mixes containing 20 mM 1,5-PD, 1 mM NAD^+, 0.15 mM FAD^+, 200 mM sodium phosphate buffer pH 8 at 30°C.

Interestingly, the outlet samples were colorless indicating that FAD^+ was either absorbed to the surface of HB13 as reported for other heterogeneous biocatalysts coated with cationic polymers or reduced to $FADH_2$ and not reoxidized due to the absence of oxygen. This latter hypothesis is supported by the poor solubility of oxygen in the aqueous media and the lack of aeration within the PBR, explaining why the PBR fails to transform 1,5-PD into 5-HPA due to the inefficient FAD and NAD^+ in situ regeneration. To surpass the mass transport limitations posed by the poor solubility of oxygen (0.25 mM), we flushed the PBR with an air-saturated solution but unfortunately neither did we detect product.

Inspired by previous work from Nidetzky´s[204] and Turner´s[205] groups who managed to release soluble oxygen in a flow reactor flushing hydrogen peroxide in presence of catalase, we decided to follow a similar approach to enable the NOX recycling action. As HB-13 integrates CAT, we run the PBR packed with this multi-functional heterogeneous biocatalyst using 20 mM 1,5-PD at varying H_2O_2 concentration and 0.02 mL min^{-1}. At 45 mM of H_2O_2, we achieved a maximum substrate conversion and product yield of 80% and 60% determined by GC, respectively (**Figure 6.16**).
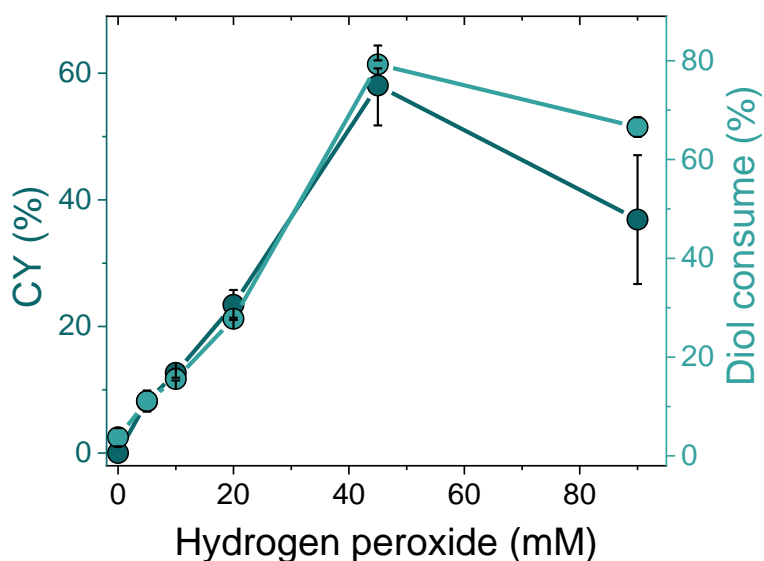

Figure 6.16: Optimization of biocatalyst in flow reaction. Ramp of hydrogen peroxide concentrations. All reaction mixes containing 20 mM 1,5-PD, 1 mM NAD$^+$, 0.15 mM FAD$^+$, 200 mM sodium phosphate buffer pH 8 at 30°C.

However, at 90 mM H_2O_2 we observed a dramatic decay in the CY likely due to the harmful effect of the hydrogen peroxide in enzyme stability. The UV-Vis analysis of the samples collected in the reactor outlet evidenced that 10 mM H_2O_2 is enough to completely maintain the redox cofactor in its oxidized form; NAD$^+$, favoring its utilization in the two consecutives dehydrogenase-mediated oxidations (**Figure 6.17**).
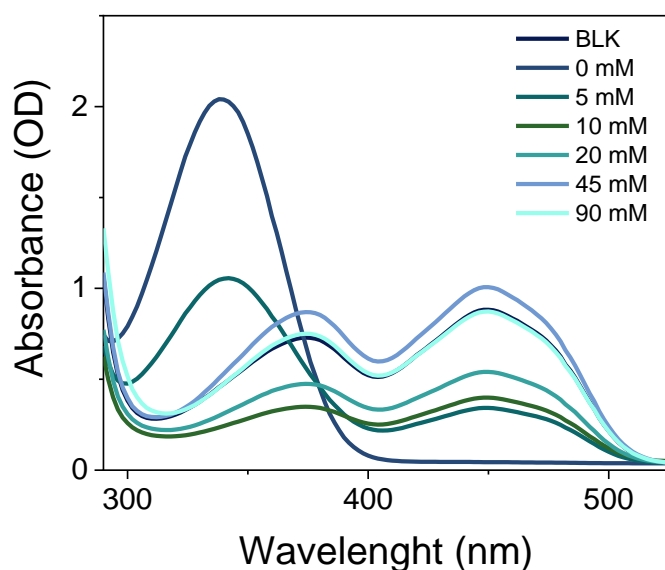
Figure 6.17: Spectra of the mix reaction at different concentrations of hydrogen peroxide after reaction. All reaction mixes containing 20 mM 1,5-PD, 1 mM NAD^+, 0.15 mM FAD^+, 200 mM sodium phosphate buffer pH 8 at 30°C.

Unlike in absence of H_2O_2, the flavin cofactor left the PBR in its oxidized form (yellow color), supporting the fact that immobilized NOX was saturated with the oxygen in situ formed by the co-immobilized CAT. As expected, we also observed a linear correlation between the pH drop at the reactor outlet and the product titer due to the accumulation of higher concentrations of the target hydroxy acid (**Figure 6.18**).
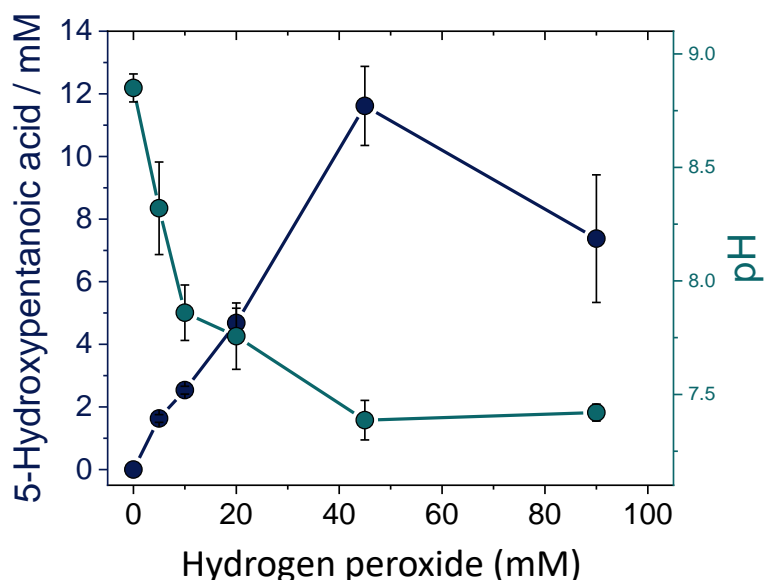

Figure 6.18: 5-Hydroxy pentanoic acid production and pH level at different hydrogen peroxide concentrations. All reaction mixes containing 20 mM 1,5-PD, 1 mM NAD^+, 0.15 mM FAD^+, 200 mM sodium phosphate buffer pH 8 at 30°C.

Once the optimal H_2O_2 concentration was found, we next challenged the PBR to a flow rate ramp to find its productivity limits. **Figure 6.18.A** shows that the maximum product CY is achieved at the lowest flow rate, giving as result the lowest STY. In contrast, the highest STY productivity was at flow rate of 0.1 mL·min^{-1} at the expense of the product titer with a CY as low as 18%.
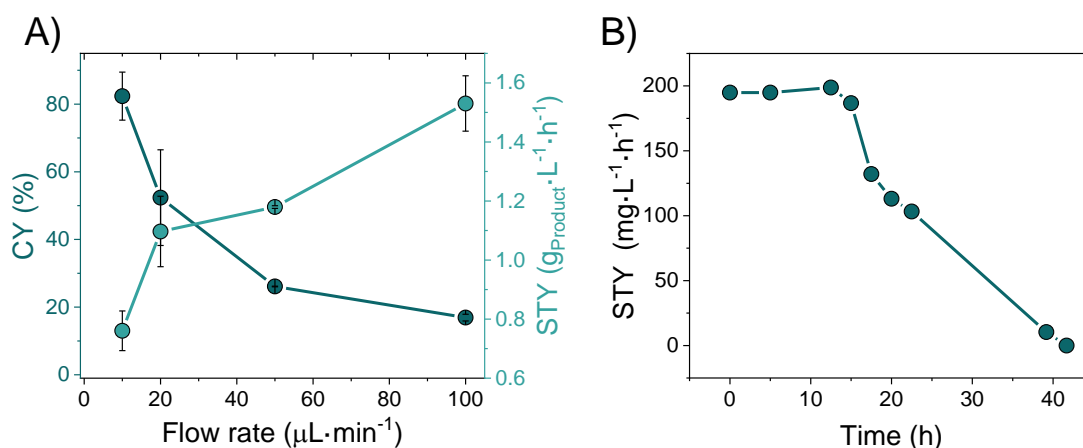

Figure 6.19: Optimization of biocatalyst in flow reaction. A) Ramp of flow operational stability. All reaction mixes containing 20 mM 1,5-PD, 1 mM NAD$^+$, 0.15 mM FAD$^+$, 45 mM of H_2O_2, 200 mM sodium phosphate buffer pH 8 at 30°C.

Thus, we selected 0.01 mL·min^{-1} and 45 mM H_2O_2 as the optimal conditions to operate the PBR. Under these conditions, we achieve 8.3 mM 5-HP in 150 min (residence time) with a STY = 200 mg·L^{-1}·h^{-1} (**Figure 6.19.B**). This STY is 4 times higher than the volumetric productivity achieved with the batch reactor using the same heterogeneous biocatalyst at a similar load. Moreover, the 1H-NMR of the sample collected directly from the outlet of the PBR shows a purer product than the sample separated from batch process catalyzed by the free enzyme system (**Figure 6.20**).
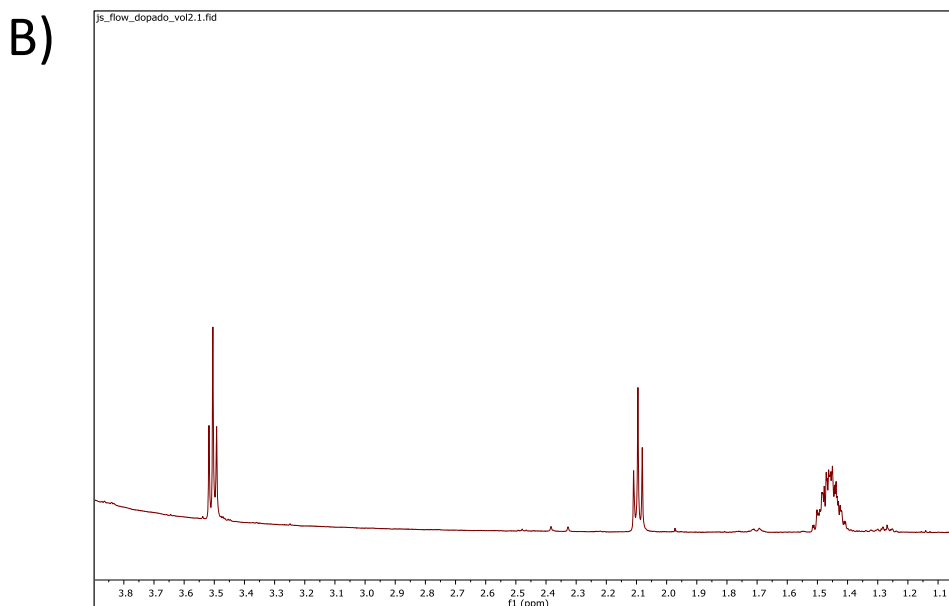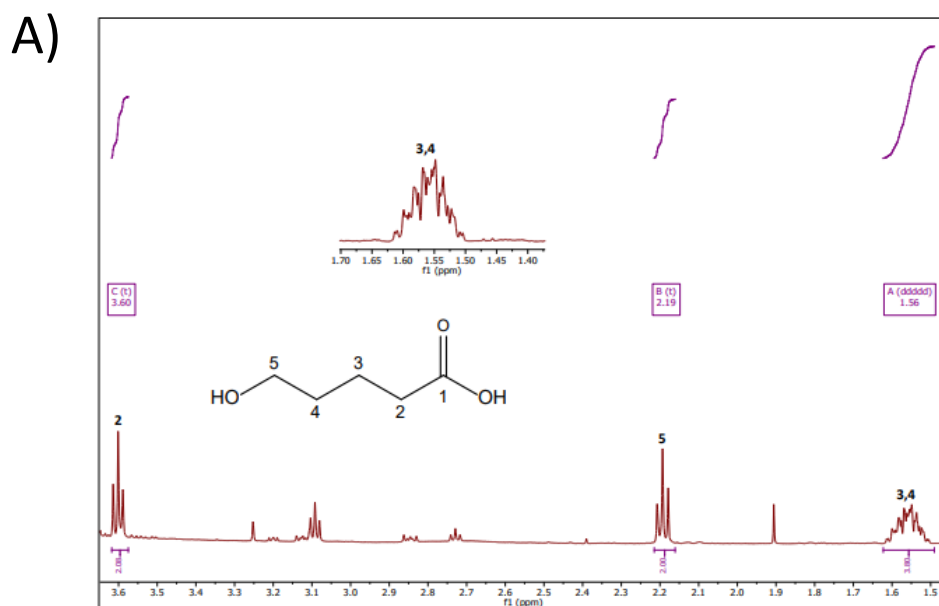
Figure 6.20: NMR spectra of our product a) Velasco-Lozano et al 2022 b) current work. The assigned signals correspond to the produced ω-HA, 5hydroxypentanoic acid (2d). 1H NMR (500 MHz, Deuterium Oxide) δ 3.60 (t, J = 6.3 Hz, 2H, H2), 2.19 (t, J = 7.1 Hz, 2H,H5), 1.56 (m, 4H,H3,H4)[206].

By analyzing the product and intermediate profile in the PBR outlet under these conditions, we can determine the specific productivity of each reaction step catalyzed for each enzyme participating in the cascade. Table 6.2 shows that the rate-limiting step is the intermediate oxidation of the lactol to the lactone as the specific productivity of ADH2 is 7- and 16-fold lower than those of ADH1 and LAC, respectively. Remarkably, the in situ generation of oxygen is the most catalytically efficient step assuring the efficient recycling of the redox cofactor.

Table 6.2: Table of operational stability flow parameters under best conditions.

Flow rate[a]	Productivity (%)	R_T (min)	STY[b]	ADH1[c] (h⁻¹)	ADH2[c] (h⁻¹)	LAC[c] (h⁻¹)
10	80,5 ± 7,1	150	760 ± 70	3019,3 ± 86,4	437,7 ± 25,7	6909,2 ± 406,5

[a]Flow rate ($\mu L \cdot min^{-1}$). [b]Space-Time Yield ($mg_{Prodcut} \cdot L^{-1} \cdot h^{-1}$). [c]Specific activity.

Under the optimal reaction conditions described above, the PBR was continuously operated for 44 hours (**Figure 6.19.B**). The STY was maintained during the first 12 hours of operation and afterwards steadily decreased to reach a value of zero after 44 hours of operation, detecting no product in the reactor outlet. Ex situ activity assays demonstrated that the STY decay during the continuous operation is related to the inactivation of the co-immobilized ADH1 and ADH2, since the ADH activity of 44 hours operated HB10-PAL was 2 times lower than its fresh counterpart, unlike NOX, which retained 90% of its initial activity in the exhausted biocatalysts.

6.4. CONCLUSION

Encouraged by the capacity of an cell-free biosynthetic cascade to transform 1,ω-diols into ω-hydroxy acids in one-pot through concurrent manner. We intended to assemble this 5-enzymes cascade into porous carriers as artificial chassis to enhance the biocatalysts performance and enable the biocatalyst reutilization and integration in flow reactors. To that aim, we first tuned the spatial organization of the enzymes involved the cascade, finding that the optimal spatial configuration is having the 5 enzymes co-immobilized on the same carrier bead and co-localized at its most outer region. The resulting heterogeneous biocatalyst was further improved by increasing the enzyme load of the NAD^+ recycling system to boost the in situ cofactor regeneration and H_2O_2 removal and coating the immobilized enzymes a cationic polymer to increase the quaternary. As result, the multi-functional heterogeneous biocatalyst (HB13) we present here offers an excellent performance and operational stability for the biosynthesis of 5-hydroxy pentanoic acid (5-HPA) starting from 1,5-pentanodiol (1,5-PD) under both discontinuous and continuous operation in batch and flow reactor, respectively. During the implementation HB13 in packed-bed reactors (PBR) to perform the process in flow, we faced the limitation of oxygen solubility within the reaction as aeration under atmospheric pressure was inefficient. As solution we decided to supply H_2O_2 to the reactor to in situ and within the PBR generate the oxygen demanded by the NAD^+ recycling systems based on the NADH oxidase catalase pair. The optimal spatial configuration of these two enzymes together the robustness of whole enzymatic system tolerated up to 45 mM H_2O_2 and used it efficiently within the micrometric particle that HB13. As far as we know this process holds the record in number of enzymes ever assembled in a cell-free biosynthetic cascade operated in flow, exhibiting a reasonable productivity despite oxygen-dependent enzymes are involved. Our work illustrates the potential of rationally arrangement the spatial localization of enzymes to fabricate more productive and heterogeneous biocatalytic systems able to access to complex biosynthetic cascades. The results herein presented demonstrate how several enzymes can be

confined into porous materials to assemble an artificial metabolic pathway. Although this system with three tandem reactions coupled with two orthogonal ones catalyzed by 5 different enzymes is still too small to be considered as cell-free metabolic pathway, we forecast that ratio enzyme co-immobilization can bring the complexity of metabolism to continuous biosynthesis of industrially relevant products, contributing to expand the portfolio of the chemical biomanufacturing.

CHAPTER 7. CONCLUSIONS

Esta tesis tenía como objetivo en el ensamblaje de un robusto y eficiente biocatalizador heterogéneo para la producción de omega-hidroxiácidos a partir de dioles renovables. Para esta tarea, se diseñó un camino para abordar todos los aspectos necesarios para la optimización de la cascada inmovilizada en la reacción. Las conclusiones son:

• Hemos desarrollado un sistema multienzimático que de forma orquestada y secuencial cataliza la doble oxidación de dioles a lactonas y su hidrolisis para, finalmente, producir omega-hidroxiácidos, integrando un eficiente sistema de regeneración de NAD+ que utiliza oxigeno como aceptor final de electrones.

• Este sistema multienzimático fue probado para transformar una amplia colección de dioles de cadena corta en sus correspondientes hidroxiácidos, demostrando una excelente enantioselectividad para la desimetrización de del diol proquiral 3-metil-1,5-pentanodiol.

• Hemos analizado una batería de materiales porosos y químicas de inmovilización para aumentar la robustez de una variante de la ADH1 con cola de histidinas. A través de una caracterización de la actividad y de cambios estructurales de la enzima inmovilizada, revelamos el impacto de los diferentes protocolos de inmovilización en las propiedades enzimáticas.

• La determinación de la anisotropía a través del marcaje con fluoróforos de la enzima inmovilizada reveló ser una parámetro muy importante que muestra una correlación de actividad/estabilidad que depende directamente de las dinámicas estructurales de la enzima inmovilizada.

• El biocatalizador heterogéneo seleccionado fue acoplado de forma exitosa con una NADH oxidasa y una catalasa, ambas co-inmovilizadas en diferentes materiales porosos para la oxidación de dioles, integrando, in situ, un sistema de regeneración de NAD+ en batch. Este sistema multienzimático inmovilizado pudo ser reciclado hasta 5 veces, manteniendo más del 50% de su conversión inicial.

• Describimos la preparación de un soporte heterofuncional que permite la coinmovilización de una variedad de enzimas que requieres distintas químicas de inmovilización. El soporte desarrollado posee tres funcionalizaciones químicas distintas (amino, aldehído y cobalto) las cuales permiten una rápida e irreversible inmovilización a pH neutro de enzimas, tanto con cola de histidinas como sin ellas.

• Así mismo, expandimos la química de funcionalización a diferentes materiales porosos, como celulosa y metacrilato. Sin embargo, las propiedades fisicoquímicas de la superficie del soporte influyen de manera importante en la actividad operacional y en la estabilidad del sistema coinmovilizado.

• Inmovilizamos la cascada enzimática en materiales porosos como chasis artificial para aumentar la capacidad del biocatalizador y ampliar su reutilización e integración en sistema de flujo. Para ese propósito, primero estudiamos la organización espacial de las enzimas de la cascada, encontrando que la configuración espacial óptima es tener las 5 enzimas co-inmovilizadas en la misma partícula y co-localizadas en su región externa.

• El biocatalizador heterogéneo resultante fue mejorado incrementando la cantidad de enzima inmovilizada del sistema regenerador de NAD+ para su reciclaje y eliminación de peróxido de hidrógeno, y la cobertura de las enzimas inmovilizadas con un polímero catiónico para incrementar la estabilidad de la estructura cuaternaria.

• El biocatalizador heterogéneo multifuncional ofrece un excelente rendimiento y estabilidad operacional para la biosíntesis del ácido 5-hidroxipentanoico a partir de 1,5-pentanodiol a través de procesos continuos y discontinuos de batch y flujo respectivamente.

This thesis aimed to assemble a robust and efficiency heterogenous biocatalyst to yield ω-HA from renewable diols. For that task, a path was designed to assess all the needed aspects to optimize the immobilized cascade in reaction. The final conclusions:

- We have developed an orchestrated multi-enzyme system that sequentially catalyzes the double oxidation of diols into lactones and their hydrolysis to ultimately yield ω-HA, integrating an efficient NAD^+ regeneration system that uses oxygen as the ultimate electron acceptor.

- This multi-enzyme system was proven to transform a wide scope of linear and branched short-chain diols into their corresponding ω-HAs, demonstrating an excellent enantioselectivity for the desymmetrization of prochiral 3-methyl-1,5-pentanediol.

- We have screened a battery of porous carriers and immobilization chemistries to enhance the robustness of a His-tagged variant of ADH1. Through characterizing the activity and structural changes undergone by the enzyme upon the immobilization, we reveled the impact of the different immobilization protocols on the enzyme properties.

- The determination of the anisotropy exhibited by the fluorophore-labelled and immobilized enzymes is revealed as a very informative parameter that unveils an activity/stability trade-off that depends on the structural dynamics of the immobilized enzyme.

- The selected heterogeneous biocatalyst was successfully mixed with a NADH oxidase and a catalase co-immobilized on a different porous carrier to selectively oxidize 1,ω-diols, integrating an in situ NAD^+ recycling system in batch. This immobilized multi-enzyme systems could be recycled up to 5 cycles, retaining more than 50% of its initial conversion.

- We describe the preparation of a heterofunctional support that enables the coimmobilization of a variety of enzymes requiring different immobilization chemistries. The herein-characterized support possesses three chemical functionalities, namely, amino, aldehyde, and cobalt moieties, which synergistically permit a fast irreversible enzyme immobilization at neutral pH values of His-tagged and untagged enzymes.

- We also showed the possibility to expand this surface chemistry to different porous materials such as cellulose and methacrylate microbeads; however, the physicochemical properties of the support surface impact the operational performance and stability of the coimmobilized systems.

- We intended to assemble this 5-enzymes cascade into porous carriers as artificial chassis to enhance the biocatalysts performance and enable the biocatalyst reutilization

and integration in flow reactors. To that aim, we first tuned the spatial organization of the enzymes involved the cascade, finding that the optimal spatial configuration is having the 5 enzymes co-immobilized on the same carrier bead and co-localized at its most outer region.

- The resulting heterogeneous biocatalyst was further improved by increasing the enzyme load of the NAD$^+$ recycling system to boost the in situ cofactor regeneration and H$_2$O$_2$ removal and coating the immobilized enzymes a cationic polymer to increase the quaternary structure stability.

- The multi-functional heterogeneous biocatalyst offers an excellent performance and operational stability for the biosynthesis of 5-hydroxy pentanoic acid (5-HPA) starting from 1,5-pentanodiol (1,5-PD) under both discontinuous and continuous operation in batch and flow reactor, respectively.
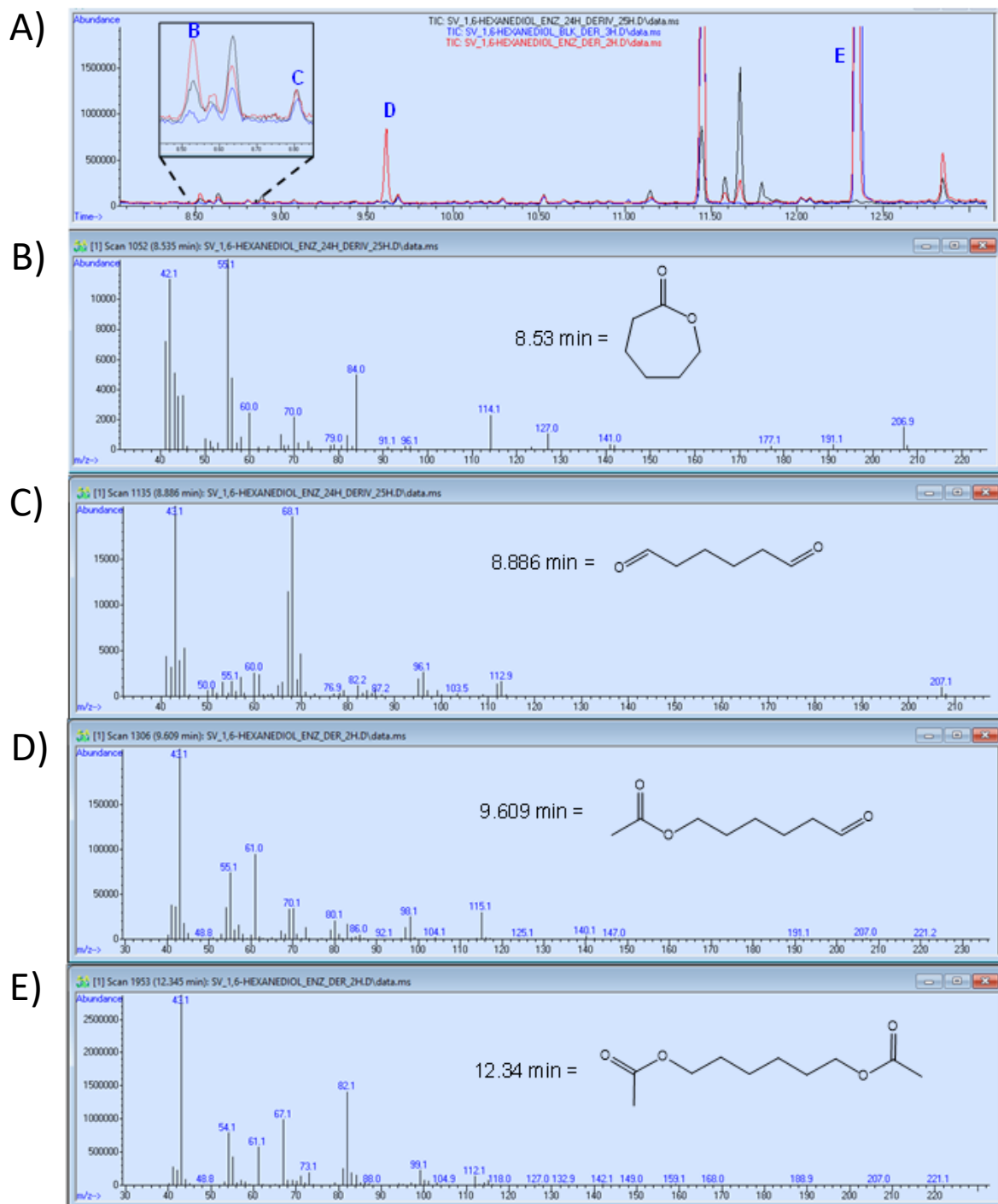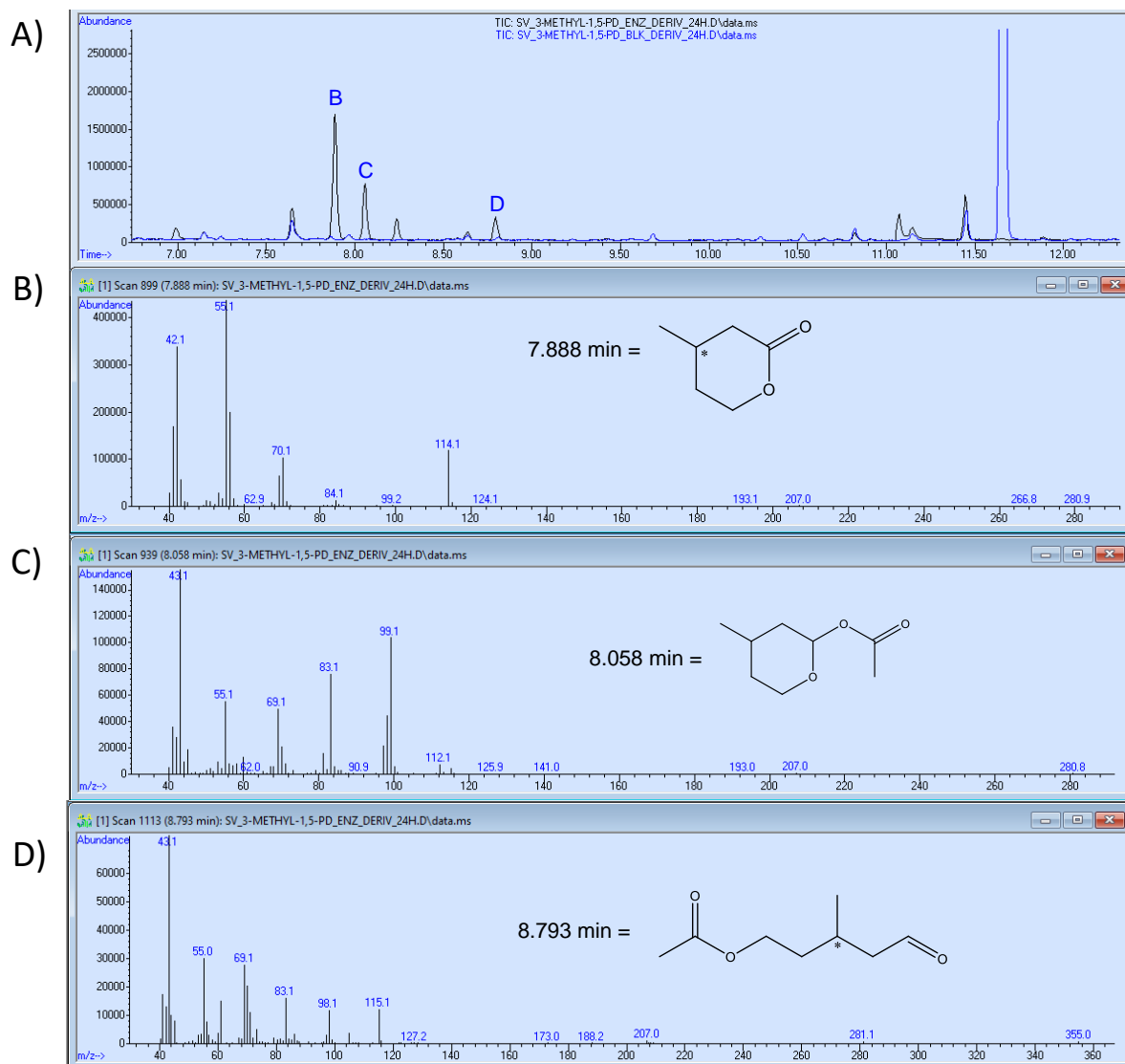
ANNEX
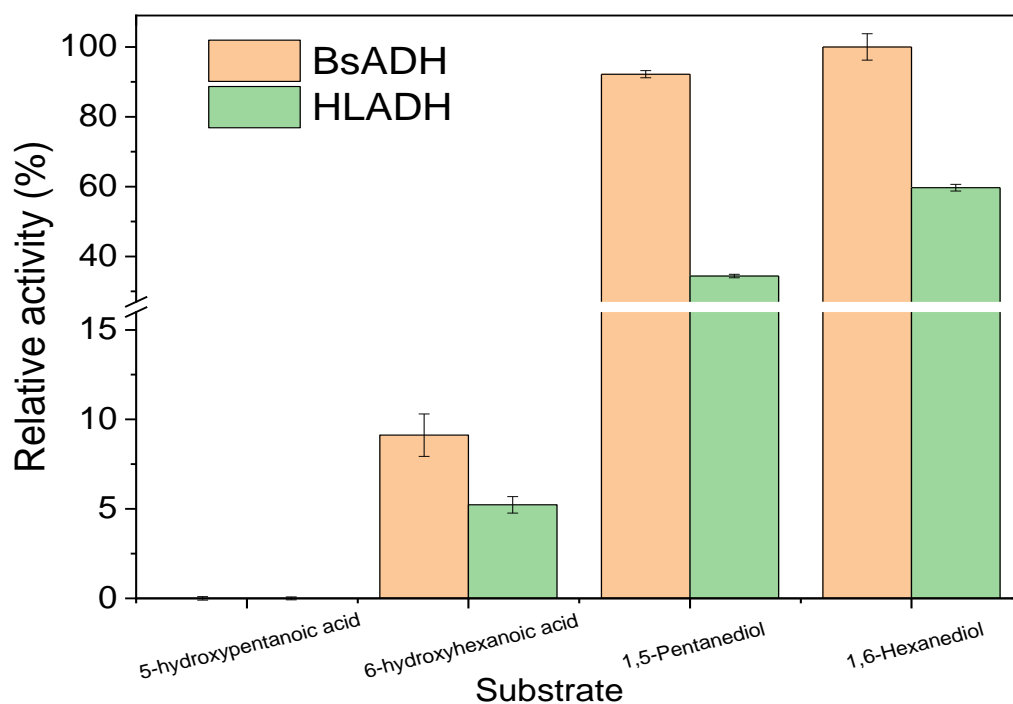
Annex 3.1: Activity of ADHs towards ω-HAs. In all cases reactions were spectrophotometrically measured employing reaction mixtures containing: 10 mM of substrate, 1 mM NAD+ in 100 mM sodium phosphate buffer 100 mM pH 8 at 30 ° (100% of relative activity corresponds to the activity of ADH2 towards substrate 1,5-pentanodio (3a) (2.17 U·mg-1).
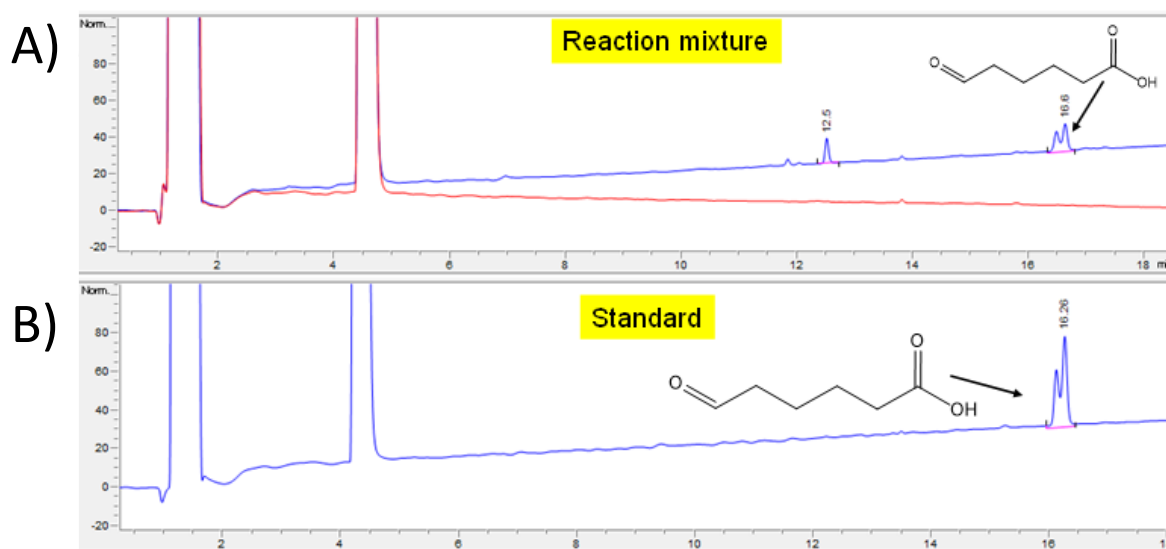
Annex 3.2: HPLC chromatograms of derivatized 6-oxohexanoic acid. A) Overlay HPLC chromatograms of reaction products (blue line) and reaction blank (red line) after 24 h starting from 3a. B) 6-oxohexanoic acid standard (3e). In both, A) and B) chromatograms, samples were derivatized as described elsewhere[180] obtaining O-benzylhydroxylamine derivatives of aldehydes. Retention time of O-benzylhydroxylamine derivative of 6-oxohexanoic acid (3e) is 16.6 min.

Annex 3.3: GC-MS chromatograms of reaction products starting from 3a. A) Overlay chromatograms of reaction products after 0 h (black line), 2 h (red line) and 24 h (blue line) starting from 3a. B) GC-MS analysis of peak retained at 8.53 min, corresponding to ε-caprolactone formed during the sample organic-phase extraction of the acetylated ω-HA (3d). C) GC-MS analysis of peak retained at 8.886 min corresponding to adipaldehyde. D) GC-MS analysis of peak retained at 9.609 min corresponding to acetylated adipaldehyde E) GC-MS analysis of peak retained at 12.34 min corresponding to acetylated 1,6-hexanediol (3a).
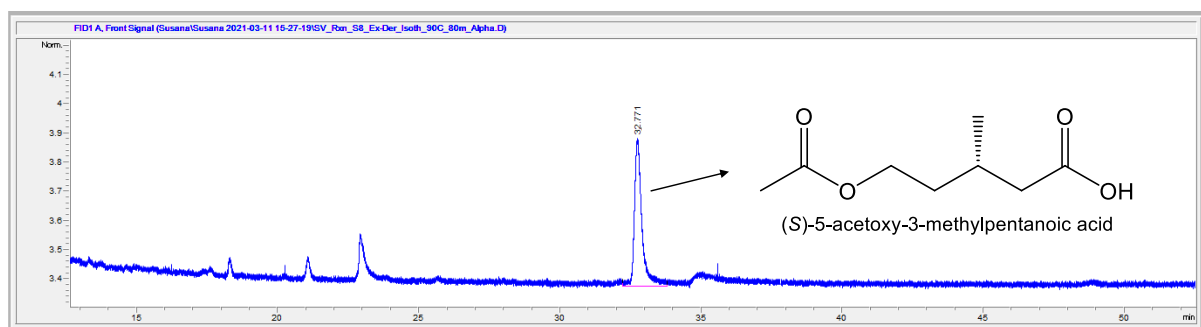
Annex 3.4: GC-MS chromatograms of reaction products starting from 6a. A) Overlay chromatograms of reaction products at 0 h (blue line) and 24 h (black line) starting from 6a. B) GC-MS analysis of peak retained at 7.888 min, corresponding to 4-methyl-tetrahydro-2H-pyran-2-one, which is formed during sample preparation for GC-MS analysis from the acetylated ω-HA (6d) in aqueous medium and later extracted with DCM. C) GC-MS analysis of peak retained at 8.058 min, corresponding to acetylated 4-methyl-tetrahydro-2H-pyran-2-ol (6b). D) GC-MS analysis of peak retained at 8.793 min, corresponding to acetylated 5-hydroxy-3-methylpentanal.
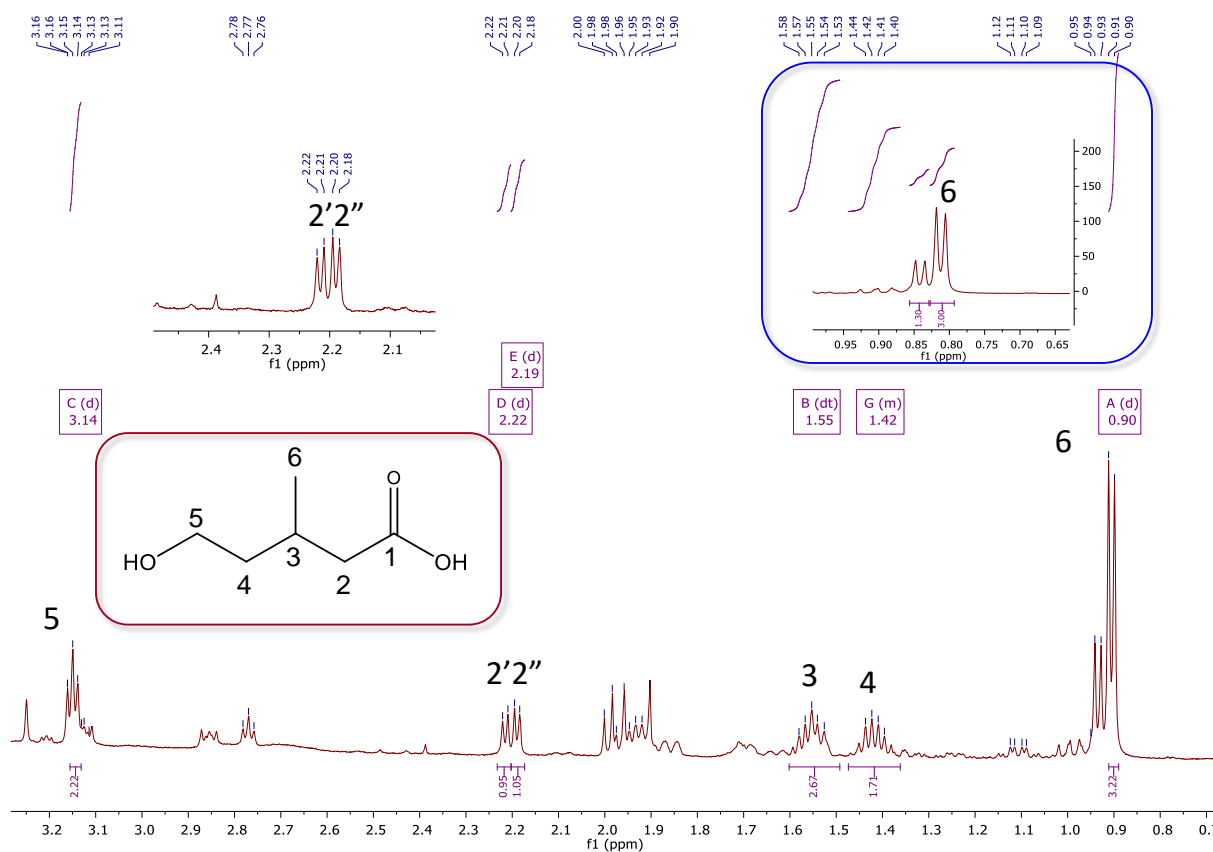
Annex 3.5: ^{1}H NMR of the reaction crude in presence of the cell-free enzyme system after 24 h using 6a as substrate. The assigned signals correspond to the produced ω-HA, 5-hydroxy-3-methylpentanoic acid (6d). ^{1}H NMR (500 MHz, Deuterium Oxide) δ 3.14 (d, J = 5.4 Hz, 2H, H5), 2.22 (d, J = 5.8 Hz, 1H, H2'), 2.19 (d, J = 5.6 Hz, 1H, H2''), 1.55 (dt, J = 13.6, 7.1 Hz, 1H, H3 (overlaps with a CH_2 of an unknown compound, hence it integrates 3), 1.42 (m, 2H, H4), 0.90 (d, 3H, H6).

Annex 3.6: Chiral chromatography of reaction products after 24h starting from 6a. Retention times of acetylated S-6d corresponds to 32.77min.
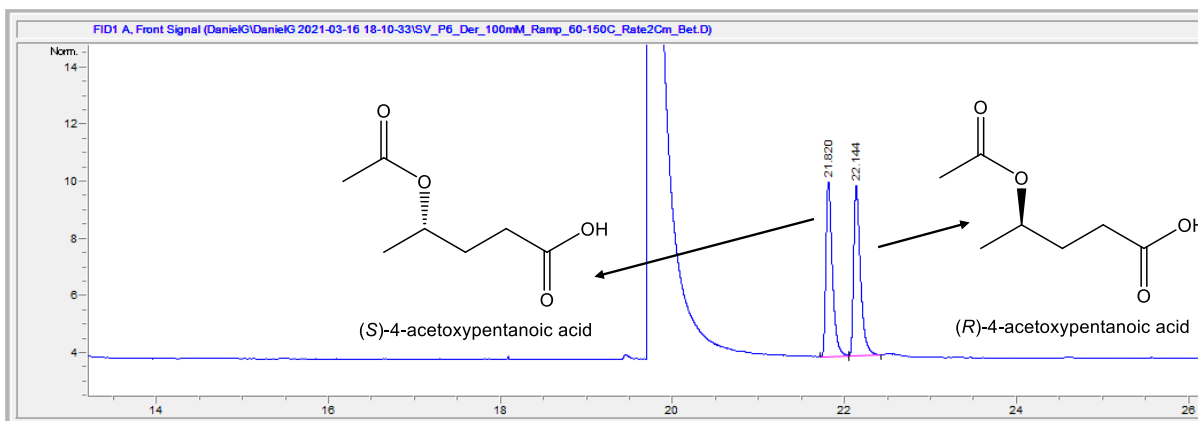
Annex 3.7: Chiral chromatography of rac-7d standard. Retention times of acetylated ω-HA enantiomers: R-7d and S-7d correspond to 21.8 min and 22.15 min, respectively. Enantiomer assigning was done using the enzymatically synthesized R-7d by the reduction of levulinic acid catalyzed by the R-specific ketoreductase from Lactobacillus kefir[207].
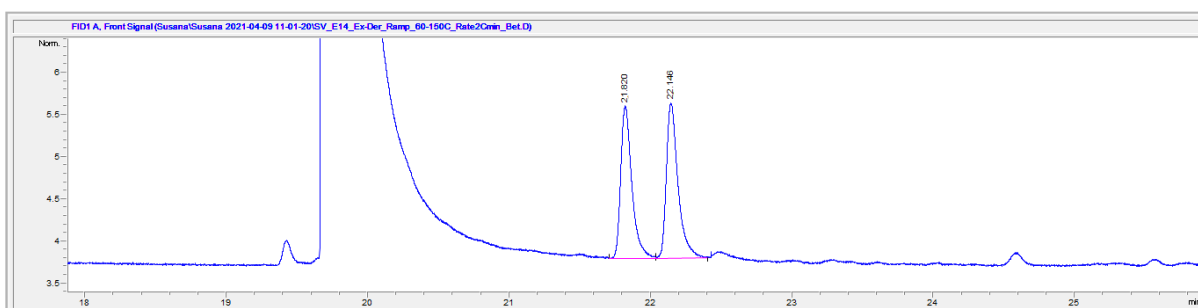
Annex 3.8: Chiral chromatography of reaction crude in presence of the cell-free system after 24 h starting from rac-7a. Retention times of acetylated ω-HA: R-7d and S-7d correspond to 21.8 min and 22.15 min, respectively.
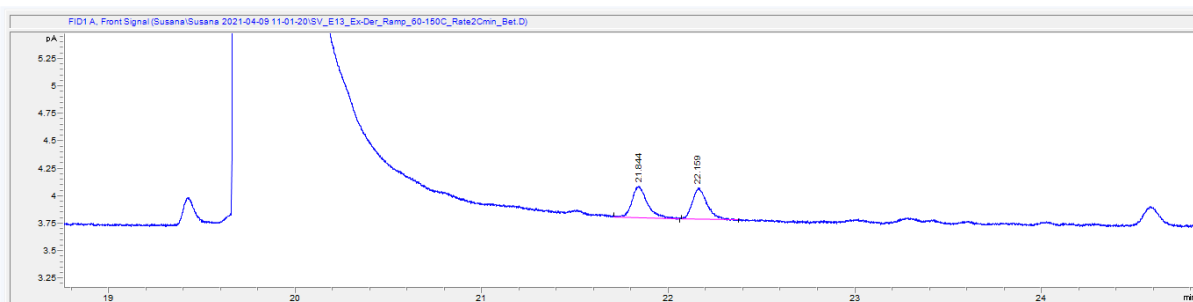
Annex 3.9: Chiral chromatography of lactone hydrolysis after 24h starting from lactone rac-7c (20 mM) catalyzed by ReLAC. For the lactone hydrolysis determination, we first extracted the remaining lactone by liquid-liquid extraction with ethyl acetate and then the sample was derivatized. Retention times of acetylated ω-HA enantiomers: R-7d and S-7d correspond to 21.83min and 22.15min, respectively.

A)

B)
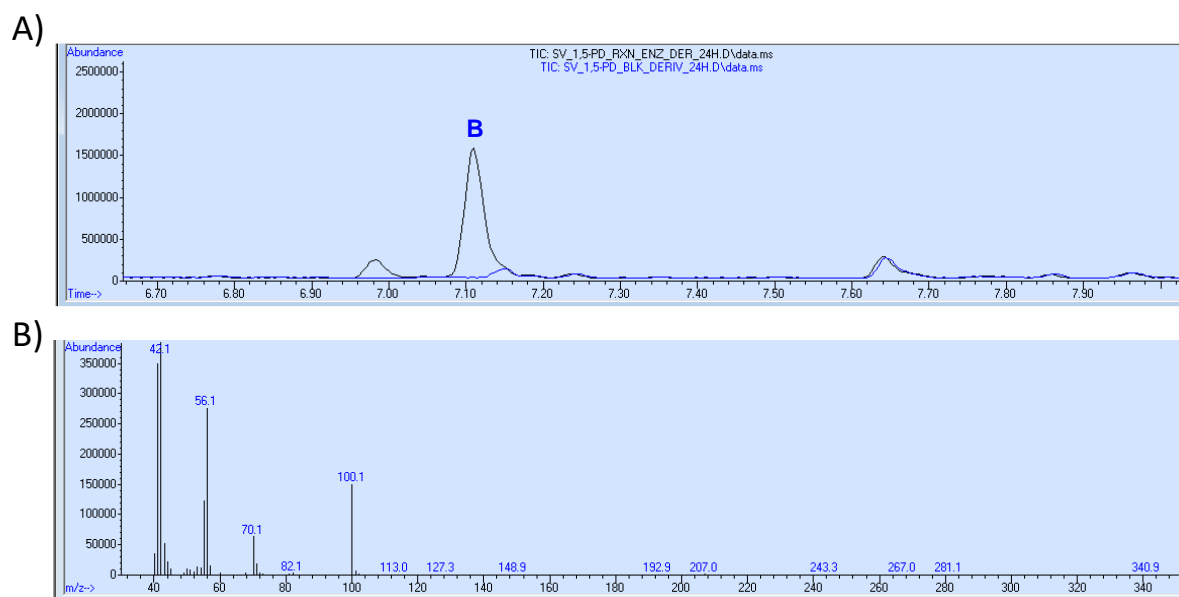
Annex 3.10: GC-MS chromatograms of reaction products starting from 2a. A) Overlay GC chromatograms of reaction products (black line) and reaction blank (blue line) after 24 h. B) MS analysis of peak retained at 7.11 min corresponding to δ-valerolactone (2d), which is formed during the sample organic-phase extraction of the acetylated ω-HA (2d) for GC-MS analysis.
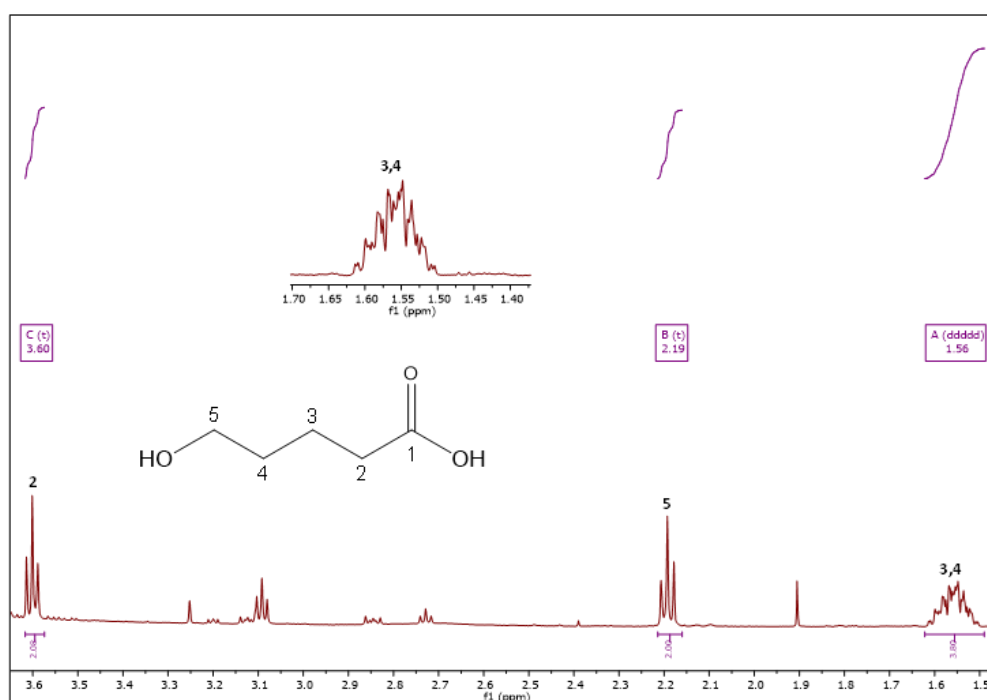
Annex 3.11: ^{1}H NMR of the reaction mixture after 24 h starting from 2a. The assigned signals correspond to the produced ω-HA, 5-hydroxypentanoic acid (2d). 1H NMR (500 MHz, Deuterium Oxide) δ 3.60 (t, J = 6.3 Hz, 2H, H2), 2.19 (t, J = 7.1 Hz, 2H,H5), 1.56 (m, 4H,H3,H4)[206].
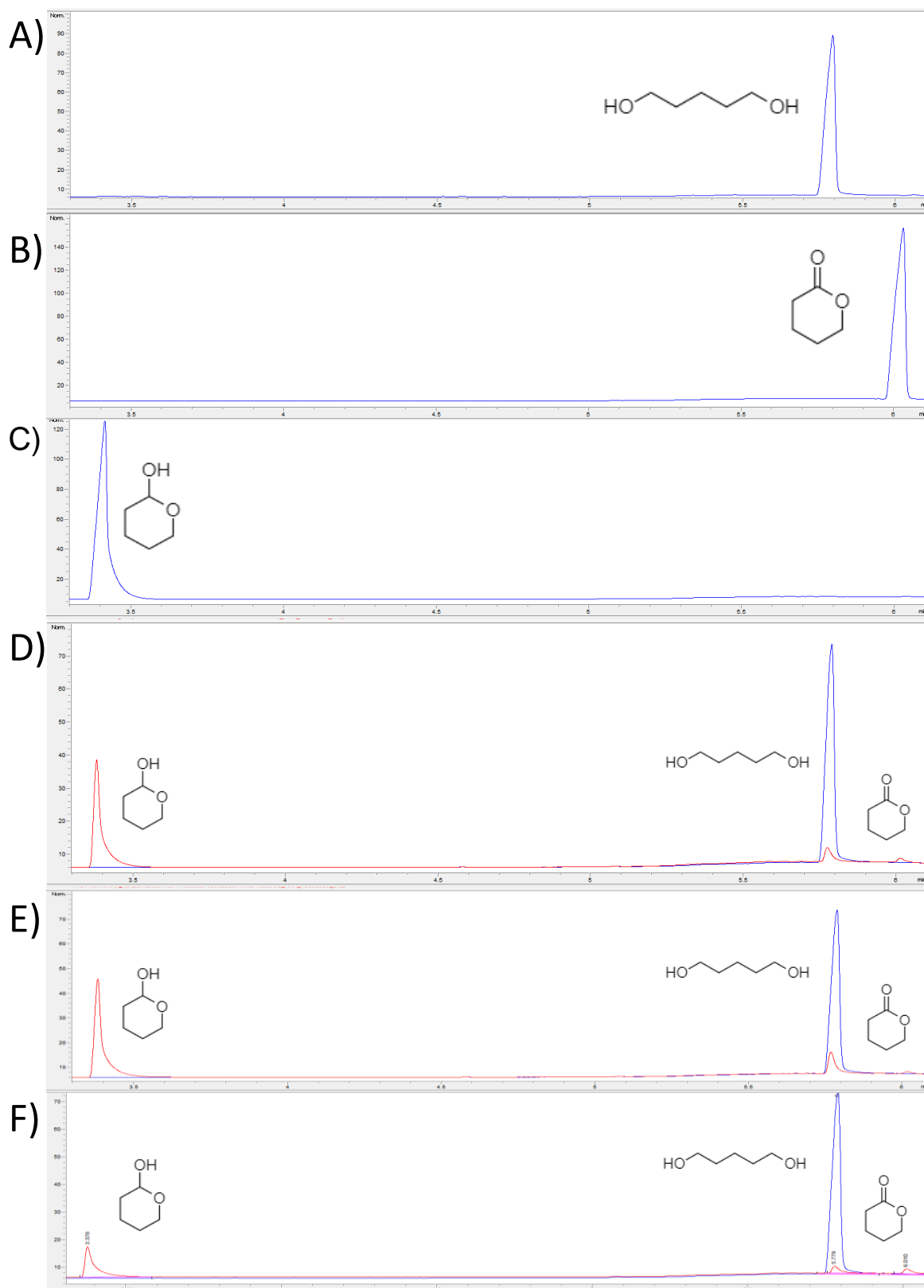
Annex 4.1: GC-FID chromatograms. Standards: A) 1,5-Pentanediol; B) 2-Hydroxytetrahydropyran (lactol); C) δ-varelolactone. Overlayed reaction mix at time zero (blue) and 24 hours reaction crude (red) using His-ADH1 immobilized on D) LdAG-Co^{2+}, E) AG-Co^{2+}/E, and F) EziG1.
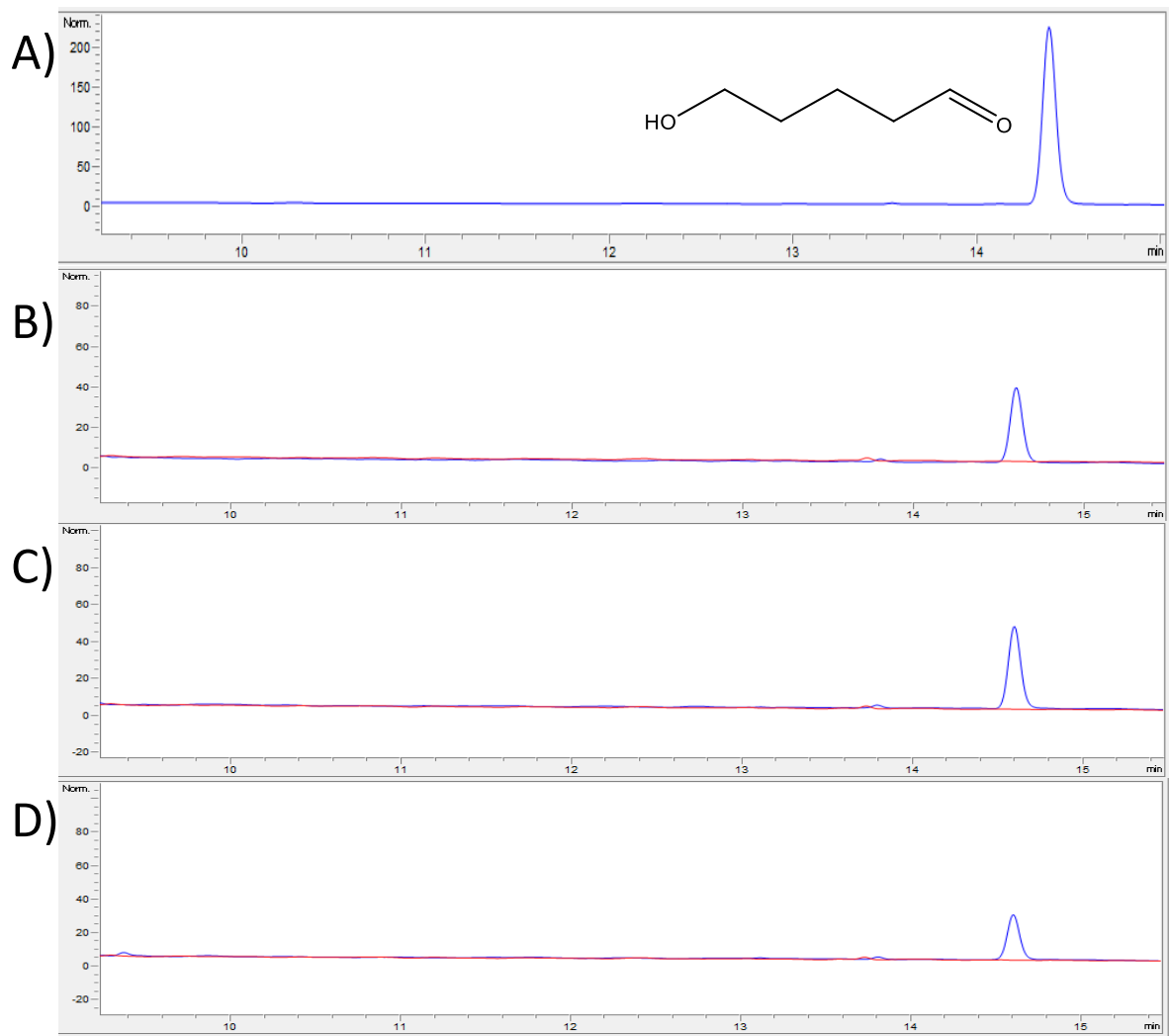
Annex 4.2: HPLC chromatograms. A) Standard of 5-hydroxypentanal. Overlayed reaction mix at time zero (blue) and 24 hours reaction crude (red) using His-ADH1 immobilized on B) LdAG-Co^{2+}, (C) AG-Co^{2+}/E, and (D) EziG1.
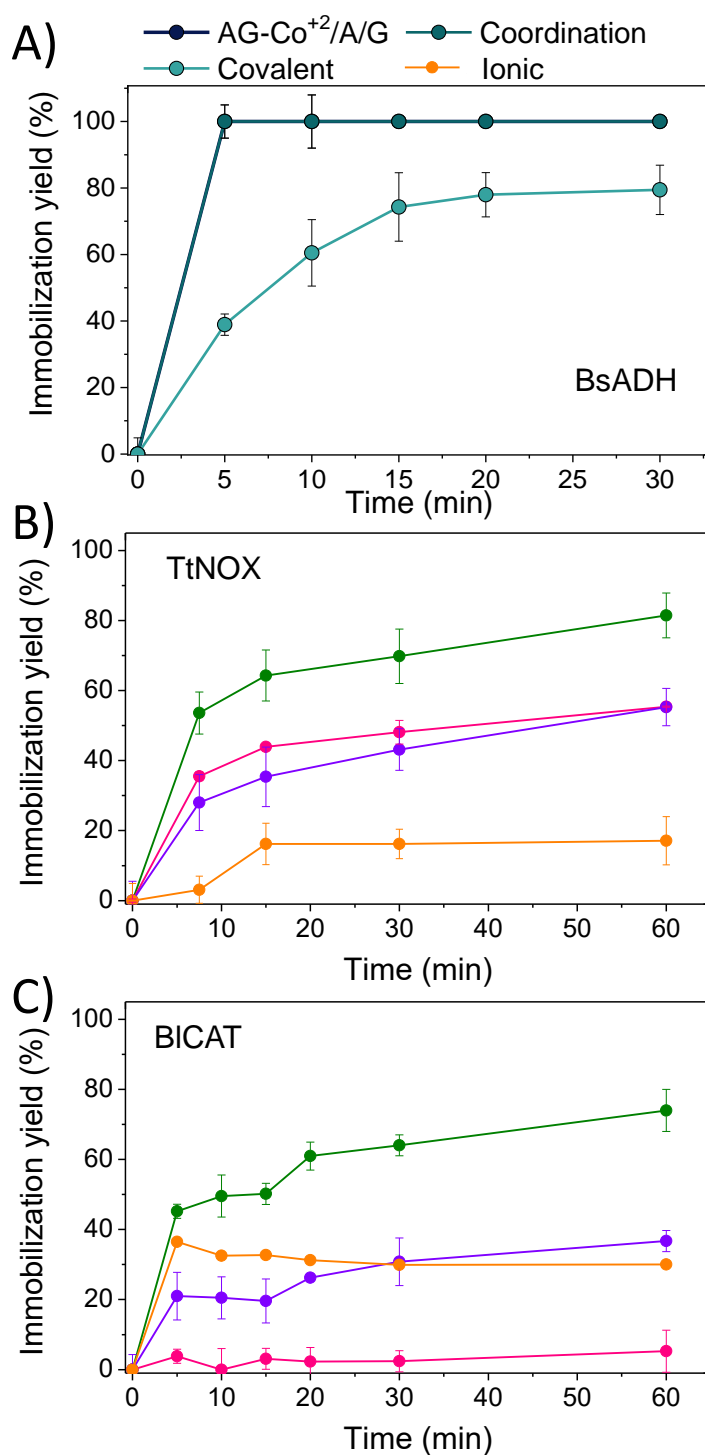
Annex 5.1: Driving immobilization chemistry of different enzymes, A) histidine tagged ADH1, B) untagged NOX, and C) untagged CAT, on triheterofunctional activated agarose microbeads. For AG-Co²⁺/A/G, the immobilization was carried out at 100 mM sodium phosphate buffer pH 8 (green lines and symbols). To only assess the coordination chemistry (pink line), the immobilization was conducted by previously blocking the G groups of AG-Co²⁺/A/G (with glycine1M for 16h) and performing the immobilization at 1 M NaCl. To only assess the covalent chemistry (purple line), the immobilization was conducted at 0.3 M imidazoleand1 M NaCl. To only assess the ionic chemistry (orange line), the immobilization was conducted by previously blocking G groups of AG-Co²⁺/A/G (with glycine 1 M for 16h) and performing the immobilization at 0.3 M imidazole. The green line represents the immobilization course on AG-Co2+/A/G where the three chemistries can participate. In all cases, the immobilization was conducted at 4°C and 250 rpm.
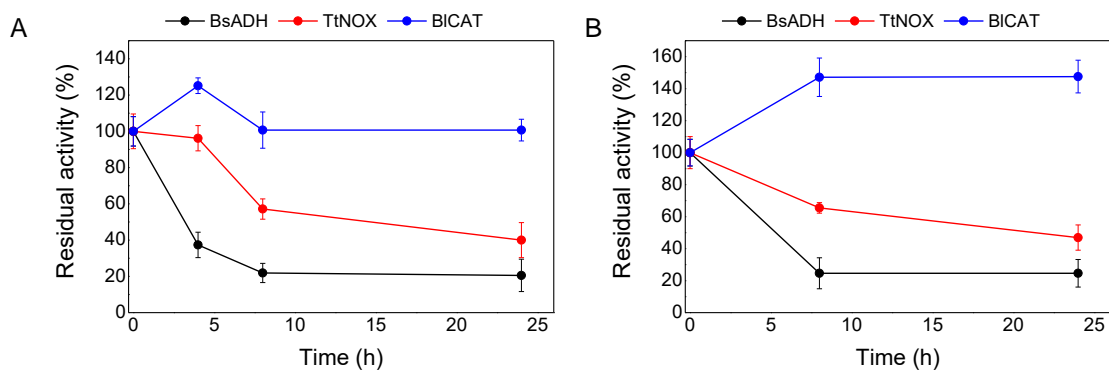
Annex 5.2: Residual activity of HB1 (A) and HB2 (B) under operation conditions. Reaction mixture consisted in 50 mg of HB and 0.3 mL of 20 mM 1,5-pentanediol, 1 mM NAD$^+$, 0.15 mM FAD$^+$ in 100 mM sodium phosphate buffer pH 8 at 30°C.

Distribution	HBs	Enzymes	mg biocatalyst /rxn	Enzyme load (mg/g)
1	HB-1	HLADH	20	15.00
	HB-2	BsADH	20	5.00
	HB-3	NOX	20	0.51
	HB-4	CAT	20	0.016
	HB-5	SiLAC	20	1.58
2	HB-6	HLADH	40	7.50
		NOX		0.21
		CAT		0.0066
	HB-7	BsADH	40	2.50
		NOX		0.13
		CAT		0.0043
	HB-5	SiLAC	20	1.58
3	HB-8	HLADH	80	4.21
		BsADH		1.26
		NOX		0.23
		CAT		0.01
	HB-5	SiLAC	20	1.58
4	HB-9	HLADH	100	3
		BsADH		1
		NOX		0.18
		CAT		0.012
		SiLAC		0.32

Annex 6.1: Table of the different contain of the distributions of the different heterogenous biocatalysts.
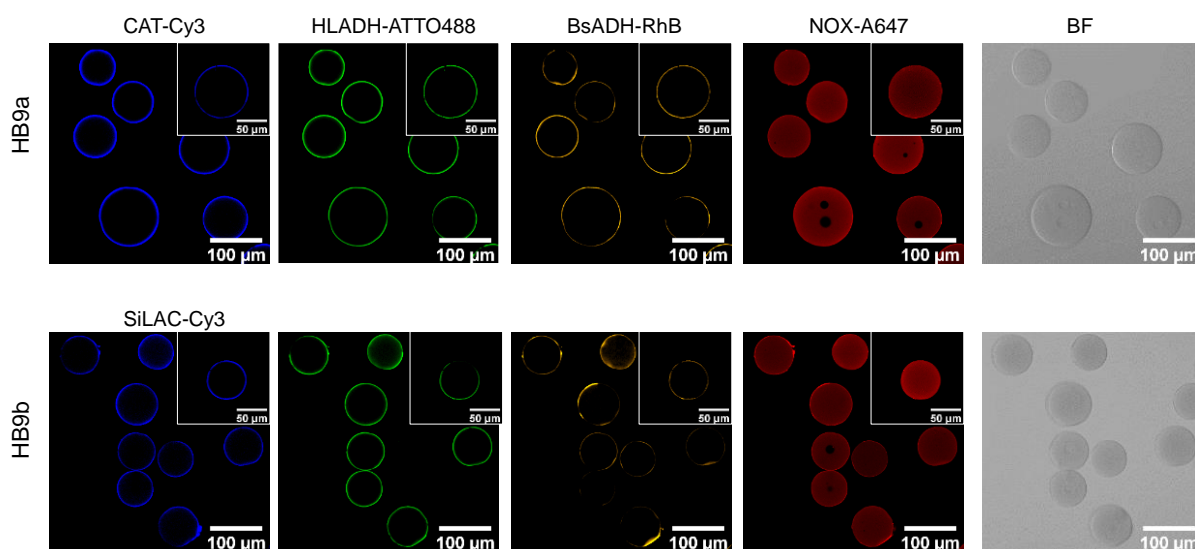
Annex 6.2: Uncontrolled spatial distribution of co-immobilized multi-enzyme system.

Enzyme	NaCl (M)	Immobilization Time (h)	Offered enzyme load (mg/g)	Immobilization Yield (%)
NOX-Tt- A647	0.0	2	0.5	69
	0.1	2	0.5	51
	0.5	2	0.5	47
	1.0	2	0.5	57

0 M   **0.1 M**   **0.5 M**   **1 M**

- ⟶ **NaCl concentration** ⟶ **+**
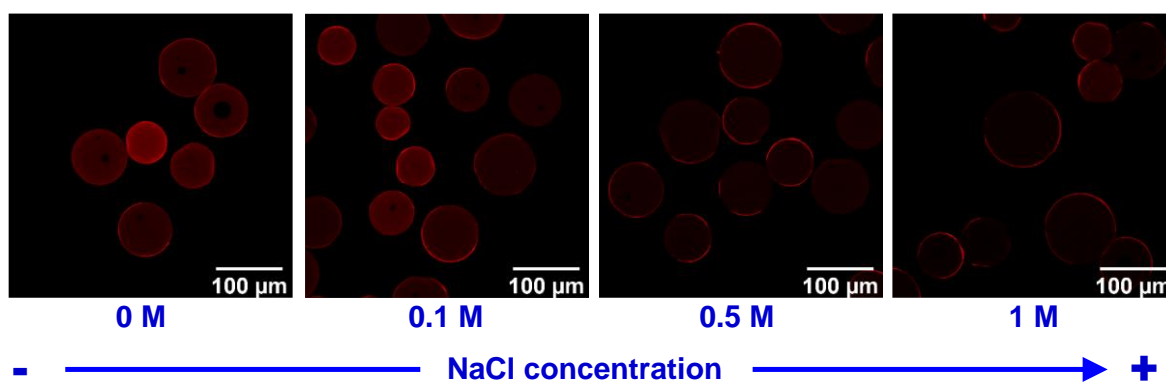
Annex 6.3: Control of the spatial distribution of TtNOX by ionic strength.

HB10a: BsADH-RhB/HLADH-ATTO488/**SiLAC**/CAT-Cy3/NOX-A647

CAT-Cy3   HLADH-ATTO488   BsADH-RhB   NOX-A647   Merged   Merged/BF
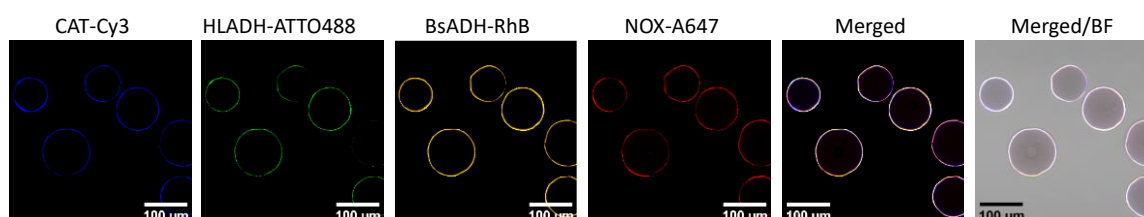
HB10b: BsADH-RhB/HLADH-ATTO488/SiLAC-Cy3/**CAT**/NOX-A647

SiLAC-Cy3   HLADH-ATTO488   BsADH-RhB   NOX-A647   Merged   Merged/BF
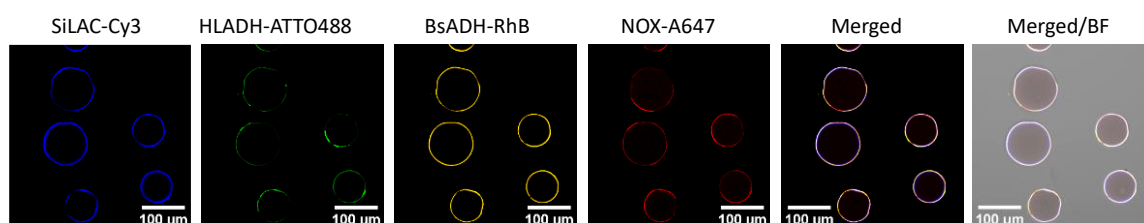
Annex 6.4: Controlled spatial distribution of co-immobilized multi-enzyme system.
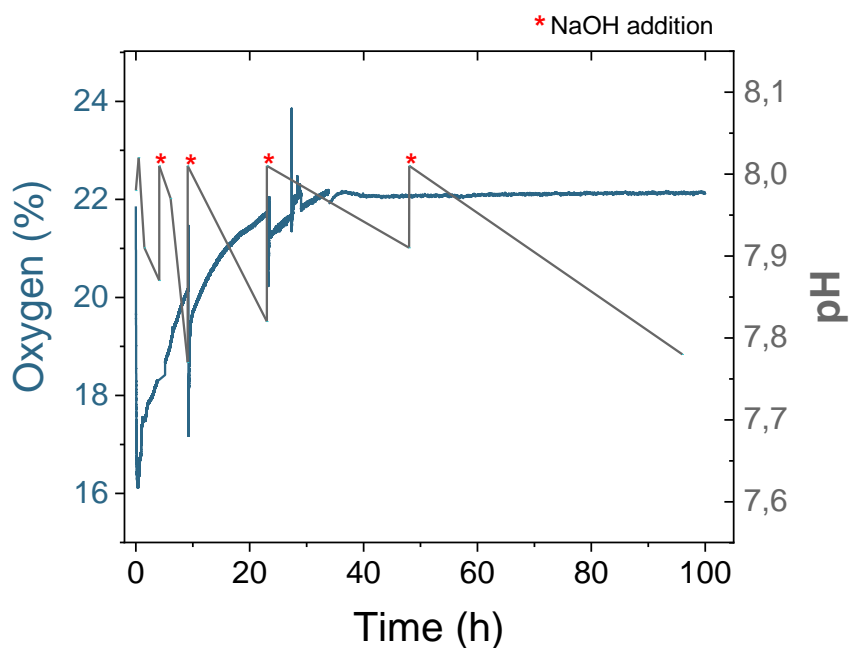
Annex 6.5: Oxygen and pH level of the batch scale-up reaction. Red start indicates pH adjustment by adding NaOH till medium reaches pH 8.

Operatinal Time	Diol conversion [%]	TTN of BsADH (first oxidation)[b]	TTN of HlADH (second oxidation)[c]	ω-HA yield [%]	TTN of HlADH (hydrolysis)[d]	TTN of Regeneration cofactor (NOX)[d]
0,5	2	2254	0	0	0	856
1	9	8749	0	0	0	3324
2	16	15569	997	3	8811	6991
4	28	27930	3408	10	30131	14292
6	36	35750	5356	14	42420	19366
9	45	43754	7412	20	60260	24627
23	60	59100	12620	35	107349	36083
36	65	64089	15542	44	135333	41133
48	68	66766	16068	47	142049	42719
96	94	91929	28377	82	250858	65572

Annex 6.6: Table of the operational parameters of the batch scale-up reaction. Reaction mix containing 20 mM 1,5-PD, 1 mM NAD+, 0.15 mM FAD+, 200 mM sodium phosphate buffer pH 8 at 30°C.

REFERENCES

1.   Roduner, E., *Understanding catalysis.* Chemical Society Reviews, 2014. **43**(24): p. 8226-8239.

2.   Sheldon, R.A. and H. Van Bekkum, *Fine chemicals through heterogeneous catalysis.* 2008: John Wiley & Sons.

3.   Ertl, G., H. Knözinger, and J. Weitkamp, *Handbook of heterogeneous catalysis.* Vol. 2. 1997: VCH Weinheim.

4.   McNaught, A.D. and A. Wilkinson, *Compendium of chemical terminology.* Vol. 1669. 1997: Blackwell Science Oxford.

5.   Bugaenko, D.I., A.V. Karchava, and M.A. Yurovskaya, *Transition metal-free cross-coupling reactions to form carbon–heteroatom bonds.* Russian Chemical Reviews, 2022. **91**(6): p. RCR5022.

6.   Wu, L., et al., *Carbonylations of alkenes with CO surrogates.* Angewandte Chemie International Edition, 2014. **53**(25): p. 6310-6320.

7.   Hajos, Z.G. and D.R. Parrish, *Asymmetric synthesis of bicyclic intermediates of natural product chemistry.* The Journal of organic chemistry, 1974. **39**(12): p. 1615-1621.

8.   Hajos, Z. and D. Parrish, *Werkwijze Voor de Bereiding van 1, 3-dioxycycloalkanen.* German Patent DE, 1971. **2102623**.

9.   Hajos, Z.G. and D.R. Parrish, *2-Alkyl-2-(3-oxoalkyl)-1, 3-cyclopentadiones.* 1976, Google Patents.

10.   Huang, X.-R., et al., *Solvent-effects tuning the catalytic reactivity of prolinamides in asymmetric aldol reactions.* Tetrahedron: Asymmetry, 2014. **25**(24): p. 1590-1598.

11.   Wilson, J. and E.Y.-X. Chen, *Organocatalytic cross-coupling of biofuranics to multifunctional difuranic C11 building blocks.* ACS Sustainable Chemistry & Engineering, 2016. **4**(9): p. 4927-4936.

12.   Hauer, B., *Embracing nature's catalysts: a viewpoint on the future of biocatalysis.* Acs Catalysis, 2020. **10**(15): p. 8418-8427.

13.   Loew, O., *On the chemical nature of enzymes.* Science, 1899. **10**(261): p. 955-961.

14.   Stein, R.L., *Kinetics of enzyme action: essential principles for drug hunters.* 2011: John Wiley & Sons.

15.   Sancar, A., *Structure and function of photolyase and in vivo enzymology: 50th anniversary.* Journal of Biological Chemistry, 2008. **283**(47): p. 32153-32157.

16.   Pravda, L., et al., *Anatomy of enzyme channels.* BMC bioinformatics, 2014. **15**(1): p. 1-8.

17.   Fischer, E., *Einfluss der Configuration auf die Wirkung der Enzyme.* Berichte der deutschen chemischen Gesellschaft, 1894. **27**(3): p. 2985-2993.

18.   Luk, L.Y., E.J. Loveridge, and R.K. Allemann, *Protein motions and dynamic effects in enzyme catalysis.* Physical Chemistry Chemical Physics, 2015. **17**(46): p. 30817-30827.

19.   Liu, W. and P. Wang, *Cofactor regeneration for sustainable enzymatic biosynthesis.* Biotechnology advances, 2007. **25**(4): p. 369-384.

20.   Bornscheuer, U. and K. Buchholz, *Highlights in biocatalysis–historical landmarks and current trends.* Engineering in Life Sciences, 2005. **5**(4): p. 309-323.

21.   Judge, A. and Michael S. Dodd, *Metabolism.* Essays in Biochemistry, 2020. **64**(4): p. 607-647.

22.   Gröger, H., F. Gallou, and B.H. Lipshutz, *Where chemocatalysis meets biocatalysis: in water.* Chemical Reviews, 2022. **123**(9): p. 5262-5296.

23.   Siedentop, R., et al., *Getting the Most Out of Enzyme Cascades: Strategies to Optimize In Vitro Multi-Enzymatic Reactions.* Catalysts, 2021. **11**(10): p. 1183.

24. Wang, X., et al., *Cofactor NAD (P) H regeneration inspired by heterogeneous pathways.* Chem, 2017. **2**(5): p. 621-654.

25. Schrittwieser, J.H., et al., *Artificial biocatalytic linear cascades for preparation of organic molecules.* Chemical reviews, 2018. **118**(1): p. 270-348.

26. Post, J.V. *Simulation of metabolic dynamics*. in *Proceedings of the Annual Symposium on Computer Application in Medical Care*. 1980. American Medical Informatics Association.

27. Anselmi, S., et al., *Discovery and Rational Mutagenesis of Methionine Sulfoxide Reductase Biocatalysts To Expand the Substrate Scope of the Kinetic Resolution of Chiral Sulfoxides.* ACS catalysis, 2023. **13**(7): p. 4742-4751.

28. Finnigan, W., et al., *RetroBioCat Database: A Platform for Collaborative Curation and Automated Meta-Analysis of Biocatalysis Data.* ACS catalysis, 2023. **13**: p. 11771-11780.

29. López-Gallego, F., E. Jackson, and L. Betancor, *Heterogeneous systems biocatalysis: the path to the fabrication of self-sufficient artificial metabolic cells.* Chemistry–A European Journal, 2017. **23**(71): p. 17841-17849.

30. Abdelraheem, E.M., et al., *Biocatalysis explained: from pharmaceutical to bulk chemical production.* Reaction Chemistry & Engineering, 2019. **4**(11): p. 1878-1894.

31. Basso, A. and S. Serban, *Industrial applications of immobilized enzymes—A review.* Molecular Catalysis, 2019. **479**: p. 110607.

32. Guzik, U., K. Hupert-Kocurek, and D. Wojcieszyńska, *Immobilization as a strategy for improving enzyme properties-application to oxidoreductases.* Molecules, 2014. **19**(7): p. 8995-9018.

33. Schmidt-Dannert, C. and F. Lopez-Gallego, *A roadmap for biocatalysis–functional and spatial orchestration of enzyme cascades.* Microbial biotechnology, 2016. **9**(5): p. 601-609.

34. Velasco-Lozano, S., J. Rocha-Martin, and J. Santos, *Designing carrier-free immobilized enzymes for biocatalysis.* Frontiers in Bioengineering and Biotechnology, 2022. **10**: p. 924743.

35. Kumari, A., et al., *Isolation and immobilization of alkaline protease on mesoporous silica and mesoporous ZSM-5 zeolite materials for improved catalytic properties.* Biochemistry and biophysics reports, 2015. **2**: p. 108-114.

36. Ricardi, N.C., et al., *Highly stable novel silica/chitosan support for β-galactosidase immobilization for application in dairy technology.* Food chemistry, 2018. **246**: p. 343-350.

37. Batsalova, K., et al., *Hydrolysis of lactose by β-galactosidase immobilized in polyvinylalcohol.* Applied microbiology and biotechnology, 1987. **26**: p. 227-230.

38. Vasconcelos, A., et al., *Detergent formulations for wool domestic washings containing immobilized enzymes.* Biotechnology letters, 2006. **28**: p. 725-731.

39. Ibrahim, A.S.S., et al., *Enhancement of alkaline protease activity and stability via covalent immobilization onto hollow core-mesoporous shell silica nanospheres.* International journal of molecular sciences, 2016. **17**(2): p. 184.

40. Shukla, R.J. and S.P. Singh, *Structural and catalytic properties of immobilized α-amylase from Laceyella sacchari TSI-2.* International journal of biological macromolecules, 2016. **85**: p. 208-216.

41. Heikinheimo, L., et al., *Treating denim fabrics with Trichoderma reesei cellulases.* Textile Research Journal, 2000. **70**(11): p. 969-973.

42. Yu, Y., et al., *Immobilization of cellulases on the reversibly soluble polymer E udragit S-100 for cotton treatment.* Engineering in Life Sciences, 2013. **13**(2): p. 194-200.

43.   Yu, Y., et al., *Noncovalent immobilization of cellulases using the reversibly soluble polymers for biopolishing of cotton fabric.* Biotechnology and Applied Biochemistry, 2015. **62**(4): p. 494-501.

44.   Smith, E., et al., *Covalent bonding of protease to different sized enteric polymers and their potential use in wool processing.* Enzyme and Microbial Technology, 2010. **47**(3): p. 105-111.

45.   Silva, C.J., G. Gübitz, and A. Cavaco-Paulo, *Optimisation of a serine protease coupling to Eudragit S-100 by experimental design techniques.* Journal of Chemical Technology & Biotechnology: International Research in Process, Environmental & Clean Technology, 2006. **81**(1): p. 8-16.

46.   Husain, Q. and R. Ulber, *Immobilized peroxidase as a valuable tool in the remediation of aromatic pollutants and xenobiotic compounds: a review.* Critical reviews in environmental science and technology, 2011. **41**(8): p. 770-804.

47.   Bayramoglu, G., et al., *Immobilization of laccase on itaconic acid grafted and Cu (II) ion chelated chitosan membrane for bioremediation of hazardous materials.* Journal of Chemical Technology & Biotechnology, 2012. **87**(4): p. 530-539.

48.   Mohammadi, M., et al., *Immobilization of laccase on epoxy-functionalized silica and its application in biodegradation of phenolic compounds.* International journal of biological macromolecules, 2018. **109**: p. 443-447.

49.   Santos, J.C.S.d., et al., *Importance of the support properties for immobilization or purification of enzymes.* ChemCatChem, 2015. **7**(16): p. 2413-2432.

50.   Romero-Fernández, M., et al., *Designing continuous flow reaction of xylan hydrolysis for xylooligosaccharides production in packed-bed reactors using xylanase immobilized on methacrylic polymer-based supports.* Bioresource technology, 2018. **266**: p. 249-258.

51.   Chen, B., et al., *Effects of macroporous resin size on candida a ntarctica lipase b adsorption, fraction of active molecules, and catalytic activity for polyester synthesis.* Langmuir, 2007. **23**(3): p. 1381-1387.

52.   Johnson, C.R. and S.J. Bis, *Enzymatic asymmetrization of meso-2-cycloalken-1, 4-diols and their diacetates in organic and aqueous media.* Tetrahedron letters, 1992. **33**(48): p. 7287-7290.

53.   De Maio, A., et al., *Influence of the spacer length on the activity of enzymes immobilised on nylon/polyGMA membranes: Part 1. Isothermal conditions.* Journal of Molecular Catalysis B: Enzymatic, 2003. **21**(4-6): p. 239-252.

54.   De Maio, A., et al., *Influence of the spacer length on the activity of enzymes immobilised on nylon/polyGMA membranes: Part 2: Non-isothermal conditions.* Journal of Molecular Catalysis B: Enzymatic, 2003. **21**(4-6): p. 253-265.

55.   Bakker, M., et al., *Highly efficient immobilization of glycosylated enzymes into polyurethane foams.* Biotechnology and bioengineering, 2000. **70**(3): p. 342-348.

56.   Van de Velde, F., et al., *Carrageenan: A food-grade and biocompatible support for immobilisation techniques.* Advanced Synthesis & Catalysis, 2002. **344**(8): p. 815-835.

57.   de Souza, S.P., et al., *Cellulose as an efficient matrix for lipase and transaminase immobilization.* RSC advances, 2016. **6**(8): p. 6665-6671.

58.   K. de S. Lira, R., et al., *Agroindustrial wastes as a support for the immobilization of lipase from Thermomyces lanuginosus: Synthesis of hexyl laurate.* Biomolecules, 2021. **11**(3): p. 445.

59. Benítez-Mateos, A.I., et al., *Dual valorization of lignin as a versatile and renewable matrix for enzyme immobilization and (Flow) bioprocess engineering.* ChemSusChem, 2021. **14**(15): p. 3198-3207.

60. Fernandez-Lafuente, R., C.M. Rosell, and J. Guisán, *Enzyme reaction engineering: synthesis of antibiotics catalysed by stabilized penicillin G acylase in the presence of organic cosolvents.* Enzyme and microbial technology, 1991. **13**(11): p. 898-905.

61. Rosell, C.M., et al., *A criterion for the selection of monophasic solvents for enzymatic synthesis.* Enzyme and Microbial Technology, 1998. **23**(1-2): p. 64-69.

62. Fernandez-Lafuente, R., R. CM, and G. JM, *Dynamic reaction design of enzymic biotransformations in organic media: equilibrium-controlled synthesis of antibiotics by penicillin G acylase.* Biotechnology and applied biochemistry, 1996. **24**(2): p. 139-145.

63. Hudson, S., J. Cooney, and E. Magner, *Proteins in mesoporous silicates.* Angewandte Chemie International Edition, 2008. **47**(45): p. 8582-8594.

64. Cabrera, K., *Applications of silica-based monolithic HPLC columns.* Journal of separation science, 2004. **27**(10-11): p. 843-852.

65. David, A.E., et al., *Chemically surface modified gel (CSMG): an excellent enzyme-immobilization matrix for industrial processes.* Journal of Biotechnology, 2006. **125**(3): p. 395-407.

66. Cassimjee, K.E., et al., *A general protein purification and immobilization method on controlled porosity glass: Biocatalytic applications.* Chemical Communications, 2014. **50**(65): p. 9134-9137.

67. Thompson, M.P., et al., *A generic platform for the immobilisation of engineered biocatalysts.* Tetrahedron, 2019. **75**(3): p. 327-334.

68. Böhmer, W., et al., *Continuous Flow Bioamination of Ketones in Organic Solvents at Controlled Water Activity using Immobilized ω-Transaminases.* Advanced Synthesis & Catalysis, 2020. **362**(9): p. 1858-1867.

69. Rodrigues, R.C., et al., *Immobilization of lipases on hydrophobic supports: immobilization mechanism, advantages, problems, and solutions.* Biotechnology Advances, 2019. **37**(5): p. 746-770.

70. Ortiz, C., et al., *Novozym 435: the "perfect" lipase immobilized biocatalyst?* Catalysis Science & Technology, 2019. **9**(10): p. 2380-2420.

71. De Simone, A., et al., *Immobilized enzyme reactors: an overview of applications in drug discovery from 2008 to 2018.* Chromatographia, 2019. **82**: p. 425-441.

72. Thompson, M.P., et al., *Biocatalysis using immobilized enzymes in continuous flow for the synthesis of fine chemicals.* Organic process research & development, 2018. **23**(1): p. 9-18.

73. Homaei, A., *Enzyme immobilization and its application in the food industry.* Advances in food biotechnology, 2015: p. 145-164.

74. Facin, B.R., et al., *Driving immobilized lipases as biocatalysts: 10 years state of the art and future prospects.* Industrial & Engineering Chemistry Research, 2019. **58**(14): p. 5358-5378.

75. Beatriz, B., G. Paula, and F. Batista-Viera, *Immobilization of enzymes: A literature survey.* Immobil. Enzym. Cells, 2013. **1051**: p. 15-31.

76. Guisan, J.M., et al., *The science of enzyme immobilization.* Immobilization of Enzymes and Cells: Methods and Protocols, 2020: p. 1-26.

77. Guisan, J.M., et al., *Correction to: immobilization of enzymes and cells.* Immobilization of Enzymes and Cells: Methods and Protocols, 2020: p. C1-C1.

78.   Miletić, N., A. Nastasović, and K. Loos, *Immobilization of biocatalysts for enzymatic polymerizations: possibilities, advantages, applications.* Bioresource Technology, 2012. **115**: p. 126-135.

79.   Sardar, M., I. Roy, and M.N. Gupta, *Simultaneous purification and immobilization of Aspergillus niger xylanase on the reversibly soluble polymer EudragitTM L-100.* Enzyme and Microbial Technology, 2000. **27**(9): p. 672-679.

80.   Barbosa, O., et al., *Strategies for the one-step immobilization–purification of enzymes as industrial biocatalysts.* Biotechnology advances, 2015. **33**(5): p. 435-456.

81.   Abbaszadeh, M. and P. Hejazi, *Metal affinity immobilization of cellulase on Fe3O4 nanoparticles with copper as ligand for biocatalytic applications.* Food chemistry, 2019. **290**: p. 47-55.

82.   Bayramoglu, G., et al., *A facile and efficient method of enzyme immobilization on silica particles via Michael acceptor film coatings: immobilized catalase in a plug flow reactor.* Bioprocess and Biosystems Engineering, 2016. **39**: p. 871-881.

83.   Ortega-Munoz, M., et al., *Vinyl sulfone functionalized silica: a "ready to use" pre-activated material for immobilization of biomolecules.* Journal of Materials Chemistry, 2010. **20**(34): p. 7189-7196.

84.   Morales-Sanfrutos, J., et al., *Vinyl sulfone: a versatile function for simple bioconjugation and immobilization.* Organic & biomolecular chemistry, 2010. **8**(3): p. 667-675.

85.   dos Santos, J.C., et al., *Characterization of supports activated with divinyl sulfone as a tool to immobilize and stabilize enzymes via multipoint covalent attachment. Application to chymotrypsin.* RSC advances, 2015. **5**(27): p. 20639-20649.

86.   dos Santos, J.C., et al., *Bovine trypsin immobilization on agarose activated with divinylsulfone: improved activity and stability via multipoint covalent attachment.* Journal of Molecular Catalysis B: Enzymatic, 2015. **117**: p. 38-44.

87.   Zucca, P., R. Fernandez-Lafuente, and E. Sanjust, *Agarose and its derivatives as supports for enzyme immobilization.* Molecules, 2016. **21**(11): p. 1577.

88.   Prikryl, P., et al., *Magnetic bead cellulose as a suitable support for immobilization of α-chymotrypsin.* Applied biochemistry and biotechnology, 2012. **168**: p. 295-305.

89.   Medina-Castillo, A.L., et al., *Novel synthetic route for covalent coupling of biomolecules on super-paramagnetic hybrid nanoparticles.* Journal of Polymer Science Part A: Polymer Chemistry, 2012. **50**(19): p. 3944-3953.

90.   de Andrades, D., et al., *Preparation of immobilized/stabilized biocatalysts of β-glucosidases from different sources: Importance of the support active groups and the immobilization protocol.* Biotechnology Progress, 2019. **35**(6): p. e2890.

91.   Xiong, Y., et al., *Microscale colocalization of cascade enzymes yields activity enhancement.* ACS nano, 2022. **16**(7): p. 10383-10391.

92.   Arana-Peña, S., et al., *Enzyme co-immobilization: Always the biocatalyst designers' choice… or not?* Biotechnology Advances, 2021. **51**: p. 107584.

93.   Trobo-Maseda, L., et al., *Immobilization of enzymes on hetero-functional supports: Physical adsorption plus additional covalent immobilization.* Immobilization of Enzymes and Cells: Methods and Protocols, 2020: p. 159-174.

94.   Zaak, H., M. Sassi, and R. Fernandez-Lafuente, *A new heterofunctional amino-vinyl sulfone support to immobilize enzymes: Application to the stabilization of β-galactosidase from Aspergillus oryzae.* Process Biochemistry, 2018. **64**: p. 200-205.

95. Barbosa, O., et al., *Heterofunctional supports in enzyme immobilization: from traditional immobilization protocols to opportunities in tuning enzyme properties.* Biomacromolecules, 2013. **14**(8): p. 2433-2462.

96. Roura Padrosa, D., V. Marchini, and F. Paradisi, *CapiPy: python-based GUI-application to assist in protein immobilization.* Bioinformatics, 2021. **37**(17): p. 2761-2762.

97. Rocha-Martín, J., et al., *Rational co-immobilization of bi-enzyme cascades on porous supports and their applications in bio-redox reactions with in situ recycling of soluble cofactors.* ChemCatChem, 2012. **4**(9): p. 1279-1288.

98. Bié, J., et al., *Enzyme immobilization and co-immobilization: Main framework, advances and some applications.* Processes, 2022. **10**(3): p. 494.

99. Velasco-Lozano, S., et al., *Sustainable and Continuous Synthesis of Enantiopure l-Amino Acids by Using a Versatile Immobilised Multienzyme System.* ChemBioChem, 2018. **19**(4): p. 395-403.

100. Benítez-Mateos, A.I., et al., *Design of the enzyme–carrier interface to overcome the O2 and NADH mass transfer limitations of an immobilized flavin oxidase.* ACS Applied Materials & Interfaces, 2020. **12**(50): p. 56027-56038.

101. Ledesma-Fernandez, A., et al., *Engineered repeat proteins as scaffolds to assemble multi-enzyme systems for efficient cell-free biosynthesis.* Nature Communications, 2023. **14**(1): p. 2587.

102. Liese, A. and L. Hilterhaus, *Evaluation of immobilized enzymes for industrial applications.* Chemical Society Reviews, 2013. **42**(15): p. 6236-6249.

103. Oh, C., et al., *New approach to the immobilization of glucose oxidase on non-porous silica microspheres functionalized by (3-aminopropyl) trimethoxysilane (APTMS).* Colloids and Surfaces B: Biointerfaces, 2006. **53**(2): p. 225-232.

104. Bolivar, J.M., et al., *Modulation of the distribution of small proteins within porous matrixes by smart-control of the immobilization rate.* Journal of biotechnology, 2011. **155**(4): p. 412-420.

105. Green, D.W. and R.H. Perry, *Perry's chemical engineers' handbook.* 2008: McGraw-Hill Education.

106. Benítez-Mateos, A.I., et al., *Flow biocatalysis 101: design, development and applications.* Reaction chemistry & engineering, 2021. **6**(4): p. 599-611.

107. Crotti, M., et al., *What's new in flow biocatalysis? A snapshot of 2020–2022.* Frontiers in Catalysis, 2023. **3**: p. 1154452.

108. Yamanè, T. and S. Shimizu, *Fed-batch techniques in microbial processes*, in *Bioprocess parameter control*. 2005, Springer. p. 147-194.

109. De Santis, P., L.-E. Meyer, and S. Kara, *The rise of continuous flow biocatalysis–fundamentals, very recent developments and future perspectives.* Reaction Chemistry & Engineering, 2020. **5**(12): p. 2155-2184.

110. Mallia, C.J. and I.R. Baxendale, *The use of gases in flow synthesis.* Organic Process Research & Development, 2016. **20**(2): p. 327-360.

111. Lawrence, J., et al., *Microfluidic multi-input reactor for biocatalytic synthesis using transketolase.* Journal of Molecular Catalysis B: Enzymatic, 2013. **95**: p. 111-117.

112. Britton, J., S. Majumdar, and G.A. Weiss, *Continuous flow biocatalysis.* Chemical Society Reviews, 2018. **47**(15): p. 5891-5918.

113. Santi, M., et al., *Flow biocatalysis: A challenging alternative for the synthesis of APIs and natural compounds.* International journal of molecular sciences, 2021. **22**(3): p. 990.

114.   Wohlgemuth, R., et al., *Microscale technology and biocatalytic processes: opportunities and challenges for synthesis.* Trends in biotechnology, 2015. **33**(5): p. 302-314.

115.   Yao, X., et al., *Review of the applications of microreactors.* Renewable and sustainable energy reviews, 2015. **47**: p. 519-539.

116.   Tomaszewski, B., A. Schmid, and K. Buehler, *Biocatalytic production of catechols using a high pressure tube-in-tube segmented flow microreactor.* Organic Process Research & Development, 2014. **18**(11): p. 1516-1526.

117.   Ringborg, R.H., A. Toftgaard Pedersen, and J.M. Woodley, *Automated determination of oxygen-dependent enzyme kinetics in a tube-in-tube flow reactor.* ChemCatChem, 2017. **9**(17): p. 3285-3288.

118.   Cen, Y.K., et al., *Immobilization of enzymes in/on membranes and their applications.* Advanced Synthesis & Catalysis, 2019. **361**(24): p. 5500-5515.

119.   Ranieri, G., et al., *Use of a ceramic membrane to improve the performance of two-separate-phase biocatalytic membrane reactor.* Molecules, 2016. **21**(3): p. 345.

120.   Salvi, H.M., M.P. Kamble, and G.D. Yadav, *Synthesis of geraniol esters in a continuous-flow packed-bed reactor of immobilized lipase: Optimization of process parameters and kinetic modeling.* Applied biochemistry and biotechnology, 2018. **184**: p. 630-643.

121.   Köckritz, A. and A. Martin, *Synthesis of azelaic acid from vegetable oil-based feedstocks.* European journal of lipid science and technology, 2011. **113**(1): p. 83-91.

122.   Girard, S.A., *Toward alternative routes to access functionalized arenes*. 2017: McGill University (Canada).

123.   Puppi, D. and F. Chiellini, *Biodegradable polymers for biomedical additive manufacturing.* Applied materials today, 2020. **20**: p. 100700.

124.   Soliday, C.L. and P. Kolattukudy, *Biosynthesis of cutin ω-hydroxylation of fatty acids by a microsomal preparation from germinating Vicia faba.* Plant Physiology, 1977. **59**(6): p. 1116-1121.

125.   Cheong, S., J.M. Clomburg, and R. Gonzalez, *Energy-and carbon-efficient synthesis of functionalized small molecules in bacteria using non-decarboxylative Claisen condensation reactions.* Nature biotechnology, 2016. **34**(5): p. 556-561.

126.   Sheppard, M.J., et al., *Retro-biosynthetic screening of a modular pathway design achieves selective route for microbial synthesis of 4-methyl-pentanol.* Nature communications, 2014. **5**(1): p. 5031.

127.   Lim, S., et al., *A multi-enzyme cascade reaction for the production of α, ω-dicarboxylic acids from free fatty acids.* Journal of Industrial and Engineering Chemistry, 2021. **98**: p. 358-365.

128.   Kim, T.-H., et al., *Multilayer engineering of enzyme cascade catalysis for one-pot preparation of nylon monomers from renewable fatty acids.* ACS Catalysis, 2020. **10**(9): p. 4871-4878.

129.   Wang, L., et al., *Efficient biosynthesis of 10-hydroxy-2-decenoic acid using a NAD (P) H regeneration P450 system and whole-cell catalytic biosynthesis.* ACS omega, 2022. **7**(21): p. 17774-17783.

130.   Ide, M.S. and R.J. Davis, *Perspectives on the kinetics of diol oxidation over supported platinum catalysts in aqueous solution.* Journal of catalysis, 2013. **308**: p. 50-59.

131.   Pyo, S.-H., et al., *A sustainable synthetic route for biobased 6-hydroxyhexanoic acid, adipic acid and ε-caprolactone by integrating bio-and chemical catalysis.* Green Chemistry, 2020. **22**(14): p. 4450-4455.

132. Wang, F., et al., *One-pot biocatalytic route from cycloalkanes to α, ω-dicarboxylic acids by designed Escherichia coli consortia.* Nature Communications, 2020. **11**(1): p. 5035.

133. Sarak, S., et al., *One-pot biocatalytic synthesis of nylon monomers from cyclohexanol using Escherichia coli-based concurrent cascade consortia.* Green Chemistry, 2021. **23**(23): p. 9447-9453.

134. Pennec, A., et al., *One-pot conversion of cycloalkanes to lactones.* ChemCatChem, 2015. **7**(2): p. 236-239.

135. Song, J.W., et al., *Multistep enzymatic synthesis of long-chain α, ω-dicarboxylic and ω-hydroxycarboxylic acids from renewable fatty acids and plant oils.* Angewandte Chemie International Edition, 2013. **52**(9): p. 2534-2537.

136. Lorenzen, J., *Enzymatic functionalization of bio based fatty acids and algae based triglycerides.* 2019, Technische Universität München.

137. Ren, Y., et al., *Structure and function of aldopentose catabolism enzymes involved in oxidative non-phosphorylative pathways.* Biotechnology for Biofuels and Bioproducts, 2022. **15**(1): p. 147.

138. van der Vlugt-Bergmans, C.c.J.B. and M.t.J. van der Werf, *Genetic and biochemical characterization of a novel monoterpene ε-lactone hydrolase from Rhodococcus erythropolis DCL14.* Applied and environmental microbiology, 2001. **67**(2): p. 733-741.

139. Velasco-Lozano, S., et al., *Cell-Free Biosynthesis of ω-Hydroxy Acids Boosted by a Synergistic Combination of Alcohol Dehydrogenases.* ChemSusChem, 2022. **15**(9): p. e202200397.

140. Velasco-Lozano, S., et al., *Co-immobilization and Colocalization of Multi-Enzyme Systems for the Cell-Free Biosynthesis of Aminoalcohols.* ChemCatChem, 2020. **12**(11): p. 3030-3041.

141. Wu, S., et al., *Biocatalysis: enzymatic synthesis for industrial applications.* Angewandte Chemie International Edition, 2021. **60**(1): p. 88-119.

142. Puetz, H., et al., *Biocatalytic oxidation of alcohols.* Catalysts, 2020. **10**(9): p. 952.

143. Kara, S., et al., *Access to lactone building blocks via horse liver alcohol dehydrogenase-catalyzed oxidative lactonization.* Acs Catalysis, 2013. **3**(11): p. 2436-2439.

144. Kirmair, L., D.L. Seiler, and A. Skerra, *Stability engineering of the Geobacillus stearothermophilus alcohol dehydrogenase and application for the synthesis of a polyamide 12 precursor.* Applied microbiology and biotechnology, 2015. **99**: p. 10501-10513.

145. Schrittwieser, J.H., et al., *Recent biocatalytic oxidation–reduction cascades.* Current Opinion in Chemical Biology, 2011. **15**(2): p. 249-256.

146. Dickinson, F.M. and G.P. Monger, *A study of the kinetics and mechanism of yeast alcohol dehydrogenase with a variety of substrates.* Biochemical Journal, 1973. **131**(2): p. 261-270.

147. Pham, N.H., et al., *Engineering an enzymatic regeneration system for NAD (P) H oxidation.* Journal of Molecular Catalysis B: Enzymatic, 2015. **120**: p. 38-46.

148. Nowak, C., et al., *A water-forming NADH oxidase from Lactobacillus pentosus suitable for the regeneration of synthetic biomimetic cofactors.* Frontiers in Microbiology, 2015. **6**: p. 957.

149. Castillo Pacheco, S.F., et al., *Chemoenzymatic Oxidation of Diols Catalyzed by Co-Immobilized Flavins and Dehydrogenases.* ChemCatChem, 2023. **15**(14): p. e202300140.

150. Díaz-Rodríguez, A., et al., *From diols to lactones under aerobic conditions using a laccase/TEMPO catalytic system in aqueous medium.* Advanced Synthesis & Catalysis, 2012. **354**(18): p. 3405-3408.

151. Martin, C., M. Trajkovic, and M.W. Fraaije, *Production of hydroxy acids: selective double oxidation of diols by flavoprotein alcohol oxidase.* Angewandte Chemie International Edition, 2020. **59**(12): p. 4869-4872.

152. Sheldon, R.A., A. Basso, and D. Brady, *New frontiers in enzyme immobilisation: robust biocatalysts for a circular bio-based economy.* Chemical Society Reviews, 2021. **50**(10): p. 5850-5862.

153. Garcia-Galan, C., et al., *Potential of different enzyme immobilization strategies to improve enzyme performance.* Advanced Synthesis & Catalysis, 2011. **353**(16): p. 2885-2904.

154. Contente, M.L., et al., *Flow-based enzymatic synthesis of melatonin and other high value tryptamine derivatives: A five-minute intensified process.* Green chemistry, 2019. **21**(12): p. 3263-3266.

155. Liu, J., et al., *Metal–organic frameworks as a versatile materials platform for unlocking new potentials in biocatalysis.* Small, 2021. **17**(32): p. 2100300.

156. Zhang, M., et al., *Enzyme-inorganic hybrid nanoflowers: Classification, synthesis, functionalization and potential applications.* Chemical Engineering Journal, 2021. **415**: p. 129075.

157. Mateo, C., et al., *Immobilization of enzymes on heterofunctional epoxy supports.* Nature Protocols, 2007. **2**(5): p. 1022-1033.

158. Liu, N., et al., *An ultrasensitive amperometric immunosensor for zearalenones based on oriented antibody immobilization on a glassy carbon electrode modified with MWCNTs and AuPt nanoparticles.* Microchimica Acta, 2017. **184**: p. 147-153.

159. Mateo, C., et al., *One-step purification, immobilization, and stabilization of poly-histidine-tagged enzymes using metal chelate-epoxy supports.* Immobilization of Enzymes and Cells, 2006: p. 117-128.

160. Patel, S.K., et al., *Protein–inorganic hybrid system for efficient his-tagged enzymes immobilization and its application in L-xylulose production.* RSC advances, 2017. **7**(6): p. 3488-3494.

161. Marchesi, A., et al., *Enzymatic Building-Block Synthesis for Solid-Phase Automated Glycan Assembly.* Angewandte Chemie, 2020. **132**(50): p. 22642-22645.

162. Bolivar, J.M., et al., *Stabilization of a formate dehydrogenase by covalent immobilization on highly activated glyoxyl-agarose supports.* Biomacromolecules, 2006. **7**(3): p. 669-673.

163. Padrosa, D.R., et al., *Cell-free biocatalytic syntheses of l-pipecolic acid: A dual strategy approach and process intensification in flow.* Green chemistry, 2020. **22**(16): p. 5310-5316.

164. Latour, X., et al., *Rhodococcus erythropolis and its γ-lactone catabolic pathway: an unusual biocontrol system that disrupts pathogen quorum sensing communication.* Agronomy, 2013. **3**(4): p. 816-838.

165. Lim, S.H. and P. Beak, *Kinetic Resolution of Racemic Lactones by Conjugate Additions of Allylic Organolithium Species: Direct Formation of Three Contiguous Centers with High Diastereo-and Enantioselectivities.* Organic Letters, 2002. **4**(16): p. 2657-2660.

166.   Mateo, C., et al., *Glyoxyl agarose: a fully inert and hydrophilic support for immobilization and high stabilization of proteins.* Enzyme and Microbial Technology, 2006. **39**(2): p. 274-280.

167.   Rocha-Martín, J., et al., *New biotechnological perspectives of a NADH oxidase variant from Thermus thermophilus HB27 as NAD+-recycling enzyme.* BMC biotechnology, 2011. **11**: p. 1-11.

168.   Wu, J., et al., *Determination of dihydroxyacetone and glycerol in fermentation process by GC after n-methylimidazole catalyzed acetylation.* Journal of chromatographic science, 2011. **49**(5): p. 375-378.

169.   Takakura, Y., et al., *K. Hernandez, J. Bujons, J. Joglar, SJ Charnock, P. Domínguez de María, WD Fessner and P. Clapés.* ACS Catal, 2017. **7**: p. 1707.

170.   Velasco-Lozano, S., et al., *Selective oxidation of alkyl and aryl glyceryl monoethers catalysed by an engineered and immobilised glycerol dehydrogenase.* Chemical Science, 2020. **11**(44): p. 12009-12020.

171.   Santiago-Arcos, J., et al., *Immobilization Screening and Characterization of an Alcohol Dehydrogenase and Its Application to the Multi-Enzymatic Selective Oxidation of 1,-Omega-Diols.* Frontiers in Catalysis, 2021. **1**: p. 715075.

172.   Rocha-Martin, J., et al., *Immobilizing systems biocatalysis for the selective oxidation of glycerol coupled to in situ cofactor recycling and hydrogen peroxide elimination.* ChemCatChem, 2015. **7**(13): p. 1939-1947.

173.   López-Gallego, F. and L. Yate, *Selective biomineralization of Co 3 (PO 4) 2-sponges triggered by His-tagged proteins: efficient heterogeneous biocatalysts for redox processes.* Chemical Communications, 2015. **51**(42): p. 8753-8756.

174.   Bradford, M.M., *A rapid and sensitive method for the quantitation of microgram quantities of protein utilizing the principle of protein-dye binding.* Analytical biochemistry, 1976. **72**(1-2): p. 248-254.

175.   Holmes, K.L. and L.M. Lantz, *Protein labeling with fluorescent probes.* Methods in cell biology, 2001. **63**: p. 185-204.

176.   Schindelin, J., et al., *Fiji: an open-source platform for biological-image analysis.* Nature methods, 2012. **9**(7): p. 676-682.

177.   Aymard, C. and A. Belarbi, *Kinetics of thermal deactivation of enzymes: a simple three parameters phenomenological model can describe the decay of enzyme activity, irrespectively of the mechanism.* Enzyme and microbial technology, 2000. **27**(8): p. 612-618.

178.   Fixler, D., et al., *Influence of fluorescence anisotropy on fluorescence intensity and lifetime measurement: theory, simulations and experiments.* IEEE transactions on biomedical engineering, 2006. **53**(6): p. 1141-1152.

179.   Huang, L., et al., *Modeling alcohol dehydrogenase catalysis in deep eutectic solvent/water mixtures.* ChemBioChem, 2020. **21**(6): p. 811-817.

180.   Hernández Sánchez, K., et al., *Combining aldolases and transaminases for the synthesis of 2‐amino-4-hydroxybutanoic acid.* 2017.

181.   Mateo, C., et al., *Advances in the design of new epoxy supports for enzyme immobilization–stabilization.* Biochemical society transactions, 2007. **35**(6): p. 1593-1601.

182.   Royer, C.A., *Probing protein folding and conformational transitions with fluorescence.* Chemical reviews, 2006. **106**(5): p. 1769-1784.

183. Orrego, A.H., et al., *Two-photon fluorescence anisotropy imaging to elucidate the dynamics and the stability of immobilized proteins.* The Journal of Physical Chemistry B, 2016. **120**(3): p. 485-491.

184. Weltz, J.S., et al., *Reduced enzyme dynamics upon multipoint covalent immobilization leads to stability-activity trade-off.* Journal of the American Chemical Society, 2020. **142**(7): p. 3463-3471.

185. Bolivar, J.M. and F. López-Gallego, *Characterization and evaluation of immobilized enzymes for applications in flow reactors.* Current Opinion in Green and Sustainable Chemistry, 2020. **25**: p. 100349.

186. Bosch, S., et al., *Thermostability engineering of a class II pyruvate aldolase from Escherichia coli by in vivo folding interference.* ACS Sustainable Chemistry & Engineering, 2021. **9**(15): p. 5430-5436.

187. Rodrigues de Melo, R., et al., *New heterofunctional supports based on glutaraldehyde-activation: A tool for enzyme immobilization at neutral pH.* Molecules, 2017. **22**(7): p. 1088.

188. Guisán, J., *Aldehyde-agarose gels as activated supports for immobilization-stabilization of enzymes.* Enzyme and Microbial Technology, 1988. **10**(6): p. 375-382.

189. Snyder, S.L. and P.Z. Sobocinski, *An improved 2, 4, 6-trinitrobenzenesulfonic acid method for the determination of amines.* Analytical biochemistry, 1975. **64**(1): p. 284-288.

190. Miksch, R.R., et al., *Modified pararosaniline method for the determination of formaldehyde in air.* Analytical Chemistry, 1981. **53**(13): p. 2118-2123.

191. Huynh, K. and C.L. Partch, *Analysis of protein stability and ligand interactions by thermal shift assay.* Current protocols in protein science, 2015. **79**(1): p. 28.9. 1-28.9. 14.

192. Diamanti, E., et al., *Intraparticle macromolecular migration alters the structure and function of proteins reversibly immobilized on porous microbeads.* Advanced Materials Interfaces, 2022. **9**(18): p. 2200263.

193. Montoya, N.A., et al., *Review on porous materials for the thermal stabilization of proteins.* Microporous and Mesoporous Materials, 2022. **333**: p. 111750.

194. Mateo, C., et al., *Increase in conformational stability of enzymes immobilized on epoxy-activated supports by favoring additional multipoint covalent attachment ☆.* Enzyme and Microbial Technology, 2000. **26**(7): p. 509-515.

195. Rocha-Martin, J., et al., *Functional characterization and structural analysis of NADH oxidase mutants from thermus thermophilus HB27: Role of residues 166, 174, and 194 in the catalytic properties and thermostability.* Microorganisms, 2019. **7**(11): p. 515.

196. Hiblot, J., et al., *Structural and enzymatic characterization of the lactonase sis lac from Sulfolobus islandicus.* 2012.

197. Nannenga, B.L., et al., *Structure of catalase determined by MicroED.* Elife, 2014. **3**: p. e03600.

198. Switala, J. and P.C. Loewen, *Diversity of properties among catalases.* Archives of biochemistry and biophysics, 2002. **401**(2): p. 145-154.

199. Romero-Fernández, M. and F. Paradisi, *Protein immobilization technology for flow biocatalysis.* Current opinion in chemical biology, 2020. **55**: p. 1-8.

200. Pessela, B.C., et al., *Ion exchange using poorly activated supports, an easy way for purification of large proteins.* Journal of Chromatography A, 2004. **1034**(1-2): p. 155-159.

201. García-Marquina, G., et al., *Immobilization and stabilization of an engineered acyltransferase for the continuous biosynthesis of simvastatin in packed-bed reactors.* ACS Sustainable Chemistry & Engineering, 2022. **10**(30): p. 9899-9910.

202. Santiago-Arcos, J., S. Velasco-Lozano, and F. López-Gallego, *Multienzyme coimmobilization on triheterofunctional supports.* Biomacromolecules, 2023. **24**(2): p. 929-942.

203. Diamanti, E., et al., *Intraparticle kinetics unveil crowding and enzyme distribution effects on the performance of cofactor-dependent heterogeneous biocatalysts.* ACS catalysis, 2021. **11**(24): p. 15051-15067.

204. Schelch, S., J.M. Bolivar, and B. Nidetzky, *Monitoring and control of the release of soluble O2 from H2O2 inside porous enzyme carrier for O2 supply to an immobilized D-amino acid oxidase.* Biotechnology and Bioengineering, 2022. **119**(9): p. 2374-2387.

205. Chapman, M.R., et al., *Highly productive oxidative biocatalysis in continuous flow by enhancing the aqueous equilibrium solubility of oxygen.* Angewandte Chemie International Edition, 2018. **57**(33): p. 10535-10539.

206. Zhou, Z.z., et al., *Silver (I)-catalyzed widely applicable aerobic 1, 2-diol oxidative cleavage.* Angewandte Chemie International Edition, 2018. **57**(10): p. 2616-2620.

207. Weckbecker, A. and W. Hummel, *Cloning, expression, and characterization of an (R)-specific alcohol dehydrogenase from Lactobacillus kefir.* Biocatalysis and biotransformation, 2006. **24**(5): p. 380-389.